Development of a human pluripotent stem cell-derived *in vitro* model of myelination

Owen Gwydion James

THE UNIVERSITY *of* EDINBURGH

Doctor of Philosophy

The University of Edinburgh

2019

Declaration

I declare that this thesis has been composed by myself and is the result of my own work except where indicated by reference or acknowledgement. The work presented here has not been previously submitted for another degree or qualification.

Owen Gwydion James

Acknowledgements

Firstly, I would like to acknowledge the Euan McDonald Centre, the College of Medicine and Veterinary Medicine and the MS Society for providing the funding that made this work possible.

To my supervisor, Siddarthan: thank you for your continued belief in me and enthusiasm for this project. You took a chance on me and have had my back ever since. You helped me see the big picture when things were tough, and I'll always be grateful for how you supported and channelled my development at every step.

I owe a great deal to Bhuvaneish: you taught me how to be a scientist! I have so much respect for your patience and integrity. Your calm and consistent guidance made all the difference. Aside from the first-rate mentorship, I'm grateful for the compassion, time, and friendship you've given me over the years.

To Charles and Dave, you are the thesis committee dream team. Thank you for your openness and the constructive discussions throughout this PhD and, in particular, for your encouragement and for pushing me on.

Thank you to Karen and the lab technicians for the first-rate stem cells! And to Bertrand, for teaching me macros and the baby steps of coding—you set me off on the right foot.

Thanks specifically to Arpan, Sam, Poulomi, and Navneet for the kind supervision and friendship you've given me over the years. Thanks also to everyone in the lab for the laughs that made being at work a real pleasure, and to my wonderful friends on the outside who have filled my memories of this city with pubs, games, and trips, without which these past four years would have been far less magical: "it does not do to dwell on dreams and forget to live".

I Mam and Dad, dwi mor ddiolchgar i cael chi fel rhieni. Diolch am eich cariad a gefnogaeth i wastad fynd amdani.

And lastly to Chloë: you've lived this PhD with me and at the very least deserve a certificate in neuroscience for all the unsolicited knowledge you now have on myelin (even if you still can't pronounce it properly). You cheered me on during the highs and lows. I'm so grateful to have had you there, each step of the way. You're my editor supreme and the 3-minute thesis coach of the year.

Graphical abstract

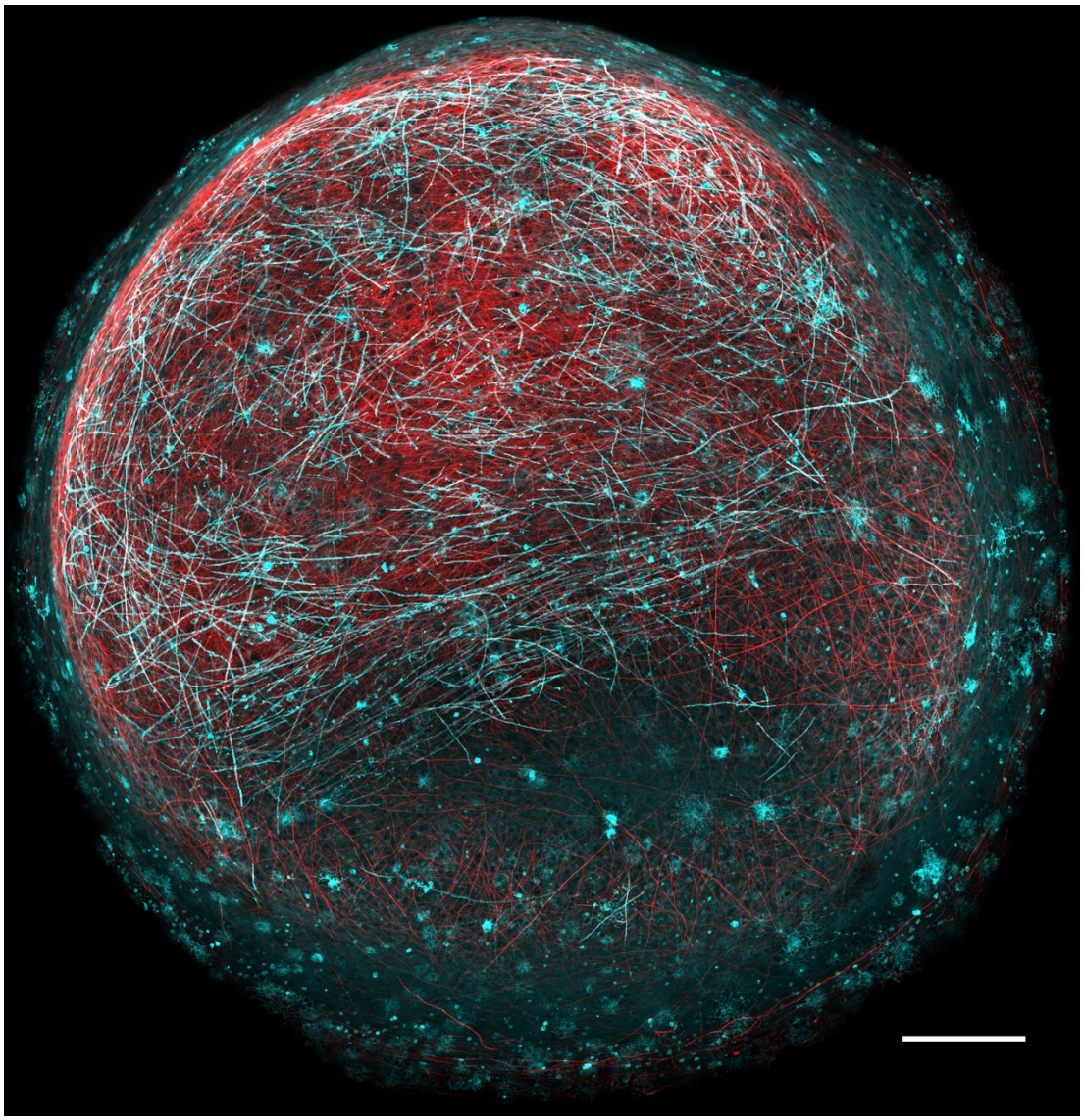

Myelinoids: three-dimensional human pluripotent stem cell-derived cultures comprising CNS-patterned cells and demonstrating compact myelination as a model to study human myelin development and disease. Myelinating oligodendrocytes in cyan (CNP staining) and neuronal axons in red (neurofilament; NF-H staining), scale = 250μm.

Abstract

Myelination is essential for central nervous system (CNS) formation, health, and function. Its development is an adaptive and regulated process that, when perturbed, leads to disease. However, our understanding of myelin formation in health and disease is limited by the paucity of human models of myelination. I sought to develop a human stem cell-derived in vitro model of myelination that would enable studies of myelin development in the context of pharmacological, physiological, or genetic perturbations.

Three-dimensional human induced pluripotent stem cell-derived, spinal cord organoids were generated containing NF-H$^+$ neurons, GFAP$^+$ astrocytes, PDGFRα$^+$ oligodendrocyte progenitor cells, and MBP$^+$ oligodendrocytes. With prolonged culture, myelin formation was evident, demonstrated by (i) thick MBP$^+$ tubular structures co-localising with NF-H$^+$ axons; (ii) organisation of myelinated axon domains, as determined by appropriate clustering of paranodal and nodal proteins; and (iii) compact myelin lamellae visualised by transmission electron microscopy. iPSC 'myelinoids' demonstrate temporal development of myelination, with both myelin sheath length and compaction increasing over time. The morphology of individual myelinating oligodendrocytes could also be analysed, and exposure to a pharmacological cytoskeletal modulator potentiated myelin sheath number per cell, as expected. Furthermore, a novel automated pipeline to quantify myelin volume across entire myelinoids was developed, which showed that myelin volume—specific to myelinated axons—increased over time. Automated analysis of oligodendrogenesis and myelin formation was demonstrated as an alternative method for investigating the effects of small molecules or trophic factor signalling on oligodendrogenesis and myelin development.

Neuronal activity can regulate myelination by oligodendrocytes in model organisms. However, whether myelination by human oligodendrocytes is responsive to neuronal activity has not previously been investigated. I found that blocking synaptic vesicle release via tetanus toxin (TeNT) impaired myelin sheath generation by individual oligodendrocytes and led to a reduction in total myelin volume across myelinoids.

These results demonstrate that human myelinating oligodendrocytes respond to changes in neuronal activity.

An advantage of iPSC-based models is the generation of patient-derived cultures that enable aspects of human disease to be modelled in vitro. In order to demonstrate that myelinoids could be used to model disorders of myelin, myelinoids were generated from a patient with a homozygous recessive mutation in the gene for Neurofascin (NFASC). This nonsense mutation is predicted to specifically affect the glial-expressed form of Neurofascin, Nfasc155 (a component of the paranodal axoglial junction assembly expressed by glia), the deficiency of which results in a neurodevelopmental disorder characterised by hypotonia, amimia, and areflexia. Patient-derived myelinoids demonstrated impaired formation of paranodal axoglial junctions, while nodal Neurofascin remained intact, recapitulating the major pathology of this disease.

Finally, oligodendrocyte pathology is prevalent in amyotrophic lateral sclerosis (ALS), a rapidly progressing neurodegenerative disorder of both upper and lower motor neurons. However, the mechanism by which oligodendrocytes contribute to disease is not yet understood. TDP-43 is a critical DNA/RNA binding protein involved in RNA metabolism whose cytoplasmic misaccumulation and aggregation in neurons and glia is a pathological hallmark of ALS. Disease causing mutations in the encoding gene, TARDBP, account for 5-10% of familial forms of ALS. To determine whether mutant TDP-43 affects myelin development, myelinoids were generated from both patient-derived and CRISPR/Cas9 gene-corrected iPSCs. I found that myelinoids derived from mutant and gene-corrected iPSCs showed no difference in oligodendrogenesis or myelin formation.

Collectively, this work shows that iPSC myelinoids provide a robust platform for investigating human myelin development in both health and disease.

Lay Summary

Communication within the brain and between the brain and the rest of the body, occurs via electrical signals that travel along nerve cells called neurons. Approximately half of these neurons are covered in a dense insulating sleeve, called myelin, which is made by cells called oligodendrocytes. Much like insulation on an electrical wire, myelin enables signals between different parts of the brain and other body parts to be carried by neurons up to ten times more quickly than they could travel otherwise. Myelin plays other important roles too, helping to provide the optimal chemical environment for neuron function. It is unsurprising then that damage to, or loss of, myelin (or oligodendrocytes) has drastic consequences on neuron function and can cause these cells to die. This happens in disorders such as the leukodystrophies, multiple sclerosis, and motor neuron disease. Moreover, there is some evidence that subtle changes to myelin development might be involved in causing psychiatric conditions such as schizophrenia.

Currently, most of our understanding of myelin development in health and disease has come from animal models. Such studies are an integral part of biomedical and drug discovery research. However, the development of new therapies to treat human disease is very inefficient, particularly for brain disorders. Recent studies have identified important differences between mice and human cells that might be contributing to inefficient drug development. In order to address this, many have turned to human stem cells: 'ground-state', embryonic-like cells that have the potential to be made into any cell in the body. Stem cells can be derived by reprogramming skin cells or blood cells, making it possible to source stem cells from healthy adults as well as people with neurological disorders. We can grow these cells into the cell type of our choice and use them to study how disease-causing mutations effect cellular processes and to test the effectiveness of different drugs on rescuing any disease-associated defects.

Human stem cell-derived oligodendrocytes can be made through a process sometimes referred to informally as 'chemical cookery'. However, unlike the same cells from rodents, human oligodendrocytes do not readily form myelin when placed together with neurons. Therefore, in order to study human myelin development using

healthy and patient-derived oligodendrocytes, I first aimed to find the right conditions that would support human stem cell-derived myelin formation in the lab. I found that cultures of stem cells that were grown as three-dimensional spheres generated both neurons and oligodendrocytes and that myelin wrapping around neurons could be seen after maintaining these cultures for long periods of time. I characterised myelin development in these cultures and found that myelinating spheres, or 'myelinoids', demonstrated the expected characteristics of mature, compactly wrapped myelin. I also showed that, when exposed to different drugs, the number and morphology of myelinating oligodendrocytes changed predictably, providing evidence that human stem cell-derived myelin looked and behaved as we would expect.

Next, I asked whether human oligodendrocytes could respond to changes in neuronal activity. Studies in animal models have shown that neurons with either higher or lower levels of electrical activity had either more or less myelin along their lengths and also affected the amount of myelin made per oligodendrocyte. This has important implications for the idea of 'plasticity', which refers to a range of physical and functional changes in the brain that accompany certain tasks, for example, learning to juggle, play the piano or learning a second language. Human brain imaging studies have shown structural changes in response to learning specific motor tasks that are suggestive of changes in myelin. However, it has not yet been possible to test whether human myelinating oligodendrocytes are responsive to neuronal activity. I found that reducing neuronal activity led to a reduction in myelin formation. These findings show, for the first time, that human oligodendrocytes respond to changes in neuronal activity.

Subsequently, using patient-derived stem cells that carry a defective gene involved in myelin formation, I show that myelinoids acquire the same myelination defect that was observed in the patient and animal models of this particular disease. This validates this platform for modelling neurological disorders. Finally, I investigated whether a disease-causing mutation that results in motor neurone disease (MND) had an impact on myelin development. To do so, I used stem cells from someone with MND and, using the CRISPR/Cas9 'genetic scissors' approach to cut and repair the disease-causing mutation, created gene-corrected stem cells that can be used to compare against the unhealthy 'cell line'. Using these two stem cell lines, I show that the presence of the MND-causing mutation does not affect myelin formation in stem cell derived myelinoids.

Collectively, this work shows that human stem cells can be used to generate a model of myelination for the study human myelin development and the factors that regulate it, as well as to study myelination in the context of human disease, through the use of patient-derived stem cells.

Abbreviations

95% CI	95 percent confidence interval
ALS	Amyotrophic lateral sclerosis
AMPA	α-amino-3-hydroxy-5-methyl-4-isoxazolepropionic acid
ATP	Adenosine triphosphate
BDNF	Brain-derived neurotrophic factor
BoNT/A	Botulinum neurotoxin
$Ca2^{+}$	Calcium
CASPR	Contactin-associated protein
ChAT	Choline Acetyltransferase
CNP	2',3'-Cyclic-nucleotide 3'-phosphodiesterase
CNS	Central nervous system
DMSO	Dimethyl sulfoxide
DNA	Deoxyribonucleic acid
dNTP	Deoxynucleoside triphosphates
DRG	Dorsal root ganglion
E(#)	Embryonic day
ESC	Embryonic stem cell
FA	Fractional anisotropy
FdU	Fluorodeoxyuridine
FGF	Fibroblast growth factor
GDNF	Glial cell-derived neurotrophic factor
GFAP	Glial fibrillary acidic protein
GLM	Generalised linear mixed model
HDR	Homology directed repair
hnRNP	Heterogeneous nuclear ribonucleoprotein
hNu	Human Nuclei
IGF	Insulin growth factor

iPSC	Induced pluripotent stem cell
Islet1/2	LIM-homeodomain transcription factors Islet 1 and 2
JXP	Juxtaparanode
K^+	Potassium
KCl	Potassium chloride
MAG	Myelin-associated glycoprotein
MBP	Myelin basic protein
MCT1	Monocarboxylate transporter 1
MI	Myelin induction
MN	Motor neuron
mRNA	Messenger ribonucleic acid
MS	Multiple sclerosis
MYRF	Myelin regulatory factor
Na^+	Sodium
NAWM	Normal appearing white matter
NF-H	Neurofilament heavy polypeptide
Nfasc	Neurofascin
NGF	Nerve growth factor
NHEJ	Non-homologous end-joining
NMDA	N-methyl-D-aspartate
NoR	Node of Ranvier
NPC	Neural precursor cell
OLIG2	Oligodendrocyte transcription factor 2
OPC	Oligodendrocyte progenitor cell
P(#)	Postnatal day
PAM	Protospacer adjacent motif
PBS	Phosphate-buffered saline
PCR	Polymerase chain reaction
PDGFRα	Platelet Derived Growth Factor Receptor Alpha
PFA	Paraformaldehyde

PLP	Proteolipid protein
PNJ	Paranodal axoglial junction
PNS	Peripheral nervous system
PTFE	Polytetrafluoroethylene
PV	Parvalbumin
RA	Retinoic acid
RNA	Ribonucleic acid
RT	Room temperature
SAG	Smoothened agonist
SD	Standard deviation
SHH	Sonic hedgehog
SOX10	SRY-related HMG-box 10
ssODN	Single-stranded donor oligonucleotides
SVZ	Subventricular zone
TDP-43	Transactive response DNA-binding protein 43
TEM	Transmission electron microscopy
TeNT	Tetanus neurotoxin
TGF-β	Transforming growth factor beta
Trk	Tropomyosin receptor kinase
TTX	Tetrodotoxin

Table of contents

Table of figures

Chapter 1 Aims

The overarching aim of this thesis is to establish a robust and efficient *in vitro* model of myelination using human induced pluripotent stem cells that recapitulates the three-dimensional architecture of myelinated axons. This will enable future studies of human myelin development and the factors that regulate it, as well as provide a platform from which to investigate myelin formation in the context of human disease. Specifically, I aim to:

a) Establish an *in vitro* human stem cell derived myelination model by exploring co-culture and three-dimensional organoid models.

b) Interrogate whether human myelination responds to pharmacological and physiological cues, including neuronal activity.

c) Develop an automated method of quantifying *in vitro* myelin that enables higher experimental throughput.

d) Investigate whether human disorders of myelin can be recapitulated in an *in vitro* model of myelination using patient-derived iPSCs.

Chapter 2 Introduction

Myelination is a remarkable example of reciprocal communication between two very different cell-types. This process profoundly affects axon function and has had considerable bearing on the expansion and connectivity of the central nervous system (CNS) over time (Zalc et al. 2008). Ensheathment of axons by specialised glial cell membrane leads to the formation of a dynamic axo-myelin unit that is associated with substantial rearrangement of ion channels and cytoskeletal proteins, modified signal propagation and altered metabolic support (Sherman & Brophy 2005; Hartline & Colman 2007; Simons & Nave 2015). Many axons are myelinated in the CNS and disruption to or loss of myelin has dramatic consequences on CNS health and function as a whole.

Myelin related disorders may be inherited or acquired, appear in young and old age and are a source of substantial economic burden (Powers 2004; Noseworthy 2000). Currently however, our understanding of myelin pathology in human disorders is limited by the paucity of human models of myelination. Induced pluripotent stem cell technology has enabled researchers to generate distinct CNS-derived cells, including oligodendrocytes, from both healthy individuals and those with neurological disorders, *in vitro* (Livesey et al. 2016). However, only transplantation studies using the dysmyelinating shiverer mouse model has faithfully recapitulated the appropriate three-dimensional architecture of myelinated axons by human oligodendrocytes so far (Windrem et al. 2017). In this thesis I will establish a robust method of generating iPSC-derived myelin with appropriate architecture and nodal organisation using organoid-like cultures and will characterise myelin development therein. I will demonstrate that human myelin formation is sensitive to pharmacological manipulation and that regulation of synaptic vesicle release modulates myelinating oligodendrocyte morphology as well as global levels of myelin. Finally, I will show that patient-derived cultures recapitulate key features of a disorder of myelinated axon organisation (Nfasc155 deficiency) and that presence of the ALS-causing mutation, *TARDBP*^{G298S}, does not impact myelin formation in these cultures.

In this introduction, I will summarise the functions of myelin as well as its development and pathology in disease. I will discuss recent evidence outlining the role of neuronal activity in modulating several aspects of myelin formation and emphasise the importance of studying human oligodendroglia by summarising species-specific differences related to myelin development. Lastly, I will discuss the models used to

study oligodendroglia and their contemporary equivalents, making the case that iPSC-derived organoids are well-suited to the study of complex interactions between human CNS-derived cells *in vitro.*

2.1 Myelin form and function

The acquisition of myelinated fibres in a subset of vertebrates 425 million years ago is considered to be a major contributing factor to the evolution of nervous systems with greatly enhanced information processing capacity (Zalc et al. 2008). The reason for this lies in the propagation of electrical impulses.

Action potential propagation along the axons of neurons relies on a strongly maintained negative charge on the intracellular surface of the axolemma. The initiation involves membrane depolarization beyond a certain threshold that results in a conformational change in nearby voltage-gated sodium channels, which are dispersed throughout the axolemma, and an influx of sodium cations. In turn, the change in voltage is extended into neighbouring areas, opening sodium channels further down the axolemma, generating a unidirectional depolarization wave, which travels down the axon at a rate of approximately 1m/s. The culmination of this process is the arrival of the depolarization wave at the presynaptic terminal and release of neurotransmitter containing vesicles onto another neuron (Hartline & Colman 2007).

Increasing conduction velocity is thought to have been advantageous for both predatory and escape behaviours and has been achieved in two ways: axon gigantism and the acquisition of myelin. In non-myelinated axons, the longitudinal resistance to electric current is inversely proportional to the square root of the fibre diameter, resulting in faster propagation in larger fibres. Axon gigantism is seen across taxa and primarily involved in circuits related to escape responses (Hartline & Colman 2007).

Alternatively, myelin—a dense, lipid rich and multilamellar membrane that ensheaths axons in a tightly wound helix—acts as an insulator that reduces the transverse capacitance of the axolemma, preventing the build-up of charge and membrane depolarization. Sodium channels are instead sequestered to gaps (~1μm) in the myelin sheath termed nodes of Ranvier where the axolemma is free to depolarise, resulting in an influx of sodium cations (Salzer 2003). Due to the increased membrane resistance inferred by myelin internodes, cations flow longitudinally through the cytoplasm towards the next node of Ranvier to propagate the depolarization wave (Figure 2.1). This saltatory (meaning ‘to leap’, from the Latin, *saltare)* conduction of action potentials at nodes of Ranvier increases the speed of propagation tenfold for

axons greater than 1μm. It is also more energetically efficient as the active transport of ions that restores the resting membrane potential of the axolemma occurs only at nodes. Finally, by avoiding the need for axon gigantism, myelin has enabled the development of large neural circuits with an economic use of space, as the same ten-fold increase in conduction velocity would require 100-times thicker axons.

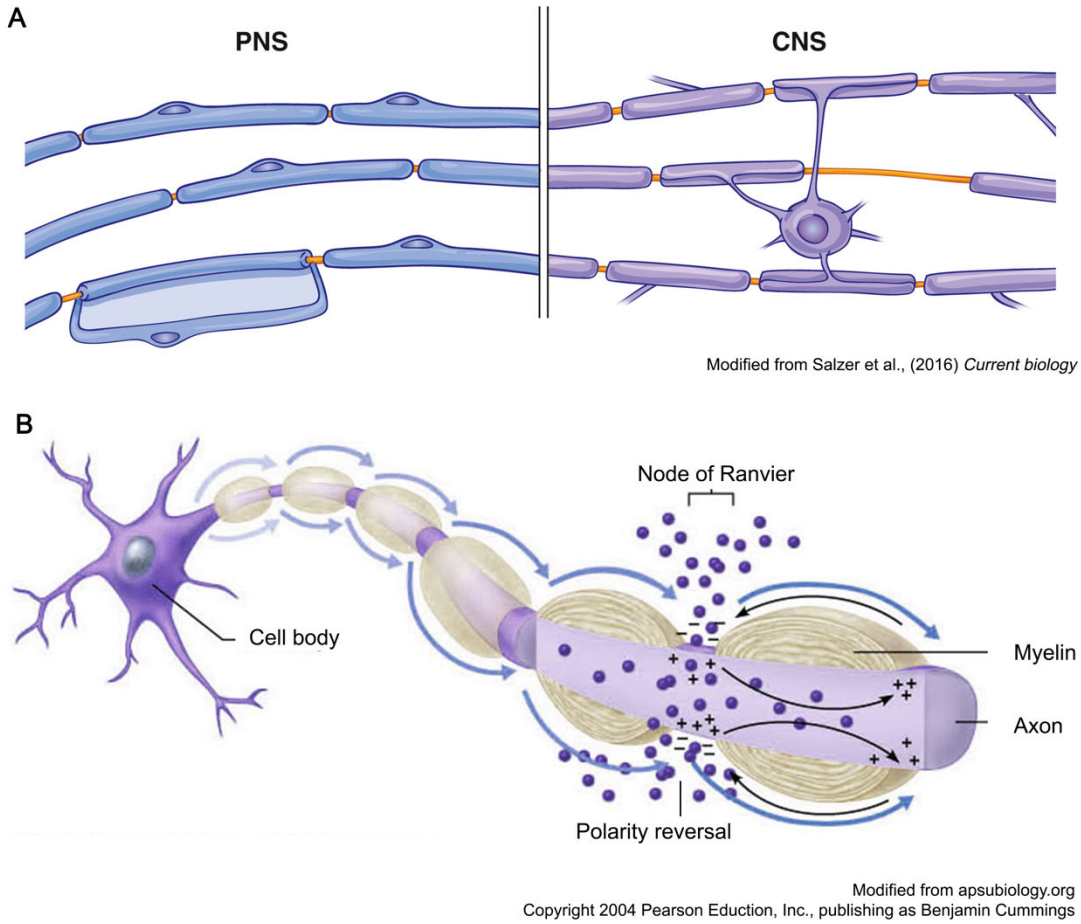

Figure 2.1 Myelin form and function

A) Schwann cells in the peripheral nervous system (PNS) form a single internode per cell and oligodendrocytes in the CNS myelinate many axons per cell (modified from Salzer et al., (2016) *Current Biology*).

B) Illustration of saltatory conduction along myelination axons (modified from apusbiology.org, Copyright Pearson Education).

In the CNS, myelin is laid down by oligodendrocytes and is predominantly found in white matter (WM), which in humans, makes up approximately 40–50% of intracortical brain volume (Ge et al. 2002). In contrast to grey matter (GM), where local networks between neurons are established with relatively sparse myelination, white matter contains both short and long-range axonal projections, which are heavily myelinated and typically gathered into bundles that link different cortical areas with each other and with subcortical structures (Schmahmann et al. 2008; Quan Wen 2005; Ouyang et al. 2017) . Deep, long-range, white matter tracts are the first to be myelinated with somatosensory pathways preceding motor tracts, reflecting the temporal sequence of their functional maturation (Geng et al. 2012). GM myelination in the frontal and temporal cortices takes place during adolescence and continues well into adulthood (Westlye et al. 2010; Walhovd et al. 2005; Benes 1989). White matter myelin contributes to processing speed in infants between 2 and 5 and is also correlated with cognitive decline later in life (Deoni et al. 2015; Grydeland et al. 2013; Deary et al. 2006; Lu et al. 2013).

However, many axons remain unmyelinated and there is tremendous variation in the length, thickness, and distribution of myelin across others. Discontinuously myelinated axons are found in the juvenile and adult CNS (Tomassy et al. 2014; Hughes et al. 2018; Hill et al. 2018) and are believed to reflect local control of signal transduction and a mechanism to fine-tune circuit function. Indeed, changes to myelin sheath parameters including internodal length, thickness, and node length have been demonstrated to influence conduction velocity (Arancibia Carcamo et al. 2017; Brill et al. 1977). Even subtle changes have potentially dramatic effects on neural circuit function by affecting synchronicity and oscillation frequency (Pajevic et al. 2014). This supports the growing appreciation that precise timing of conduction, rather than maximal velocity, may represent the optimal state for the function of certain circuits (Suminaite et al. 2019). Thalamocortical afferents for example display selective myelination to ensure consistent latency across a range of travelling distances (Salami et al. 2003). Intriguingly, discontinuous myelination has also been demonstrated along individual axons in sound localization circuitry within the brainstem (Seidl & Rubel 2015; Ford et al. 2015). Here, coincident detection of signals at medial superior olivary (MSO) neurons on either side of the brain is essential for circuit function. This is achieved, in part, through differential internode lengths along

ipsilateral and contralateral bifurcations of single axons projecting from each cochlear nucleus (Seidl & Rubel 2015). Thus, precise myelination, even along single axons, supports optimal CNS function and suggests that myelin sheath length optimisation is regulated via local adaptive mechanisms. That myelin not only modulates signal transduction but is reciprocally regulated in an activity-dependent process is further discussed in Chapter 2.5.

Myelin has also been recently attributed with additional functions in the metabolic support of axons (Figure 2.2). Axons can reach very long lengths of up to 1m in human adults and lack significant energy stores, which makes them vulnerable to increased neuronal activity due to the energetic demands of re-establishing the membrane potential via Na^+/K^+ channels (Thomas Philips 2017). Extra-axonal supply of lactate (or pyruvate) is considered a mechanism by which these energy demands are met. This was demonstrated in acute optic nerve preparations whereby the rapid deterioration of evoked compound action potentials (CAPs) observed in aglycemic conditions was rescued by bath application of L-lactate (Brown et al. 2004). Astrocyte-vasculature coupling and astrocytic glycogen stores are integral to the metabolic support of axons, and astrocytes may shuttle monocarboxylates to axons directly. However, panglial coupling of astrocytes and oligodendrocytes via gap junctions enables the diffusion of metabolites into oligodendrocytes, which are well placed to support the metabolic demands of axons, particularly in densely myelinated tracts. Axo-myelin metabolic coupling involves the release of pyruvate and lactate via oligodendroglial monocarboxylate transporter 1 (MCT1) into the internodal space. Subsequent take-up by axons for mitochondrial ATP production fuels neuronal energy homeostasis (Y. Lee, Morrison, Y. Li, Lengacher, Farah, Hoffman, Y. Liu, Tsingalia, Jin, Zhang, Pellerin, Magistretti & Rothstein 2012a; Fünfschilling, Supplie, Mahad, Boretius, Saab, Edgar, Brinkmann, Kassmann, Tzvetanova, Möbius, Diaz, Meijer, Suter, Hamprecht, Sereda, Moraes, Frahm, Goebbels & Nave 2012a; Saab et al. 2013; Thomas Philips 2017). It is also thought that axonal glutamate release and activation of N-methyl-D-aspartate receptors (NMDAR) on oligodendrocytes regulates this process, thereby coupling neuronal activity and metabolic supply (Saab et al. 2016) (Figure 2.2).

Interestingly, a distinct mode of axo-myelin metabolic coupling was identified in the corpus callosum, which rather than being fully myelinated, displays a large proportion

(60-70%) of non-myelinated axons (Mack et al. 1995). When mouse coronal sections were placed in aglycemic conditions, L-lactate perfusion was not sufficient to sustain the rapidly deteriorating evoked CAPs within the corpus callosum (Meyer et al. 2018). Rather, loading of individual oligodendrocytes (and not astrocytes) with glucose was able to rescue the loss of CAPs. This effect was abolished by reducing glial network coupling or by pharmacological blockade of MCTs and glucose transport. That alternate modes of metabolic coupling exist between different WM tracts underlines the importance of oligodendrocytes in supporting neuronal function but leaves open further questions about the generalisability of axo-myelin metabolic coupling across the CNS and the functional heterogeneity of myelinating oligodendrocytes across different regions. A failure to support axon metabolism is thought to underlie several neurodegenerative disorders, discussed in Chapter 2.4.

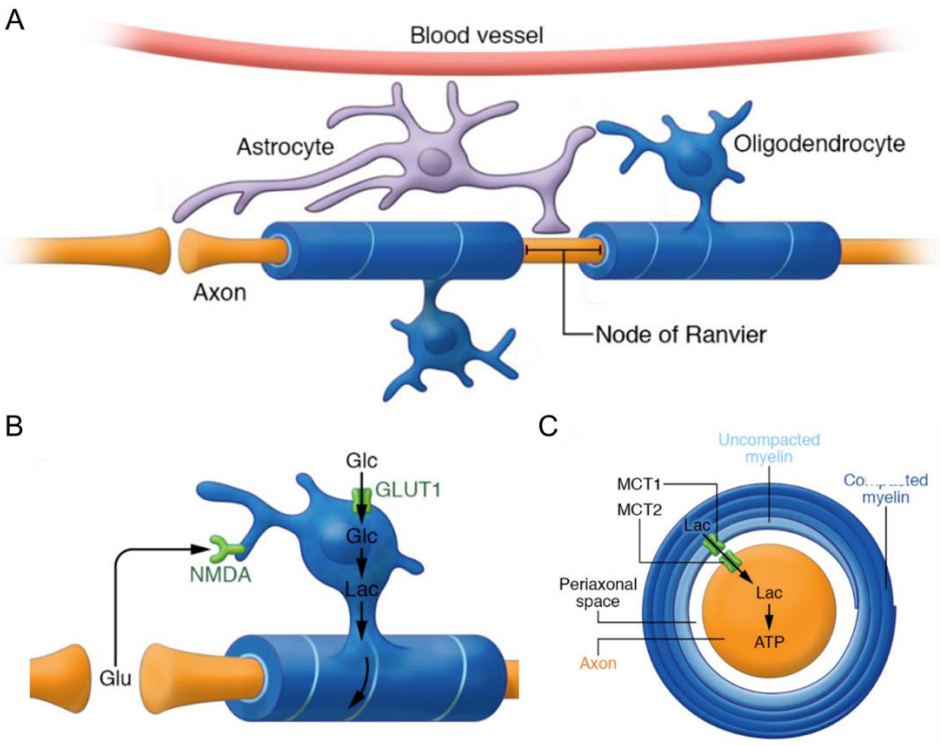

Figure 2.2 Oligodendrocyte metabolically support axons

A) Astrocytes couple the vasculature to both oligodendrocytes and axons by shuttling glucose or its glycolytic products to other cell-types.

B) Glycolytic oligodendrocytes import glucose and shuttle lactate (or pyruvate) to the underlying axon, which is thought to be modulated by activity dependent release of glutamate.

C) Glycolytic substrates are shuttled to the axon via MCT1 on the inner tongue of oligodendrocytes and subsequently taken up by the axon via MCT2 on the axonal surface, where it can be used in oxidative phosphorylation to generate ATP.

Image adapted from Phillips and Rothstein, (2017) *The Journal of Clinical Investigation*.

2.2 Oligodendrocyte development

Myelinated fibres were first identified by van Leeuwenhoek in 1717 but it wasn't until the 1920s and the work of Rio-Hortega and Penfield that oligodendrocytes were confirmed to be the myelinating cell of the CNS (Boullerne 2016). In contrast to the myelinating Schwann cells of the PNS, which form only one internode per cell, oligodendrocytes extend several processes to form as many as 50–60 internodes per cell (Figure 2.1). With internodal lengths varying between 20 and over 200 μm, and up to 100 myelin wraps per internode, oligodendrocytes generate an estimated 5-50,000μm^2 of membrane area per cell, which is significantly more than any other cell type (Mikael Simons 2016).

Oligodendrocytes first appear in the cervical spinal cord around mid-gestation in humans and just prior to birth in both mice and rats. They arise from the pMN domain of the ventral spinal cord, which is patterned into multiple domains in the ventral-dorsal axis by contrasting gradients of sonic hedgehog (SHH) and bone morphogenetic proteins (BMP) released by the floor plate and roof plate, respectively (Fu et al. 2002; Lai et al. 2016) (Figure 2.3). Whilst a second, minor wave of oligodendrogenesis occurs in the dorsal spinal cord and three separate waves of cortical oligodendrogenesis arise from the ganglionic eminences, this thesis relates only to the derivation of pMN-derived oligodendrocytes. The key stages of differentiation, however, are shared across all oligodendroglial cells.

In the developing neural tube, the positioning of neural progenitor cells along the ventral-dorsal axis determines their exposure to particular concentrations of SHH and BMP. This induces the expression of unique combinations of transcription factors and, in turn, define the cellular subtypes derived from each domain. Each population of progenitors first gives rise to neurons and then glial cells. The pMN domain is defined by the expression of OLIG2, which is critical for the transcription of genes related to both motor neuron and oligodendrocyte generation. Olig2-dependent expression of Ngn2 and Lhx3 trigger motor neuron generation and the ratio of Ngn2 relative to Olig2 in progenitor cells acts as a gate for timing the switch between neurogenesis and gliogenesis, and appropriate cell production (S.-K. Lee et al. 2005). However, the exact mechanisms by which pMN progenitors switch from neurogenesis to

gliogenesis is not precisely known. Live imaging of developing zebrafish revealed that in fact distinct progenitors drove the sequential generation of motor neurons (MNs) and oligodendrocyte progenitor cells (OPCs). Radial migration of MN progenitors away from the spinal cord lumen was followed by ventral migration of dorsally positioned progenitor cells, which initiate Olig2 expression in response to higher SHH, replenishing the pMN domain with progenitors destined to be OPCs (Andrew M Ravanelli 2015). Thus, spatial and temporal patterning mediated by SHH signalling drives diversification of neural cell types within the developing neural tube.

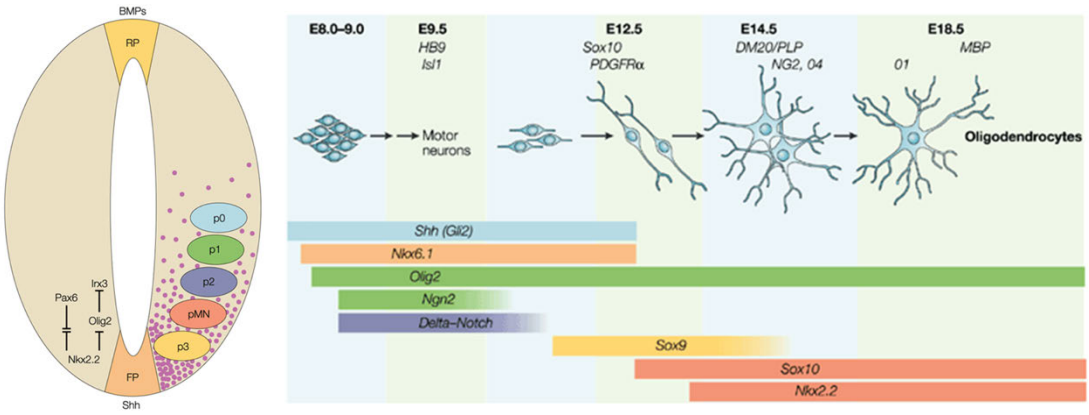

Figure 2.3 Oligodendrocyte development and differentiation

A gradient of Floor Plate derived Sonic Hedgehog establishes discrete domains along the dorsal-ventral axis of the developing spinal cord. Oligodendrocytes are generated from the pMN domain after the generation of motor neurons. Antagonistic actions of Olig2 and Ngn2 control the temporal switch to gliogenesis. PDGFRα^{+} OPCs differentiate into pre-myelinating oligodendrocytes expressing O4 and PLP. Maturation of differentiated oligodendrocytes is denoted by the expression of MBP. Image modified from Rowitch et al., (2004) *Nature Reviews Neuroscience*.

Whilst Olig2 expression is maintained throughout oligodendroglial production, differentiation and myelination, a number of stage-specific markers have been identified which enable the study of the temporal development of oligodendrocytes. OPCs are identified by their expression of NG2, platelet derived growth factor receptor (α subunit, PDGFRα) and Sox10, a key transcription factor that regulates the expression of myelin genes and is necessary for terminal oligodendrocyte differentiation. pMN domain derived OPCs are highly migratory and repulse one another to achieve unique territories throughout spinal cord grey and white matter (Hughes et al. 2013). Interestingly, not all OPCs go on to differentiate and represent approximately 5% of the total cells in the adult CNS. They comprise the majority of proliferative cells in the adult CNS, respond to injury and have been implicated in axo-glial communication by the discovery of bona fide synapses between OPCs and axons (Hughes et al. 2013; Bergles et al. 2000). It was recently shown that non-differentiating OPCs may arise from distinct progenitors through an expanded programme of progenitor recruitment outlined above. In zebrafish, sequential initiation of Olig2 expression in distinct spinal cord progenitors appeared to first gives rise to motor neurones, then rapidly myelinating oligodendrocytes followed by OPCs that persisted without differentiation (Ravanelli et al. 2018).

Terminal differentiation of OPCs into pre-myelinating oligodendrocytes is associated with translocation of the Olig1 transcription factor to the cytosol, an increase in morphological complexity, and induction of the transcription factor myelin gene regulatory factor (MRF) which has been shown to be critical for the expression of late myelin genes, including MOG (Ben Emery et al. 2009; Niu et al. 2012). Three highly conserved signalling pathways have been associated with oligodendrocyte differentiation including Wnt/β-catenin, PI3K/AKT/mTOR, and ERK/MAPK (Jenna M Gaesser 2016). Further detail regarding the transcription factors (Ben Emery 2015), epigenetic modifications (J. Liu et al. 2016), microRNAs (Dylan A Galloway 2016), and signalling pathways (Jenna M Gaesser 2016) involved in oligodendroglial lineage progression have been reviewed.

Surprisingly, oligodendrocytes are over-produced during development with the majority of newly differentiated oligodendrocytes undergoing programmed cell death (Barres et al. 1992; Hughes et al. 2018). Recently it was shown that this process is regulated, in part, by the expression of transcription factor EB (TFEB) in

premyelinating oligodendrocytes and that suppression of TFEB leads to ectopic myelination (Sun et al. 2018; Meireles et al. 2018). Whilst the factors that regulate TFEB expression are poorly understood, it is well established that axonal contact and axoglial communication promote oligodendrocyte survival and the regulation of myelin formation.

2.3 Myelin formation

Individual oligodendrocytes can myelinate multiple axons of varying diameters and demonstrate a range of myelin sheath lengths and thickness per cell. However, myelin sheath lengths are also precisely distributed along certain axons to fine-tune action potential conduction velocities, suggesting that the physical dimensions of individual myelin sheaths are locally regulated (Waxman & Sims 1984). Remarkably however, oligodendrocytes establish each of their internodes (up to ~60 in the mammalian cortex) across different axons in concert. This process is rapidly completed following the initiation of myelination (5 hours for zebrafish spinal cord oligodendrocytes (Czopka et al. 2013) and, in the intact CNS, fluctuations in sheath number or sheath length following this critical period are minimal.

Non-cell autonomous and cell-intrinsic regulation of myelination

Myelin formation follows in a stepwise manner of oligodendrocyte process extension, axoglial contact, membrane outgrowth and axonal wrapping, trafficking of membrane proteins, compaction, and node formation (Simons & Nave 2015). Several axonally-regulated signals have been identified to positively and negatively regulate these distinct processes. For example, oligodendrocyte processes are sensitive to axon calibre and a minimum threshold of ~1μm for PNS axons and ~0.2μm for CNS axons exists, below which it is thought myelin ensheathment is unlikely to confer significantly enhanced conduction velocity (Voyvodic 1989; Mayoral et al. 2018; Sherman & Brophy 2005). In the PNS, unmyelinated small diameter axons can be stimulated to grow in calibre, which leads to their myelination (Voyvodic 1989). This is thought to be signalled through increased expression of Neuregulin 1 (Nrg1) type III expression on the surface of axons. Larger calibre axons express more Nrg1 than smaller axons and overexpression of Nrg1 leads to increased myelin sheath thickness and induced myelination of typically non-myelinated peripheral axons (Taveggia et al. 2005; Michailov et al. 2004). In the CNS, Nrg1 has been shown to support the survival of newly differentiated oligodendrocytes but its role in myelination is largely dispensable (Fernandez et al. 2000; Brinkmann et al. 2008). Integrin signalling via Lamininα2 has been shown to be important in regulating oligodendrocyte number, enhancing myelin membrane formation *in vitro* and its absence leads to dysmyelination in both mice and

humans (Buttery & ffrench-Constant 1999; Colognato et al. 2002; Jones et al. 2001; Chun et al. 2003). Several inhibitory cues of oligodendrocyte differentiation and myelination have also been found. Lingo-1, a transmembrane protein expressed by neurons and oligodendrocytes inhibits oligodendrocyte differentiation with Lingo-1 knockout mice demonstrating increased numbers of mature oligodendrocytes and myelination (Mi et al. 2005). JAM2 is a somatodendritic protein that inhibits myelin wrapping and whose knockout leads to ectopic myelination of neuronal cell bodies (Redmond et al. 2016). Increasing evidence also demonstrates neuronal activity as an important regulator of oligodendrocyte differentiation and myelination, discussed further in 2.5. Finally, intrinsic properties of oligodendrocytes also regulate myelination as myelin sheath length around inert microfibres were found to differ between cortical and spinal cord-derived oligodendrocytes (Bechler et al. 2015).

Myelin wrapping

The mode of myelin wrapping has proven to be an elusive process to define with several hypotheses put forward over the years. With the advent of techniques such as live *in vivo* imaging and serial section electron microscopy analysis, a clearer picture has begun to form. Oligodendrocyte processes appear to first encircle axons before the bilateral growth of outer myelin layers (Snaidero et al. 2014). F-actin polymerisation at the leading edge of the oligodendrocyte process drives its continued wrapping of the underlying axon. F-actin disassembly and bilateral elongation of myelin membrane follows, resulting in a stepwise reduction in myelin thickness towards the distal end of elongating sheaths (Figure 2.4).

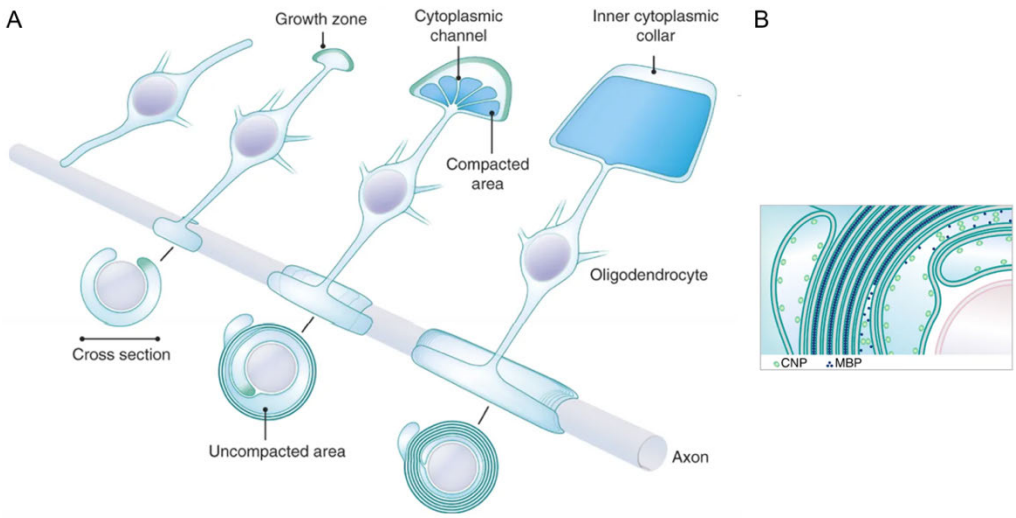

Figure 2.4 Myelin wrapping and compaction

A) Illustration of myelin wrapping. The active growth zone (green) proceeds to encircle the axon as sheath elongation occurs at the distal ends of nascent sheaths. B) Cross-sectional illustration of myelinated axon shows that MBP is pivotal to compaction of myelin lamellae, which is achieved by extruding CNP^+ cytoplasm. Images taken from Chang et al., (2017) *Nature Neuroscience*.

The myelin sheath is biochemically distinct to that of plasma membrane at the oligodendrocyte cell soma and is segmented into compact and non-compact domains (Krämer et al. 2001; Morell & Quarles 1999). The biochemical composition of myelin by dry weight consists of 70% lipid (predominantly galactoceramide and cerebroside) with most (80%) of the remaining mass accounted for by two proteins, myelin basic protein (MBP) and proteolipid protein (PLP/DM20) (Morell & Quarles 1999; Krämer et al. 2001). Precise localisation of these proteins to compact myelin and others, including 2'3'-cyclic nucleotide 3'-phosphodiesterase (CNP), myelin-associated glycoprotein (MAG) and myelin-oligodendrocyte glycoprotein (MOG) to uncompacted regions or the border between these two domains (e.g. CLAUDIN-11) requires organised synthesis, sorting and trafficking of myelin components. Several pathways have been implicated in myelin membrane trafficking including directed transport, transcytosis or 'bulk flow' of myelin membrane, exocytosis of vesicles that deliver new myelin to the inner tongue via the cytoplasmic channels of non-compacted myelin and the assembly of myelin rafts, which involves lipid-protein interactions and delivery via cytoplasmic adapter molecules (Snaidero et al. 2014; Krämer et al. 2001). The delivery of PLP appears largely dependent on myelin rafts (Simons et al. 2000). MBP, however, is locally translated at the cell periphery following the translocation of Mbp mRNA in microtubule-associated granules to sites of myelin growth. This suggests that sheath growth can be locally regulated. Indeed, nascent myelin sheaths engaged with electrically active axons *in vitro* demonstrate increased expression of newly synthesized MBP (Wake, Lee & Fields 2011a).

MBP is a small, positive protein that interacts with membranes by binding to negatively charged lipid head groups, which then leads to conformational changes and the formation of ordered α-helices and β-sheets (Aggarwal et al. 2011). During myelin compaction it is thought MBP neutralises the repulsive charges on opposing membranes to create a 'zipper' type effect that extrudes cytoplasmic proteins such as CNP (Snaidero & Simons 2017) (Figure 2.4B). This is exemplified in $CNP^{+/}$ and in $MBP^{+/}$ mice that show either advanced or delayed intracellular compaction, respectively (Snaidero et al. 2014).

Node formation

Myelinated axon function requires two specializations: the compaction of myelin lamellae around axons to reduce transverse capacitance and the organisation of nodal and paranodal proteins into discrete domains to enable saltatory conduction of action potentials.

Mature myelinated axons are morphologically divided into discrete domains that include the node of Ranvier (NoR), paranodal axoglial junctions (PNJ), juxtaparanodes (JXP) and internodes. The intricate formation of these domains is an extraordinary demonstration of reciprocal communication between axons and glia, involving extracellular matrix proteins, cell adhesion molecules and cytoskeletal scaffolds. Figure 2.5 is an illustrated representation of a myelinated axon cut along its sagittal axis, adapted from (Derfuss et al. 2010).

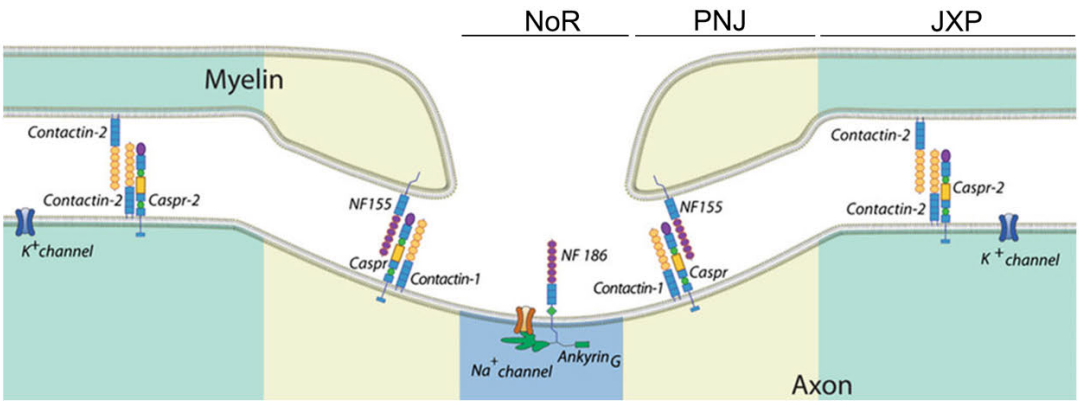

Figure 2.5 Organisation of myelinated axon sub-domains

Sagittal section of a myelinated axon depicting distinct domains. NoR: node of Ranvier; PNJ: paranodal junction; JXP: juxtaparanode. Adapted from Derfuss et al., (2010) *Journal of Molecular Medicine*.

The nodes of Ranvier are composed of a diverse arrangement of voltage-gated Na^+ channels, which mediate ion flow across the membrane and, together with K^+ channels, regulate action potential propagation. In addition, the NoR contains a number of scaffolding proteins essential to its assembly and maintenance. Flanking the nodes of Ranvier are PNJ, which tether the myelin sheath to the axolemma via specialised septate-like junctions. The PNJ serves as a major boundary that constrains electrical activity to the node of Ranvier and prevents lateral diffusion of axonal membrane proteins. The JXP domain highlights a dense cluster of Kv1 K^+ channels, which are thought to function as delayed rectifier K^+ channels that maintain internodal resting potential. Finally, the internode is where dense layers of compact myelin can be viewed in cross-section. Several cell adhesion or scaffolding proteins are involved in establishing myelinated axon domain organisation, which are useful markers used to determine the formation of these structures.

The PNJ is a specialised axoglial contact between the axolemma and the spiralling cytoplasmic loops of myelin lamellae located at the distal ends of myelin sheaths. The septate-like junctions formed at this site constitute the largest known intercellular junctions in vertebrates (Rasband & Peles 2015). The PNJ is composed of the cell adhesion molecules CASPR and CONTACTIN, expressed on the surface of axons, which form a complex that binds with the 155-kDa isoform of Neurofascin, Nfasc155, expressed on the surface of oligodendrocytes. The heterotrimeric complex formed bridges the two cell-types together.

Neurofascins are a family of proteins, encoded by alternative transcripts of the NFASC gene, involved in the assembly of the axon initial segment (AIS) and NoR in myelinated axons. The two major isoforms, Nfasc155 and Nfasc186 (named corresponding to their molecular weight in kDA) are differentially expressed by myelinating glia and axons, respectively. Nfasc186 is central to and initiates NoR assembly by recruiting Ankyrin-G, a large cytoskeletal protein that acts as a multivalent organiser in the assembly and maintenance of both the AIS and NoR (Dzhashiashvili et al. 2007; Gasser et al. 2012).

Myelin wrapping is also demonstrated by CLAUDIN-11, otherwise known as oligodendrocyte-specific protein (OSP). CLAUDIN-11 forms tight-junctions between the cytoplasmic loops of myelin lamellae, which is distinct from, but structurally

overlaps with, the PNJ. CLAUDIN-11 also demarcates Schmidt-Lantermann incisures of the CNS, which are cytoplasmic channels that spiral through compact CNS myelin, permitting the trafficking of products to the inner myelin tongue (Gow et al. 1999; Blakemore 1969; Pérez-Cerdá et al. 2015) (Figure 2.6).

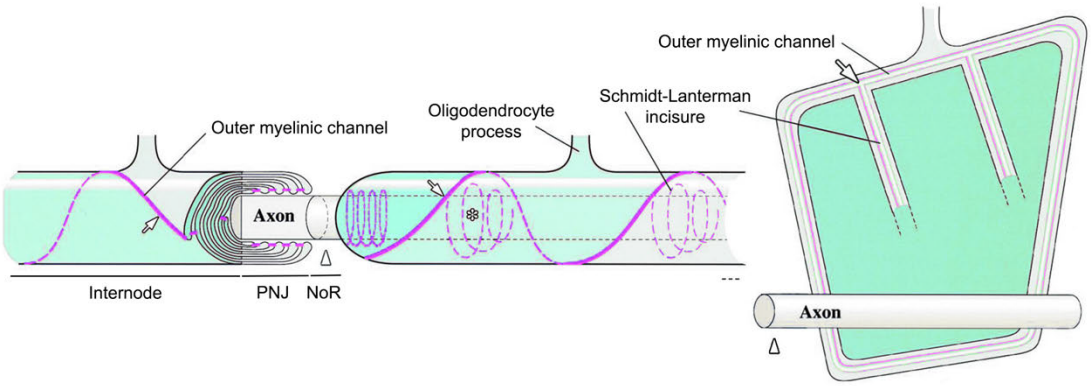

Figure 2.6 The myelinic channel
Claudin-11 labels tight junctions between terminal myelin lamellae at the PNJ as well as the outer myelinic channel and Schmidt-Lanterman incisure (uncompacted structures beneath the outer myelin loop that spirals through compact myelin towards the axon at regular intervals). Adapted from Gow et al., (1999) *Cell.*

2.4 Disorders of myelin

The evidence provided above supports the notion that oligodendrocytes are not simply passive members of the CNS whose sole purpose is to insulate axons but are instead dynamic modulators of neural circuits and axon function. This is best exemplified by inherited and acquired disorders of myelin such as the leukodystrophies and multiple sclerosis, demonstration that cell-autonomous defects profoundly affect the integrity and function of the CNS as a whole.

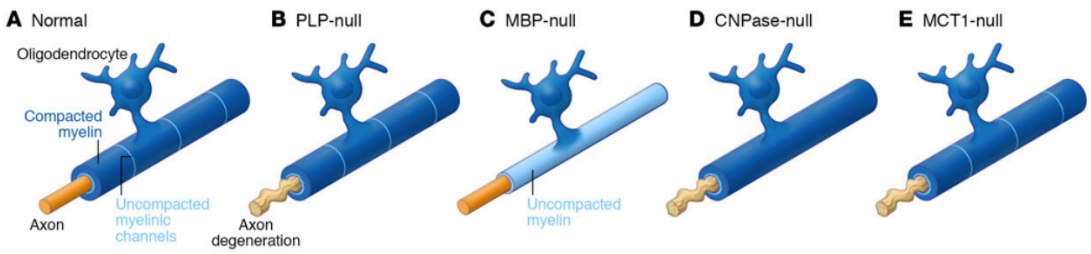

Figure 2.7 Oligodendrocyte mutations impact on axonal health

Mutations in oligodendrocyte-specific genes have differing effects on myelinated axon health. MBP-null mutations lead to uncompacted myelin without affecting axonal health. PLP-, CNPase- and MCT1-null mutations lead to neurodegeneration. Image adapted from Phillips and Rothstein, (2017) *The Journal of Clinical Investigation*.

Mouse models

Mice that lack the myelin proteins proteolipid protein (PLP), myelin associated glycoprotein (MAG) or 2'3'-cyclic nucleotide 3'-phosphodiesterase (CNP) generate compact myelin sheaths but exhibit widespread axonal swellings and degeneration (Griffiths et al. 1998; Lappe-Siefke et al. 2003; Pan et al. 2005). Shiverer mice, discussed below, lack the structural protein myelin basic protein (MBP) and so fail to generate compact myelin, leading to tremors, convulsions and early death (Chernoff 1981). Knockout mutations in the genes encoding oligodendrocyte-specific gap junction proteins Cx32 and Cx47 exhibit extensive myelin pathology and loss of axons (Menichella et al. 2003). Mice lacking expression of the myelin tight junction protein Claudin-11 show neurotransmitter imbalances in the absence of neurodegeneration, which lead to perturbed auditory processing and neuropsychiatric disease-associated phenotypes (Maheras et al. 2018). These data underlie the importance of myelin in global CNS health and point towards additional functions of oligodendrocytes besides accelerating signal conduction (Figure 2.7).

Inherited and acquired disorders of myelin

The leukodystrophies are a group of heritable metabolic disorders that result from defective myelination of the CNS (Schiffmann & van der Knaap 2009; Powers 2004). Several types of leukodystrophies exist and have been classified accordingly: hypomyelinative disorders are those in which the CNS myelin is not properly formed. They arise from mutations in myelin related genes and include Pelizaeus Merzbacher disease (PMD), which arises from mutations in the gene for PLP (Gow et al. 1998). Metabolic demyelinating diseases such as Krabbe disease arise from enzymatic deficiency and lipid misaccumulation (Svennerholm et al. 1980) and leukoencephalopathy disorders such as vanishing white matter disease display gross tissue loss (Leegwater et al. 2001). Myelin abnormalities are also found in several disorders of perinatal injury, including cerebral palsy, where hypoxia-ischaemia events lead to oligodendrocyte injury (Haynes et al. 2003).

Multiple sclerosis

The most common acquired disorder of myelin is multiple sclerosis (MS), a chronic autoimmune inflammatory disease of the CNS that leads to myelin destruction and progressive neurodegeneration. Approximately 85% of MS patients present with a relapse-remitting form of the disorder in which exacerbations of clinical symptoms are followed by periods of remission, which are thought to reflect resolution of inflammation and/or remyelination (Goldenberg 2012). However, the majority of patients after c.10 years will move into the progressive phase of disease characterised by accumulating and irreversible disability due to underlying neurodegeneration. In addition, 10–15% of patients have a purely progressive form of the disease from the outset. MS is thus the most common form of neurodegeneration in younger adults (majority of patients present with the relapse-remitting form between 20 and 40 years of age) with a prevalence of 100–200 per 100,000 in the UK. A complex disease, that affects woman c.2.5 x more than men, both genetic and environmental factors have been identified to play a part (Noseworthy et al. 2000; Visser et al. 2012; Patrikios et al. 2006). Inflammatory-mediated demyelination detrimentally impacts conduction speed. Interestingly however, remyelination of denuded axons by newly differentiated oligodendrocytes restores conduction speeds and is associated with functional recovery of the affected circuits, albeit remyelinated sheaths appear thinner and shorter in length (Blakemore 1974; Smith et al. 1979; Franklin & ffrench-Constant 2008). In contrast to the development of many effective disease modifying treatments for the inflammatory dominant relapse – remitting phase of disease there are no effective treatments for the progressive phase of disease. There is therefore an unmet need for neuroprotective therapies (discussed further in Chapter 7).

Neuropsychiatric disorders

Considerable interest has also been placed on white matter pathology in several neuropsychiatric disorders including autism, schizophrenia, bipolar disorder and major mental illness where changes in white matter integrity have been observed (Haroutunian et al. 2014; Roussos & Haroutunian 2014; Fields 2008; Nave & Ehrenreich 2014; J. Liu et al. 2012; Sehmbi et al. 2019). Genome-wide association

studies of neuropsychiatric conditions regularly highlight dysregulated expression of myelin-related genes (Hakak et al. 2001; Witt et al. 2017) and, in some cases, white matter alterations precede the onset of psychosis (Carletti et al. 2012).

Neuropsychiatric conditions such as schizophrenia typically present during adolescence between the second and third decade of life, a period of time that overlaps with the development of inhibitory pathways and myelination of the pre-frontal cortex (Insel 2010). This has led many to suggest that disrupted connectivity and aberrant modulation of synaptic efficacy underlies the pathogenesis of this disorders (Friston et al. 2016). Indeed others have speculated on the convergence of interneuron and white matter abnormalities in schizophrenia (Stedehouder & Kushner 2016). Further work is needed to determine cell-intrinsic deficits and dysfunctional interactions between different neural cells in schizophrenia. Several studies have already highlighted the utility of iPSCs to probe oligodendrocyte dysfunction in schizophrenia (Vasistha et al. 2019; de Vrij et al. 2019).

Amyotrophic laterals sclerosis

Oligodendrocyte dysfunction is also prevalent in amyotrophic lateral sclerosis (ALS), a rapidly progressing neurodegenerative disease characterised by the selective death of motor neurons. Though the majority (90%) of ALS cases are sporadic, several mutations have been identified to cause ALS, including in the gene for TDP-43 (*TARDBP)* (Kabashi et al. 2008; Sreedharan et al. 2008; Lagier-Tourenne et al. 2010). TDP-43 is a DNA/RNA binding protein that plays critical roles in RNA splicing, translation and transport (Ratti & Buratti 2016) and also represents a defining pathological hallmark for the majority of ALS cases by the accumulation of large TDP-43^{+} cytoplasmic aggregates in both neurons and glial cells (Neumann et al. 2006; Arai et al. 2006; Mackenzie et al. 2010). TDP-43 mislocalization and aggregation is present in oligodendrocytes in spinal cord grey matter of human ALS (Rohan et al. 2014; Philips et al. 2013) and demyelination in both the spinal cord and grey matter regions of the motor cortex has been observed (S. H. Kang et al. 2013). The SOD1^{G93A} mouse model of ALS is a well characterised model in which expression of mutant human Cu, Zn superoxide dismutase (SOD1; which accounts for ~2% of familial ALS) leads to

MN degeneration (Gurney et al. 1994). Here, enhanced proliferation of $NG2^{+}$ oligodendrocyte progenitor cells and degeneration of new-born oligodendrocytes was observed (S. H. Kang et al. 2013). In addition, selective depletion of mutant SOD1 from oligodendrocytes delayed disease onset in $SOD1^{G93A}$ mice, suggesting a deleterious non-cell autonomous effect on motor neuron survival (S. H. Kang et al. 2013).

A possible mechanism by which oligodendrocyte integrity might negatively impact neuronal survival is via MCT1 and the shuttling of glycolytic substrates from the myelin sheath to the underlying axon to be used in oxidative phosphorylation (Fünfschilling, Supplie, Mahad, Boretius, Saab, Edgar, Brinkmann, Kassmann, Tzvetanova, Möbius, Diaz, Meijer, Suter, Hamprecht, Sereda, Moraes, Frahm, Goebbels & Nave 2012a; Y. Lee, Morrison, Y. Li, Lengacher, Farah, Hoffman, Y. Liu, Tsingalia, Jin, Zhang, Pellerin, Magistretti & Rothstein 2012b; Saab et al. 2013) (Figure 2.2). Spinal cord MNs depend on MCT1 for survival and MCT1 was shown to be downregulated in the motor cortex of ALS patients (Fünfschilling, Supplie, Mahad, Boretius, Saab, Edgar, Brinkmann, Kassmann, Tzvetanova, Möbius, Diaz, Meijer, Suter, Hamprecht, Sereda, Moraes, Frahm, Goebbels & Nave 2012b; Y. Lee, Morrison, Y. Li, Lengacher, Farah, Hoffman, Y. Liu, Tsingalia, Jin, Zhang, Pellerin, Magistretti & Rothstein 2012b).

The exact mechanism by which oligodendrocyte dysfunction and disease exacerbation occurs is unclear. One suggestion centres around dysfunctional RNA metabolism. Myelin proteins, including MBP, are locally translated in the cell periphery (Campagnoni et al. 1980; Colman et al. 1982) and can be bound and sequestered by TDP-43 (Jia Wang et al. 2018). Additionally, translocation of myelin mRNAs is regulated by the activity of a number of trans-acting factor heterogeneous nuclear ribonucleoprotein (hnRNP) RNA binding proteins (Barton et al. 2019; White et al. 2008), which in turn are regulated by TDP-43 (Deshaies et al. 2018; Highley et al. 2014). Finally, it was recently shown that increasing concentrations of TDP-43 in the cytoplasm leads to formation of long-lived liquid droplets of cytosolic TDP-43 that accumulate a number of nucleocytoplasmic transport proteins as well as hnRNPA1, thereby disrupting normal RNA trafficking (Gasset-Rosa et al. 2019). A possible framework therefore is established whereby stress-related imbalances in posttranscriptional regulation of oligodendroglial mRNAs may lead to reduced

oligodendrocyte integrity, dysfunction, demyelination and neurodegeneration (Hoch-Kraft et al. 2019).

Whilst the exact role of TDP-43 in oligodendrocytes remains unclear, it was recently shown that selective depletion of TDP-43 from mature oligodendrocytes (Cnp^{+}) resulted in a shortened lifespan, progressive motor deficits, progressive myelin disruption, degeneration of mature oligodendrocytes and enhanced oligodendrogenesis, though no loss of spinal cord MNs or muscle denervation observed (Jia Wang et al. 2018). Further studies investigating endogenous expression of mutant TDP-43 are needed to unpick oligodendrocyte pathophysiology in this disease.

Finally, the importance of axon-oligodendrocyte coupling has resulted in a shift in how we perceive axonal physiology and raises the possibility that oligodendrocytes are important contributors to the pathogenesis of other neurodegenerative disorders that display white matter and oligodendrocyte pathology including Alzheimer's disease, multiple system atrophy and Huntington's disease (Alexandra I et al. 2018; J. Zhang et al. 2018; B. Huang et al. 2015; Nasrabady et al. 2018).

2.5 Activity regulated myelination

White matter volume steadily increases until the fifth decade of life (Westlye et al. 2010), is positively correlated with intelligence (Grydeland et al. 2013) and can be potentiated by learning novel motor tasks including juggling (Scholz et al. 2009), piano playing and following musical training (Bengtsson et al. 2005), riding a unicycle (Weber et al. 2019) and also by bilingualism (Schlegel et al. 2012; Anderson et al. 2018). It has also been shown that social isolation or enrichment likewise modulates the extent of cortical myelination (J. Liu et al. 2012; Hughes et al. 2018; Makinodan et al. 2012). Experience-dependent structural changes in both grey and white matter relative to task performance is an indication of the plasticity of the CNS and one which highlights physical activity as a potential intervention for modulating cognitive and brain functions (Weber et al. 2019; Erickson et al. 2011; Colcombe et al. 2006). However, the cellular mechanisms underlying these changes are not completely understood (Zatorre et al. 2012).

Magnetic resonance imaging (MRI) can be used to investigate both the structural and functional integrity of white matter *in vivo.* The latter makes use of the constrained diffusion of water molecules along similarly oriented fibres, creating a directional 'anisotropy' of water diffusion that reveals microstructural properties of the brain (Alexander et al. 2007). It was estimated that a single white matter 100 x 100 x 100 μm voxel contains between 1,000 and 13,000 axons and is occupied by approximately 48% myelin volume and 48% astrocyte membrane volume. Oligodendrocytes outnumber astrocytes 4:1 and the number of microglia and OPCs were less and in equal proportions (Walhovd et al. 2014). Changes in fractional anisotropy (FA) or mean diffusivity may reflect modifications to each or several of these compartments (Cassandra Sampaio-Baptista 2017). However, histological examination of myelin has been shown to correlate with *in vivo* measurements, supporting the use of *in vivo* imaging to reflect myelin-specific changes (Blumenfeld-Katzir et al. 2011; Sampaio-Baptista et al. 2013).

Understanding how neuronal activity modulates myelin development has interested researchers for decades: since the identification that dark reared mice demonstrate reduced myelination of optic nerve tracts (Gyllensten & Malmfors 1963). The role of

axons in regulating oligodendrocyte development was eluded to following the observation that neonatal optic nerve transection reduces the number of proliferating OPCs (Barres & Raff 1993). Furthermore, pharmacological suppression of neuronal activity within the optic nerve—via tetrodotoxin (TTX)-mediated blockade of voltage gated Na^+ channels—reduced OPC proliferation and the number of myelinating oligodendrocytes (Barres & Raff 1993; Demerens et al. 1996). TTX was also found to reduce the number of myelinated fibres in optic nerve cultures. In contrast, potentiation of neuronal activity via α-scorpion-toxin (Na^+ channel activator) had an opposite effect by greatly increasing the number myelinated fibres (Demerens et al. 1996).

In vivo, electrical stimulation of the dorsal corticospinal tract in adult mice selectively promoted the proliferation and differentiation of oligodendrocyte progenitor cells (Q. Li et al. 2010). However, white matter changes are also associated with pathological perturbations of electrical activity, including accelerated myelin development following epileptic seizures (Goldsberry et al. 2011) and oligodendrocyte injury due to glutamate receptor-mediated excitotoxicity in hypoxia-ischemia (Follett et al. 2000).

More recently, sophisticated genetically encoded modulators of neuronal activity have been used to address this question. Using transgenic mice expressing channelrhodopsin 2 under the control of the Thy 1 promoter, optogenetic-mediated enhancement of neuronal activity in the mouse premotor cortex increased OPC proliferation, differentiation and myelination with functional behavioural changes in normal gait (Gibson et al. 2014). In another study, optogenetic activation of toxin-induced demyelinated lesions increased OPC numbers, enhanced oligodendrocyte differentiation, promoted remyelination and aided functional recovery (Ortiz et al. 2019). Using Designer Receptors Exclusively Activated by Designer Drugs (DREADD)-based modulation of neuronal activity, stimulation of the somatosensory cortex led to increased OPC proliferation and differentiation in the underlying white matter, a myelination bias for activated axons and thicker myelin sheaths on activated axons (Mitew et al. 2018). DREADD-activated $parvalbumin^+$ interneurons in the medial prefrontal cortex also led to selectively increased myelination mediated by enhanced axonal arborisation and the number of internodes (Stedehouder et al. 2018). These data highlight the potential of neuronal activity to regulate OPC proliferation, differentiation and/or myelination during development, learning and

disease. Interestingly, blocking the formation of new oligodendrocytes impaired the learning of complex running tasks (Xiao et al. 2016), further supporting the role of oligodendrocytes in regulating CNS plasticity and learning.

The mechanisms underlying activity regulated myelination are not completely understood. However, a number of key observations have been made that have begun to explain this phenomenon. A landmark paper discovered that OPCs form bona fide synapses with axons of hippocampal pyramidal neurons with AMPA receptor-mediated calcium responses produced by local release of glutamate-filled synaptic vesicles (Bergles et al. 2000). Indeed, many of the canonical postsynaptic constituents have been shown to be express by OPCs, including PSD-95 (Almeida & Lyons 2014). Vesicular release of glutamate also occurs along unmyelinated callosal axons during action potential propagation, which activates Ca^{2+}-permeable AMPA receptors at OPC-axon synapses within the corpus callosum, as identified by VGLUT1^{+} puncta at axon-NG2^{+} cell junctions (Ziskin et al. 2007; Kukley et al. 2007). ATP is also released by electrically active DRG axons and activity-induced differentiation of OPCs and myelination in co-culture was shown to be mediated by adenosine (Stevens et al. 2002). These studies have led to a leading hypothesis that OPC-axon synapses represent a mechanism for activity-dependent signalling that modulates OPC behaviour to promote myelination of electrically active axons, thereby modulating the speed and efficiency of signal propagation.

Evidence that nonsynaptic release of neurotransmitter is mediated via exocytosis of vesicles—rather than membrane channels (Fields 2011)—was demonstrated by Wake et al. who showed botulinum neurotoxin (BoNT/A)-mediated blockade of vesicular release significantly reduced Ca^{2+} responses in OPCs when co-cultured with DRGs (Wake, Lee & Fields 2011a). The authors also identify a reduction in the number of myelin segments per cell in BoNT/A-treated cultures, preferential myelin targeting to a subset of neurons that had not been pre-treated with BoNT/A, and preferential translation of MBP on OPC processes in contact with electrically active axons (Wake et al. 2015; Wake, Lee & Fields 2011b).

Further evidence for the role of vesicle exocytosis in mediating myelin development *in vivo* came from live imaging of transgenic zebrafish reporter lines expressing the tetanus toxin (TeNT) light chain. TeNT is another clostridial neurotoxin that blocks

synaptic transmission via proteolytic cleavage and inactivation of Synaptobrevin 1/2 (VAMP2), one of three neuronal SNARE (soluble N-ethylmaleimide-sensitive factor attachment protein receptor) proteins that mediate rapid exocytosis of neurotransmitter containing synaptic vesicles at the pre-synaptic terminal, in all known synapses (Söllner et al. 1993). Clostridial neurotoxin exposure blocks both spontaneous and action-potential-evoked synaptic vesicle release (Y. I. Kim et al. 1984). TeNT-expressing zebrafish showed a 40% reduction in the number of myelinated axons, which was accounted for by individual oligodendrocytes myelinating fewer (30% reduction) axons per cell (Mensch et al. 2015). In a parallel study, (Hines et al. 2015) identified under normal conditions, the motility of synaptic vesicles was reduced at points of myelin ensheathment. Additionally, selective TeNT expression in Phox2b^{+} neurons reduced the stabilisation of nascent sheaths and total myelin along these neurons. Importantly, it was recently shown that social isolation reduces the number of myelin sheaths per cell, providing evidence that experience dependent changes can also negatively modulate oligodendrocyte morphology *in vivo* (Swire et al. 2019; Mensch et al. 2015).

Finally, neuronal activity has also been shown to be important in driving myelin repair. Using organotypic brain slices from a rat model of toxin-induced demyelination, recruited OPCs were found to form *de novo* synapses with demyelinated axons in the corpus callosum (Gautier et al. 2015). Furthermore, activity-dependent myelination (mediated by newly born oligodendrocytes) also occurs in the adult mammalian CNS (Gibson et al. 2014; Mitew et al. 2018). As such, experience-dependent plasticity has been suggested as a tractable method for the management of multiple sclerosis (Jensen & Yong 2016). It is inconclusive however, whether established oligodendrocytes and their myelin sheaths are capable of activity regulated adaptation. Myelin remodelling by established oligodendrocytes was recently demonstrated in zebrafish following selective ablation of oligodendrocytes. The sparse loss of internodes along myelinated axons led to radial growth of neighbouring myelin sheaths to cover the portion of denuded axon (Auer et al. 2018). Whether or not this process may be modulated by neuronal activity remains to be seen. It is more likely that adaptation by established oligodendrocytes will involve changes in myelin thickness. However, this remains to be determined.

2.6 The argument for complementary human models

The understanding of human development and disease would ultimately be best served by the study of living human models that are experimentally tractable. Animal models provide accessible and genetically amenable tools with which to investigate cellular mechanisms and disease-associated pathogenesis. Moreover, their use in preclinical studies of therapeutic interventions and drug safety is integral to the drug discovery process. However, the underlying pathology for many neurological disorders are still not fully understood and there is high attrition in the development of new therapies, particularly for neurological disorders (Garner 2014; McGraw et al. 2017). Both disease- and species-specific differences have been suggested to contribute to the attrition of drug development and suggests that human models of development and disease may complement existing capacities for both mechanistic and drug discovery/validation purposes. This is also true for myelin development and disease. Here, I will summarise the differences in neuroanatomy as well as in the temporal development, signalling pathways and transcriptional profile of oligodendroglial cells and emphasise the potential of human stem cell-derived cultures to study the biology and pathology of myelin development.

Evolutionary divergences in the density of glial cells are surprisingly minimal across clades with absolute numbers of nonneuronal cells best explained by the average mass of glial cells and the relative neuronal mass (Mota & Herculano-Houzel 2014). However, the relative proportion of white matter within the cerebral cortical volume differs significantly between species as it increases relative to brain size and is linked to the degree of cortical folding in mammals (Hofman 1985; Schoenemann et al. 2005; Smaers et al. 2010; Mota et al. 2019). As I will describe below, however, species-specific differences are primarily attributed to functional differences, rather than in the distribution and types of cells.

Human myelin development is a particularly protracted process, even amongst primates (Miller et al. 2012; Bakken et al. 2016). The phylogenetically close chimpanzee, for example, demonstrates a more rapid acquisition of neocortical myelin relative to developmental stage (Miller et al. 2012). Additionally, whilst myelination peaks in the chimpanzee around the time of sexual maturity, human

myelin development extends past adolescence into adulthood and steadily increases until the fourth or fifth decade of life (Miller et al. 2012; Westlye et al. 2010; Yeung et al. 2014). This distinction has important implications for the development of neuropsychiatric conditions in humans, which appear during an intense period of neocortical myelination. Indeed, perturbed myelin development is a leading hypothesis for the development of disorders including autism, schizophrenia, and bipolar disorder (Haroutunian et al. 2014; Roussos & Haroutunian 2014; Fields 2008; Nave & Ehrenreich 2014; J. Liu et al. 2012).

Currently, there is some contradictory evidence over the turnover rate of oligodendrocytes in the adult CNS, whether mature oligodendrocytes can contribute to remyelination and whether species-specific differences may exist.

Retrospective ^{14}C birth-dating takes advantage of the enormously elevated ^{14}C content in all biological material synthesized during the atomic bomb testing of the early 1960s and the fallout thereafter to identify the respective age of cellular material (Spalding et al. 2005). Using this technique on autopsied human brains, the majority of oligodendrocytes of the human corpus callosum were found to be nearly as old as the individual, supporting very long survival of integrated oligodendrocytes, similar to what was recently indicated in mice (Yeung et al. 2014; Hughes et al. 2018). However, fractionally isolated myelin of the same region appears to be relatively contemporary, indicating myelin turnover occurs in long-lived oligodendrocytes (Yeung et al. 2014). Additionally, the authors identify an annual 'turnover rate' (which may also reflect new additional oligodendrocytes) of 0.3% for WM oligodendrocytes after the age of 5, which is at least 100-fold lower than mice at comparable ages. Indeed, while over 98% of human callosal oligodendrocytes were established by 9 years of age, as many as 20% of callosal oligodendrocytes in the mouse are born during adulthood (Rivers et al. 2008). Given the recently established paradigm of activity regulated myelination—whereby experience dependent elevations in myelination are dependent on the integration of newly differentiated oligodendrocytes (McKenzie et al. 2014; Hughes et al. 2018)—the authors suggest that the rate of oligodendrogenesis in human white matter could not account for the increase in myelin content observed during learning (determined by proxy using FA) and that mature oligodendrocytes might instead contribute to myelin plasticity in the human

adult CNS (Yeung et al. 2014). However, the changes observed by FA in humans have not yet been corroborated at the level of oligodendrocyte/myelin ultrastructure.

The apparent plasticity of human myelinating oligodendrocytes was further developed in the context of remyelination in MS. Yeung et al. once again employed ^{14}C dating to show that a greater proportion of recently generated OPCs and oligodendrocytes exist in normal appearing white matter (NAWM) of a subset of MS patients with a severe course of disease, compared to unaffected individuals. Significantly, oligodendrocytes residing in shadow plaques (believed to be indicative of lesions undergoing remyelination), were found to be old in 'age' and could not have been generated from neighbouring progenitor cells (Yeung et al. 2019). This suggests that oligodendrocytes that survive demyelination may contribute to remyelination in humans. Support for this notion recently came from large animal models of remyelination, where mature oligodendrocytes were found associated with both thick and thin myelin sheaths (indicative of remyelination) in the cat spinal cord following irradiated food induced demyelination; and also from a model of vitamin B12 deficiency in the rhesus monkey which resulted in demyelination, survival of oligodendrocytes, and association with thin myelin sheaths (Duncan et al. 2018). This is in contrast to the rodent, where pre-existing mature oligodendrocytes were shown not to contribute to remyelination (Crawford et al. 2016). Whilst not generalizable across models of demyelination, these results indicate species-specific differences in myelin repair and, at the very least, highlight an important consideration for the development of future therapies that aim to promote remyelination.

Further insight into species-specific differences has come from transcriptomic analysis of mouse and human cells. A study by the Allen Institute for Brain Science used single-nuclear RNA sequencing of mouse cerebral cortex and the middle temporal gyrus (MTG) of autopsied human tissue to show that, despite a 65 million year old common ancestor, many cell-types matched up 1:1 with no major class of cell missing a homolog (Hodge et al. 2019). However, divergent gene-expression was identified between mouse and human and—most notably—in nonneuronal cells and in genes associated with connectivity and signalling, indicating that evolutionary adaptations in humans have focussed on cell-cell interactions within a relatively comparable cellular architecture. A similar conclusion was drawn from another single nuclear RNA sequencing study comparing mouse, rat, and human cerebellar

transcriptomes (Xu et al. 2018). They conclude that, whilst cell-type specific genes are highly conserved across species, a significant number of genes demonstrate divergent expression profiles not defined by any particular gene ontology pathway, including in OPCs and oligodendrocytes. Promoter chromatin accessibility was identified as a potential driver of evolutionary differences and changes in the expression of cell-type specific transcription factors was suggested to underlie the common failure of mouse models to recapitulate features of human disease (Xu et al. 2018). In addition, divergent DNA sequences was found to underlie the difference in activity-dependent gene-responsiveness of mouse and human ESC-derived cortical neurons (Qiu et al. 2016).

Substantial evidence indicates that human astrocytes are functionally and morphologically specialised compared with rodent, demonstrating different laminar distributions, up to tenfold difference in size, different gene expression profiles and altered cytokine responses (Y. Zhang et al. 2016; Oberheim et al. 2009; Hodge et al. 2019; Du et al. 2017). Their role in regulating aspects of myelination and remyelination are beginning to be uncovered (Molina-Gonzalez & Miron 2019). However, species-specific differences have also been identified in oligodendroglial cells. The study by Hodge et al. identified 14% of genes expressed by OPCs to be highly divergent between mouse and human (Hodge et al. 2019). Additionally, comparisons between mouse and human fetal A2b5^{+} cells, isolated by magnetic sorting, showed significant differences in their gene expression profiles (Sim et al. 2009). After filtering out astrocyte-related genes, an OPC-enriched dataset identified 92 differentially expressed genes between mouse and human and over 200 genes not identified in mouse. Furthermore, proteomic analysis of mouse and human myelin identified shared and differentially expressed proteins (308 proteins shared, 167 mouse-specific, and 370 human-specific). However, the authors conclude these differences may be overestimated by the technical limitations of their study (Ishii et al. 2009).

More in-depth investigation by single cell RNA sequencing of isolated oligodendroglial cells revealed surprising heterogeneity within oligodendrocytes. Based on their gene expression profiles, Marques et al., identified 13 subpopulations of cells across the juvenile and adult mouse CNS that included 6 distinct populations of mature oligodendrocytes (Marques et al. 2016). Jäkel et al. showed that a similar scenario exists in the human brain, where 7 subpopulations of oligodendrocytes were

identified. Whilst a comparison of oligodendrocyte heterogeneity between healthy mice and humans is currently lacking, the authors demonstrated altered heterogeneity between control human and MS brains. Additionally, comparison between MS brains and cells isolated from the EAE mouse model of the disease showed only partly overlapping populations (Jäkel et al. 2019). This research supports the need for human models of myelin development, especially in the context of disease. An interesting consequence of this work will be to determine whether different subtypes of mature oligodendrocytes identified by RNA sequencing show differential responses to physiological cues and whether comparable oligodendrocyte subtypes behave equally across species. This is yet to be investigated.

Finally, species-specific differences have also been identified regarding the behaviour and function of oligodendroglial cells. For example, fibroblast growth factor 2 (FGF2) is a trophic factor that promotes mouse—but not human—OPC specification and proliferation (Chandran et al. 2004) and the transcription factor ASCL1 regulates the induction of mouse—but not human—OPC genes (Jing Wang et al. 2014). Additionally, the expression pattern of muscarinic receptor (MR) subtypes is different between mouse and human OPCs, which has implications for the development of pro-myelinating therapeutics as MR antagonism is frequently identified from rodent-based drug screens of oligodendrocyte differentiation (Welliver et al. 2018).

Intrinsic differences have also been identified in the proliferation, colonisation and myelination of the demyelinated mouse CNS by either transplanted human fetal or mouse glial progenitor cells (Sim et al. 2009; Windrem et al. 2008; Windrem et al. 2014; Mozafari et al. 2015; Buchet et al. 2011; Chanoumidou et al. 2019) with human cells showing increased proliferation for a prolonged period of time before differentiation and myelination begins. Given that human oligodendrocyte differentiation occurs comparatively quicker *in vitro,* this suggests that human and mouse OPCs differentially respond to the same niche-derived signals and that rodent models of remyelination therefore may not accurately reflect the dynamics of human OPC-mediated repair (Dietz et al. 2016).

Altogether, these findings demonstrate significant differences in the dynamics and degree of human myelination, the transcriptomic signature of oligodendroglial cells and that novel disease-associated states of oligodendroglia are not recapitulated by

mouse models. In light of this, the development of a humanised model of myelination is warranted, as it would support our understanding of normal and pathogenic myelin formation whilst maintaining appropriate interactions with neurons and astrocytes (whose species-specific differences are well documented) and provide confidence that any potential disease-modifying treatments have a desired effect in human cells.

2.7 Modelling myelin development

The use of tissue culture as a tool to study developmental and pathological processes has become an integral component of biomedical research. Since the demonstration that tissue explants derived from embryonic sources could be cultivated and propagated *ex vivo* in the earliest twentieth century, tissue culture techniques have been used to study developmental events in detail (Harrison et al. 1907; Carrel 1912; Ambrose 2017). Furthermore, access to the cellular environment permits pharmacological manipulation and physiological evaluation of cellular processes.

Two dimensional cultures: primary oligodendrocytes and co-cultures

Oligodendrocyte progenitor cells may be specifically isolated from the rat or mouse cerebral cortex and have been instrumental in understanding the behaviour and function of these cells (McCarthy & de Vellis 1980). Interestingly, in the absence of neurons, oligodendrocyte differentiation is not impeded. However, without a substrate to myelinate, large, flat, leaf-shaped sheets of myelin membrane are generated (Szuchet et al. 1987). Surprisingly, it was found that oligodendrocytes could myelinate both inert microfibres that mimic the physical dimensions of myelinated axons *in vivo* and fixed axons, demonstrating that myelin formation is not dependent on neuron-derived signals (Althaus et al. 1984; Rosenberg et al. 2008; Bechler et al. 2015). However, the extent of wrapping is much greater in the presence of live axons and the factors that regulate non-cell autonomous induction of myelination in neuron co-cultures has been of considerable interest (Allamargot et al. 2001; Brinkmann et al. 2008; Câmara et al. 2009; Ishibashi et al. 2006; Demerens et al. 1996; Wake et al. 2015). Indeed, two-dimensional co-cultures derived from dissociated CNS explants were highly informative and used to conclude that myelin is only targeted to axons, that the number of processes per cell was equivalent to that *in vivo,* that individual oligodendrocytes myelinate multiple axons in concert, and that myelination typically occurred in areas of high axonal density (S. U. Kim 1972; Lubetzki et al. 1993).

Another well-established method of studying myelin formation *in vitro* is through co-culture with dorsal root ganglion (DRG) neurons. DRG neurons are pseudo-unipolar sensory neurons that project an axon both to the periphery and to the spinal cord and so are myelinated both by oligodendrocytes and schwann cells *in vivo* (Wood et al. 1980). Wide-spread myelination occurs 10–14 days after the addition of OPCs (Chan et al. 2004; J. K. Huang et al. 2011). Due to the independent preparations of DRGs and OPCs, the ability to tightly control and manipulate each compartment prior to their co-culture provides a highly flexible model for studying both cell autonomous and non-cell autonomous regulators of myelination (Jarjour et al. 2012).

Three-dimensional cultures: organotypic and aggregate cultures

Cultures that more closely mimic the *in vivo* environment have also be devised. Crain and colleagues showed that organotypic slice cultures of embryonic spinal cord develop a high degree of electrophysiological and biochemical maturity with prolonged culture (Crain 1966). Given the preservation of histotypical architecture and neuronal circuitry in brain organotypic slice cultures, they became—and remain—a powerful model for investigating neuronal physiology and function in a physiologically relevant environment. Organotypic cultures have also been extensively used to study myelination and helped to elucidate which cells were responsible for myelin formation (Jarjour et al. 2012; Field et al. 1969). A robust response to chemically induced demyelination with a substantial and well-defined time course of repair makes them well suited to study the process of remyelination and the factors that regulate it (Miron et al. 2013).

Another interesting and relevant culture method to this thesis, that was popularised during the 1970s, is that of CNS aggregate cultures. Interest in recapitulating developmental processes *ex vivo* led to the demonstration that enzymatic digestion and mechanical dissociation of limb buds from the chick embryo would aggregate and self-organise *in vitro* and re-establish the expected tissue architecture with continued differentiation (Moscona & Moscona 1952). This method was soon applied to fetal cortical tissue, which gave rise to numerous spherical cultures displaying neural rosette formation, typical of the developing neural tube (Moscona 1957). Indeed, CNS

aggregate cultures became popular with optimised conditions yielding diverse neuronal and glial differentiation, synapse formation, expression of multiple neurotransmitters and, significantly, myelination (Seeds & Vatter 1971; Matthieu et al. 1978; Trapp et al. 1979). Aggregate cultures were used to study modulators of myelination (Almazan et al. 1985), as well as de- and remyelination (de Rosbo et al. 1990; Duvanel et al. 2001; Diemel et al. 2004), and were also generated using human fetal material (Pulliam et al. 1988). Aggregate cultures were advantageous due to the full complement of CNS cells present and their ability to mirror both the temporal maturation of the *in vivo* brain and appropriate cell-cell interactions therein. Aggregate cultures were often referred to as organoids (i.e. resembling an organ) and represent the methodological foundation to contemporary organoid cultures, which have been loosely defined as "derived from primary sourced material or pluripotent stem cells to generate restricted or diverse cell-types to study developmental and pathological processes in a 3D environment" (Lancaster & Knoblich 2014b).

Pluripotent stem cells

The derivation of embryonic stem cell lines from the mouse and human blastocyst was a landmark event that enabled the propagation and differentiation of mammalian cells *in vitro* and led to the generation of experimental mammalian genetics (Evans & Kaufman 1981; Martin 1981). Then came the seminal discovery that somatic cells both from mouse and human could be reprogrammed to a comparably pluripotent state via the transduction of 4 transcription factors (Oct3/4, Sox2, Klf4, c-Myc), revolutionising the field and bypassing the ethical controversy of using human ES cell lines (Takahashi & Yamanaka 2006; Takahashi et al. 2007). So called 'induced' pluripotent stem cells (iPSC) promised the ability to generate patient and disease-specific cell lines to understand developmental and disease mechanisms, for drug screening and toxicology purposes and for application in regenerative medicine.

Furthermore, another major advancement in recent years was the development of gene editing tools—most notably of CRISPR/Cas9—that enabled accessible and precise targeting of the genome. In particular, for iPSC research, targeted gene-correction of known genetic mutations in patient-derived iPSCs has provided

researchers with a valuable tool to create isogenic cell lines for investigating genotype-phenotype correlations and begin to unpick mechanisms of disease.

iPSC-derived oligodendrocytes.

Developmental studies of the 20th century provided the foundation and necessary information to induce precise differentiation of pluripotent stem cells into defined germ-layers and cell-types (Rossant 2011) (Figure 2.8). The generation of stem cell-derived oligodendrocytes was viewed as an attractive method to study normal as well as dysfunctional oligodendrocyte development in disease, as a screening tool to find chemical inducers of oligodendrogenesis to treat demyelinating disorders and as a potential cell-based therapeutic intervention for childhood leukodystrophies and cerebral palsy (Billon et al. 2002; Goldman & Kuypers 2015; Goldman et al. 2012).

Oligodendrocytes were first derived from mouse ES cells (Fraichard et al. 1995) and then from human ES (S.-C. Zhang et al. 2001) inefficiently amongst a mix of neuronal cell-types. However, protocol optimisation eventually led to efficient generation of oligodendrocytes from human ES cells (S. M. Kang et al. 2007) and iPSC cells (Ogawa et al. 2011; Su Wang et al. 2013; Livesey et al. 2016; Douvaras et al. 2014) using the principle technique of reproducing the temporal signalling environment exposed to neuroepithelial cells as they differentiate into oligodendrocyte *in vivo*. This involves neural induction via retinoic acid, proliferation of NPCs via FGFs, ventralisation via sonic hedgehog signalling, expansion of OPCs via PDGF and exposure to insulin and thyroid hormone to support oligodendrocyte differentiation, survival and maturation (Goldman & Kuypers 2015; Barres et al. 1993).

Stem cell-derived oligodendrocytes demonstrate the appropriate maturation-specific physiological features that were first reported in rodent systems, including a progressive reduction in voltage-gated sodium and potassium channels, an increase in the activity of inwardly rectifying potassium channels and modifications to AMPA receptor composition (Livesey et al. 2016). Additionally, a number of studies have used this model to study the development of oligodendrocytes in response to factors

including small molecules and different oxygen tensions (Stacpoole et al. 2013; Hubler et al. 2018).

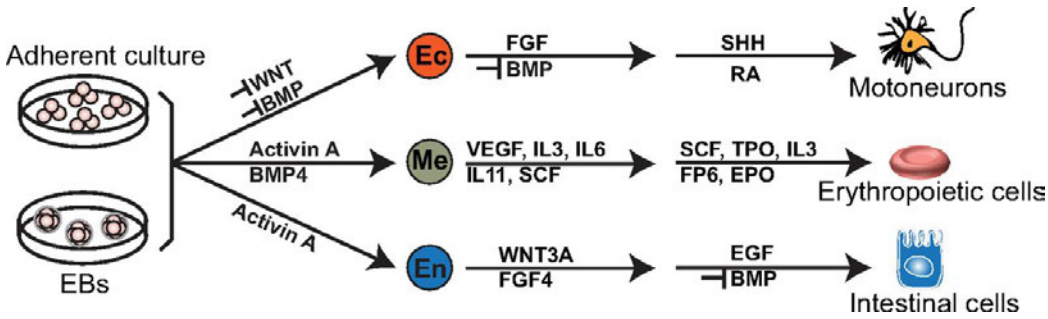

Figure 2.8 In vitro generation of different germ layers from pluripotent stem cells

Pluripotent stem cells can be differentiated into different cell-types across all three germ layers (motor neurons: ectoderm, erythropoietic: mesoderm and intestinal cells: endoderm) using precise patterning factors. Adapted from Zhu and Huangfu, (2013), *Development.*

iPSC-derived myelin

The critical function of oligodendrocytes is to myelinate and there exists a limited number of methods to study iPSC-derived myelin formation. The most robust of which involves transplantation of iPSC derived OPCs into the dysmyelinating shiverer mutant mouse. First described in 1973 (by Biddle et al in the F38 generation of Swiss Vancouver stock), the shiverer mouse contains an autosomal recessive mutation in the gene for myelin basic protein (MBP) (Chernoff 1981). As a result of the large deletion, shiverer mice do not express MBP mRNA and have trace amounts of compact myelin in the CNS, while peripheral myelin is intact. Consequently, transplantation of exogenous OPCs into either the neonatal mouse brain, or organotypic slice cultures derived from the shiverer mouse, leads to oligodendrocyte differentiation and myelination, which can be ascribed to the transplanted cells by their expression of MBP. This technique has been used to investigate the myelinating potential of normal and patient-derived iPSC-derived oligodendrocytes (Su Wang et al. 2013; Douvaras et al. 2014; Osipovitch et al. 2018; Windrem et al. 2017; Vasistha et al. 2019).

Whilst useful for demonstrating the potential of human oligodendrocyte to form myelin, the constrained circumstances by which human cells must replace endogenous oligodendrocytes that fail to compactly myelinate the shiverer mouse, as well as the inherent variability of transplantation studies and the restrictive conditions of an *in vivo* environment highlight the need for a reliable, accessible, *in vitro* human-based model of myelination.

In vitro assays of myelination are readily available using rodent material, involving co-culture between primary rat OPCs and either retinal or dorsal root ganglion cells (Svenningsen et al. 2003). So far, similar efforts using strictly iPSC-derived cell-types has failed to give rise to myelin formation (Su Wang et al. 2013). Recently, mixed-species approaches have been more successful, where co-culture of iPSC-derived oligodendrocytes with rat DRGs does lead to myelin formation (Nevin et al. 2017). Whilst suitable for analysis of cell-autonomous defects in human oligodendrocytes, the longevity of co-cultures is low, thereby limiting maturation of iPSC-derived myelin (e.g. assembly of nodal domains). Furthermore, there may be differences in axonally-regulated signals between human and rat that are not accounted for in this system.

This may be particularly important in the context of modelling familial human diseases *in vitro* as such gene mutations will be globally expressed throughout the CNS.

In order to model myelin disorders *in vitro* or to inform accurately on the factors that regulate human myelination, an improved *in vitro* model of myelination is needed that demonstrates robust, compact myelin development and which mirrors the *in vivo* physiological maturity of myelin.

Pluripotent stem cell-derived organoids

Until recently, the emphasis on refining iPSC-based protocols was placed on deriving more homogenous populations of defined cell-types to attribute any phenotype accordingly. However, though a reductionist approach is often warranted, it has long been established that cells behave differently in the presence of other cell-types. Most notably, astrocytes promote CNS synaptogenesis via thrombospondin-gabapentin receptor signalling (Christopherson et al. 2005; Eroglu et al. 2009). This has led to a resurgence in three-dimensional cultures that aim to preserve appropriate cell-cell interactions *in vitro* as a more physiologically relevant model system to study organ development.

As indicated to earlier, organoids represent the methodological evolution of both pluripotent stem cell-derived embryoid bodies and aggregate cultures derived from dissociated embryonic tissue (Lancaster & Knoblich 2014b; Clevers 2016). They have been defined as *"collections of organ-specific cells types that develop from stem cells or organ progenitors and self-organise through cell sorting and spatially restricted lineage commitments in a manner that is similar to in vivo"* (Lancaster & Knoblich 2014b). The advent of human pluripotent stem cells brought with it the possibility of modelling human organ development *in vitro.* In 2013, Madeline Lancaster demonstrated an organoid model of the developing brain that recapitulated species-specific differences in cortical volume and outer radial glial cell number, compared to mouse ES-derived organoids. Furthermore, cerebral organoids generated from patient-derived iPSCs recapitulated the major hallmarks of primary microcephaly (Lancaster et al. 2013). Cerebral organoids develop a variety of regional identities that self-organised into discrete domains and opened up the possibilities of modelling

other neurodevelopmental conditions to study the pathogenesis of disease (Kelava & Lancaster 2016a).

Over the following years a number of protocols have established slightly more restrictive, CNS region-specific cultures, made up of multiple, developmentally associated cell-types that avoids the unrestricted differentiation observed in cerebral organoids. A useful figure to illustrate the spectrum of stem cell-derived neural cultures with regard to cellular complexity is shown in Figure 2.9 (taken from Kelava & Lancaster 2016b). This depicts the trade-off between homogeneity and cellular complexity across different types of cultures, which is controlled by the degree of patterning factors supplemented into the medium and how the cells are handled. Whilst neural stem cells can be maintained in a highly pure population by controlling their growth and limiting their differentiation, spheroid cultures are exposed to inductive cues that pattern neuroepithelial cells to defined domains of the developing CNS. The complexity of whole-brain organoids is due to the absence of inductive cues. This results in highly heterogenous cultures that are established by intrinsic differentiation cues, which leads to regionalisation of different CNS domains. So far, region-specific organoids have been generated to resemble the dorsal and ventral forebrain, midbrain and hypothalamus (Birey et al. 2017; Qian et al. 2016). Of note, the term organoid has more recently become associated with any three-dimensional culture derived from either stem cells or primary tissue and is increasingly used interchangeably with ‘spheroid’ cultures.

Techniques have emerged to study neuronal function and network formation (Paşca et al. 2015; Giandomenico et al. 2019) and the cellular composition of forebrain organoids has been shown to resemble that of the human fetal brain (Velasco et al. 2019). Importantly, organoids give rise to cells that are functionally more mature than through conventional differentiation protocols, which is exemplified by the dynamic cell-cell interactions observed between astrocytes and neurons in cortical spheroids and so called ‘asteroids’ (Paşca et al. 2015; Krencik et al. 2017).

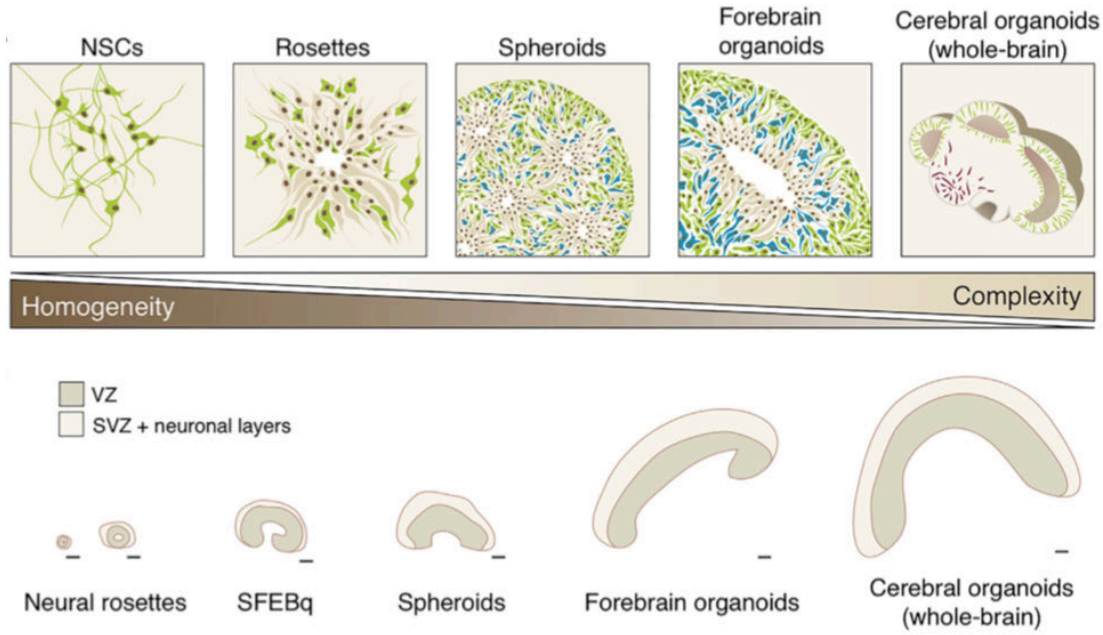

Figure 2.9 Complexity and homogeneity in stem cell-derived spheroids and organoids

An inverse relationship between homogeneity and complexity exists in stem cell-derived neural cultures. Increasing cellular diversity is evident between neural stem cell and spheroids cultures with cerebral organoids demonstrating grater complexity again. (s)VZ : (sub)-ventricular zone.

Recently, several studies have investigated oligodendrogenesis in spheroid/organoid cultures (Madhavan et al. 2018; Marton et al. 2019; H. Kim et al. 2019). Given the heterogenous mixture of neurons and astrocytes, advanced functional maturity and the enhanced longevity of organoid culture (Lancaster & Knoblich (2014a) were the first to demonstrate cultures maintained for over 1 year) — organoids are an attractive model to study human myelin development. Evidence of oligodendrocyte-axon interaction and compaction has been shown in three-dimensional human stem cell-derived cultures (Madhavan et al. 2018; Marton et al. 2019; H. Kim et al. 2019). However, wide-spread myelin formation and organisation of myelinated axon domains (eg. node of Ranver) have not been recapitulated *in vitro*, highlighting the immaturity of currently available model systems.

Against this background, this thesis set out to develop a robust and physiologically mature model of myelination derived from human pluripotent stem cells in order to investigate the physiology and pathology of human myelin development.

Chapter 3 Methods and materials

3.1 Materials

Advance DMEM/F12 (Life Technologies, 12634-010)

Accutase (Sigma, A6964)

Antibiotic-Antimycotic (Life Technologies, 15240062)

Murine bFGF (Peprotech, 450-33)

GFR BD Matrigel basement membrane matrix (SLS, 354230)

Laminin (Sigma, L2020-1MG)

DPBS (Ca-/Mg-) (Life Technologies, 14190-094)

DMSO (Sigma, D2438)

Activin Inhibitor (R & D Sytems, 1614/1)

LDN193189 (Stratech, S2618)

IMDM (Life Technologies 21980-32)

F12 (Life Technologies 31765-027)

BSA (Europa EQBAC62 0050)

CD Lipid 100x (Life technologies) 11905-031)

Monothioglycerol (Sigma M6145)

Insulin (Roche 1376497)

Transferrin (Roche 10652202001)

Glutamax (Life Technologies, 35050-038)

B27 (Life Technologies 17504-044)

N2 (Life Technologies, 17502-048)

BDNF (R & D Systems248-BD-025)

GDNF (R & D Systems212-GD-050)

Forskolin (R & D Systems1099/10)

Retinoic acid (Sigma R2625)

Puromorphamine (Merck 540220-5MG)

Heparin (Sigma H3149)

4% paraformaldehyde (PFA) (Sigma, 158127)

3.2 Buffers and reagents

10X Phosphate Buffered Saline (PBS)	Product code	**Weight**
NaH_2PO_4 . $2H_2O$ (MW 156.01)	Fisher Chemical 10315770	5.93 g
Na_2HPO_4 anhydrous (MW 141.96)	VWR 28026.292	23 g
NaCl	Fisher Chemical 10428420	87.68 g
H_20		1 L
		pH 7.2

Citrate buffer	Product code	Weight
Tri-sodium citrate $C6H5Na307.$ $2H_2O$ (MW 294.09)	Fisher Chemical 10112880	2.94 g
H_20		1 L
Tween-20 (100%)	P1379	500 µl
		pH 6

10X TAE buffer	Product code	Weight
Tris base (MW 121.14)	T1503	48.5 g
glacial acetic acid (17.4M)	A/0360/PB08	11.4 mL
0.5 M EDTA (pH 8)	15575020	20 mL
H_20		1 L

3.3 iPSC maintenance and generation of oligodendrocytes

Media compositions

Chemically defined medium (CDM)	Product code	Stock conc.	Working conc.
IMDM	21980-032	100%	50%
F12	31765-027	100%	50%
Bovine Serum Albumin, Powders, Cohn Fraction V (BSA)	EQBAC62-100	100%	5%
Chemically Defined Lipid Concentrate (100x)	11905031	100%	1%
Monothioglycerol	M6145	108 mg/ml	4.32 µg/ml
Insulin	11376497001	10 mg/ml	7 µg/ml
Transferrin	10652202001	30 mg/ml	15 µg/ml
Antibiotic-Antimycotic	15240062	100%	1%

Phase 1 medium	Product code	Stock conc.	Working conc.
CDM		100%	100%
N-acetyl cysteine	A8199	500 mM in ddH2O	1 mM
Activin Inhibitor	1614/1	10 mM in DMSO	10 μM
LDN	SML0559	100uM in DMSO	100 nM

Phase 2 medium	Product code	Stock conc.	Working conc.
CDM		100%	100%
N-acetyl cysteine	A8199	500 mM in ddH2O	1 mM
FGF2/Heparin	450-33	20 μg/ml	5 ng/ml
Retinoic Acid	R2625	1 mM in ethanol	100 nM

Phase 3 medium	Product code	Stock conc.	Working conc.
100 mL Adv DMEM/F12	12634-028	100%	100%
Antibiotic-Antimycotic	15240062	100%	1%
B-27	17504044	50 X	0.5 X
N-2	17502048	100 X	0.5 X
Glutamax	35050038	100%	1%
FGF2	450-33	20 µg/ml	5 ng/ml
Purmorphamine	540220	1 mM in DMSO	1 µM
Retinoic Acid	R2625	1 mM in ethanol	1 µM

Phase 3 medium - FGF	Product code	Stock conc.	Working conc.
Adv DMEM/F12	12634-028	100%	100%
Antibiotic-Antimycotic	15240062	100%	1%
B-27	17504044	50 X	0.5 X
N-2	17502048	100 X	1 X
Glutamax	35050038	100%	1%
Purmorphamine	540220	1 mM in DMSO	1 µM
Retinoic Acid	R2625	1 mM in ethanol	1 µM

Oligodendrocyte proliferation medium	Product code	Stock conc.	Working conc.
Adv DMEM/F12	12634-028	100%	100%
Antibiotic-Antimycotic	15240062	100%	1%
B-27	17504044	50 X	0.5 X
N-2	17502048	100 X	1 X
Glutamax	35050038	100%	1%
Heparin	H3149	5 mg/ml	5 μg/ml
FGF2	450-33	20 μg/ml	10 ng/ml
PDGF-α	AF-100-13A	20 μg/ml	20 ng/ml
Purmorphamine	540220	1 mM in DMSO	1 μM
IGF	AF-100-11	20 μg/ml	10 ng/ml
3,3′,5-Triiodo-L-thyronine sodium salt (T3)	T6397	40 μg/ml	60 ng/ml
Smoothened Agonist, SAG	566660	1 mM in H2O	1 μM

Oligodendrocyte differentiation medium	Product code	Stock conc.	Working conc.
Adv DMEM/F12	12634-028	100%	100%
Antibiotic-Antimycotic	15240062	100%	1%
Heparin	H3149	5 µg/ml	5 ng/ml
B-27	17504044	50 X	0.5 X
N-2	17502048	100 X	1 X
ITS	51500-056	100 X	1 X
Glutamax	35050038	100%	1%
IGF	AF-100-11	20 µg/ml	10 ng/ml
3,3′,5-Triiodo-L-thyronine sodium salt (T3)	T6397	40 µg/ml	60 ng/ml

Plate coating	Product code	Solution	Stock conc.	Working conc.
Poly-L-ornithine hydrobromide	P3655	Embryo transfer water	100%	1%
Laminin	L2020	Adv DMEM/F12	1 mg/ml	10 µg/ml

GFR BD Matrigel Basement Membrane matrix	354230	Adv DMEM/F12	100%	0.5%
Fibronectin	F2006-5MGX5	Adv DMEM/F12	1 mg/ml	50 μg/ml

Method: iPSC maintenance

All iPSC lines used in this study were obtained under full Ethical/Institutional Review Board approval from the University of Edinburgh. CS02iCTR-NTn1 (iPSC1), CS25iCTRL-18n2 (iPSC2) were obtained from Cedars-Sinai and the CS00iNK-n1 and / CS00iNK-n2 lines (Nfasc155 $^{/}$) were generated in collaboration with Professor Peter Brophy and Cedars-Sinai. The two ALS patient-derived cell lines used, harbouring either the G298S or M337V *TARDBP* mutations, were provided as fibroblasts from Professor Chris Shaw, King's College London and reprogrammed to iPSCs by Dr Karen Burr and Dr Bilada Bilican via either episomal or retroviral-based methods.

All iPSCs were maintained on Matrigel (BD Biosciences)-coated plates in Essential 8 medium (Life Technologies) at 37°C and 5% CO2. Medium was replenished every day until cells had reached 80% to 90% confluency. To passage, cells were washed in 1 mL of DPBS before being lifted from the surface of the plate with 1 mL of a 1:1 ratio of Dispase: Collagenase and incubated at 37˚C for 15–25 min. 1 mL of DPBS is added to the cell solution and used to flush remaining colonies from the surface of the plate. Cells were transferred to a 15mL falcon tube, gently separated by pipetting and allowed to settle. The supernatant was removed by aspiration and the pellet resuspended in 5 mL of DPBS to wash the cells, which were again left to settle. The supernatant was removed once more, the pellet was resuspended in E8 medium $^{+}$ PSF, and the cells were split accordingly.

Method: Generation of iPSC derived oligodendrocytes

iPSC-derived oligodendrocytes were generated using the protocol published by (Livesey et al. 2016). On day 0, confluent iPSC colonies were lifted using Dispase/Collagenase (similarly to passaging iPSCs) and, after washing the cells without breaking the colonies up, were reconstituted in 10mL phase 1 medium, transferred to 90mm plastic dishes and placed on rotating shakers to encourage embryoid body and neurosphere formation. Phase 1 medium contains LDN and Activin inhibitor to direct cells towards a neuroectoderm fate by blocking BMP and TGF-β respectively (dual SMAD inhibition) and was replenished every 2–3 days. On day 7, the medium was changed to phase 2 medium, which contains the caudalising agent retinoic acid (RA) to pattern the cells towards the spinal cord. On day 14, neurospheres were plated on to laminin-coated 6 well plates for 2–3 days to allow for adhesion to the plate surface. Since only viable spheres attached to the plate surface, this process enriched the cultures for healthy spheres. In addition, non-neuralised spheres that did not show neural rosettes or any neural precursor cells (NPCs) migrating out of attached spheres were selectively removed using a p200 pipette. Neurospheres were lifted from 6 well plates using a cell scraper, transferred to 90mm dishes and cultured for a further 7 days in phase 3 medium containing the ventralising agent purmorphamine, to pattern the cells towards the pMN domain of the ventral telencephalon, and FGF2 to support the proliferation of NPCs. After 7 days, neurospheres were transferred to phase 3 medium-FGF for a further 14 days to prevent further growth of the spheres and promote differentiation of NPCs. Following this phase, spheres were transferred to oligodendrocyte proliferation medium, which contains the mitogens PDGF-α and FGF2, to promote oligodendrocyte progenitor generation and proliferation; smoothened agonist (SAG), as an additional ventralising factor; IGF; and T3, which support oligodendrocyte differentiation. Oligodendrocyte progenitor spheres were mechanically dissociated at this stage to enrich the OPC population and maintained for a further 3–4 weeks with regular pruning of any aggregated spheres.

For two-dimensional analysis of oligodendrocyte differentiation, oligodendrocyte progenitor spheres were dissociated using the papain kit (Worthington Biochemical).

0.5 mL of spheres are collected in a 15 mL falcon tube and allowed to settle. A Papain/DNase solution is added to the cells and returned to the incubator for 15–20 minutes. Using a P1000 pipette, spheres were gently dissociated into a single cell suspension and centrifuged at 2500 rpm for 2.5 minutes to remove the supernatant. The cell pellet was reconstituted in an inhibitor/DNase solution and gently layered on to 1mL of Ovomucoid inhibitor in a fresh falcon tube. This allowed for larger clumps of cells to sink to the bottom of the discontinuous density gradient. Using a P1000, the upper layer of cells was carefully removed from the gradient, centrifuged at 2.5rpm for 3 minutes, and the was supernatant removed. The pellet was resuspended in oligodendrocyte proliferation medium and the cells counted using a haemocytometer and 40 μl of cells at 1000 cells per μl was added as a droplet onto the centre of pre-coated coverslips. After 2 hours, the cells had adhered to the surface and the well was flooded with oligodendrocyte proliferation medium. The next day, half the medium was changed with oligodendrocyte differentiation medium. Cultures were maintained for 3–4 weeks with medium changes every 2–3 days. Cultures were fixed in 4% PFA, washed in PBS, and used for immunocytochemistry.

Method: coating coverslips

To coat coverslips for oligodendrocyte plate down, acid-treated and autoclaved coverslips were submerged in a 1% polyornithine solution (in embryo transfer water) overnight at room temperature. The next day, coverslips were washed three times in Embryo Transfer Water. A 40 μl droplet of coating reagents laminin, matrigel, and fibronectin (LMF) was added and the coverslips were stored at 4°C for up to 7 days or placed in an incubator at 37 °C for 2–3 hours prior to plate down.

3.3.1 Co-culture with iPSC derived motor neurons

iPSC-derived MN co-culture medium	Product code	Stock conc.	Working conc.
Neurobasal	21103049	100%	100%
Glutamax	35050-038	100%	1%
Antibiotic-Antimycotic	15240062	100%	1%
Non-essential amino acids	11140035	100%	1%
β-mercaptoethanol	31350010	14.3 M	100 μM
B-27	17504044	50 X	1 X
N-2	17502048	100 X	1X
Retinoic acid	R2625	1 mM	1 μM
Ascorbic acid	A4403	10 mM	2.5 μM
BDNF	248-BD-025	10 μg/ml	10 ng/ml
GDNF	212-GD-050	10 μg/ml	10 ng/ml
IGF	AF-100-11	20 μg/ml	10 ng/ml
ITS	51500-056	100 X	1 X
3,3′,5-Triiodo-L-thyronine sodium salt (T3)	T6397	40 μg/ml	60 ng/ml

Method

iPSC derived MNs were provided by Dr Bhuvaneish Selvaraj and were generated via the protocol published (Selvaraj et al. 2018). In a 40μl droplet, 20,000 MNs were added to the LMF-coated coverslips. After 1 hour, 25 μl of media was removed and replaced with 25 μl of a single cell suspension of OPCs. Between 35,000 and 125,000 cells were added per well. After a further 2 hours, the well was flooded with MN co-culture medium. Co-cultures were maintained for 3 weeks and the medium was replaced every 2–3 days. Cultures were fixed in 4% PFA, washed in PBS, and used for immunocytochemistry.

3.3.2 Co-culture with DRG neurons

Medium compositions

DRG medium	Product code	Stock conc.	Working conc.
DMEM	41966029	100%	100%
FBS	11550356	100%	1%
Antibiotic-Antimycotic	15240062	100%	1%
β-mercaptoethanol	31350010	14.3 M	100 μM
NGF	PMP04Z	100μg/ml	100 ng/ml

DRG co-culture medium	Product code	Stock conc.	Working conc.
Neurobasal	21103049	100%	100%
DMEM	41966029	100%	1%
Antibiotic-Antimycotic	15240062	100%	1%
B-27	17504044	50 X	0.5 X
N-2	17502048	100 X	1X
N-acetyl cysteine	A8199	500 mM	1 mM

3,3′,5-Triiodo-L-thyronine sodium salt (T3)	T6397	40 μg/ml	60 ng/ml

Method

Dr Marie Bechler in the ffrench-Constant lab provided technical support in establishing DRG cultures. DRGs were dissected from E15 rats and were incubated in 1 ml of papain digestion mix (1 ml MEM, 1.2 U/ml papain (Worthington), 0.24 mg/ml L-cysteine solution (Sigma) and 40μg/ml of DNase (Sigma) for 1 hour at 37ºC. DRG medium supplemented with NGF was used to quench the reaction and, after washing once in DRG medium, the cell pellet was dissociated. Between 1.7 and 2.0 x 10^6 cells were added as a 200 μl droplet onto Poly-D-Lysine and matrigel-coated 22 mm wide coverslips. The next day, each well was flooded with DRG medium supplemented with NGF and FdU. Cells were maintained in DRG medium supplemented with NGF for 21 days and were exposed to a total of three doses of FdU every other media change. After 21 days, DRGs were slowly exposed to DRG co-culture medium by gradual incorporation over 3 days. Subsequently, between 50,000 and 250,000 iPSC derived OPCs were added and maintained for 4 weeks. Cultures were fixed in 4% PFA, washed in PBS, and used for immunocytochemistry.

3.3.3 Co-culture with shiverer slice cultures

Medium and buffers compositions

Slice culture medium – serum containing	Product code	Stock conc.	Working conc.
MEM	31095029	100%	100%
FBS	12360273	100%	25%
EBSS	14155048	100%	25%
PSF	15240-062	100%	1%
Gluatamax	35050-038	100%	1%
Glucose	G6152	45%	0.65%

Slice culture medium – serum free	Product code	Stock conc.	Working conc.
MEM	31095029	100%	50%
F12 nut mix	21765029	100%	50%
B-27	17504044	50 X	1 X
N-2	17502048	100 X	0.5 X
PSF	15240-062	100%	1%
Glucose	G6152	45%	0.65%

ITS	51500-056	100 X	1 X
IGF	AF-100-11	20 mg/ml	10 μg/ml
3,3′,5-Triiodo-L-thyronine sodium salt (T3)	T6397	40 mg/ml	60 μg/ml

Lysis buffer	Product code	Working concentration.
Tris-HCl (MW 157.60)	10812846001	100 mM (pH 8.5)
EDTA	15575020	5 mM (pH 8)
NaCl	10626272	200 mM
Sodium dodecyl sulfate	436143	0.2%
Proteinase K	V3021	100 μg/ml

Method: Genotyping shiverer mice

Tail clippings for each P0-P2 mouse were digested in 400 μl lysis buffer at 55°C in a water bath over night or for 5–6 hours. Samples were then transferred to a heat block at 99°C for 10 minutes to denature proteinase K and centrifuged for 5 minutes at max speed. The supernatant was transferred to a fresh eppendorf and an equal volume of was isopropanol added. After centrifuging for 10 minutes, the supernatant was

discarded and the DNA pellet was washed in 70% EtOH. DNA was resuspended in 10-20 μl of buffer EB and used in a PCR reaction to test for presence of full-length MBP gene.

Method: Preparing organotypic slice cultures and OPC co-cultures

The brains of homozygous shiverer MBP$^{-/-}$ mice were dissected in cold EBSS and placed in plastic moulds containing pre-heated 4% low-melting agarose (Lonza). Once hardened, 300 μm sections of forebrain were cut using a vibratome and up to three sections each were transferred to PTFE-coated cell culture inserts in serum containing slice culture medium. Between days 1 and 7, the medium was slowly replaced with increasing concentration of serum free slice culture medium. Between 10 to 20,000 OPCs were added onto organotypic slice cultures in 1–2 μl. Alternatively, whole spheroids that had not been dissociated were transferred onto slice cultures using a p200 pipette. Cultures were maintained in serum free slice culture medium for 2–8 weeks. Cultures were fixed in 4% PFA by adding 1ml below and 1ml above each insert, washed in PBS, and used for immunocytochemistry.

3.4 Generation of myelinoids

Medium composition

Myelination medium	Product code	Stock conc.	Working conc.
Adv DMEM/F12	12634-028	100%	100%
Antibiotic-Antimycotic	15240062	100%	1%
Heparin	H3149	5 mg/ml	5 µg/ml
B-27	17504044	50 X	0.5 X
N-2	17502048	100 X	1 X
ITS	51500-056	100 X	1 X
Glutamax	35050038	100%	1%
IGF	AF-100-11	20 µg/ml	10 ng/ml
3,3′,5-Triiodo-L-thyronine sodium salt (T3)	T6397	40 µg/ml	60 ng/ml
GDNF	212-GD-050	10 µg/ml	10 ng/ml

Method

To generate myelinating spheroids, the protocol for deriving iPSC oligodendrocytes was modified as follows: mechanical dissociation of spheroids was avoided as they entered oligodendrocyte proliferation medium and, after 2–3 weeks of culture, intact spheres (size 700-1500 µm) were individually transferred on to PTFE-coated cell culture membrane inserts in 6 well plates, using a p200 µl pipette. Up to 6 spheres

were added to each insert and maintained in myelination medium for 4–12 weeks (1 ml of medium was replaced every 2–3 days). To pharmacologically modulate myelin development, blebbistatin (10 μM, Sigma), TeNT (3 nM, Sigma), and BDNF (10 ng/μl) were added to myelination medium at MI and maintained throughout the remainder of the culture period. Myelinoids were exposed to 15 mM KCl (myelination medium supplemented with 10mM KCl) for 2 hours at a time, either once or three times per week, before being returned to normal medium.

3.5 CRISPR/Cas9 gene targeting

In order to correct the TDP-43 G298S mutation in patient-derived iPSCs, a CRISPR/Cas9 gene targeting approach was used to induce a double stranded DNA break near the mutation site and a single stranded oligo DNA nucleotide (ssODN) was supplied with the correct gene sequence as a substrate for homology directed repair (HDR). A schematic overview of the targeting strategy is provided in Figure 7.2A.

Testing gRNA targeting efficiency

Dr Bhuvaneish Selvaraj designed guide RNAs (gRNA) targeting the mutant allele using the gRNA design resource at http://crispr.mit.edu/. gRNAs were cloned into the pMTL23 vector, which was used to drive expression of CRISPR RNA, transactivating CRISPR RNA and gRNA via the U6 promoter. The targeting efficiency of each gRNA was tested via a T7 assay on transfected cells. To do so, patient-derived iPSCs were lifted using accutase, pelleted, washed, and reconstituted in E8 medium $^{+}$ Rock inhibitor. Once counted, 800,000 iPSCs were reconstituted with a transfection solution containing a pMTL23 plasmid to drive expression of each gRNA, the pspCas9-2A-GFP plasmid that drove expression of the Cas9 mRNA and an EGFP-PUROMYCIN plasmid that enabled positive selection of transfected cells. The Lonza 4D nucleofector (programme CA137) and P3 Primary Cell 4D-Nucleofector kit was used was used to transect iPSCs in a total of 500 μl. Per well, 250 μl of cells were plated in E8 medium $^{+}$ Rock inhibitor per well. The next day, the medium was replaced and supplemented with 0.5 μg/ml puromycin for 24 hours. DNA was isolated from the transfected cells after a further 5 days of culture using the Promega kit (Wizard Genomic DNA Purification Kit).

T7 surveyor assay

Following Cas9-mediated DNA cleavage, the dominant repair process is non-homologous end-joining, which being highly error prone, introduces mis-matched

nucleotides. Firstly, TDP-43 exon 6 was amplified by PCR using the primers listed below. The PCR product was then purified using the Invitrogen ChargeSwitch PCR Clean-Up Kit. For the T7 assay, 200ng of DNA was incubated with 2 µl NEBuffer 2 and H_2O in a 19 µl reaction. A hybridisation reaction was performed by placing samples in a thermocycler and running the RAMP down PCR programme. 1 µl T7 Endonuclease was added to the solution and incubated at 37ºC for 15 minutes. 1µl 0.5M EDTA was then added and the solution immediately loaded onto a 2% gel. The resulting bands at 262bp and 191bp indicate efficient cutting and imperfect repair events at the target locus (Figure 7.2B).

Primer	Sequence 5' - 3'	Size
TARDBP ex 6 F	TTGCGCAGTCTCTTTGTGGA	452 bp
TARDBP ex 6 R	TTGGTTGGGGATCAGCATCC	

T7 assay	Volume	Step
200ng DNA	/	RAMP down PCR
NEBuffer 2	2 µl	
H_2O	Up to 19µl	
T7 Endonuclease I	+ 0.5 µl	37°C 15 min
EDTA (0.5M)	+ 1 µl	Gel electrophoresis

RAMP down PCR	time
95˚C	5 min
95˚C to 85˚C	–2˚C / s
85˚C to 25 ˚C	–0.1˚C / s
25˚C	forever

ssODN design

A 180bp ssODN containing the WT genomic sequence with 90bp flanking arms upstream and downstream of the cut site was designed to be used as a substrate for homology directed repair following Cas9-mediated cleavage. The ssODN was designed using SnapGene Viewer and the WT sequence obtained from Ensembl (ENSG00000120948). To prevent Cas9-mediated cleavage of the incorporated ssODN, silent mutations were created in the repair template by swapping out redundant nucleotides at the 3' end of the gRNA binding site (Figure 3.1).

Genomic region being targeted

TDP43 G298S mutation (red)
gRNA binding site (blue)
PAM site (yellow)

AATAGCAGAGGGGGTGGAGCTAGTTTGGGAAACAATCAAGGTAGTAATAT

Repair template

Corrected mutation (green)
gRNA binding site (blue)
Silent mutations (pink) AAC --> AAT and AAT--> AAC
PAM site (yellow)

AATAGCAGAGGGGGTGGAGCTGGTTTGGGAAATAACCAAGGTAGTAATAT

Figure 3.1 TARDBP gene targeting ssODN

A 180bp ssODN was designed that included the corrected G298S mutation (red to green) and two silent mutations (pink) created by substituting redundant nucleotides without affecting the coded amino acid.

iPSC transfection

Once the targeting efficiency of each gRNA was demonstrated, gene correction could be performed. Patient-derived iPSCs were transfected as before with the addition of the ssODN repair template. The mass of each plasmid is provided below. The cells were similarly plated and treated with puromycin after 24 hours. Three days later, transfected iPSCs were dissociated into single cells and plated onto 2 laminin-coated 10cm dishes in E8 + Rock inhibitor. Isolated colonies grew from individual cells over 7 days. Using an EVOS video microscope, 480 colonies were manually picked and plated into discrete wells in matrigel-coated 96-well plates. Clonal targeted iPSCs were maintained in E8 medium. To passage cells in 96-well plates, each well was washed in PBS using a multi-channel pipette and 50μl of 0.5mM EDTA was added to each well. Once colonies had rounded up (5–8 minutes at RT or 4-5 minutes at 37°C), EDTA was removed and 100 μl of E8 medium was added to break colonies into smaller pieces. Each plate was passaged 1:2 by transferring 50 μl of cells each to fresh matrigel-coated plates. One set of plates was used for continued culture and the other set was used for screening targeted iPSC clones.

Component	Amount
Cas9-2A-GFP	1.5μg
pMTL23-gRNA7	0.5μg
EGFP-PURO	1μg
ssODN repair template	10μl of 10μM stock

DNA isolation from cells in 96 well plates

Lysis Buffer for 96wp	20µl / well
10% NP40	4.5µl
10% Tween 20	4.5µl
20mg/ml Proteinase K	1µl
PCR buffer (5X)	20µl
dH_20	70.2µl

On-plate DNA isolation was performed to quickly screen individual iPSC colonies. First, iPSC colonies were washed in PBS and lysed by incubating with 20 µl of lysis buffer for 2 or more hours in a 55°C oven. Supernatants were then transferred to a PCR plate, centrifuged to remove bubbles and incubated at 95°C for 10 minutes (with a sealed cover). From each well, 2 µl of DNA was used to PCR amplify TDP-43 exon 6.

BsaJ1 restriction digest

To identify ssODN integration, 2µl of TDP-43 exon 6 PCR amplified DNA were incubated with BsaJ1 restriction enzyme at 60°C for 3 hours. Next, 15 µl were loaded onto a 2% agarose gel for restriction fragment length polymorphism analysis. The presence of a band corresponding to 191bp confirmed transgene integration (Figure 7.2). iPSC clones that showed positive integration were expanded into 24-well-plates, their DNA isolated, the targeting region amplified by PCR, purified, and sent for Sanger sequencing (Source Bioscience).

Restriction digestion	20µl reaction
BsaJ1	0.7µl
Cutsmart	2µl
PCR product	10µl
dH_2O	7.3µl

3.6 RT-PCR

RNA was extracted from MI spheroids using the RNeasy kit with additional clearance of genomic DNA using the Turbo DNA free kit (Invitrogen): 250ng of RNA was used to prepare cDNA via reverse transcription.

3.6.1 cDNA synthesis

In a total of 12µl RNase-free H20 containing 1µl random hexamers, 250–500ng of RNA was incubated for 5 minutes at 65°C. To this, 4µl of 5X Reverse Transcriptase buffer + 2µl dNTPs + 1µl Reverse Transcriptase were added, and placed in a thermocycler, and the following cycle was run. cDNA was stored at –20°C.

Temp	Time
25°C	10 min
45°C	60 min
70°C	10 min
12°C	Forever

3.6.2 Polymerase chain reaction (PCR)

The following primers were used during this thesis:

Target	Sequence	Temp (°C)	Size (bp)
hMBP mRNA ex1 F	CTTCCTCCCAAGGCACAGAG		
hMBP mRNA ex2 R	TGTACATGTTGCACAGCCCA	68	170bp
SOX10 mRNA ex4 F	CCAGGCCCACTACAAGAGC		
SOX10 mRNA ex5 R	CTCTGTCTTCGGGGTGGTTG	69	136bp

hFOXG1 R2	CCGTCGTAAAACTTGGCAAAG		
hFOXG1 F2	CCGCACCCGTCAATGACTT	65	133bp
hOtx2 F	AGAGGACGACGTTCACTCG		
hOtx2 R	TCGGGCAAGTTGATTTTCAGT	66	115bp
hHoxB4 ex1 F	GTGAGCACGGTAAACCCCAAT		
hHoxB4 ex2 R	CGAGCGGATCTTGGTGTTG	67	243bp
hGbx2 R	CGCCTTGTCGAAGTTACCG		
hGbx2 F	CTCACCTCTACGCTCATGGC	67	126bp
hPax6RT F	ATGTGTGAGTAAAATTCTGGGCA		
hPax6RT R	GCTTACAACTTCTGGAGTCGCTA	65	103bp
hNkx2.2 R	GCGCTTCATCTTGTAGCGG		
hNkx2.2 F	CGGCGAGTGCTTTTCTCCAA	68	165bp
SYT1 F	TCATCTGATGCAGAATGGTAAGAGG		
SYT1 R	GTAGCCCACAAAGACTTTGCC	67	199bp
PSD95 F	GGGAGAAGCAGCTCAACTCCAATCC		
PSD95 R	CCAGCAAGGCCTGGAAGAG	70	180bp
VAMP2 F	GTGGATGAGGTGGTGGACAT		
VAMP2 R	TTCTCTAGGCAGGGCAGACT	68	267bp
TDP-43 exon 6 Forward	TTGCGCAGTCTCTTTGTGGA		
TDP-43 exon 6 Reverse	TTGGTTGGGGATCAGCATCC		452bp

PCR reaction mix and cycle settings

Reagent	25µl reaction
Q5 reaction buffer	5µl
10mM dNTP	0.5µl
10µM F primer	1.25µl
10µM R primer	1.25µl
cDNA	1µl
Q5 polymerase	0.25µl
dH_2O	Up to 25µl

Step	Temp (˚C)	Time (s)	
1	98	120	
2	98	30	**X 32**
3	66	30	
4	72	30	
6	72	180	
7	12	Forever	

Gel electrophoresis

For products 50-2000bp in size, a 2% agarose gel was prepared in 1X TAE buffer with 5ul of nucleotide staining reagent GelRed. Gel electrophoresis was run at 100V for 1 hour 15 minutes.

3.7 Immunocytochemistry

MI-4, MI-8, and MI-12 myelinoids were fixed by submerging in 4% PFA (myelinoids: 2 hours at room temperature (RT), co-cultures: 15–20 minutes RT). Cells were washed twice in PBS and stored at 4°C until they were ready for processing. For analysis of myelin sheath length and myelin volume across the spheroid, whole spheroids were stained as follows. Membranes containing myelinoids were cut out from each insert and placed in 24 well plates with fresh PBS. Cells were permeabilised with 0.3% Triton-X-100 in PBS for 45 minutes and then placed in blocking solution for 2 hours (10% normal goat serum, 0.3% Triton-X-100 in PBS) at RT. For CNP staining, antigen retrieval was performed by transferring membranes into 1.5 mL eppendorfs containing 1mL of citrate buffer pH 6 and placed in a shaking heatblock at 95°C for 20 minutes. Myelinoids were then washed in PBS and placed in blocking solution for another 1 hour. Primary antibodies were diluted in blocking solution and added to myelinoids for overnight incubation at 4°C. The next day, spheres were washed in PBS + 0.1% Tween-20 (PBS-T) and incubated with secondary antibody (all 1/1000) for 2 hours at RT. DAPI was used at a dilution of 1:20,000 and incubated for 15 minutes. After further washing in PBS-T, membranes containing myelinoids were mounted onto microscope slides (Thermo Scientific) with FluorSave (Calbiochem) and No. 1.5 coverslips (Thermo Scientific).

Where cryosections were used, myelinoids were fixed (as before) and immersed in a 30% sucrose solution overnight at 4°C. The next day, myelinoids were transferred to a 1:1 solution of 30% sucrose and OCT and frozen in a bath of isopentane over dry ice. Cryosections of 10μM were cut and stored at –20°C until ready for staining. To stain cryosections, slides were immersed in 0.3% Triton-X-100 in PBS for 30 minutes and blocked using the same blocking solution as above for 1 hour. For CNP staining, slides were immersed in citrate buffer pH 6 and placed in a microwave for 4 minutes at full power, then for 3 minutes at 80% power, and washed in PBS. The sections were incubated with primary antibody in blocking solution overnight at RT. The next day, sections were washed in PBS-T and incubated with secondary antibodies for 2 hours. DAPI was added to the sections for 7 minutes, which were washed in PBS-T and mounted with FluorSave.

3.7.1 Antibodies

1˚ Antibody	Species	Dilution	Company	Cat #
ANKYRIN-G	mIgG2a	1:100	Gift from Peter Brophy	
CASPR	Rabbit	1:1000	Abcam	AB34151
ChAT	Goat	1:200	Sigma	AB144P
CLAUDIN-11	Rabbit	1:75	Thermo Fisher Scientific	36-4500
CNP	mIgG2b	1:2000	Atlas	AMAB91072
GFAP	m-Cy3	1:500	Sigma	C9205
IBA1	Goat	1:500	Abcam	AB5076
ISLET1/2	mIgG2b	1:50	DSHB	39.4D5
MBP	Rat	1:100	Abcam	AB3749
NESTIN	mIgG1	1:300	Millipore	MAB5326
NEU-N	mIgG1	1:300	Millipore	CLONE A60 MAB377
NF-H	Chicken	1:100	Biolegend	822601
pan-NFASC	Chicken	1:50	Thermo Fisher Scientific	PA5-47468
O4	mIgM	1:300	R&Do Systems	MAB1326
OLIG2	Rabbit	1:250	Abcam	AB42453

P2RY12	Rabbit	1:200	Abcam	AB188968
PARVALBUMIN	Rabbit	1:500	SWant	PV27
PDGFR-α	Rabbit	1:250	CellSignaling	5241S
SOX10	Rabbit	1:500	Abcam	AB155279
TMEM119	Rabbit	1:200	Abcam	AB185333

Dyes	Dilution	Company	Cat #
DAPI	1:20000	Thermo Fisher Scientific	D1306

2˚ antibody	Fluorophore (λ)	Dilution	Company
Goat anti-chicken	Brilliant Violet 421	1:1000	Biolegend
Goat anti-mouse	488, 555, 647	1:1000	Abcam
Goat anti-rabbit	568, 647	1:1000	Abcam
Goat anti-rat	488	1:1000	Abcam
Goat anti-chicken	568, 647	1:1000	Abcam
Donkey anti-goat	488, 648	1:1000	Abcam

3.8 Confocal microscopy and image analysis

A Zeiss 710 confocal was used for each of the following: for cell counts, two z-stacks per myelinoid were acquired with a 40X (1.3 NA) objective. For manual tracings of individual oligodendrocytes, a 40X objective was used to create tiled z-stacks (typically 3x4 tiles, 20 μm z-depth with 0.25 μm z-steps), a minimum of 5 cells per myelinoid was measured. To acquire PNJs, a 63X oil objective (1.4 NA) was used. Image analysis was performed using FIJI with the cell counting plugin and Simple Neurite Tracer plugin (Longair et al. 2011). Nearest neighbour analysis was performed by plotting a 100 μm radius circle around individual cells and counting the number of myelinating oligodendrocytes within that area. All cell counts and analysis between experimental conditions were performed blinded by either blinding samples before image acquisition and/or running an ImageJ macro to blind and randomise files (see appendix).

3.9 Transmission electron microscopy

To demonstrate myelin compaction, myelinoids were fixed in phosphate buffer (PB) containing 4% PFA and 2% glutaraldehyde for 2 hours, post-fixed in 0.1% glutaraldehyde for 24 hours at 4°C and washed in 0.1 M PB (2 x 15 min). Samples were transferred to 1% OsO_4 in 0.1 M PB for 45 min at RT, washed in 0.1 M PB and then dehydrated in increasing concentrations of EtOH for 15 minutes each (50%, 70%, 90%, 100% x 3). Samples were then incubated in a 1:1 mix of Araldite-DDSA (Agar Scientific):acetone for 1 hour then transferred to Araldite-DDSA for overnight incubation, before being cured in Araldite embedding mix at 60°C for 48 hours. Ultrathin sections (60 nm thick) were cut, stained in Uranyl Acetate, and Lead Citrate then viewed using a JEOL JEM-1400 Plus TEM. Images were captured on a GATAN OneView camera.

3.10 ImageXpress image acquisition and metaxpress image analysis of myelin volume

An ImageXpress micro confocal was used to acquire whole-mounted myelinoids for automated analysis of myelin volume. Low magnification (4X) scans for each microscope slide were taken and acquisition areas were drawn around each myelinoid. Z-stacks of 12 μm (1 μm z-step) beginning at the superficial edge of each acquisition area were acquired using a 20X plan Apo objective, a 42 μm pin hole confocal mode with 10% overlap for stitching.

A custom module was designed to segment myelin volume in 3D. First, an adaptive threshold was used to segment either MBP or CNP staining. The Filter Mask tool was then used to remove objects with a Fiber Breadth > 16 μm, a Fiber Length < 10 μm and an Area < 45 μm^2. Objects were then shrunk by 4 pixels and a subsequent filter step removed objects that had an Elliptical Form Factor < 3.7, Fiber Breadth of > 8 μm, and an Intensity Standard Deviation < 1000. Keep Marked Objects was then used to retain objects from the first Filter Mask that overlaid with the second Filter Mask of shrunk objects. This step specifically helped remove the non-myelin objects including cell bodies and debris. The Find Blobs tool was used to further identify non-myelin objects with an approximate width between 8-100 μm, which were then enlarged by 5 pixels and subtracted from the Filter Mask. This step was repeated with blobs approximately 4-6 μm in width. Next, a 3D filter mask was obtained by connecting neighbouring z-steps using the Connect Touching Objects tool. A final filter step removed 3D objects with a volume ≤ 450 μm^3 and a diameter ≤ 45 μm. In order to measure NF-H intensity, a simple threshold was performed to segment the total image area and Connect by Touching was used to segment the total image volume. $DAPI^+$ nuclei were similarly identified using the 'find round objects' tool with typical dimensions between 5.7 and 9 μm and z-steps were stitched by connect best match. The volume of segmented myelin (μm^3), integrated intensity of $NF\text{-}H^+$ staining, DAPI number and SOX10 number were measured within the total image volume, summated for each acquisition site. Downstream analysis was performed using RStudio to process exported data tables, aggregate measurements for each myelinoid, and normalise data to a batch control.

3.11 Distribution correlations of myelinoid cell-types

To determine how the regional distribution of different cell-types correlated with each other in iPSC myelinoids, automated measurements were gathered from all control MI-12 myelinoids processed at the time (51 myelinoids from 11 conversions). In order to identify robustly myelinated samples, the maximum myelin score for each myelinoid was ranked and the top 50th percentile myelinoids were taken forward for correlation analysis (28 myelinoids from 6 conversions). The dataset was filtered to remove redundant acquisition sites with fewer than 100 DAPI+ cells. As the dataset was not large enough to run a mixed linear model with random effects, a linear model with robust standard errors was used.

3.12 Statistical analysis using R

Statistical analyses were performed using RStudio and the generalised mixed models plugin glmmTMB (Brooks et al. 2017). Analysis of myelin sheath length over time was performed using mean sheath length as the dependent variable. Individual myelinoids were included as a random effect (with random intercepts) to accommodate for nesting of data (Aarts et al. 2014). Analysis of sheath number and mean sheath length per cell were performed with treatment conditions as fixed effects (e.g. TeNT) and each myelinoid and cell line were included as random effects. Automated analysis of myelin volume was performed with TeNT as a fixed effect and each conversion of iPSCs included as a random effect. For correlating automated measurements of cell densities, a linear model was used with robust standard errors.

Chapter 4 Human iPSC-derived CNS-patterned spheroids demonstrate compact myelin formation.

4.1 Introduction

In vitro generation of iPSC-derived oligodendrocytes has provided a major advancement in our ability to ask questions related to human oligodendrocyte biology in development, in response to pharmacological manipulation, in the context of genetic perturbations (Vasistha et al. 2019; Osipovitch et al. 2018; Ehrlich et al. 2017; Ferraiuolo et al. 2016) and to explore the recently identified gene-expression differences between both between mouse and human oligodendroglia (Hodge et al. 2018; Xu et al. 2018) and in human disease (Jäkel et al. 2019). However, there exists a paucity of methods to investigate the most critical function of iPSC-derived oligodendrocytes: forming myelin. Currently, the most reliable method involves transplantation of iPSC derived OPCs into the shiverer mouse brain, which is devoid of endogenous compact myelin (Wang et al. 2013; Vasistha et al. 2019). *In vitro* models of myelin development are desired due to the advantages of an accessible environment for pharmacological modulation, increased experimental throughput and improved reproducibility. Currently, human pluripotent stem cell-derived models have so far failed to give rise to robustly myelinating cultures with appropriate myelinated axon organisation. Against this background, I set out to generate a humanised model of myelination using iPSC-derived cells to understand the cellular processes that regulate human myelin development and also permit investigations of normal and pathogenic myelin development using patient-derived cell lines.

As I will describe in this chapter, an iPSC-derived organoid model that demonstrates temporal formation of compact myelin was developed following a series of unsuccessful approaches in which dissociated iPSC-derived OPCs were added to human and rodent neuronal cultures. I characterise the cell-types and temporal development of myelin formation within myelinating organoid and assessed the thickness and integrity of myelin and the organisation of myelinated axon sub-domains. Finally, I identify the regional distribution of myelin within these cultures and investigate the sub-types of neurons being myelinated in this model.

4.2 Results

4.2.1 Generation of iPSC-derived oligodendrocytes

The healthy control human induced pluripotent stem cell (iPSC) lines used for the completion of this thesis were CS02iCTR-NTn1 (iPSC1), CS25iCTRL-18n2 (iPSC2), which were purchased from Cedars Sinai. These and other cell lines were maintained on Matrigel-coated culture plates in E8 medium. iPSCs were positive for pluripotency markers TRA-1-60, OCT3/4, and NANOG, and were shown to be karyotypically normal (Figure 4.1A).

In order to generate oligodendrocytes from iPSCs, I used a protocol that was established by a previous post-doctoral researcher in the Chandran lab, Dr Dario Magnani (Figure 4.1B) (Livesey, Magnani, Cleary, Vasistha, James, Selvaraj, Burr, Story, Shaw, Kind, Hardingham, Wyllie & Chandran 2016a). This protocol—similarly to others that have been established by different research groups (Wang et al. 2013; Douvaras et al. 2014)—involves patterning neuroepithelial cells towards the pMN domain of the developing spinal cord, which gives rise to both motor neurons and oligodendrocytes during development, in a time-dependent manner (Rowitch 2004). Specification of the pMN domain begins by enzymatic detachment of confluent iPSC colonies, transfer to orbital shakers to encourage embryoid body formation, and patterning with dual SMAD inhibition to direct cells towards neuroectoderm. Subsequent exposure to retinoic acid and sonic hedgehog agonist pattern cells towards a caudal and ventral fate, respectively. Efficient targeting of the pMN domain can be determined by the expression of OLIG2. At week 5, the mitogens PDGF-AA and FGF-2 are used to induce oligodendroglial cell-fate and expand the cycling population of oligodendrocyte progenitor cells (OPCs). During this period, oligodendrocyte progenitor spheroids are mechanically dissociated and re-formed to yield a higher proportion of OPCs by expanding the surface area of cells exposed to media growth factors. This process also reduces the neuronal contamination of cultures by axotomisation and prevents the aggregation of spheroids into large clumps. Two to four weeks after oligodendroglial induction, spheroids are enzymatically dissociated into single cells and plated on matrigel-laminin-fibronectin-

coated coverslips, or plates, and maintained in medium devoid of growth factors for up to 21 days. Successful generation of iPSC-derived oligodendrocytes at d14 post-plate down is shown in Figure 4.1C, where OPCs and oligodendrocytes are labelled by PDGFR-α and O4, respectively. The full range of cell-types generated from this protocol which includes OLIG2^{+} pMN derived cells, GFAP^{+} astrocytes, and NF-H^{+} neurons, are shown in Figure 4.1D.

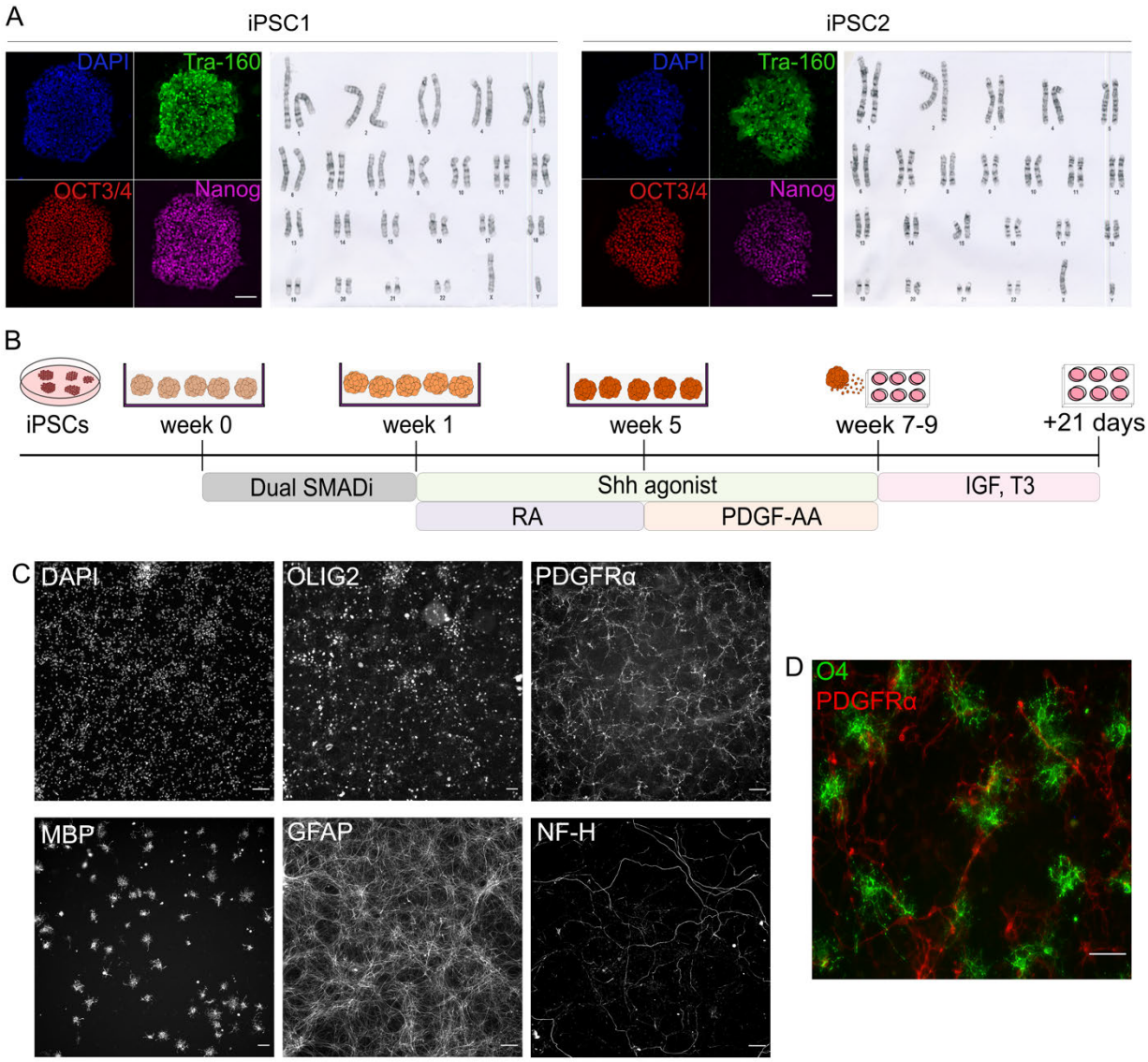

Figure 4.1 Generation of iPSC derived oligodendrocytes

A) Immunocytochemical staining of iPSC colonies demonstrating positive expression of pluripotency markers TRA-1-60, OCT3/4 and NANOG, and normal karyotype analysis for two different iPSC lines.

B) Schematic overview of the protocol to generate iPSC-derived oligodendrocytes.

C) Representative images for other cell-types present in glia-progenitor spheroids including DAPI$^+$ nuclei, OLIG2$^+$ pMN derived cells, PDGFRα$^+$ OPCs, MBP$^+$ oligodendrocytes, GFAP$^+$ astrocytes and NF-H$^+$ axons.

D) Representative images of iPSC-derived OPCs and oligodendrocytes.

All scale bars = 100 μm .

4.2.2 Co-culture with iPSC-derived motor neurons

In order to determine whether iPSC-derived oligodendrocytes have the capacity to form myelin *in vitro,* I performed a series of co-culture experiments using different neuronal substrates.

As our aim was to develop an entirely human-derived culture system, I first performed two-dimensional co-culture experiments with human iPSC-derived neurons. iPSC-derived motor neuron (MN) cultures were chosen, as they comprise a purely neuronal composition without contamination by glial cells and reflect the appropriate target for myelination by pMN-derived oligodendrocytes, *in vivo*. These cultures were generated by Dr Bhuvaneish Selvaraj in the Chandran lab using a protocol that similarly patterns iPSC-derived neurospheres towards the pMN domain (see Methods) (Selvaraj et al. 2018).

After 16 days, MN spheres were dissociated, plated as single cells and maintained for 3 weeks in defined neuronal medium. Oligodendrocyte differentiation medium was gradually incorporated over 2 days (final concentration 1:1) prior to the addition of OPCs. Following dissociation of oligodendrocyte progenitor spheres, between 50,000 and 300,000 cells were added to each 24-well-plate well of neurons and maintained for an additional 3 weeks in 1:1 neuronal: oligodendrocyte medium, before being fixed and stained for Tau, O4 and MBP. Figure 4.2 shows representative images of the co-culture including magnified images of individual MBP+ oligodendrocytes after 3 weeks of co-culture. Whilst some association can be seen between oligodendrocyte processes and neurons, no ensheathment was observed.

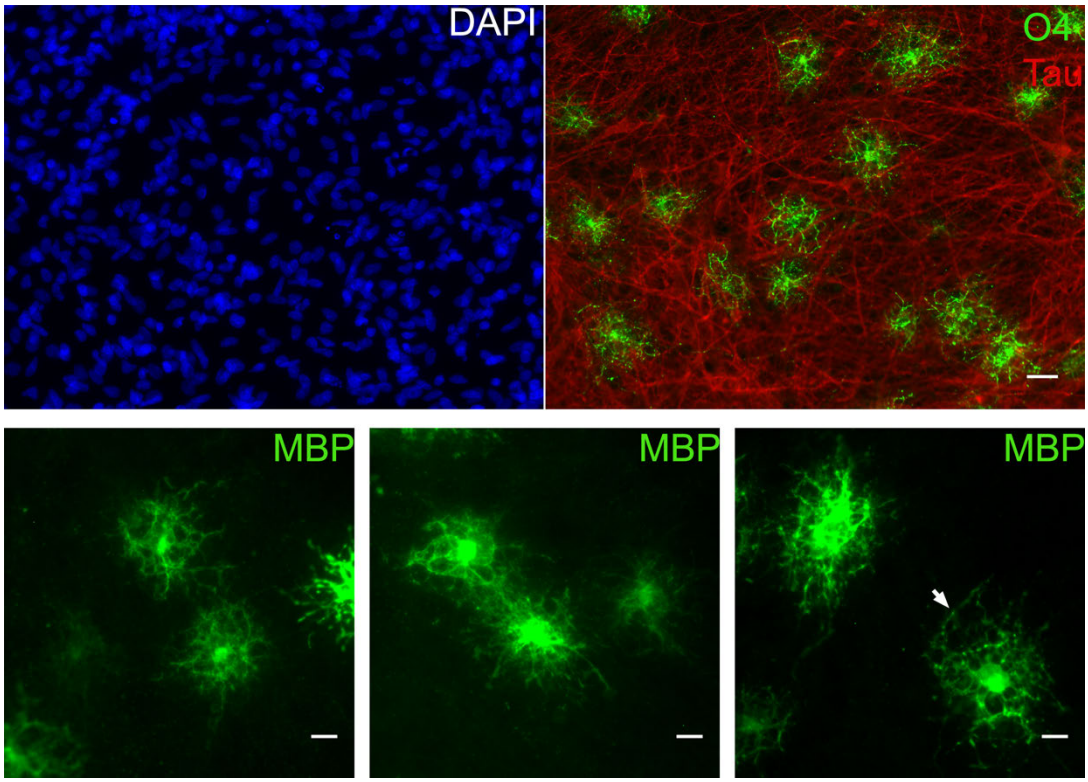

Figure 4.2 Co-culture with iPSC-derived neurons

200,000 cells dissociated from oligodendrocyte progenitor spheres were added to 3-week-old neuron cultures and co-cultured for 3 weeks.

Top panel shows the density of respective cell-types (scale 25 μm).

Lower panels show highly branched oligodendrocytes and linear arrangement of processes suggestive of axonal association (arrow), but no myelin formation (scale 10μm);

N = 2 conversions, n = 6 coverslips.

The reasons for failure are unclear. It is possible that a baseline of neuronal activity is required to induce myelin formation and that 3- to 5-week-old neurons fall beneath this threshold. This is unlikely, however, as rodent-derived oligodendrocytes have been shown to ensheath inert fibres that mimic axonal structures (Bechler et al. 2015) and one would assume that human oligodendrocytes have the capacity to behave similarly. It is possible that, for myelination to take place, human oligodendrocytes require long-term culture, which accommodates the protracted period of myelination *in vivo.* Unfortunately, in this culture paradigm, cells began to lift away from the coverslip after 3 weeks of co-culture and the experiment could not be continued. Indeed, other research groups that have performed similar humanised co-cultures have had very limited success at inducing myelin formation and have each been limited to 2–4 weeks of co-culture (Kerman et al. 2015; Wang et al. 2013).

4.2.3 Co-culture with rat dorsal root ganglion neurons

Given that our human:human co-cultures failed to give rise to myelin formation *in vitro*, I resorted to a more established model of *in vitro* myelination to test whether human iPSC-derived oligodendrocytes were capable of *in vitro* myelination: co-culture with embryonic rat dorsal-root ganglion (DRG) neurons.

Dr Marie Bechler of the ffrench-Constant lab provided training to establish cultures of E15.5 rat DRGs. Briefly, E15.5 rat embryos were dissected, and their spinal cords were removed. Dorsal root ganglia were plucked individually, dissociated, and plated at a density of 200,000 cells per coverslip. Proliferating cells were selectively removed by treatment with fluoro-deoxyuridine (FdU) and the cultures were maintained for three weeks in the presence of NGF to promote neurite extension. Subsequently, oligodendrocyte progenitor spheres were dissociated, as before, and between 150,000 and 300,000 cells were seeded onto DRG cultures. After 4 weeks of co-culture, coverslips were fixed and stained for SMI-312, GFAP, and MBP.

As found in the human neuron co-culture, oligodendrocytes were widely distributed among SMI-312$^+$ processes with highly branched morphologies. However, in contrast to the above, oligodendrocytes were occasionally associated with thick, linear MBP$^+$ processes, aligned with SMI-312$^+$ axons, indicative of early myelin sheaths (Figure 4.3). The majority of oligodendrocytes observed had 1 or 2 myelin sheaths per cell, in addition to numerous thin, arborized non-myelinating processes, reflecting the immaturity of myelin formation. Whilst this was encouraging, the survival of co-cultures was a considerable issue as the dense structure of axons would often peel away from the coverslip, terminating the experiment. Over 8 independent preparations of DRG cultures, approximately half were viable after 4 weeks of co-culture. Further optimisation would certainly have improved matters, including the addition of FdU to limit the proliferation of human cells, however, success in another culture paradigm resulted in progressing from this set-up.

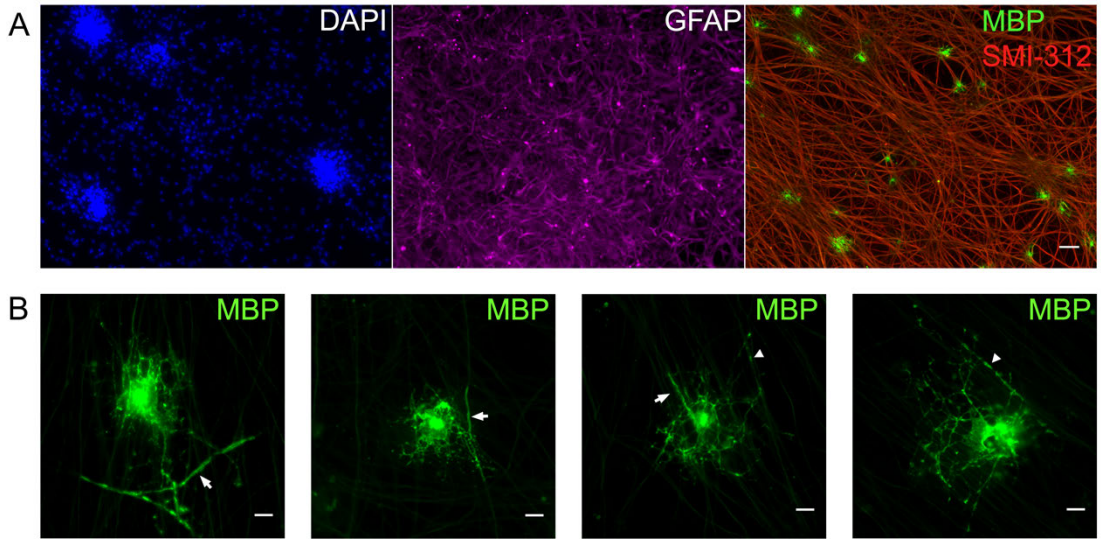

Figure 4.3 iPSC-derived oligodendrocyte co-culture with E15.5 DRGs.

250,000 cells from dissociated oligodendrocyte progenitor spheroids were added to 3-week-old DRG neuron cultures and maintained for 4 weeks.
A) representative image of co-culture demonstrating the density of GFAP+ astrocytes, MBP+ oligodendrocytes and SMI-312+ axons, scale = 50μm.
B) Individual oligodendrocytes show early signs of wrapping (arrow heads) and structures indicative of myelin sheaths (arrows). Scale = 10μm
Data collected from N = 4 independent preparations, n = 8 coverslips.

4.2.4 Co-culture with shiverer mouse organotypic slice cultures

Another routinely used model for examining the myelinating potential of OPCs *in vitro* is their co-culture with shiverer mouse organotypic slice cultures. The advantages of shiverer mouse organotypic slice co-cultures over conventional co-culture methods include a microenvironment that mimics the appropriate *in vivo* environment, preservation of the relevant cytoarchitecture and cell-types, and their ability to be maintained for longer durations (e.g. Bin et al. (2012) maintained their cultures for over two months), which contributes to the greater degree of myelination often associated with these cultures. Organotypic slice cultures of the shiverer mouse brain and spinal cord have been used to assess myelin formation *in vitro* when co-cultured with OPCs from mice, rats, and human fetal material (Bin et al. 2012) and from human embryonic stem cell-derived oligodendrocytes (Izrael et al. 2007).

Dr Navneet Vasistha of the Chandran lab provided technical assistance in optimising shiverer mouse organotypic slice cultures. Given that myelin development in heterozygous shiverer mice *mbp*$^{+/-}$ is largely unaffected (Martin et al. 2006), it was necessary to use only homozygous *mbp*$^{-/-}$ mice for co-culture experiments. P0-P1 neonatal mice were therefore genotyped for the presence or absence of the complete MBP gene by PCR, using DNA lysed from tail cuts (see Methods). Next, shiverer mouse brains were collected from P2-P4 mice and 300μm forebrain sections were cut using a vibratome and transferred onto millicell culture inserts and maintained in slice culture medium. Over 3 days, the serum content of the slice culture medium was reduced as it has been shown to be detrimental for myelin induction by transplanted cells (Bin et al. 2012). After 7 days of culture, sections became opaque as they stabilised.

To co-culture hOPCs, oligodendrocyte progenitor spheroids were dissociated as before and 250,000 cells were added to each section on day 7 in a total volume of 5μl (Figure 4.4A). After 2–4 weeks of co-culture, human cells, identified by the hNu antibody, were sparse (Figure 4.4B). MBP^{+} human cells were present but were few in number and extended only flat membranous sheets and not myelin sheaths (Figure 4.4B). Cell loss and degradation were occasionally found in co-cultured slices, which

was possibly due to disruption of the liquid-air interface that is necessary for slice culture maintenance. Stereotactic injection of hOPCs into the slice culture would potentially improve survival and yield myelin formation over time. However, success in an alternative culture set-up resulted in a change in emphasis and no further work with dissociated hOPCs was undertaken.

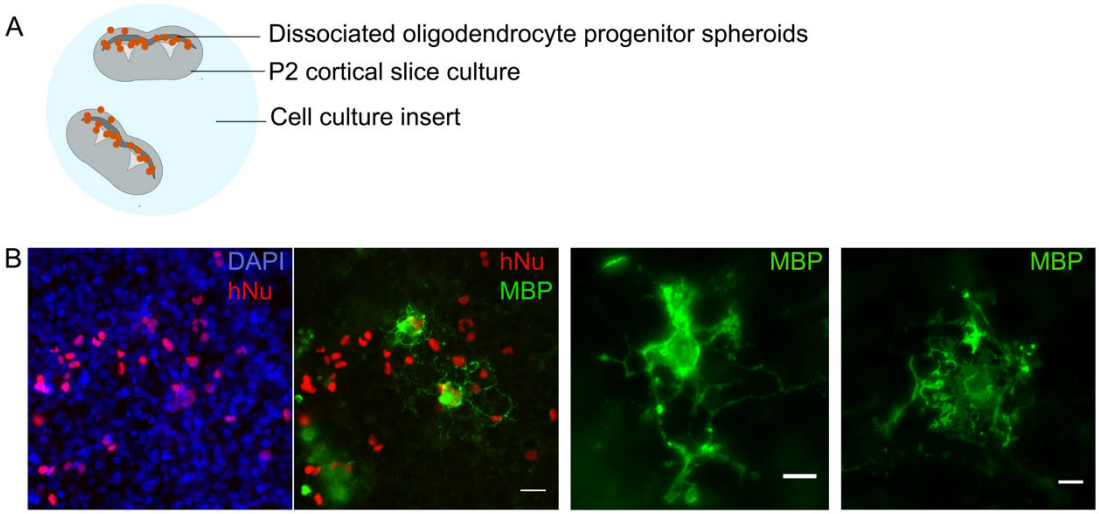

Figure 4.4 iPSC-derived oligodendrocyte co-culture with shiverer mouse organotypic slice culture.

Between 10 and 50,000 cells from dissociated oligodendrocyte progenitor spheroids were added on top of 7-day-old cortical organotypic slice cultures prepared from P2-P4 pups.

A) Schematic showing experimental set-up.

B) Human oligodendrocytes are identified by the Human Nuclei antibody and MBP. Oligodendrocytes are sparse and without myelinating processes.

N = 8 preparations, n = 6 slices each. Scale = 10μm.

4.2.5 Intra-spheroid myelination in iPSC-derived cultures

In order to improve the survival of both human cells and slice culture in co-culture, I attempted an alternative experimental paradigm that involved migration of OPCs from oligodendrocyte progenitor spheroids into the organotypic slice culture. Previously, it has been shown that cerebellar organotypic slice cultures prepared from WT newborn mice—treated with cytosine arabinoside to suppress myelination—could be rescued by overlaying explanted slice cultures that had not been exposed to cytosine arabinoside, demonstrating that oligodendrocytes could migrate from an overlaid tissue section to myelinate the underlying slice culture (Seil & Blank 1981). A similar phenomenon appeared when WT optic nerves were transplanted into shiverer mouse cerebellar cultures with resulting MBP^+ and compact myelin being found within the shiverer slice culture (Billings-Gagliardi et al. 1984). Given that when glial progenitor spheroids are dropped onto plastic or glass-coated coverslips, a large number of OPCs migrate out of adhered spheroids (In-house observations, Douvaras et al. 2015), I asked whether dropping intact spheroids onto slice cultures in close proximity to the corpus callosum would result in OPC migration into the slice culture and myelination of mouse neurons. This strategy would avoid both the mechanical dissociation of spheroids and the flooding of slice cultures with excess media. A schematic of the experimental set-up and a phase-contrast image of the co-culture is shown in Figure 4.5A-B.

After two weeks in culture, we observed (for the first time) tube-like MBP^+ segments, indicative of *in vivo* myelin sheaths, developing within the confines of the spheroid placed onto the shiverer cortical slice culture—identified by phase contrast and an antibody against human nuclei (hNu) staining (Figure 4.5C). On closer examination, individual human myelinating oligodendrocytes could be identified by co-labelling of MBP and hNu (Figure 4.5D-E). Intriguingly, the circular arrangement of MBP^+ structures and the high density of human nuclei observed in this co-culture suggested that hOPCs were not migrating out of the transplanted spheroids into the surrounding tissue but rather were forming myelin within the margins of iPSC-derived spheroids.

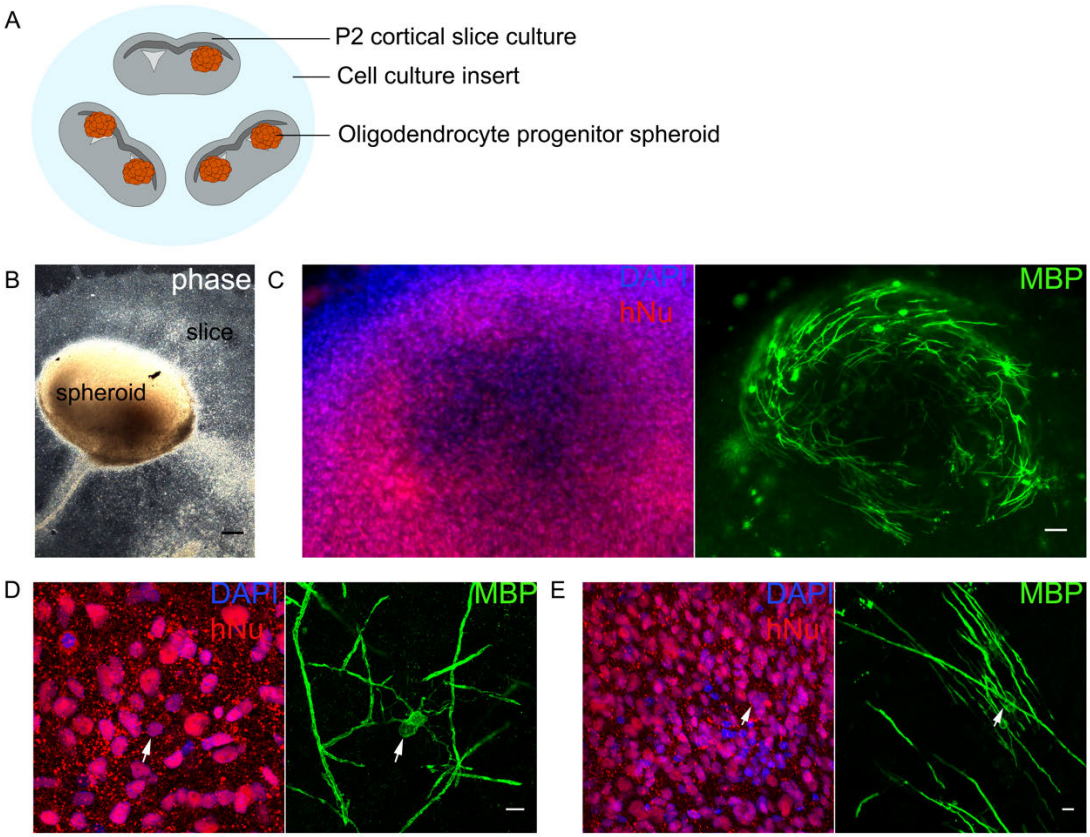

Figure 4.5 iPSC-derived oligodendrocyte progenitor spheroids co-culture with mouse shiverer organotypic slice culture.

Oligodendrocyte progenitor spheroids were added on top of cortical shiverer mouse slice cultures without dissociation.

A) Schematic showing experimental set-up.

B) Phase contrast and hNu staining shows the demarcation where individual spheroids were placed. MBP staining is constrained to the region of hNu+ cells (scale 200μm).

C) Magnified view of spheroid-slice boundary identified by human nuclei. MBP staining is constrained within the perimeter of the sphere (scale = 15μm).

D-E) Individual human oligodendrocytes associated with myelin sheaths, stained with hNu (arrows) and MBP (scale = 10μm).

Based on this pattern, I asked whether oligodendrocytes were myelinating mouse neurons present in the brain slice or human neurons present within the spheroid. As our protocol mimics the developmental trajectory of the pMN domain of the ventral telencephalon, motor-neurons are also generated at the early stages of patterning, which is followed by a switch from neurogenesis to gliogenesis (Stacpoole et al. 2013). Therefore, it is possible that intra-spheroid neurons could serve as a substrate for myelination, though the neuronal contribution to monocultures derived from dissociated spheroids is minimal (Figure 4.1C, Livesey, Magnani, Cleary, Vasistha, James, Selvaraj, Burr, Story, Shaw, Kind, Hardingham, Wyllie & Chandran 2016a).

In order to determine which neuronal population was being myelinated, I adapted the culture conditions. Instead of the direct co-culture of oligodendrocyte progenitor spheroids and cortical slices (Figure 4.6A), spheroids were transferred either onto cell culture inserts to be cultured in isolation (Figure 4.6A) or next to cortical slices without direct contact (Figure 4.6B). Analysis at 8 weeks post-plate down demonstrates the presence of MBP+ myelinating oligodendrocytes in both isolated spheroids (Figure 4.6C) and non-contact co-cultured spheroids (data not shown). Numerous MBP^+ sheaths were identified and showed co-localisation with NF-H^+ axons (Figure 4.6D-E).

These results led me to conclude that human myelin formation occurs within intact three-dimensional iPSC-derived spheroids, hereafter referred to as “myelinoids”, cultured on membrane inserts and that this is independent of soluble signals secreted by the shiverer cortical slice. Further investigations of iPSC-myelinoids were made in the absence of organotypic slice cultures.

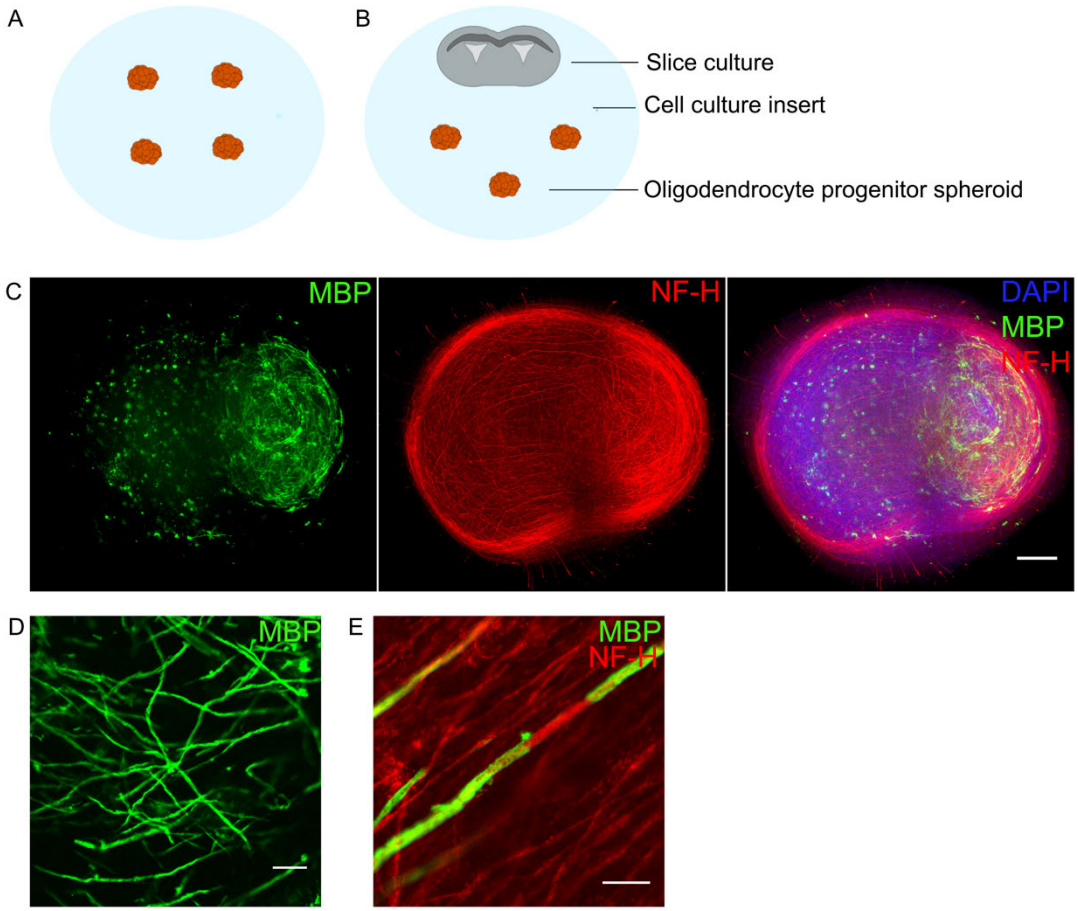

Figure 4.6 Oligodendrocyte progenitor spheroids cultured away from organotypic slice culture

A-B) Schematic of experimental set-up. Oligodendrocyte progenitor spheroids were either transferred to cell culture inserts in isolation away from organotypic slice cultures, or next to organotypic cultures.

C) Representative image of a single oligodendrocyte progenitor spheroid in isolation (experimental set-up A) showing MBP^+ myelin-like staining and NFH^+ axons (scale 50μm). D) MBP^+ structures demonstrate typical myelin morphology (scale 25μm). E) MBP^+ structures co-localise with $NF\text{-}H^+$ axons (scale 10μm).

4.2.6 Characterisation of iPSC myelinoids

The result that there was sufficient axonal content in glial progenitor spheroids to give rise to myelination was somewhat of a surprise. However, the low neuronal content observed in dissociated cultures is likely due to axotomy of neurons during the mechanical dissociation of spheroids, the short period of time that cultures were maintained (2–3 weeks) and the lack of neuronal-specific growth factors in the culture medium that would aid their recovery. Therefore, in order to characterise the starting point for iPSC-derived myelinating cultures, I first wanted to characterise the cell-types observed '*in-sphero'.*

The induction of myelin formation begins with the transfer of spheroids onto cell culture inserts after 2–3 weeks in oligodendrocyte proliferation medium. 'Myelin Induction' (MI) spheroids therefore were whole-mounted 24-hours after being transferred to cell culture inserts and used for immunocytochemical analysis of a range of cell-types.

Similar to the dissociated cultures, MI spheroids contain a large proportion of OLIG2+ cells, demonstrating efficient specification of the pMN domain *in vitro* and a high proportion of NESTIN+ neural progenitor cells (Figure 4.7). Oligodendroglial patterning was again demonstrated by the dense arrangement of SOX10+ nuclei and PDGFRα^{+} oligodendrocyte progenitor cells, as well as sparsely labelled MBP+ oligodendrocytes. Analysis of NF-H staining in MI spheroids revealed a dense arrangement of axons that can be seen to circle the periphery of the spheroid, forming close parallel tracts. Finally, a high proportion of GFAP+ astrocytes also exists within spheroids. This shows that MI spheroids contain a mixture of progenitor and differentiated cells across all CNS-derived cell-types, with an abundant axonal population that serves as a favourable environment for the *in vitro* study of human myelin development.

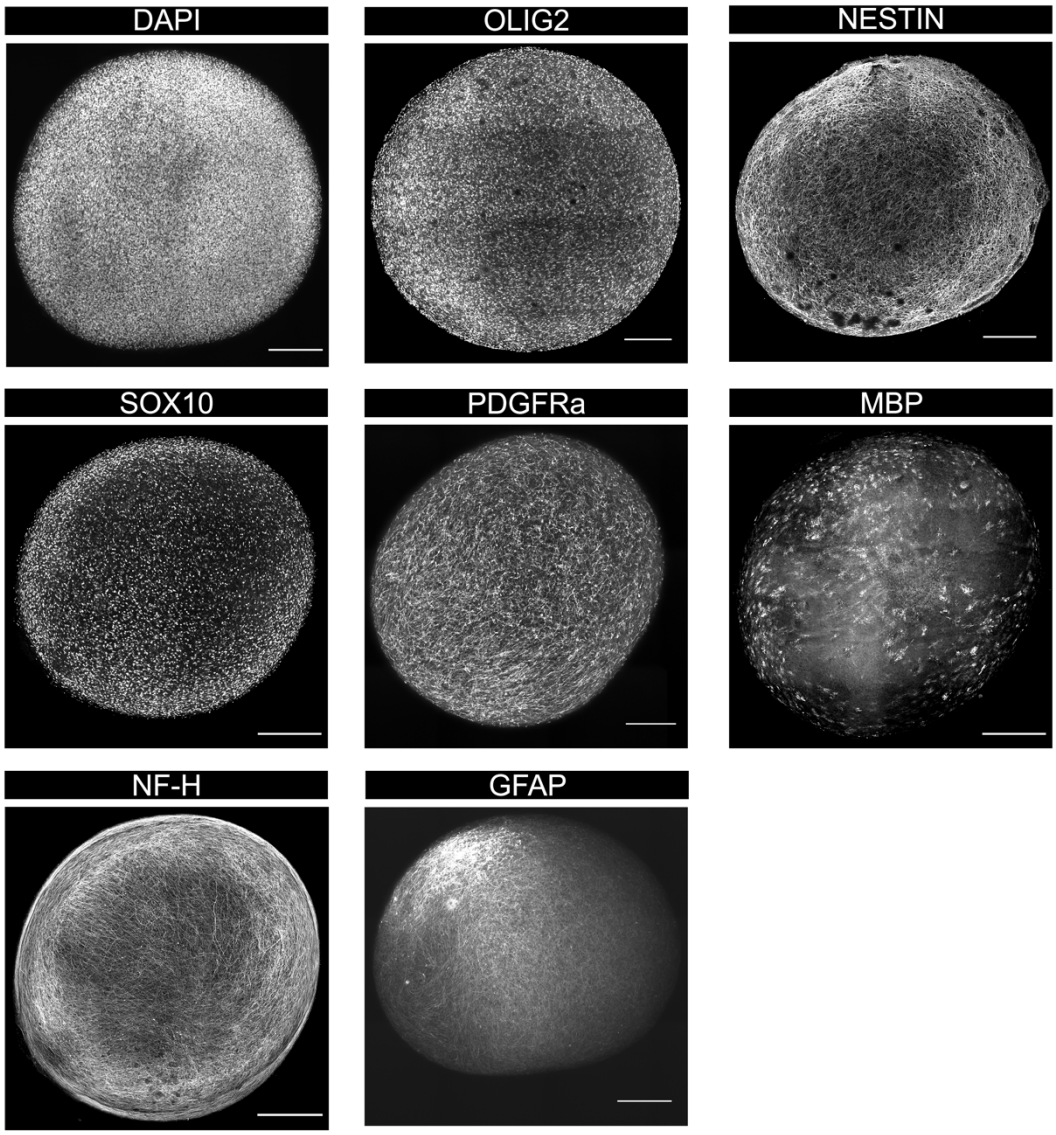

Figure 4.7 Myelin Induction (MI) spheroids contain a mixture of CNS-derived cell-types

iPSC myelinoids were fixed 24 hours after being transferred onto cell culture inserts, stained with a range of markers for different cell-types, whole-mounted, and imaged on the ImageXpress micro confocal. OLIG2 expression demonstrates pMN domain acquisition; NESTIN identifies neural progenitor cells; SOX10 identifies oligodendroglial cells; PDGFR-α identifies OPCs; MBP identifies mature oligodendrocytes; NF-H identifies neuronal axons; and GFAP identifies astrocytes. Scale 250μm.

4.2.7 Temporal development of iPSC-myelinoids

To profile the temporal development of iPSC-myelinoids, MI spheroids were cultured in differentiation medium for a further 4, 8, and 12 weeks and subjected to immunocytochemistry. These time-points are referred to as MI-4, MI-8, and MI-12, respectively. A revised schematic outlining the protocol for iPSC myelinoids is shown in Figure 4.8A.

Firstly, phase contrast images of spheroids were acquired at different time-points throughout the culture period and their diameters recorded. Figure 4.8B shows an overview of the entire culture process and the change in spheroid diameter over time. Between week 5 and MI there is a doubling of spheroid diameter due to the expansion of oligodendrocyte progenitor cells in the presence of FGF2. It is at this time-point that glial progenitor spheroids are transferred onto cell culture inserts. The subsequent increase in spheroid diameter between MI and MI-4 is due to flattening of spheroids on the membrane, a process that also occurs in the culture of organotypic slices. Subsequently, no further increase in diameter is seen, even when spheroids were maintained for an additional 20 weeks.

It is important to select spheroids of a similar size at the myelination induction phase to mitigate any potential variability in myelin formation at later time-points. During the generation of glial progenitor spheres, individual spheroid diameters can vary significantly. However, as long as there is sufficient supply of material, it is possible to be accurate in choosing spheres of a consistent size. Figure 4.8C shows the variability in the diameter of spheroids that have been transferred onto cell culture inserts (mean MI spheroid diameter = 577 μm). The standard deviation of MI spheroid diameter across conversions was 123 μm. However, the mean standard deviation of MI spheroid diameter within conversions was 76 μm, demonstrating reduced within-batch variability in spheroid diameter.

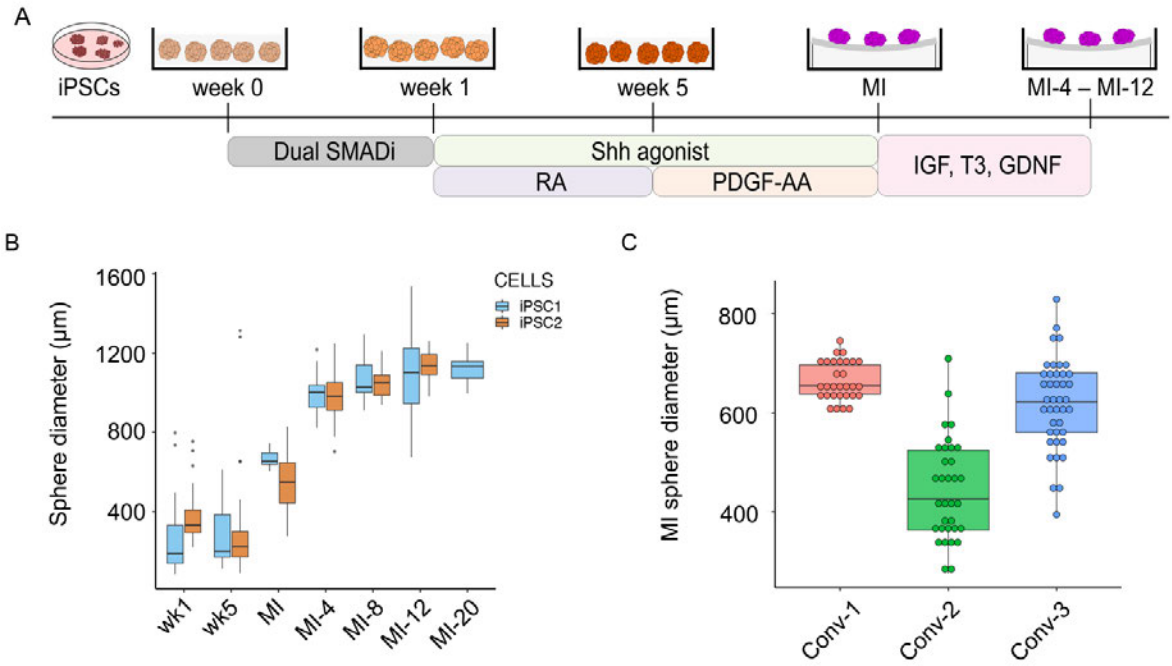

Figure 4.8 Temporal development of iPSC myelinoids 1

A) Schematic overview of the revised protocol to generate iPSC myelinoids.

B) Sphere diameter increases over time and stabilises from MI-4 onwards.

C) Sphere diameter varies within and between individual conversions.

To visualise the temporal development of myelin, iPSC-myelinoids were fixed at MI, MI-4, MI-8, and MI-12 and stained for CNP, NF-H, and SOX10 (Figure 4.9). 25 μm z-stacks were acquired on the ImageXpress spinning disc micro confocal microscope and best projection images were stitched together using an image-J macro (see Appendix, Chapter 10.2). Representative figures of whole-mounted myelinoids, acquired in a similar fashion, are shown throughout this thesis.

The profile of CNP^+ oligodendrocytes across the surface of iPSC-myelinoids changes over time. The first four weeks between MI and MI-4 show a large increase in the number of CNP^+ oligodendrocytes, which are primarily located around the periphery of the spheroid. The majority of these cells do not show evidence of myelin formation though few have begun to form myelin sheaths. Between MI-4 and MI-8, the number of myelinating oligodendrocytes, and of myelin sheaths, has increased, though many non-myelinating cells persist around the periphery. Finally, by MI-12, a dense arrangement of myelinating oligodendrocytes is observed across the surface of the spheroid. Myelin is found always in areas of high axonal density, which is something that I have analysed further in Chapter 7. The density of $SOX10^+$ cells, which identifies oligodendrocyte progenitor cells as well as differentiated oligodendrocytes, varies between spheroids over time but is uniformly distributed across the sphere (see Chapter 7).

Given that these images were acquired from whole-mounted myelinoids and re-constructed as best projection images from 25μm z-stacks, they do not provide detail as to the distribution of myelin within the spheroid. Are oligodendrocytes distributed evenly throughout the spheroid or only around the outer areas of the spheroid, as visualised in the above images? To answer these questions, cryosections were taken of myelinoids at MI-12 and the distribution of cell-types analysed.

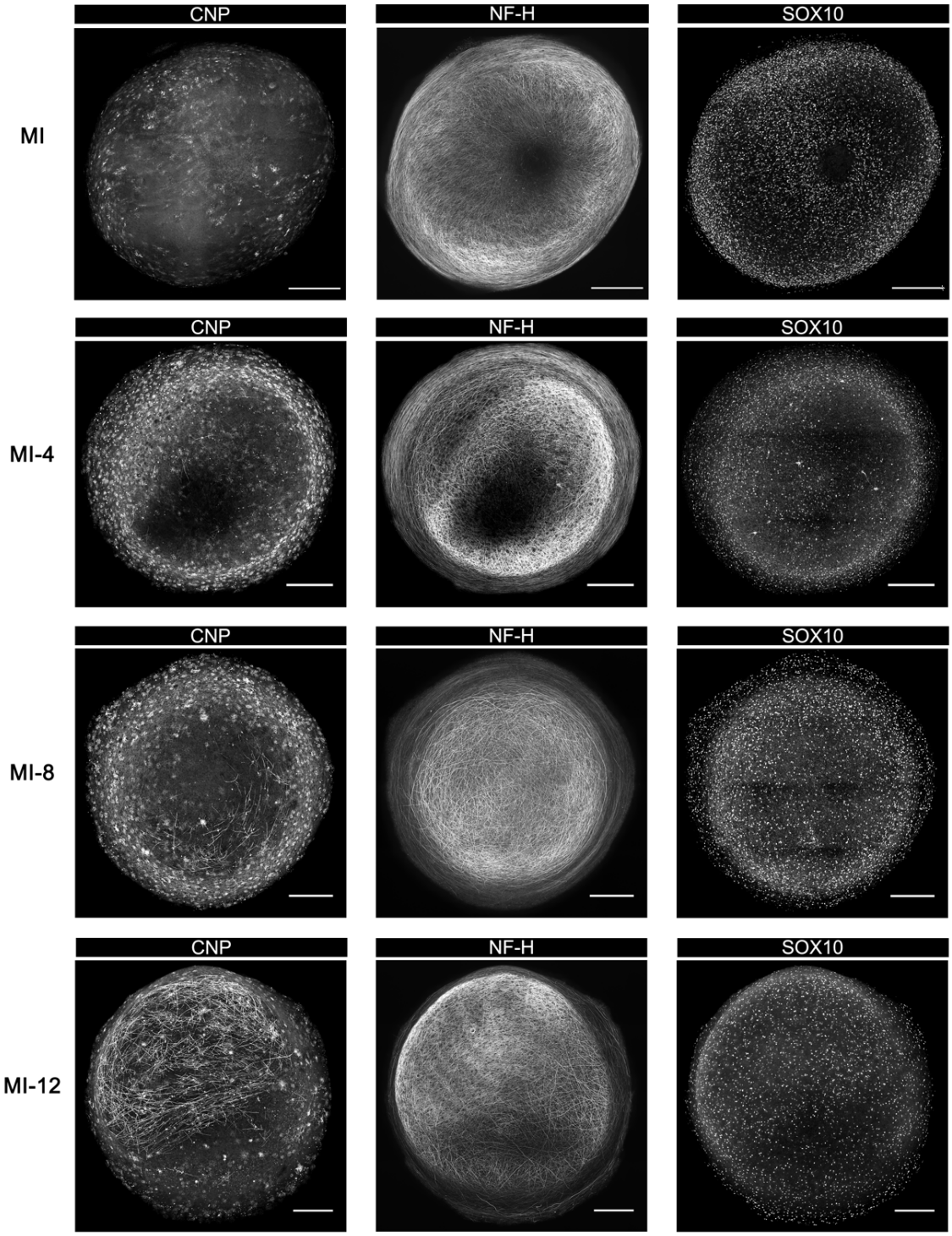

Figure 4.9 Temporal development of iPSC myelinoids 2

Myelinoids at MI, MI-4, MI-8, and MI-12 were stained for CNP, NF-H, and SOX10, whole-mounted, and imaged on the ImageXpress micro confocal. Scale = 250μm.

4.2.8 Regional distribution of myelin in iPSC myelinoids

In order to determine the distribution of myelin throughout iPSC-derived myelinoids, 10μm cryosections were cut from MI-12 spheroids and stained for MBP. Images were acquired from sections at their largest diameter and their smallest diameter, corresponding to the middle and superficial regions of myelinoids, respectively. Example images of an MI-12 mid-section and superficial-section are shown in Figure 4.10A-B.

To quantify the regional distribution of myelin across cryosections, images were thresholded and binarized. Next, a 100μm wide rectangle region of interest (ROI) spanning the diameter of the sphere was drawn and an intensity profile was measured to count the number of MBP+ pixels as a function of length across each section (illustrated in Figure 4.10C). Several intensity measurements were measured per section in both the vertical and horizontal axes. Each ROI was binned into 5 equal lengths to represent 'peripheral', 'intermediate', and 'central' domains of each region of interest, and the intensity profile for each domain was plotted on a graph.

Figures 4.10D-E show that, while in mid-sectioned myelinoids MBP+ pixels are mostly found in the periphery of the section, in superficial sections MBP+ pixels are evenly distributed across each domain. These results show that myelin is distributed around the periphery of spheroids, with highest intensity profiles in the outer domain of spheres and little to no myelin found in the inner regions of the sphere. Comparing these findings with the observations made on whole-mounted myelinoids, I have drawn a schematic representation of myelin distribution throughout iPSC-myelinoids (Figure 4.11). In addition, I have included a depiction of the imaging paradigm for whole-mounted myelinoids, which, in essence, aims to capture a z-stack of the peripheral domain of myelinoids where myelin is most dense.

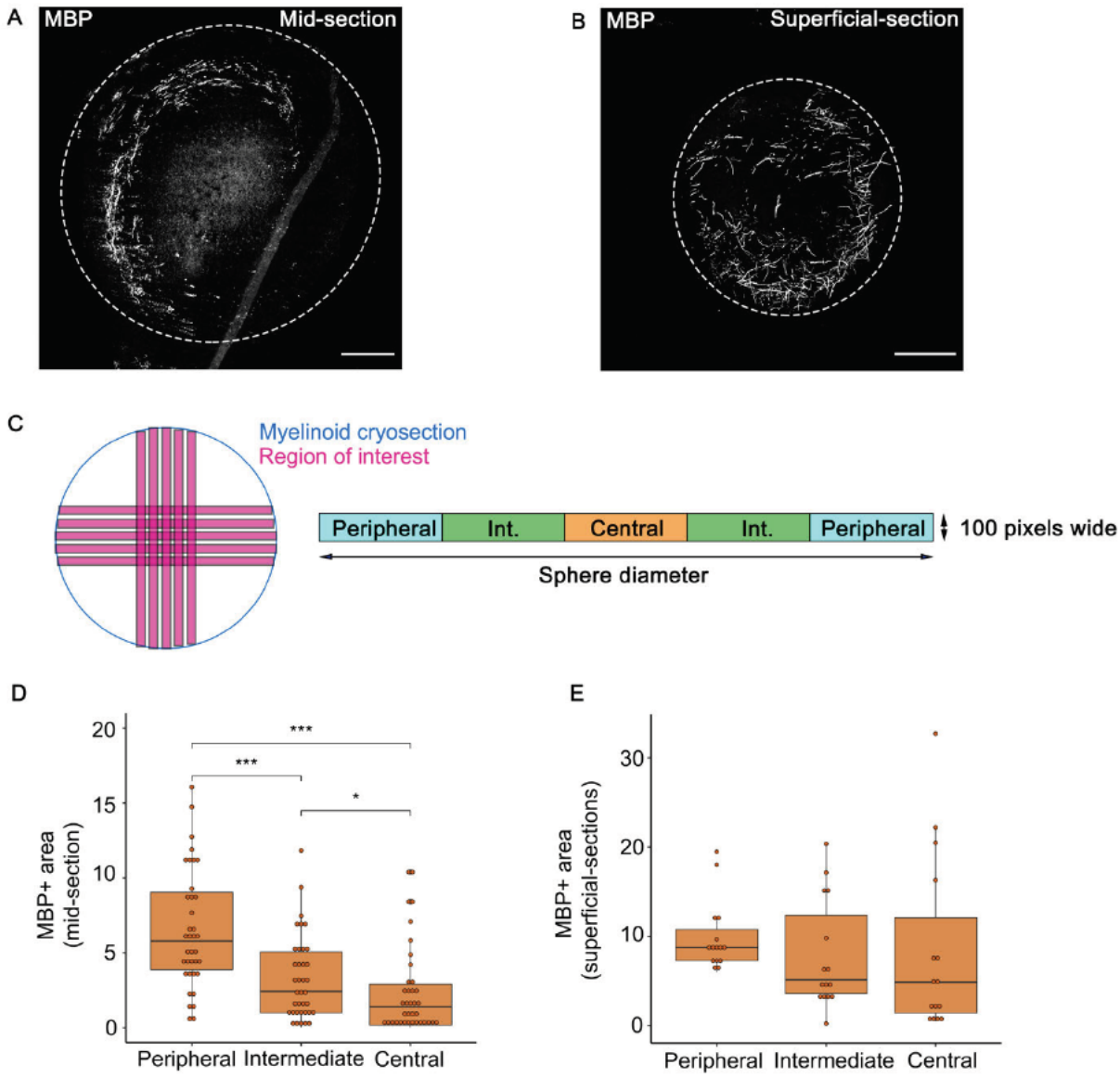

Figure 4.10 Regional distribution of myelin throughout iPSC myelinoids

10μm cryosections of MI-12 myelinoids were cut and stained for MBP to visualise the distribution of myelin throughout iPSC myelinoids.

A) Representative image of MBP+ myelin in the middle portion of myelinoids shows myelin around the periphery (dashed line indicates section perimeter), scale = 250μm.

B) Representative image of MBP+ myelin from a superficial section shows myelin across the entire area of the myelinoid (dashed line indicates section perimeter), scale = 250μm.

C) Schematic overview for quantifying distribution of MBP+ pixels (Int = intermediate).

D-E) Quantification of MBP distribution across middle and superficial myelinoid sections.

$p < 0.05$ *, $p < 0.01$ **, $p < 0.001$ *** glm with dummy variables for each region. n= 37 sections across 5 myelinoid preparations.

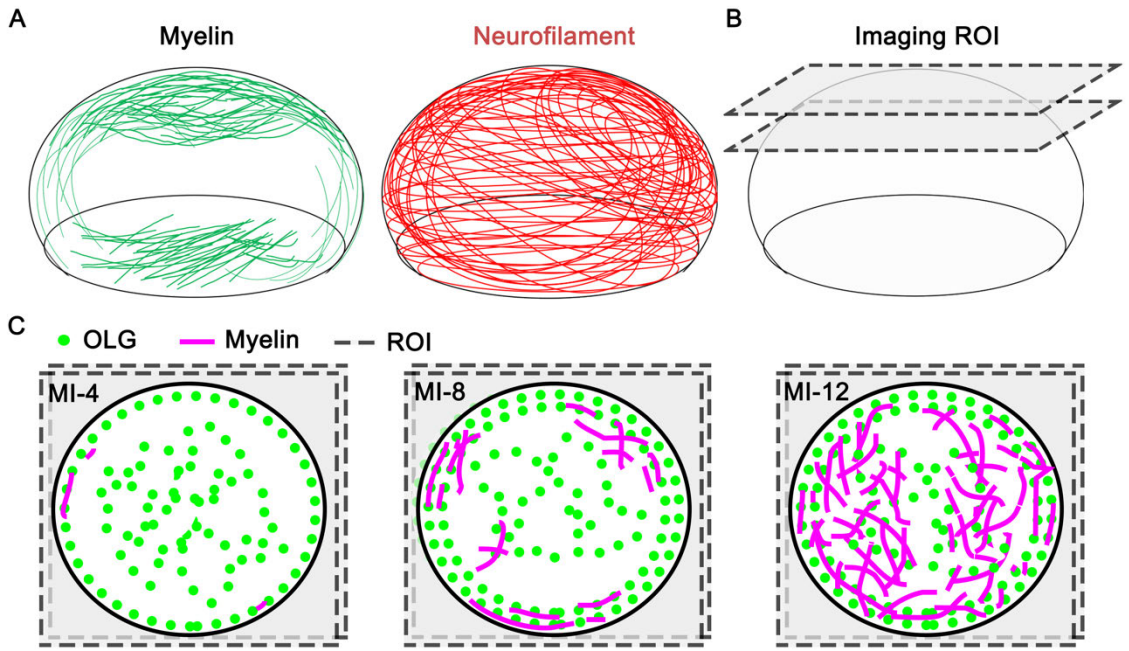

Figure 4.11 Schematic depiction of myelin distribution in myelinoids

A) Schematic depiction of the distribution of myelin and NF-H^{+} axons across iPSC myelinoids.

B) Imaging set-up for whole-mounted myelinoids captures myelin formation in the outer 1/3rd of myelinoids.

C) Schematic representation of myelin visualised within the ROI from B at MI-4, MI-8, and MI-12.

4.2.9 Oligodendrocyte morphology over time

Myelination is a process that requires extensive re-organisation of the cytoskeleton, as oligodendrocytes elaborate large swathes of membrane around multiple axons simultaneously. Many of the nascent myelin sheaths that are formed are subsequently retracted soon after. In the zebrafish, 40% of nascent sheaths are retracted within 5 hours after the initiation of myelination (Czopka et al. 2013). To capture the morphological transitions of iPSC-derived oligodendrocytes, MI-4, MI-8, and MI-12 myelinoids were stained with CNP, which labels the cell body, processes, and internodes of mature oligodendrocytes. Figure 4.12 shows that as oligodendrocytes begin to myelinate, they appear to put out many processes (MI to MI-4) and, over time, (MI-8 to MI12) the number of processes and myelin sheaths from a single oligodendrocyte is considerably reduced. Whilst temporal analysis of myelin formation by the same cell was unavailable, these results suggest that iPSC-derived oligodendrocytes conform to the expected process of overproduction and retraction of nascent sheaths during myelination.

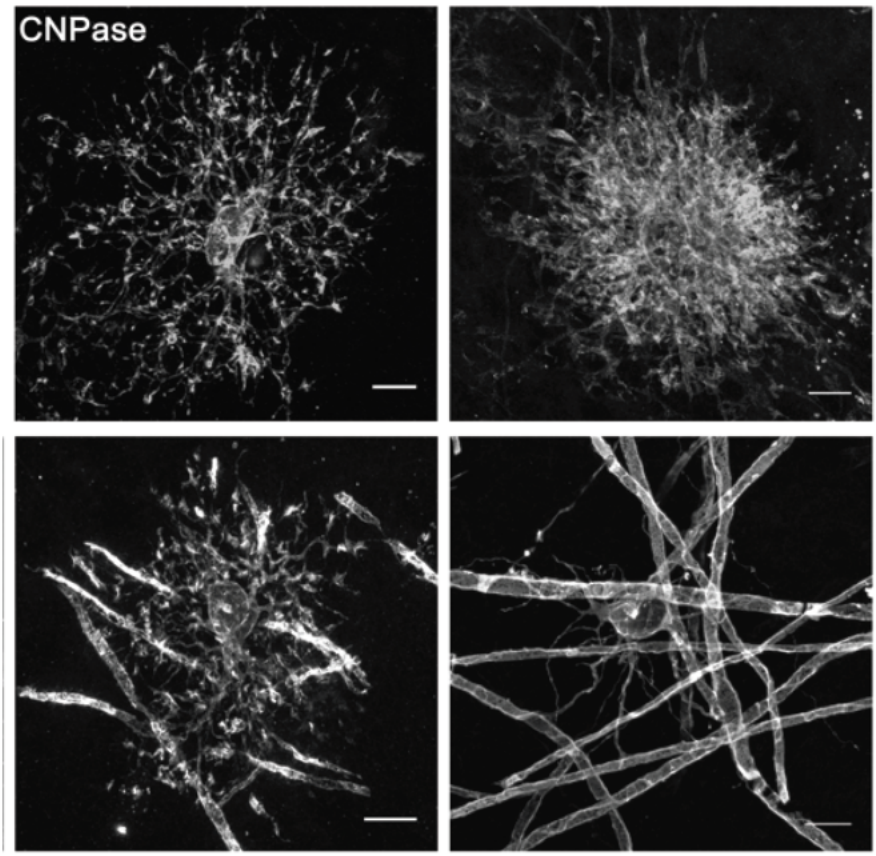

Figure 4.12 Temporal changes in oligodendrocyte morphology

Representative images of oligodendrocyte morphology between MI and MI-4 (top left and top right panes) and MI-8 to MI-12 (bottom left and bottom right panels). Scale = 10μm.

4.2.10 Quantifying the temporal development of myelin formation

To quantify the temporal relationship between oligodendrocyte differentiation and myelination, the number of SOX10+ oligodendrocyte lineage cells and the proportion of MBP+ oligodendrocytes at MI-4, MI-8, and MI-12 were assessed. In addition, the proportion of myelinating oligodendrocytes was quantified by morphological identification of thick, linear MBP+ segments that were characteristic of myelinating oligodendrocyte processes. Representative images at MI-4, MI-8, and MI-12 are shown in Figure 4.13A. Between MI-4 and MI-12, the proportion of mature MBP+SOX10+ oligodendrocytes remain unaltered at approximately 17% (Figure 4.13B). However, the proportion of mature oligodendrocytes that were observed forming at least one myelin sheath increased from 18% at MI-4 to 79% at MI-12 (Figure 4.13C).

The same cultures were also used to measured myelin sheath length over time. 20X images were acquired in z-stack to ensure whole myelin sheaths were captured in a single region of interest. Again, myelin sheaths were identified by their distinct morphology to non-myelinating processes and, using the distance between distal ends of MBP+ myelin sheaths (Figure 4.13D). Manual tracing of myelin sheath lengths showed a 52 % increase between MI-4 and MI-12 (mean 48 ± 35 μm to 74 ± 41 μm) (Figure 4.13E).

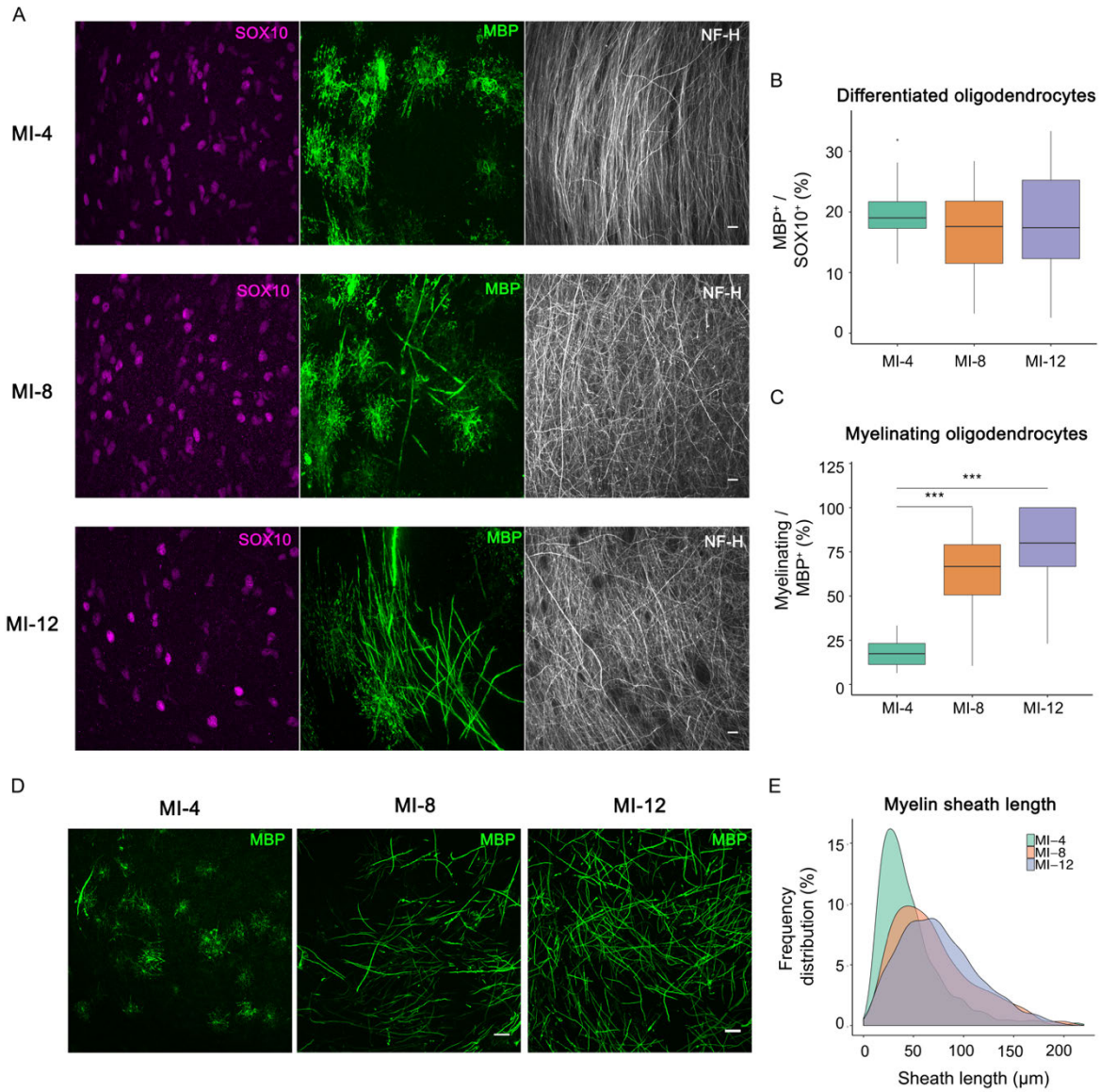

Figure 4.13 Temporal development of oligodendrocyte differentiation, myelination and myelin sheath length

A) Representative images of whole-mounted myelinoids stained with SOX10, MBP, and NF-H at MI-4, MI-8, and MI-12, scale = 10μm.

B) Quantification of the number of mature (MBP^+ $SOX10^+$) oligodendrocytes / total number of $SOX10^+$ oligodendroglial cells over time (glm with dummy variables for each timepoint, no change, 2 sites per myelinoid from n = 45 myelinoids across 2 cell lines and 5 conversions).

C) Quantification of the number of mature oligodendrocytes that could be seen forming at least one myelin sheath (glm with dummy variables for each timepoint $p < 0.001$, 95% CI: 68% to 90% increase between MI-4 to MI-12, 2 sites per myelinoid from n = 45 myelinoids across 2 cell lines and 5 conversions).

Continued overleaf

Figure 4.13 Temporal development of oligodendrocyte differentiation, myelination and myelin sheath length contd.

D) Representative images of MBP^+ myelin sheaths imaged at 20X between MI-4 to MI-12, scale = 50μm.

E) Frequency distribution plot showing the increase in sheath length between MI-4 and MI-12 (glm with dummy variables for each timepoint, *** $p < 0.001$, 95% CI: 44% to 60% increase between MI-4 and MI-12, data collected from over 2000 sheaths from 6 myelinoids from the same conversion).

4.2.11 Compact myelin formation

A critical step in the process of myelin formation is the compaction of myelin lamellae wrapped around axons. The evidence that I have demonstrated so far indicates the formation of myelin sheaths that co-localise with NF-H. However, to confirm myelin wrapping and to determine the thickness and integrity of myelin sheaths, iPSC myelinoids between MI-8 and MI-28 were processed for transmission electron micrsocopy (TEM).

Representative images of myelinated axons are shown in Figure 4.14A demonstrating the formation of compact and concentric, electron-dense layers of myelin around axons of varying size. To determine the thickness of iPSC-derived myelin, g-Ratio analysis was performed by measuring the diameters of the myelinated fibre (distance between opposing outer myelin sheaths) and of the axon alone and calculating the ratio between the two. Figure 4.14B shows the distribution of g-Ratios for individual fibres against their corresponding axon diameter. Average g-Ratio across all fibres was 0.7 ± 0.01 and showed a reduction over time (mean for MI-8 = 0.82 ± 0.01, mean for MI-12 = 0.77 ± 0.03, mean for MI-28 = 0.69 ± 0.09). Theoretical modelling of axon structure and function identify an optimal g-Ratio of between 0.6 and 0.77 (Rushton 1951; Chomiak & Bin Hu 2009), which is in line with measurements made across different species, including humans (Saliani et al. 2017).

These data show that not only are myelin lamellae compacted in iPSC myelinoids but that myelin sheaths demonstrate a thickness in line with that seen around axons *in vivo*.

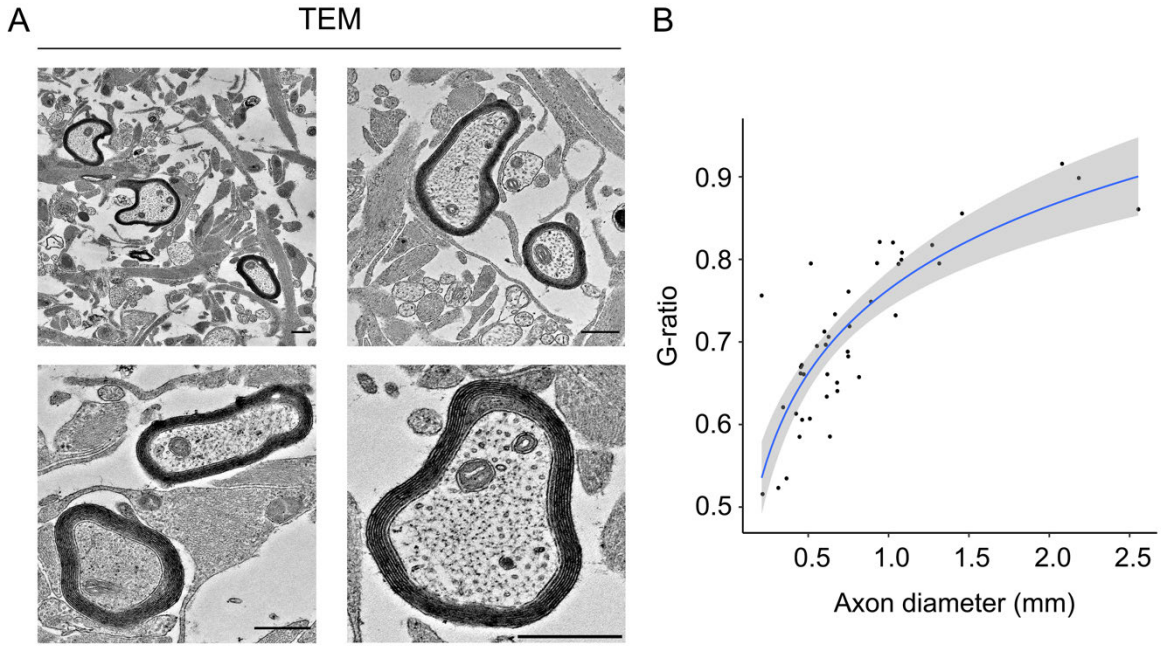

Figure 4.14 Compact myelination and g-ratio analysis

A) Representative images of myelinated axons under TEM (scale 500 nm) at MI-12.

B) Scatter plot of axon diameter against g-ratio (axon diameter/fiber diameter) with a logarithmic regression curve between MI-8 and MI-28 (43 axons from 3 myelinoids).

4.2.12 Organisation of myelinated axon domains

Myelin sheath function requires both compaction of myelin lamellae and the organisation of discrete myelinated axon domains for saltatory conduction. The assembly of nodes of Ranvier in the CNS occurs via the positioning of several cytoskeletal and tethering proteins at sites along the axolemma contacted by myelinating oligodendrocytes and is mediated by both contact-dependent and soluble factors (Susuki et al. 2013; Snaidero et al. 2014). The formation of PNJs precede nodal assembly in the CNS, which in turn is dependent on myelin wrapping (Wiggins et al. 1988; Rasband et al. 1999; Susuki et al. 2013).

Though more recently, myelin has been attributed with additional functions, including more dynamic, activity-dependent roles in CNS development, nodal assembly remains the definitive hallmark of myelin. In order to see whether iPSC-myelinoids can recapitulate definitive functions of compact myelin *in vitro,* 10 μm cryosections of MI-12 myelinoids were stained for components of the node and paranode.

PNJ formation in iPSC myelinoids was confirmed by the expression of CASPR at the distal ends of myelin sheaths (Figure 4.15A). In addition, CLAUDIN-11$^+$ tight-junctions between the cytoplasmic loops of myelin lamellae are equally prominent at the distal ends of myelin sheaths, demonstrating myelin wrapping and the sequestration of cell-type specific proteins into overlapping yet discrete domains (Figure 4.15B). At higher magnification, a Schmidt-Lantermann incisures can be seen spiralling through compact CNS myelin (Figure 4.15B).

Many closely opposed PNJs could be seen separated by a small gap, indicative of NoRs. Node formation was confirmed by staining for Neurofascin and ANKYRIN G. Both major isoforms of Neurofascin can be identified in iPSC myelinoid sections by their localisation. Nfasc155, which binds CASPR at the PNJ is found at the distal ends of myelin sheaths. Nfasc186, which is central to and initiates NoR assembly by recruiting ANKYRIN-G, is expressed brightly within the gap between CASPR+ bands (Figure 4.15C). Furthermore, ANKYRIN-G itself is clearly visualised at the node between CASPR$^+$ bands (Figure 4.15D).

These data show that human myelinating oligodendrocytes in iPSC myelinoids form appropriate axoglial interactions that lead to maturation and organisation of myelinated axon subdomains.

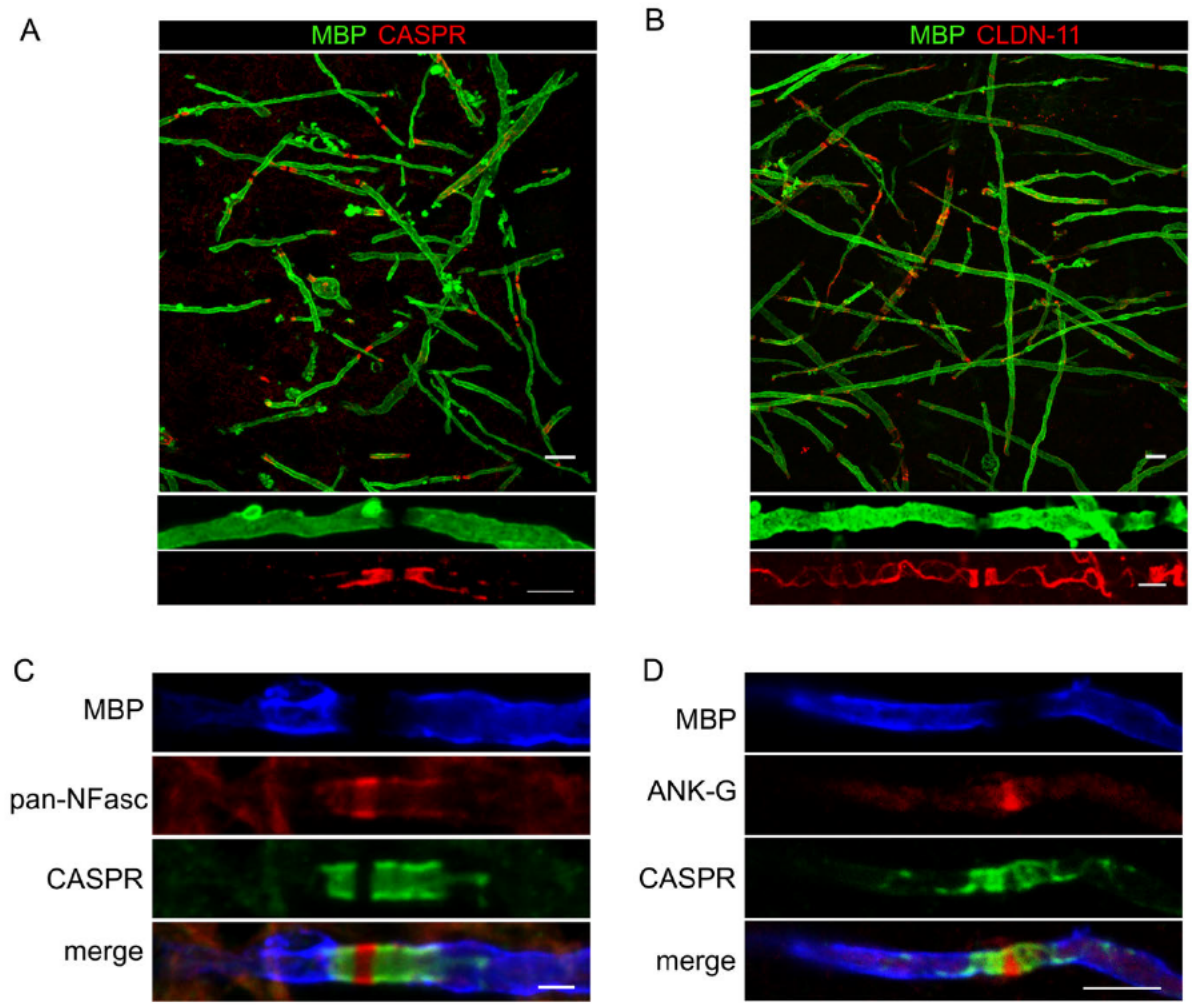

Figure 4.15 Organisation of myelinated axon domains

A) Overview and magnified images of MBP+ internodes and CASPR+ PNJ (scale 10μm and 5μm respectively).

B) Overview and magnified images of CLAUDIN-11+ tight junctions at the distal ends of MBP+ internodes (scale 10μm and 5μm respectively).

C) Neurofascin expression was identified using a pan-Nfasc antibody at the node and PNJ where distinct isoforms of Nfasc are expressed by opposing cell types (scale 1μm).

D) ANKYRIN-G expression identifies the node of Ranvier (scale 5μm).

4.2.13 Characterisation of neuronal subtypes and myelin targeting

The pMN domain of the developing spinal cord gives rise to motor neurons that are distinguished by their expression of the LIM-homeodomain transcription factors Islet 1 and 2 (Islet1/2) and Choline Acetyl Transferase (ChAT), which synthesises the neurotransmitter acetylcholine (Thaler et al. 2002). However, in patterning cells as three-dimensional spheroids, cells will naturally be exposed to a graded concentration of patterning factors—including ventralising smoothened agonist (SAG)—thereby resulting in the acquisition of additional domains neighbouring the pMN, which give rise to a range of interneuron and astrocyte subtypes (Lai et al. 2016). With this in mind, I decided to broadly investigate neuronal subtypes in iPSC myelinoids. Firstly, I asked whether interneurons were present in iPSC-myelinoids? And secondly, whether interneurons were being myelinated in iPSC myelinoids?

10μm cryosections of MI-12 myelinoids were stained for ISLET1/2, ChAT, and PARVALBUMIN (PV), which is a calcium binding protein that is expressed by a large subgroup of GABAergic interneurons (Gonchar & burkhalter 1997). Figure 4.16A shows the presence of motor neuron cell bodies by the colocalisation of ISLET1/2 and ChAT. Additionally, PV$^+$ cell bodies could be identified; these did not co-localise with ISLET1/2 (Figure 4.16B), demonstrating the acquisition of a range of neuronal subtypes in iPSC myelinoids.

Next, sections were stained with NF-H, PV, and MBP to determine the myelination status of PV$^+$ neurons. Figure 4.16C demonstrates the presence of myelinated PV$^+$ axons (red arrows) as well as the presence of myelinated PV$^-$ NF-H$^+$ axons (yellow arrows). Quantification of the number of PV$^+$ myelinated axons revealed that approximately half of all myelinated axons were PV$^+$ (mean = 52% ± 14.4%, analysed from three separate myelinoids, Figure 4.16D). Additionally, cryosections stained with CNP and PV revealed that individual oligodendrocytes could myelinate both PV$^+$ and PV$^-$ axons simultaneously (Figure 4.16E).

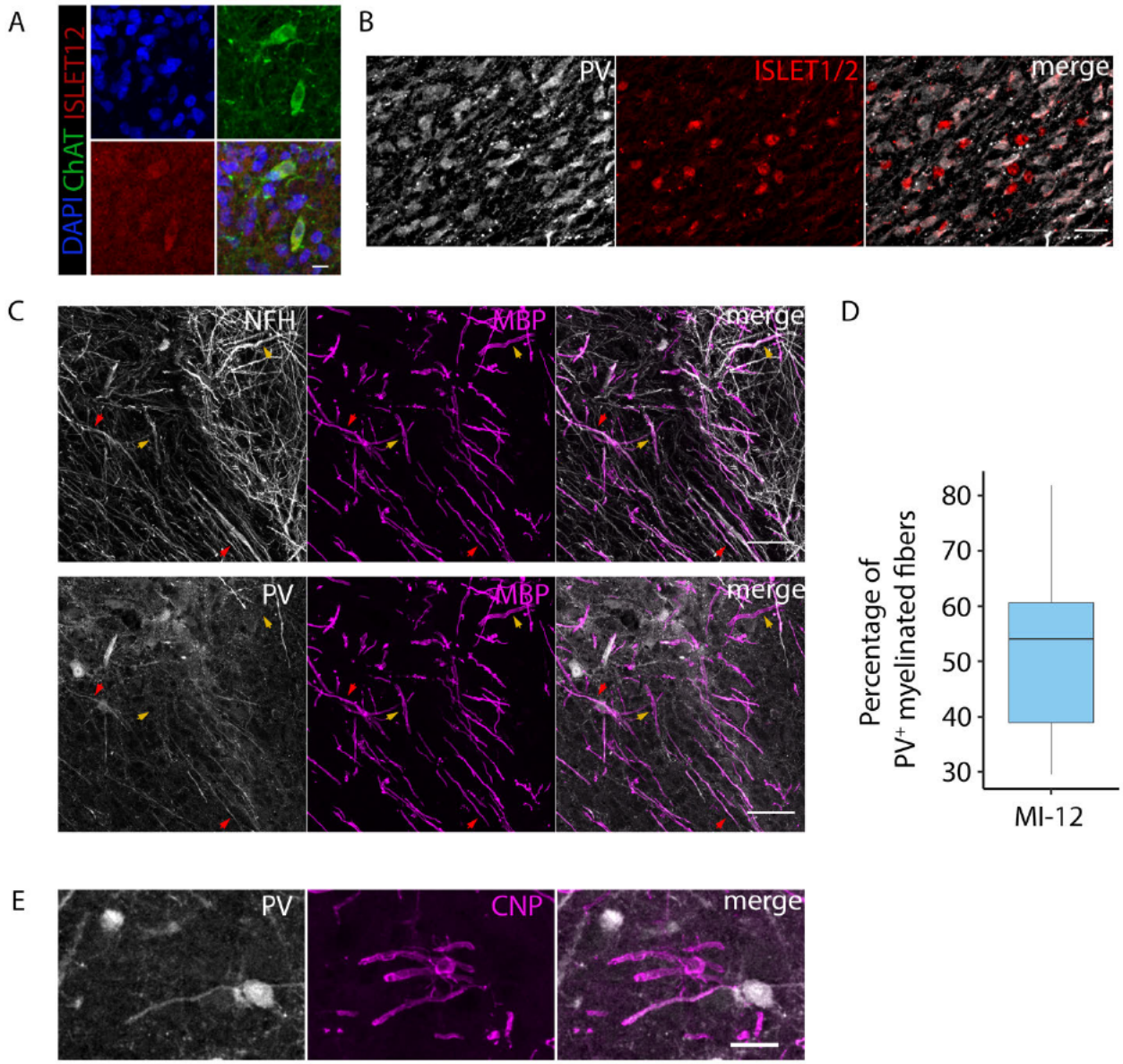

Figure 4.16 Neuronal subtypes and myelin targeting

A) Motor neurons are identified by ChAT and ISLET1/2 staining (scale 10 μm).

B) PV+ neuronal cell bodies do not co-localise with ISLET1/2, demonstrating a range of neuronal subtypes in iPSC myelinoids (scale 20 μm).

C) Analysis of myelin targeting to PV+ axons. Red arrows indicate NF-H+ PV+ myelinated axons and yellow arrows indicate NFH+ PV myelinated axons (scale 50 μm).

D) Quantification of PV+ myelinated axons / total myelinated axons (data collected from over 1000 myelinated axons from 15 sections across 4 myelinoids).

E) CNP+ oligodendrocytes myelinate both PV+ and PV axons (scale 25 μm).

These data demonstrate 1) the acquisition of multiple neuronal subtypes in iPSC myelinoids, 2) that axons of different neuronal subtypes can be myelinated, and 3) that oligodendrocytes can myelinate multiple neuronal subtypes simultaneously. Indeed, the proportion of myelinated PV+ axons suggest that oligodendrocytes indiscriminately myelinate PV+ and PV- axons without bias. It was recently shown in the mouse neocortex that some oligodendrocytes can be biased towards inhibitory neurons or excitatory neurons, or show no bias at all, suggesting that oligodendrocytes can recognise and differentially myelinate neuronal subtypes (Zonouzi et al. 2019). Further analysis of the myelination profile of different neuronal subtypes would be of great interest in determining the factors that underlie the distribution of myelin across the brain and spinal cord.

It is unclear what the identity of PV^+ neurons are. In the ventral horn of spinal cord, PV expression is high during development but is absent in both adult rats and humans following maturation of the locomotor system (Clowry et al. 2000). PV expression was found in a variety of neuronal subtypes in the ventral horn, including Renshaw cells, which are premotor inhibitory interneurons that are excited by motor neuron axon collaterals and function to inhibit motor neurons (Jankowska 2013). PV expression has also been observed in motor neurons themselves (Clowry et al. 2000). However, as all newly generated motor neurons express ISLET1/2 (Pfaff et al. 1996) and PV expression was not found to overlap with ISLET1/2 in iPSC myelinoids, observed PV^+ cells are likely to be interneurons.

PV^+ interneurons are also found in the dorsal horn of the spinal cord (Chen et al. 2016) and it is possible that incomplete ventral patterning could yield a population of dorsally derived interneurons in iPSC myelinoids. However, this is unlikely due to the substantial proportion of OLIG2+ observed in dissociated oligodendrocyte progenitor spheroids (Livesey, Magnani, Cleary, Vasistha, James, Selvaraj, Burr, Story, Shaw, Kind, Hardingham, Wyllie & Chandran 2016b). Further work to precisely identify these cells would require staining for other markers including the $Ca2^+$ binding proteins Calbindin and Calretinin as well as a range of transcription factors that establish spinal cord neuronal diversity (Lai et al. 2016).

4.3 Conclusions

The work presented in this chapter outlines the identification of a novel, completely humanised *in vitro* model of compact myelin formation, derived from human pluripotent stem cells. I have shown that iPSC-derived spheroids patterned towards the pMN domain of the ventral telencephalon generate neurons, astrocytes, and oligodendrocyte lineage cells. Following their initial patterning, spheroids that were maintained on PTFE-coated inserts for an additional 12 weeks demonstrated temporal development of myelin formation with increasing numbers of myelinating cells and elongating sheath lengths. iPSC-derived myelin was shown to be compact, with organisation of myelin axon domains. In addition, g-Ratio analysis showed appropriate myelin thickness mirroring *in vivo* measurements. The regional distribution of myelin within iPSC myelinoids was shown to be primarily located around the periphery of iPSC-myelinoids where dense tracts of NF-H$^+$ axons are also found. Finally, in characterising the subtypes of myelinated axons, I showed that approximately half of all myelinated axons are positive for the interneuron marker PV, indicating that oligodendrocytes in this culture model myelinate both excitatory and inhibitory neurons without bias.

4.4 Discussion

A number of recent papers have demonstrated the development of oligodendrocytes in iPSC-derived organoids with the aim of modelling human myelin development (Madhavan, Nevin, Shick, Garrison, Clarkson-Paredes, Karl, Clayton, Factor, Allan, Barbar, Jain, Douvaras, Fossati, R. H. Miller & Tesar 2018a; Marton et al. 2019; Kim et al. 2018). Similar to the work I have shown here, these papers show that organoid-type cultures can be generated to comprise a range of CNS-derived cells, including oligodendrocytes. However, across each of these protocols, myelin formation is sparse and evidence for compaction is limited. Furthermore, these cultures fail to acquire nodal domain organisation, highlighting the immaturity of these culture systems. A critical factor that likely explains the discrepancy between these cultures and the work presented here is that each of the reported protocols generated forebrain-patterned spheroids via the omission of RA and exposure to different FGFs. Human myelin development begins *in utero* in the cervical spinal cord as early 10–12 gestational weeks and proceeds both caudally and rostrally to the spinal cord and brain (Weidenheim et al. 1996; Hajihosseini et al. 1996). In contrast, cortical myelin development is not apparent until after mid-gestation (17-32 gestational weeks) (Jakovcevski et al. 2009). Additionally, humans in particular have a protracted development of cortical myelination characterised by a delayed period of maturation (D. J. Miller et al. 2012). It is therefore likely that recapitulating widespread myelination of forebrain patterned cells will require advanced maturity and culture time beyond what has been achieved so far.

The advanced maturity of iPSC myelinoids compared to other protocols is also demonstrated in their earlier acquisition of nascent myelin sheaths. For reference, iPSC myelinoids demonstrate MBP^+ oligodendrocytes at MI (total culture time of 56 days/8 weeks) and nascent sheath formation at MI-4 (total culture time of 84 days/12 weeks). Madhavan et al. induce oligodendrogenesis at around day 50 and PLP^+ oligodendrocytes are observed at around day 84 (14 weeks) with early myelin sheath formation evident at day 210 (30 weeks) (Madhavan, Nevin, Shick, Garrison, Clarkson-Paredes, Karl, Clayton, Factor, Allan, Barbar, Jain, Douvaras, Fossati, R. H. Miller & Tesar 2018a). Marton et al. begin inducing oligodendrogenesis much

earlier, at day 25, but do not identify evidence for myelin sheath formation (by immunofluorescence) until day 158, though evidence of myelin compaction by TEM is shown at day 103 (15 weeks) (Marton et al. 2019). The protocol published by Kim et al., which involves the independent formation and subsequent fusion of dorsal and ventral-patterned forebrain spheroids, more closely mimics iPSC myelinoid timescales as MBP^+ oligodendrocytes are identified by day 63 (9 weeks) and thick MBP^+ sheaths are identified at week 15. The authors suggest the advanced oligodendrogenesis is due to their use of BrainPhys medium (STEMCELL technologies), which likely contains neuronal growth factors including BDNF due to increased c-FOS expression observed in dorsal forebrain organoids (Kim et al. 2019). Indeed, BDNF is supplemented in each of the protocols at some point but was omitted in the generation iPSC myelinoids.

Another critical difference in the culture of iPSC myelinoids is in the transfer to cell culture inserts where they are maintained at an air-liquid interface. This technique presents a number of advantages. Firstly, it avoids the aggregation of spheroids when maintained long-term in suspension cultures. Secondly, as myelinoids flatten on the membranes, myelinoids acquire an orientation that promotes wide-spread myelination across their surface and allows for each myelinoid to be processed similarly, contributing to the reproducibility of analysis between cultures from different conversions. Finally, comparisons between myelinoids and spheroids maintained in suspension cultures for similar durations show that whilst myelin formation does occur in suspension cultures, a greater degree of myelin is found in myelinoids transferred onto PTFE-membranes. This is possibly due to more efficient gas exchange at the air-liquid interface and improved culture conditions that favour increased maturity of both neurons and glia. Indeed, a recent publication supports the culture of organoids at the air-liquid interface due to improved survival and maturity of neurons assessed by TUNNEL staining, axonal tract formation, and dendritic morphology (Giandomenico et al. 2018).

The critical advantage of iPSC myelinoids over currently available methods is the widespread acquisition of myelin with typical morphology of myelinated axons, that is, compacted to a similar degree as is observed *in vivo* and that also demonstrates appropriate organisation of nodal and paranodal domains. This demonstrates the enhanced maturity of iPSC-derived myelin in this culture model. The temporal

sequence of myelination involves first myelin wrapping, followed by formation of axoglial junctions at the distal ends of elongating sheaths, and finally, nodal assembly (Rasband et al. 1999; Susuki et al. 2013). In shiverer mice, whose oligodendrocytes wrap axons but fail to generate compact myelin due to the absence of MBP, PNJ formation is perturbed (Rasband et al. 1999). It is conceivable therefore that the failure to observe PNJs in established organoid models—as noted by (Madhavan, Nevin, Shick, Garrison, Clarkson-Paredes, Karl, Clayton, Factor, Allan, Barbar, Jain, Douvaras, Fossati, R. H. Miller & Tesar 2018b)—is due to the predominance of loose or incomplete myelin wrapping in their cultures.

Importantly, the robust acquisition of myelinated axons with appropriate three-dimensional architecture in iPSC myelinoids provides a unique platform for investigations into both the biology and pathology of human myelination, from oligodendrogenesis right through to compact myelin formation.

However, one limitation of iPSC myelinoids is that they are patterned caudally and so reflect spinal cord-derived cell-types. Intrinsic differences between forebrain and spinal cord oligodendrocytes have been identified, (Bechler et al. 2015) and recent transcriptomic studies have revealed unappreciated heterogeneity within oligodendrocytes isolated from similar regions (Jäkel et al. 2019; Leong et al. 2014). Whether or not investigations of factors that influence oligodendrocyte differentiation and myelination affect all oligodendrocytes equally is yet to be determined. However, with these caveats in mind, application of iPSC myelinoids to study myelin development in the context of neurodevelopmental or neurological diseases may still be indicative of pathological processes or disease mechanisms, irrespective of neuronal (and potentially oligodendrocyte) subtype generation.

With the description of any new model system, an in-depth characterisation is a necessary pre-requisite to experimental manipulation. The data presented here give a small window into the temporal development of myelin in iPSC-myelinoids and are by no means exhaustive. Further analysis of interneuron subtypes and their myelination profile, of synapse formation and the physiological properties of myelinoid neurons would provide an excellent foundation to pursue questions around the impact of myelin formation on network formation and circuit dynamics. Such questions may require advanced techniques to probe cellular physiology, including live imaging

reporter constructs of calcium activity, and would require successive rounds of gene-editing to report on the behaviour of individual cells. Nevertheless, iPSC myelinoids provide a novel and unique means of assessing compact human myelin formation in response to different physiological, pharmacological, and genetic perturbations.

Chapter 5 iPSC myelinoids respond to pharmacological and physiological cues

5.1 Introduction

A wealth of information is available on the regulation of rodent OPC proliferation, differentiation, and myelination including but not limited to: oxygen tension (Yuen et al. 2014), trophic factors (Barres et al. 1993; Brinkmann et al. 2008), integrins (Colognato et al. 2002), inflammatory cytokines (Yuen et al. 2013), and neuronal activity (Almeida & Lyons 2017). Whilst many of these factors are also regulated by—or indeed themselves regulate—CNS health and function more generally, deciphering their role in oligodendrocyte/myelin development will aid our understanding of normal and pathogenic myelination and will support novel treatment strategies for disorders with which these factors have been associated, including perinatal hypoxia-ischemia (Back et al. 2002), multiple sclerosis (Lock et al. 2002), schizophrenia (Stefansson et al. 2002), and glioblastoma (Venkatesh et al. 2019).

Due to the inaccessibility of human tissue, little is known about the factors that regulate human myelination and to what extent human oligodendrocytes mirror their rodent counterpart. As many orthologous, classically defined, oligodendroglial genes are expressed by human cells, core oligodendroglial functions are likely similar (X. Xu et al. 2018; Hodge et al. 2019). However, a small subset of differentially regulated genes specifically enriched in human cells may confer functional differences to human oligodendrocytes and which may play a role in human disease (Hodge et al. 2019; X. Xu et al. 2018; Jäkel et al. 2019). Similar indications have appeared from the study of human astrocytes, which have, for example, been attributed with sustaining more complex information processing (Vasile et al. 2017).

Physiologically, human oligodendrocytes appear similar to rodent cells (Livesey et al. 2016; Stacpoole et al. 2013). However, human oligodendrocytes have revealed differential responsiveness to specific trophic and transcription factors (Chandran et al. 2003; J. Wang et al. 2014) and intrinsic differences in the proliferation, colonisation, and myelination of the demyelinated mouse CNS, compared to rodent-derived cells (Sim et al. 2009; Windrem et al. 2008; Windrem et al. 2014; Mozafari et al. 2015; Buchet et al. 2011; Chanoumidou et al. 2019). Moreover, as oligodendroglial function is inextricably tied to myelin formation, our understanding of this key process in human cells is limited by the lack of robust models of human myelination.

iPSC myelinoids are well-suited for studies of the regulation of human myelination, from oligodendrogenesis through to myelin wrapping, compaction, and sub-domain organisation. Pharmacological or physiological manipulations therefore may both corroborate findings from other animal models and examine human-specific or disease-associated responses. In particular, iPSC myelinoids provide a unique platform for interrogating activity-regulated myelin development due to the presence of multiple CNS-derived cell types and a defined time-course for wide-spread, compact myelin formation. This is important as, whilst MRI studies have demonstrated experience-dependent white matter plasticity in the CNS (Scholz et al. 2009; Bengtsson et al. 2005; Weber et al. 2019; Schlegel et al. 2012; Sampaio-Baptista et al. 2013), the structural information obtained from MRI may be attributed to changes across several cell-types. This includes OPC proliferation and differentiation, new myelination, and myelin remodelling, as well as affecting axonal diameter, branching, and vascular changes (Walhovd et al. 2014; Cassandra Sampaio-Baptista 2017). Increased FA in the corpus callosum of rats following a learning and memory task and in M1-associated white matter following precise motor skill learning is associated with localised increased MBP expression (Blumenfeld-Katzir et al. 2011; Sampaio-Baptista et al. 2013), indicating that experience-dependent white matter changes by MRI may reflect myelin related changes in humans. However, direct evidence to show that human oligodendrocytes are responsive to changes in neuronal activity is lacking.

In order to demonstrate the suitability of iPSC myelinoids for use in such studies, it was first necessary to show that human oligodendrocytes in this culture model can modulate their myelin deposition predictably in response to previously identified pharmacological and physiological manipulations.

5.2 Results

5.2.1 Characterising the myelinating profile of iPSC-derived oligodendrocytes

Prior to pharmacological manipulation of iPSC myelinoids, the myelinating profile of oligodendrocytes was characterised. Using the marker CNP to label the cell body, processes, and internodes of myelinating oligodendrocytes, large tiled areas of myelin in MI-12 myelinoids were acquired using a Zeiss 710 confocal with 40X oil objective. The acquisition area was large enough to easily count 5–20 cells per field of view, per myelinoid. The number and lengths of myelin sheaths per cell were quantified. Figure 5.1A is a maximum projection image of an example tile of CNP^+ oligodendrocytes. To show that myelin sheath length can be accurately captured by CNP staining alone, segmented lengths obtained from CNP^+ myelin sheaths were overlaid onto the corresponding image of $CASPR^+$ PNJs to confirm appropriate alignment between these structures (Figure 5.1B). Human myelinating oligodendrocytes generated a median of 10 ± 6.82 sheaths per cell (Figure 5.1C). Mean standard deviation per batch of myelinoids and per myelinoid was 5.06 and 3.98, respectively, demonstrating reduced variability within batches of myelinoids. Mean sheath length per cell was 89.4 ± 23.9 μm (mean *SD* per myelinoid = 20.8 μm) (Figure 5.1C-D). The lengths of all sheaths measured were also plotted as a frequency distribution histogram (population mean sheath length = 86 μm ± 52 μm) (Figure 5.1E). Additionally, the log-transformed histogram is shown in Figure 5.1F, demonstrating the log-normal distribution of sheath lengths).

Given the variation in both sheath number and sheath lengths, I created a composite score for total myelin length per cell by summation of all sheath lengths per cell. Though not able to account for differences in axonal diameter or myelin sheath thickness, the score provides an approximate measure for the myelinogenic output per cell. The total myelin length per cell was found to be 1237.20 ± 803 μm (mean *SD* per batch of myelinoids = 382 μm and mean *SD* per myelinoid = 326 μm) (Figure 5.1E).

These data show that the myelinating profile of individual oligodendrocytes can be readily measured in iPSC myelinoids with reproducible results across two cell lines. Using this assay, investigations into those factors that modulate myelin development can be made.

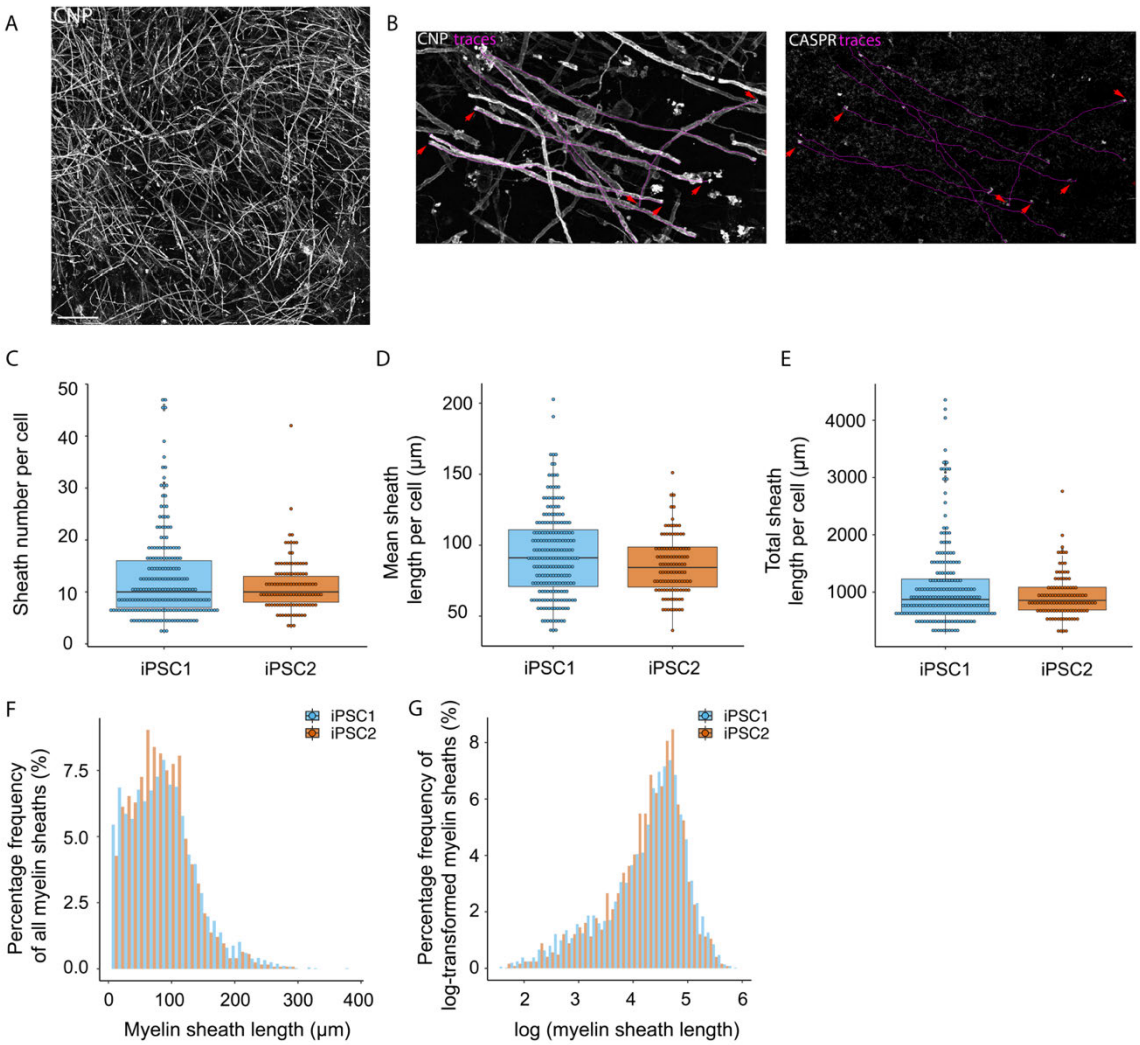

Figure 5.1 Analysis of myelin sheath number and lengths per cell

A) Maximum projection image of a representative area acquired for measuring the lengths and number of CNP+ sheaths per cell, scale = 100μm.

B) CNP marks the distal ends of myelin sheaths identified by CASPR+ PNJ (red arrows).

C) Boxplot of sheath number per cell across two control iPSC lines.

D) Boxplot of mean sheath length per cell.

E) Boxplot of total sheath length per cell.

F) Frequency distribution for all sheath lengths.

G) Log-transformed frequency distribution for all sheath lengths.

Data collected from 321 cells from 26 different myelinoids across 8 conversions.

5.2.2 Oligodendrocyte density does not influence myelin sheath number or length

The myelinogenic capacity of oligodendrocytes has been shown to be influenced by surrounding biophysical factors including changes in axonal area (Almeida et al. 2018) and the number of neighbouring oligodendroglial cells (Chong, Rosenberg, Fancy, Zhao, Shen, A. T. Hahn, McGee, Xu, Zheng, L. I. Zhang, Rowitch, Franklin, Lu & Chan 2012b). In Kif1bp mutant zebrafish for example, a 50-80% reduction in reticulospinal axon area does not limit the number of sheaths per oligodendrocyte. Instead, supernumerary oligodendrocytes mistarget myelin to neuronal cell bodies (Almeida et al. 2018). In RGC-OPC co-cultures, OPCs cultured in the presence of polystyrene beads conjugated with oligodendrocyte membrane to mimic increased oligodendrocyte densities show a reduction in the number of internodes per cell as well as a reduction in the percentage of myelinating oligodendrocytes per field of view (Chong, Rosenberg, Fancy, Zhao, Shen, A. T. Hahn, McGee, Xu, Zheng, L. I. Zhang, Rowitch, Franklin, Lu & Chan 2012b).

In order to determine whether the density of neighbouring oligodendrocytes contributes to the myelinogenetic capacity of human myelinating oligodendrocytes in iPSC myelinoids, I performed a nearest neighbour analysis. I first counted the lengths and number of internodes of individual oligodendrocytes, then plotted a circle surrounding each cell with a 100μm radius and counted the number of neighbouring CNP^+ oligodendrocytes within that area (Figure 5.2A). Figures 5.2B-C show the correlation between the number of neighbouring oligodendrocytes and myelin sheath number or mean sheath length per cell, respectively. Neither measure significantly correlated with the number of neighbouring oligodendrocytes. Therefore, in iPSC myelinoids, the density of oligodendrocytes does not affect myelin sheath number or length.

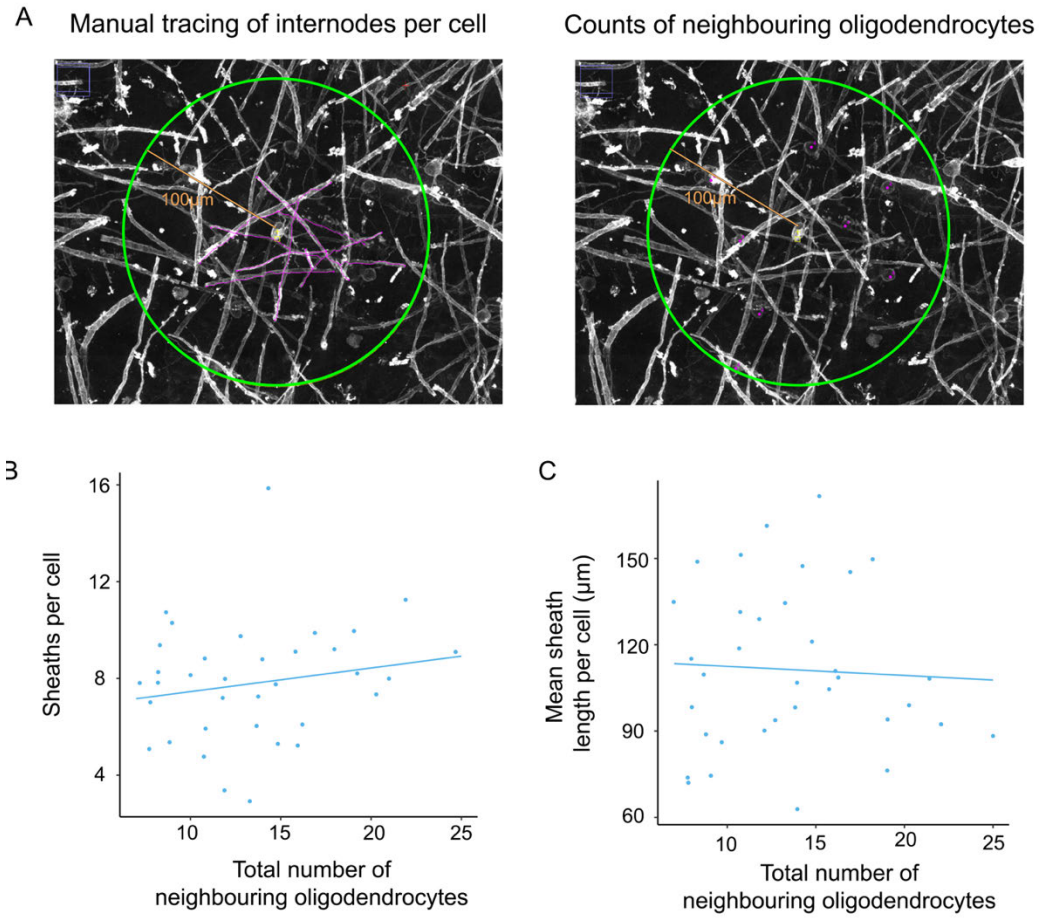

Figure 5.2 Nearest neighbour analysis of oligodendrocyte density

A) Illustration of nearest neighbour assay. 100μm radius circles were drawn around particular oligodendrocytes whose sheaths had been traced and the number of CNP$^+$ oligodendrocytes within that area was counted.

B) Scatterplot correlating the number of sheaths per cell and the total number of neighbouring oligodendrocytes (glm, no significant correlation).

C) Scatterplot comparing mean sheath length per cell and the total number of neighbouring oligodendrocytes (glm, no significant correlation).

Data from 35 cells from 8 myelinoids across 3 batches.

5.2.3 Blebbistatin increases myelin sheath number per cell

Oligodendrocyte membrane extension and subsequent wrapping involves dramatic cytoskeletal changes that is dependent on the polymerization of actin and tubulin (Wilson & Brophy 1989). Filamentous actin (F-actin) is concentrated at the leading edge of membrane protrusions in immature oligodendrocytes and also at the inner tongue of myelinating processes (Nawaz, Sánchez, Schmitt, Snaidero, Mitkovski, Velte, Brückner, Alexopoulos, Czopka, Jung, Rhee, Janshoff, Witke, Schaap, Lyons & Simons 2015a). However, the extension of myelin membrane is dependent on actin de-polymerisation, which reduces surface tension and enables myelin wrapping (Zuchero et al. 2015). A key regulator of actin dynamics in OPCs is non-muscle myosin II, which binds to F-actin in lamellipodia and provides cytoskeletal tension necessary for membrane protrusion (H. Wang et al. 2008; Domingues et al. 2017). During oligodendrocyte differentiation, Myosin II is downregulated, which coincides with F-actin depolymerisation and elaboration of myelin (Domingues et al. 2017). Importantly, blocking the function of non-muscle myosin II with the inhibitor blebbistatin modulates oligodendrocyte myelination by increasing the number of myelin sheaths elaborated per cell (H. Wang et al. 2008).

To demonstrate that the myelinating profile of individual oligodendrocytes could be modulated pharmacologically, I treated cultures with 10μM blebbistatin between MI and MI-12. Representative images of blebbistatin-treated myelinoids shows wide-spread myelination (Figure 5.3A). Blebbistatin treatment resulted in a 44.5 % increase in the number of myelin sheaths per cell (mean of 9.8 ± 4.8 sheaths per cell vs 14.2 ± 5.4 in blebbistatin-treated cultures) (Figure 5.3B-C). Mean sheath length per cell was reduced by 24 % (100.4 ± 28.5 μm to 76.3 ± 19.4 μm) (Figure 5.3D) and total sheath length per cell was not significantly different between the two conditions (Figure 5.3E).

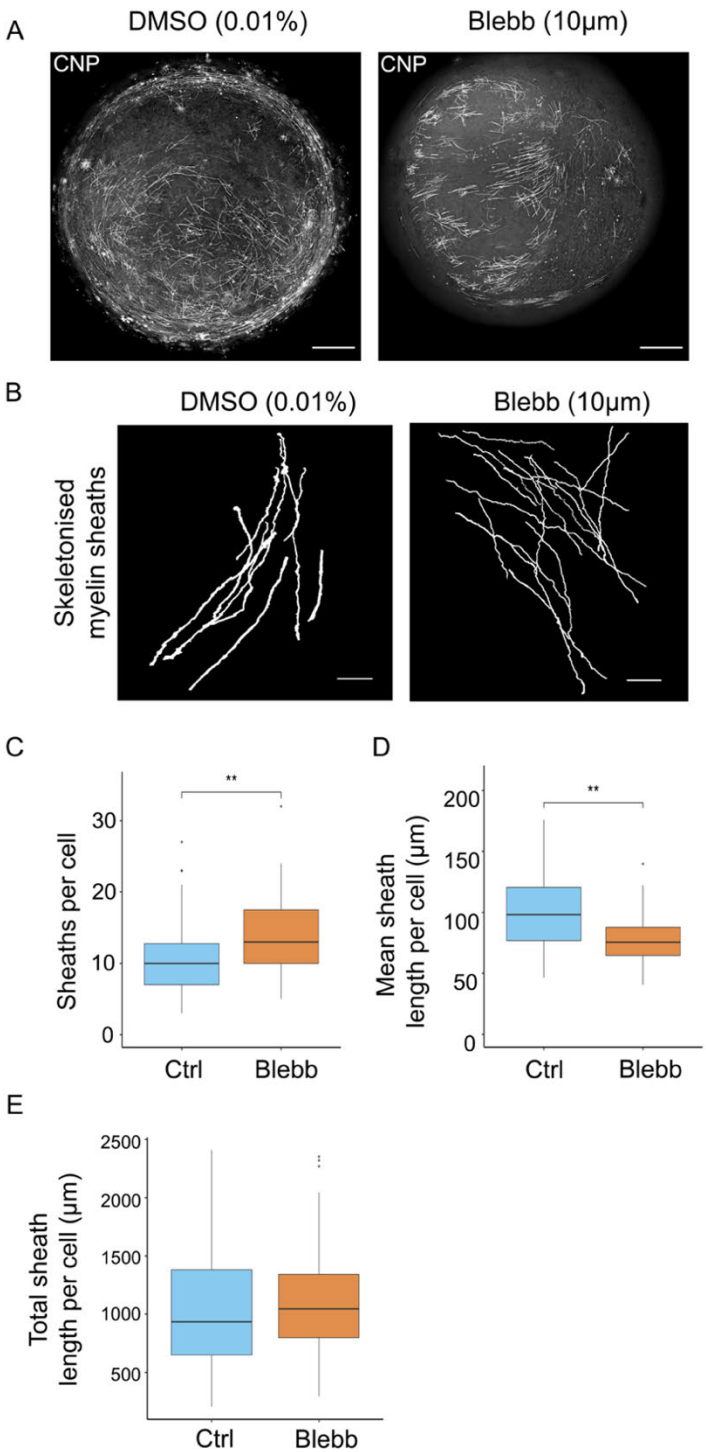

Figure 5.3 Blebbistatin increases myelin sheath number per cell

A) Representative images of CNP staining in MI-12 myelinoids treated with normal media (Ctrl) or supplemented with 10 μM blebbistatin for 12 weeks (scale 250μm).

Figure 5.3 Blebbistatin increases myelin sheath number per cell contd.
B) Skeletonised traces of myelin sheaths from Ctrl and Blebb-treated myelinoids (scale 25μm).
C) Blebbistatin increased sheath number per cell (p = 0.0078, 95% CI: 6.2% to 84.8% increase).
D) Blebbistatin reduced mean sheath length per cell (p = 0.0015, 95% CI: 10% to 36% reduction).
E) Blebbistatin did not change total sheath length per cell.
Data collected from 146 cells from 10 myelinoids across two batches.
< 0.01 ** generalised mixed model with individual myelinoids included as a random effect.

5.2.4 TeNT reduces myelin sheath number per cell

Having established that the myelinating profile of individual cells can be modulated experimentally, I aimed to test whether iPSC-myelinoids could respond to changes in neuronal excitability and modulate their myelinogenetic output accordingly.

To test whether iPSC-derived myelin development could be modulated by dampened neuronal activity, myelinoids were exposed to TeNT to suppress neuronal excitability. TeNT-induced cleavage and inactivation of VAMP2 is an efficient method to block both spontaneous and action-potential-evoked synaptic and nonsynaptic vesicle release (Söllner et al. 1993) (Kim et al. 1984), which has profound effects on myelin development (Wake et al. 2011; Mensch et al. 2015; Hines et al. 2015). TeNT has also been used to shut down synaptic transmission in stem cell-derived neurons (Beske et al. 2016).

Firstly, the expression of VAMP2 as well as PSD-95 and SYNAPTOPHYSIN was confirmed in MI spheroids by RT-PCR, demonstrating that the functional target of TeNT, as well as structural components of the synapse, are expressed at the point of treatment (Figure 5.4A). iPSC-derived myelinoids were then exposed to TeNT by supplementing the culture medium with 3nM TeNT (Sigma, heavy chain and light chain connected through an interchain disulphide bond) for 12 weeks between MI and MI-12. Myelin development was wide-spread in TeNT-treated myelinoids (Figure 5.4B).

Manual tracing of the number and lengths of myelin sheaths per cell (Figure 5.4C) demonstrated that, averaged across two independent cell lines and five biological replicates, myelin sheath number per cell was reduced by an average of 22 % (mean 9.1 ± 5.9 to 7.1 ± 3.5 TeNT*;* p = 0.005, 95% CI: 7% to 35%) (Figure 5.4D). Mean sheath length per cell was increased in TeNT-treated cultures (14.1% increase, p = 0.018, 95% CI: 2.4% to 25% increase) (Figure 5.4E) and there was no overall difference in total myelin sheath length per cell (Figure 5.4F).

To determine the effect of TeNT on oligodendrocyte differentiation, the density of myelinating oligodendrocytes was evaluated by nearest neighbour analysis. No change was observed in the number of oligodendrocytes per 100μm radius between

Ctrl and TeNT-treated cultures (Figure 5.4G). Further breakdown of mean sheath number and mean sheath length per cell in TeNT-treated cultures is provided as a table in Figure 5.4H.

These data demonstrate that blockade of vesicular release results in a predictable reduction in the myelinogenic output of human oligodendrocytes, providing the first evidence that human cells can also undergo activity regulated myelination.

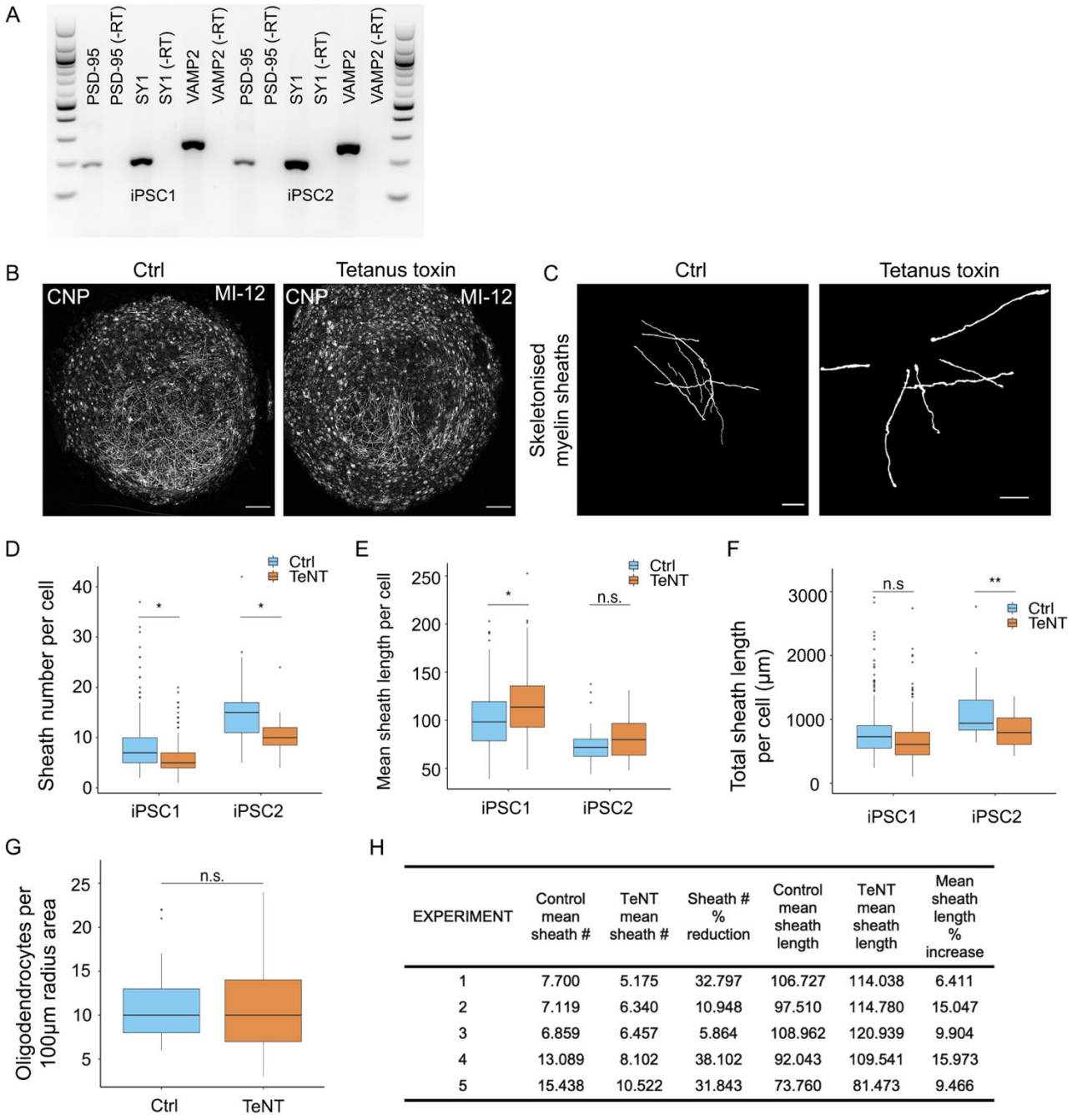

EXPERIMENT	Control mean sheath #	TeNT mean sheath #	Sheath # % reduction	Control mean sheath length	TeNT mean sheath length	Mean sheath length % increase
1	7.700	5.175	32.797	106.727	114.038	6.411
2	7.119	6.340	10.948	97.510	114.780	15.047
3	6.859	6.457	5.864	108.962	120.939	9.904
4	13.089	8.102	38.102	92.043	109.541	15.973
5	15.438	10.522	31.843	73.760	81.473	9.466

Figure 5.4 TeNT reduces myelin sheath number per cell

A) RT-PCR confirms the expression of VAMP2, PSD-95 and SYNOTPOPHYSIN in MI myelinoid-derived RNA +/- reverse transcriptase (RT).

B) Representative images of CNP staining in Ctrl and TeNT-treated myelinoids (scale 250μm).

C) Skeletonised myelin sheaths from Ctrl and TeNT-treated myelinoids (scale 25μm).

Figure 5.4 TeNT reduces myelin sheath number per cell contd.

D) Sheath number per cell is reduced in TeNT-treated myelinoids. The breakdown per cell line shows: iPSC1; 20% reduction in TeNT myelinoids, mean change 8 to 6.4 sheaths per cell, p = 0.028, 95% 95% CI: 2.2% to 33.9% reduction. iPSC2; 32% reduction in TeNT myelinoids, mean change 15.3 to 10.4 sheaths per cell, p = 0.012, 95% CI: 8.1% to 49.3% reduction. E) Mean sheath length per cell in TeNT-treated myelinoids. iPSC1; increase of 11.4 %, p = 0.0322, 95% CI: 0.97 % to 21.76 %. iPSC2; cultures did not show a difference in mean sheath length per cell.

F) Total sheath length per cell in TeNT-treated myelinoids. iPSC1; no change. iPSC2; 25 % reduction, $p < 0.01$, 95 % CI: 10.4% to 36.9%.

G) Nearest neighbours analysis shows no change in the number of oligodendrocytes per 100μm radius.

H) Breakdown of sheath number and mean sheath length per cell for each batch of myelinoids. The combined effect of TeNT across both cell lines is reported in the main text. Data collected from 588 cells from 40 myelinoids from 5 batches across two 2 cell lines. < 0.05 * < 0.01 ** generalised mixed model with individual myelinoids included as a random effect.

5.2.5 Potassium chloride does not affect myelin sheath number per cell

Given that a reduction in synaptic vesicle release led to a decrease in the number of myelin sheaths per cell, I next asked whether increasing neuronal activity would promote myelin sheath number per oligodendrocyte. In order to stimulate neuronal activity, I transiently exposed myelinoids to an increased concentration of potassium chloride (KCl), which causes membrane depolarisation by stimulating L-type Ca^{2+} channels and NMDA receptors, leading to action potential firing (Bading et al. 1993) and increased synaptic vesicle release (Freyberg et al. 2016). Establishing an appropriate treatment paradigm for KCl proved challenging. Whilst bath application of KCl to cultured neurons elicits stereotypical response within minutes, experiments conducted with organotypic slice cultures, which are arguably more similar to myelinoid cultures, display KCl-evoked responses from different concentrations and time-scales ranging from tens of minutes to several days (Croft et al. 2017; Chen et al. 2005) . However, it has also been shown that in hippocampal neurons, chronic depolarization with KCl over 7–13 days results in dampened intrinsic excitability, whereby greater currents were required to elicit action potentials (O'Leary et al. 2010). In order to stimulate myelinoids whilst avoiding plasticity-mediated adaptations, cultures were exposed to 15 mM KCl for 2 hours at a time, either once per week (KCl-1) or three times per week (KCl-3) for 12 weeks.

Representative figures of whole-mounted myelinoids from Ctrl and KCl-1 cultures are shown in Figure 5.5A. Overall, the number of myelin sheaths per cell was not different in KCl-treated cultures compared to myelinoids maintained in control medium (Figure 5.5B). Mean sheath length per cell was again not affected by KCl treatment overall (Figure 5.5C). However, the breakdown for each cell line showed that, for iPSC2 alone, there was an increase). Total myelin per cell was not significantly different between the two conditions for both cell lines (Figure 5.5D).

Whilst I was unable to directly measure the excitability of neurones in KCl-treated myelinoids, these data suggest that KCl treatment had either no effect or a slightly negative effect on the myelinogenic output per cell.

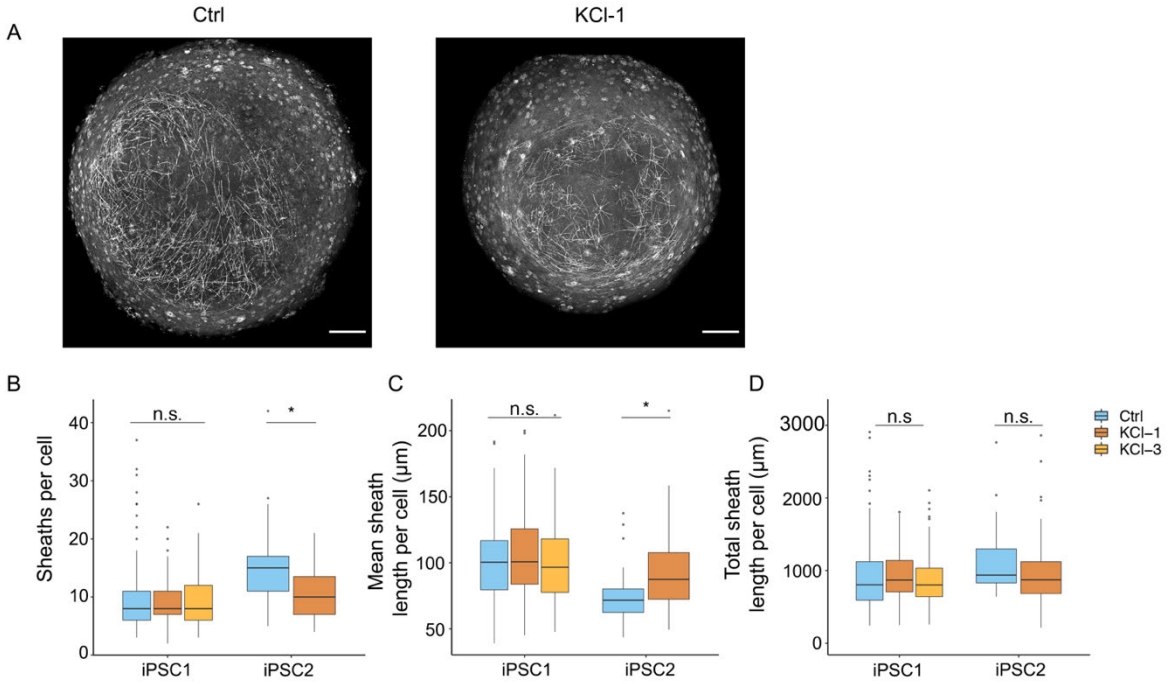

Figure 5.5 High KCl does not affect myelin sheath number per cell

A Representative images of CNP staining in Ctrl and KCl-1 treated myelinoids (scale 250μm). B) Sheath number per cell. iPSC1; no change between Ctrl, KCl-1 or KCl-3. iPSC2; 31.3% reduction, mean change of 15.2 to 10.5 sheaths per cell in KCl-1, $p = 0.03$, 95% CI: 3.5% to 51%. C) Mean sheath length per cell. iPSC1; no change between Ctrl, KCl-1 or KCl-3. iPSC2; 26% increase in mean sheath length per cell, $p = 0.013$, 95% CI: 4.9 % to 51%.

D) No change was found in total sheath lengths per cell between Ctrl and KCl-treated myelinoids. Data collected from 498 cells from 33 myelinoids from 3 batches across 2 cell lines. < 0.05 * generalised mixed model with individual myelinoids included as a random effect.

5.2.6 BDNF increases oligodendrocyte density without affecting sheath number per cell

Brain-derived neurotrophic factor (BDNF) is a member of the neurotrophin family of growth factors, which together with nerve growth factor (NGF) and neurotrophin 3 and 4 (NT-3/4), exert a wide range of actions in both the CNS and PNS via two classes of transmembrane receptors: the tropomyosin-related kinase (Trk) receptor B (TrkB) and p75 neurotrophin receptor (p75NTR). Neurotrophin signalling regulate numerous processes including cell survival, proliferation and differentiation, axon and dendrite outgrowth, synaptic activity, and myelination (E. J. Huang & Reichardt 2003; Chan et al. 2001; Xiao et al. 2009).

Regarding neuronal activity, BDNF-TrkB signalling enhances differentiation of neural precursors, as well as synapse formation and spontaneous neuronal activity (Ahmed et al. 1995; Aguado et al. 2003). In addition, BDNF has been shown to enhance quantal neurotransmitter release by increasing the number of docked vesicles in hippocampal excitatory synapses (Tyler & Pozzo-Miller 2001).

BDNF can also directly act upon oligodendroglial cells via TrkB receptors to increase the total number of oligodendrocytes, the number of myelinating oligodendrocytes and myelin area in rat DRG-OPC co-cultures (Xiao et al. 2010; Lundgaard et al. 2013). Indeed, both global haploinsufficiency of BDNF as well as conditional knockout of Bdnf in mature (MBP+) oligodendrocytes led to CNS hypomyelination (Vondran et al. 2010; Xiao et al. 2010; Nicholson et al. 2018), though different patterns of hypomyelination were observed (Fletcher et al. 2018). Intriguingly, it was shown that loss of TrkB expression in Pdgfr-α^{+} OPCs blocked activity-regulated oligodendrogenesis and myelination in optogenetically-stimulated cortical projection neurons (Geraghty et al. 2019). Additionally, BDNF has been shown to modulate the mode of myelination to one that is NMDAR-dependent (Lundgaard et al. 2013). Thus, BDNF is a pro-myelinating factor in the CNS and potentiates both developmental and activity-dependent myelination.

Against this background, I was interested in asking whether 1) BDNF treatment would potentiate myelin formation in iPSC myelinoids and 2) whether BDNF had an effect

on myelin sheath number or sheath length, which has not previously been investigated. To assess the role of BDNF in iPSC myelinoids, 10 ng/ml BDNF was supplemented to the myelination medium between MI and MI-12.

Representative images of Ctrl and BDNF-treated cultures are shown in Figure 5.6A. BDNF-treated myelinoids did not show any difference in myelin sheath number or mean sheath length per cell (Figure 5.6B-C). However, the density of oligodendrocytes was often so high in BDNF-treated cultures that accurate tracing of myelin sheaths per cell in those areas was impossible. This is demonstrated by the increased number of total and myelinating oligodendrocytes per 100 μm radius (241% increase, p = 0.0026) Figures 2.6D-E). Whilst I have shown that oligodendrocyte density does not affect sheath number or sheath length under basal conditions, it is possible that BDNF may be acting differentially on oligodendrocytes in areas of high oligodendrocyte density. Therefore, the role of BDNF in regulating sheath number and sheath length remains inconclusive.

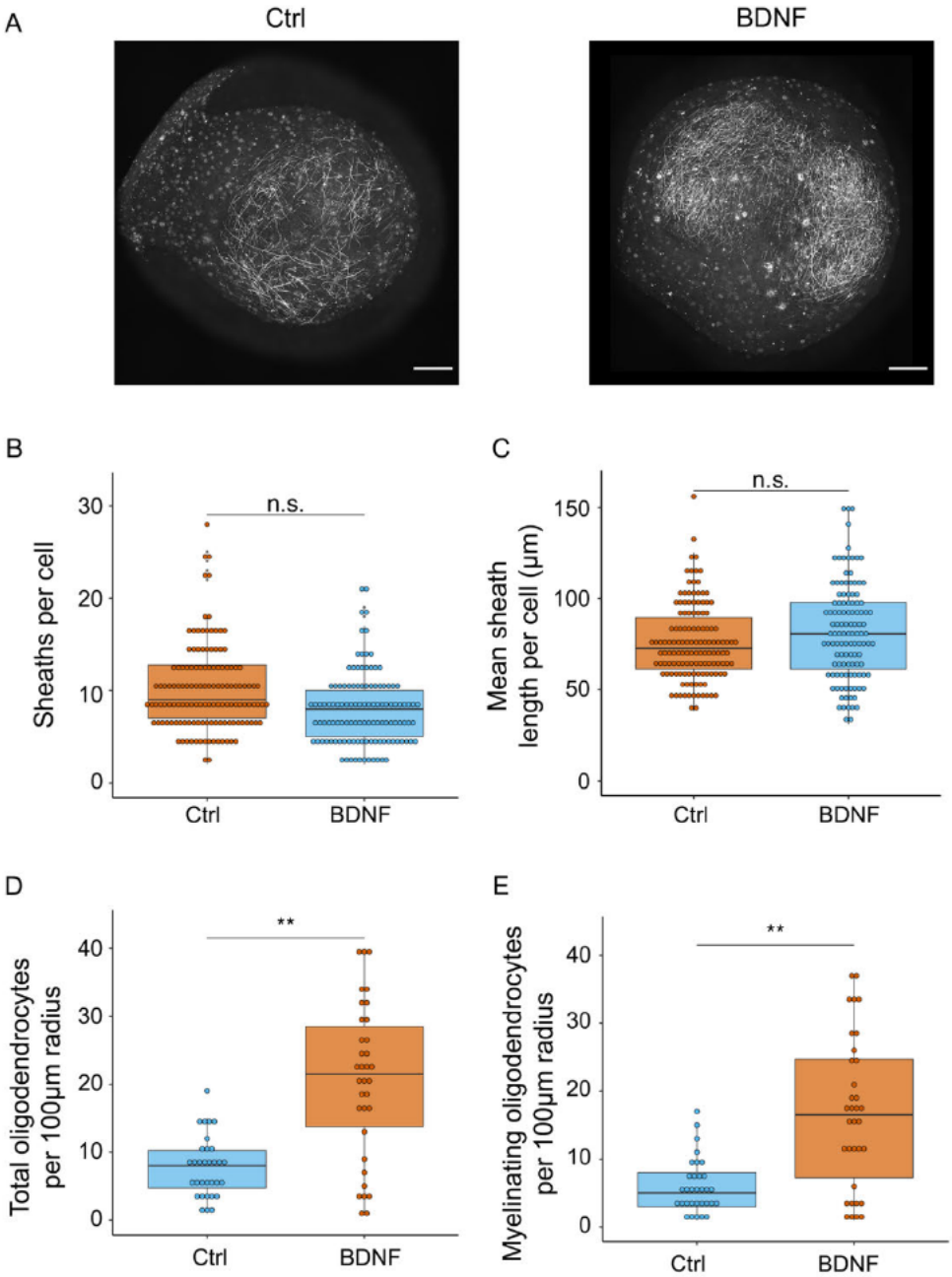

Figure 5.6 BDNF increases oligodendrocyte density but not sheath number per cell

A) Representative images of CNP staining in Ctrl and BDNF-treated myelinoids (scale = 250μm).

B) No difference in sheath number per cell between the two conditions.

C) No difference in mean sheath length per cell between the two conditions.

D-E) Nearest neighbours analysis showed a 240 % in the total number of oligodendrocytes (p = 0.0026, 95% CI: 36 % to 427 % increase) (D) and a 247 % increase in the number of myelinating oligodendrocytes (p = 0.004, 95% CI: 35 % to 458 % increase) (E) per 100 μm radius. Data collected from 251 cells from 22 myelinoids across 3 batches. < 0.05 * generalised mixed model with individual myelinoids included as a random effect.

5.3 Conclusions

In this chapter, I have characterised the myelinating profile of individual human oligodendrocytes with respect to sheath number and length per cell and demonstrated that myelin development of single cells can be pharmacologically modulated. Specifically, blebbistatin treatment increased sheath number per cell by over 40%. Furthermore, I have made preliminary investigations into the role of vesicular release in regulating activity dependent myelination by human oligodendrocytes. TeNT-induced blockade of vesicular release reduced myelin sheath number per cell by 22% on average without affecting the density of myelinating oligodendrocytes. However, the converse experiment to potentiate neuronal activity via KCl-mediated depolarisation did not affect myelin formation by individual cells. Finally, BDNF treatment had no effect on sheath number per cell but increased the number of oligodendrocytes by approximately 2.5 fold.

5.4 Discussion

Early in the myelination process, oligodendrocytes rapidly establish the number of axons they myelinate after a dynamic process of forming and retracting nascent sheaths on neighbouring axons (Czopka et al. 2013). Live imaging studies have demonstrated that the number of internodes per cell can be modulated by changes in neuronal activity and is remarkably stable thereafter (Mensch et al. 2015; Hines et al. 2015; Czopka et al. 2013; Hughes et al. 2018; Hill et al. 2018). A number of parameters regulate the conduction velocity of action potential propagation along myelinated fibres including axon diameter, periaxonal space, and myelin thickness, as well as nodal and internodal length (Halter & Clark 1991; Arancibia Carcamo et al. 2017). Modulating the number and lengths of internodes along individual axons therefore provides a mechanism to fine-tune signal transduction (Young et al. 2013).

iPSC myelinoids generate on average 11.9 myelin sheaths per cell (median = 10), though a number of cells were found to myelinate over 40 axons each. Variability in sheath number between cells of the same myelinoid was less than for sheath number between myelinoids of the same or different batches. *In vivo,* sheath number and sheath length can vary greatly both between and within CNS regions (Murtie et al. 2007; Chong, Rosenberg, Fancy, Zhao, Shen, A. T. Hahn, McGee, Xu, Zheng, L. I. Zhang, Rowitch, Franklin, Lu & Chan 2012a). Mouse cortical oligodendrocytes generate up to 60 sheaths per cell (Chong, Rosenberg, Fancy, Zhao, Shen, A. T. Hahn, McGee, Xu, Zheng, L. I. Zhang, Rowitch, Franklin, Lu & Chan 2012a) and rat spinal cord oligodendrocytes have been shown to generate as few as 1–2 sheaths per cell, possibly due to the presence of large calibre axons (Hildebrand & R. Hahn 1978; Bjartmar et al. 1994). Further comparisons with other model systems (zebrafish: approx. 10 sheaths per cell (Mensch et al. 2015), DRG-OPC co-cultures: approx. 7 sheaths per cell (H. Wang et al. 2008), rat primary oligodendrocytes on inert microfibres: approx. 7 sheath per cell (Bechler et al. 2015), shows that iPSC myelinoids generate a physiologically relevant number of myelin sheaths per cell, which performs better than other *in vitro* models. Pio del Rio-Hortega highlighted the diversity of myelinating oligodendrocyte morphologies nearly a 100 years ago (Pérez-Cerdá et al. 2015). That single oligodendrocytes in the spinal cord generate fewer sheaths surrounding large diameter axons compared to the many small diameter

axons myelinated per cell in the brain, has since been confirmed across all animal models studied so far (Hildebrand et al. 1993). Even neighbouring oligodendrocytes in iPSC myelinoids can demonstrate differing morphologies. Does this reflect different subtypes of oligodendrocytes? Does this reflect different axonal targets? Would forebrain-patterned myelinoids generate a greater number of internodes per cell? These questions remain outstanding.

Myelin sheath lengths in iPSC myelinoids are surprisingly long for an *in vitro* model. Mean sheath length per cell was found to be 89 μm and multiple sheaths over 300 μm were observed. Both co-cultures of rat primary oligodendrocytes with either DRGs, shiverer mouse organotypic slice culture or microfibres and zebrafish, generate a mean sheath length of approximately 20-40μm (Bechler et al. 2015; Mensch et al. 2015). *In vivo,* oligodendrocytes generate a range of lengths between 20 and 220μm in mice (Chong, Rosenberg, Fancy, Zhao, Shen, A. T. Hahn, McGee, Xu, Zheng, L. I. Zhang, Rowitch, Franklin, Lu & Chan 2012a) and up to 241μm in cats (Remahl & Hildebrand 1990). More than likely, the enhanced sheath length observed reflects the physiological maturity of iPSC myelinoids, resulting from the dense compaction of neurons, astrocytes, and oligodendrocytes over several months. As human post-mortem data on CNS internodal length is not available and nor is there a comparable culture model derived from rodent cells, it is difficult to determine whether species-specific differences might also be contributing to increased sheath length. *In vivo,* internode length varies considerably but has been shown to increase linearly with axon diameter (Ibrahim et al. 1995). Given the unremarkable calibre of myelinated axons observed in iPSC myelinoids (mean 0.8 μm), it is possible that human oligodendrocytes are generating comparatively long myelin sheaths. However, another factor is the non-histotypical arrangement of axons and the abundance of non-myelinated axon area, which might provide myelin sheaths with more space to elongate.

Pharmacological manipulation of iPSC myelinoids modulated the myelinogenic potential of individual oligodendrocytes. Inhibition of non-muscle myosin II with blebbistatin increased the number of myelin sheaths per cell by 44.5% and also reduced mean sheath length per cell. In DRG co-cultures, blebbistatin treatment was associated with a 3 to 4-fold increase in sheath number per cell. However, in their system, the authors report that oligodendrocytes under basal conditions only

generated 4.8 ± 3.5 sheaths per cell (H. Wang et al. 2008). This low degree of baseline myelination makes it difficult to compare the percentage increase in sheath number per cell observed between the two experiments as the therapeutic window was greater for their experiment. Nevertheless, this finding demonstrates that pharmacological modulation of human myelination is possible and opens up possibilities for future studies.

The results of the TeNT experiment are in-line with a number of other studies that have investigated blockade of synaptic vesicle release on myelin development. TeNT-treated myelinoids demonstrated an overall reduction in sheath number of 22%. However, the percentage reduction varied between individual batches of myelinoids with 3 out of 5 batches showing over 30% reduction in sheath number per cell. This mirrors in vivo data where TeNT-expressing zebrafish show a 30% reduction in sheath number per cell (Mensch et al. 2015). A possible explanation for the reduced effect of TeNT treatment in the remaining two batches is that the degree of neuronal activity may not have developed to a substantial level in those myelinoids. Given that myelination is suspected to proceed via both activity-dependent and independent mechanisms (Bechler et al. 2017), the percentage difference in sheath number from TeNT exposure is dependent on the initial degree of neuronal activity (and activity-dependent myelination) present within iPSC myelinoids. Additionally, it has been shown that vesicular release-mediated myelin development does not occur in all neurons. Whilst expression of TeNT in reticulospinal neurons of the zebrafish suppressed myelination along their lengths, myelination was normal along commissural primary ascending neurons of the zebrafish expressing TeNT (Koudelka et al. 2016). Therefore, it possible that blockade of vesicular release had varying effects on the myelination of different neuronal subtypes identified in iPSC myelinoids, which could influence overall sheath number per cell by the relative proportion of those neurons within each (or batch of) myelinoids.

In DRG-OPC co-cultures, (Wake et al. 2011) used either 3nM BoNT/A or 3μM TeNT for at least 18 hours prior to co-culture to abolish vesicular release and saw the number of myelin segments per cell reduce dramatically from approximately 8 to 1 segment per cell. It is possible that the 1000-fold increase in TeNT concentration used in their study would have suppressed myelin development further in iPSC myelinoids. However, such a high dose may have been toxic over the long time-course of myelin

development in this culture model and, as mentioned, a baseline of activity-independent myelination is expected and indeed supports the positive viability of myelinoids exposed to long-term TeNT treatment. Importantly, whilst Wake et al. abolished vesicular release prior to co-culture with OPCs, it was found that TeNT did not reduce sheath number per cell by directly acting on oligodendrocytes as expressing the TeNT light chain exclusively in zebrafish oligodendrocytes resulted in a normal number of myelin sheaths per cell (Mensch et al. 2015).

TeNT exposure resulted in a slight increase in mean sheath length per cell in iPSC myelinoids. This result was not consistent across the two cell lines used for this study and is not likely to be of biological significance as the percentage increase per batch did not correlate with the percentage difference in sheath number per cell (Figure 5.4G). Indeed, TeNT expression in the developing zebrafish did not modulate sheath length (Hines et al. 2015; Mensch et al. 2015). Finally, there is discrepancy in whether TeNT affects the number of myelinating oligodendrocytes. Whilst DRG-OPC co-cultures showed no difference in oligodendrocyte differentiation, both zebrafish studies identify a small but significant reduction in the number of myelinating oligodendrocytes (Wake et al. 2011; Hines et al. 2015; Mensch et al. 2015). As the density of oligodendrocytes was normal in iPSC myelinoids, it may simply reflect differences between zebrafish and *in vitro* culture models. Nevertheless, this is the first demonstration that human myelination responds to regulated vesicular release, indicating that human oligodendrocytes might respond to changes in neuronal activity during development and learning.

Having demonstrated myelin-related changes in response to suppressed neuronal excitability, I attempted the converse experiment: to potentiate myelin sheath number per cell by increasing neuronal activity. Whilst KCl robustly induces depolarization of cells and release of synaptic vesicles (Bading et al. 1993; Freyberg et al. 2016), KCl-treated myelinoids did not show an increase in sheath number per cell. A likely explanation is due to overstimulation with KCl in the chosen treatment paradigm that results in intrinsic adaptation and dampened excitability of neurons. Indeed, a reduction of sheath number per cell was found in iPSC myelinoids treated with KCl in a subset of experiments. It was also shown that patterned electrical stimulation, rather than continuous KCl depolarization more effectively induced release of BDNF in neuronal cultures (Balkowiec & Katz 2000). It would therefore be interesting to test

whether reducing KCl treatment to very short exposure times would result in a different outcome.

Finally, whilst oligodendroglial TrkB signalling has been shown to potentiate myelin development in a number of ways, the role of BDNF in modulating myelin sheath number has not been investigated. Interestingly, neither sheath number nor length was affected by BDNF treatment. However, as has been shown previously (Xiao et al. 2010; Lundgaard et al. 2013), BDNF induced a robust increase in the density of myelinating and total number of oligodendrocytes in iPSC myelinoids. Consequently, firm conclusions over the role of BDNF in modulating sheath number per cell is difficult to make as the increased density of cells prevented manual tracing of sheaths within those dense areas of myelin. Though under basal conditions oligodendrocyte density did not affect the myelinating profile of individual cells, it possible that BDNF-TrkB signalling may be acting directly to modulate the myelinating profile of individual oligodendrocytes, in addition to increasing the number of myelinating oligodendrocytes. TrkB signalling was shown to be critical for BDNF-mediated increases in the number of myelinating oligodendrocytes (Xiao et al. 2010; Lundgaard et al. 2013). However, it is also possible that enhanced neuronal activity from BDNF exposure supported the integration of new-born oligodendrocytes, as has been shown by both sensory enrichment and motor skill learning (Hughes et al. 2018; McKenzie et al. 2014). In order to establish, conclusively, whether BDNF modulates myelinogenic output per cell, one could employ a virus-based method to sparsely label oligodendrocytes as has been shown previously (Osanai et al. 2016).

In summary, pharmacological and physiological manipulation of iPSC myelinoids leads to predictable outcomes in the morphology of individual oligodendrocytes and highlights the plasticity of myelin development in this system for further studies of the regulators of myelination.

Chapter 6 Automated analysis of iPSC myelinoids

6.1 Introduction

A challenging feature of iPSC myelinoids is the heterogeneity of myelin formation across the surface of myelinoids. The analysis of individual oligodendrocyte morphology described above was performed with blinding and randomisation. Although regions of myelin had to be manually selected for analysis, large tiled areas were acquired to further mitigate bias. However, a completely unbiased method of measuring myelin volume across entire myelinoids would enable researchers to address questions relating to the response of global myelin volume to different conditions and support the findings made at higher resolution.

High content automated image analysis is increasingly being employed to *in vitro* cultures to increase experimental throughput, remove human error and bias, and improve reproducibility. However, myelin is a technically challenging structure for automated segmentation due to the expression of myelin proteins throughout the cell body and the processes of oligodendrocytes. A common method of measuring myelination relies on quantifying MBP^+ pixels above a certain threshold, or those pixels that co-localise with an axonal marker such as NF-H (Kerman et al. 2015; Lariosa-Willingham et al. 2016). A major challenge is to avoid the inclusion of non-compacted MBP^+ pixels that would improperly contribute to a score of 'myelin area', especially when maximum projection images are being used. The development of a more stringent segmentation method that is able to account for the three-dimensionality of myelin would enable more accurate analysis of myelin volume and improve the confidence in findings.

This is of particular relevance to studies investigating small molecule-induced potentiation of myelin formation. High-content phenotypic screens aiming to identify inducers of oligodendrogenesis have identified a number of compounds that promote the differentiation of oligodendrocytes (Deshmukh et al. 2013; Mei et al. 2014; Najm et al. 2015; Mei et al. 2016; Early et al. 2018; Hubler et al. 2018). When applied to secondary myelination assays, these compounds also promote myelin formation and aid functional recovery in experimental mouse models of demyelination. Interestingly, a miniaturised 96-well-plate myelination assay derived from embryonic rat cortical cells, identified different classes of compounds not found in differentiation screens

that promoted myelination (Lariosa-Willingham et al. 2016). Whilst not directly comparable, due to the presence of neurons in their culture model, this does support the view that differentiation and myelination are distinct cellular processes and that a combinatorial treatment that targets each of them is a favourable strategy for treating white matter disorders.

Zebrafish offer an alternative and powerful method with which to perform *in vivo* phenotypic drug discovery and was recently used to identify compounds that promoted the number of myelinating oligodendrocytes (Early et al. 2018). However, a human stem cell-derived high-content screen of oligodendrocyte differentiation has also identified novel classes of compounds that have not previously been associated with oligodendrocyte differentiation, indicating that species-specific differences might exist in regulating oligodendrogenesis (Magnani, Telford-Cooke et al., manuscript in preparation). Indeed, the high failure rate of clinical trials based on experimental data suggests that more physiological—and potentially species-specific—models of drug discovery/validation are required to improve the development of novel treatments (Silva & Haggarty 2019; Garner 2014; McGraw et al. 2017). iPSC myelinoids provide a complementary tool that bridges high-throughput models of differentiation with a human and physiologically representative environment to test the pro-myelinating potential of candidate compounds.

In order to corroborate findings made at the level of individual oligodendrocytes and to enable analysis of global changes in myelination in response to pharmacological modulation of myelinoids, I sought to develop a novel automated method of whole-myelinoid myelin segmentation.

6.2 Results

6.2.1 Image acquisition

Using the ImageXpress Micro Confocal microscope, entire myelinoids were imaged. First, a low magnification (4 X objective) scan of mounted microscope slides was performed and regions of interest (ROI) drawn around $DAPI^+$ myelinoids for subsequent image acquisition. Each ROI may be composed of between 9 and 25 sites (each 20 X site has a maximum area of 0.49 mm^2). Automated laser-based focussing was used to the superficial edge of the myelinoid in each acquisition site. Z-stacks between 12-25 μm (1 μm z-step) beginning at the superficial edge were acquired using a 20 X plan Apo objective in 42 μm pin hole confocal mode with 10 % overlap for stitching. Practically, a single myelinoid captured across a 4x4 grid in 4 wavelengths and a 12 μm z-stack may be acquired in approximately 23 minutes and is composed of 768 individual images and 5.3 GB of data.

The representative images presented throughout this thesis were acquired on the ImageXpress microscope. An ImageJ macro was used to stitch best projection images from each site (see Appendix, Chapter 10.2).

6.2.2 Image analysis

Using the MetaXpress software, a custom module was developed to detect and quantify the number of DAPI+ cells, the number of SOX10+ cells, the volume of compact myelin and NF-H+ axonal density.

In order to segment myelin, an adaptive threshold was first used to segment MBP or CNP staining to identify objects above a defined threshold of background intensity. The Filter Mask tool was used to selectively remove objects with a Fiber Breadth > 16 μm, a Fiber Length < 10 μm and an Area < 45 μm^2. The Shrink Objects tool was then used to shrink objects by 4 pixels and a subsequent filter step removed those objects that had an Elliptical Form Factor < 3.7, Fiber Breadth of > 8 μm and an Intensity Standard Deviation < 500. Keep Marked Objects was then used to retain objects from the first Filter Mask that overlaid with the second Filter Mask of shrunk objects. This step specifically helped remove the non-myelin objects including cell bodies and debris. The Find Blobs tool was used to further identify non-myelin objects with an approximate width between 7.5-100 μm, which were then enlarged by 6 pixels and subtracted from the Filter Mask. This step was repeated with blobs approximately 4-6 μm in width. This step was particularly important when segmenting compact myelin from CNP-stained myelinoids as CNP also labels myelinating cell bodies and processes. Next, another filtration step removed objects with a Total Area < 50 μm to again remove non-myelin objects and prevent the formation of interconnected non-myelin objects in the next step. The 3D tool Connect Touching Objects was used to merge objects between neighbouring z-steps to produce a three-dimensional segmentation mask. A final filtration step removed 3D objects with a volume ≤ 400 μm^3 and a diameter ≤ 45 μm. Representative images of myelin segmentation in a single acquisition site is shown in Figure 6.1A.

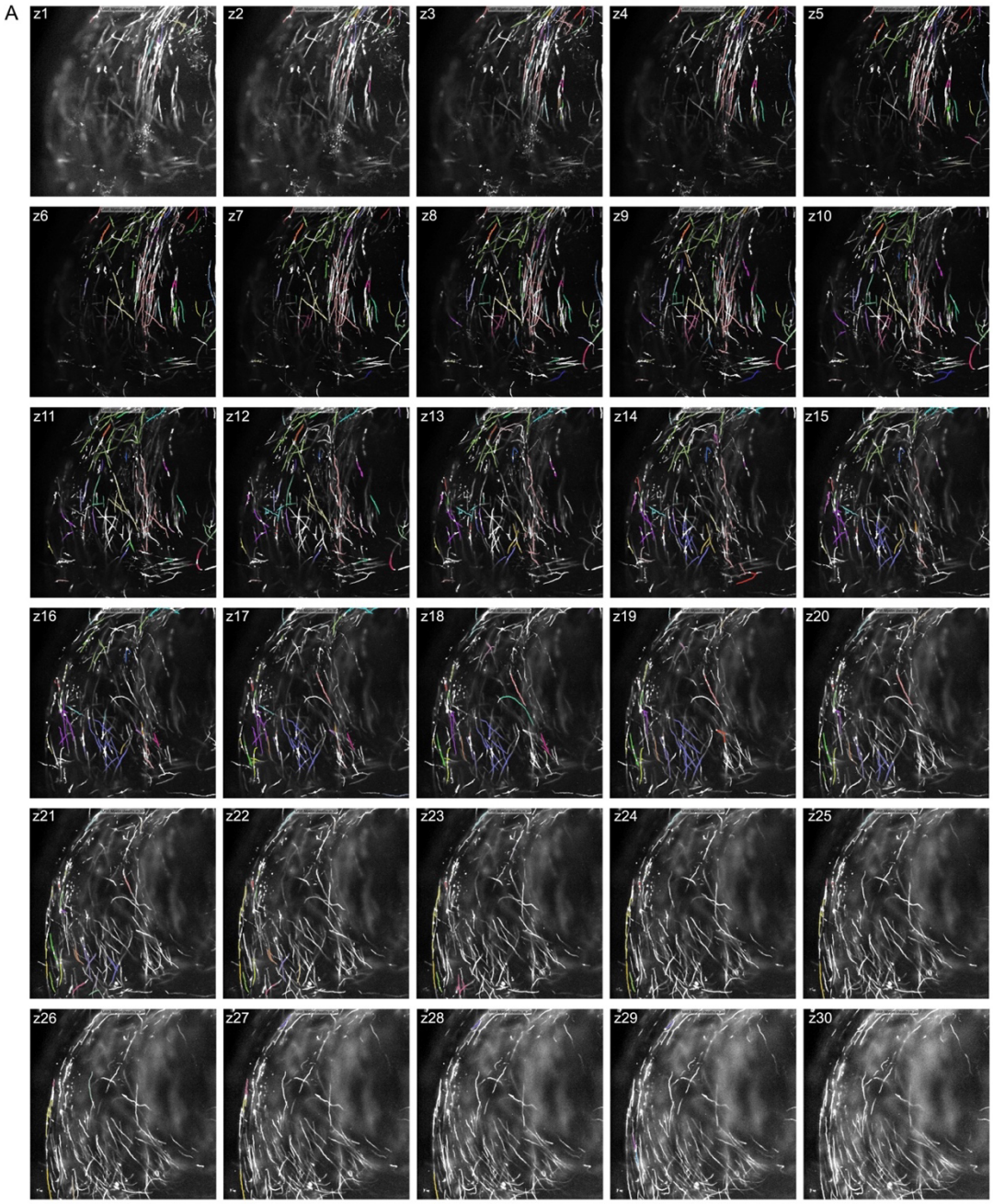

Figure 6.1 Automated segmentation of myelin formation

A) Z-stack series of MBP+ myelin in grey with segmented compact myelin overlaid in colour with 1μm steps.

The segmentation of DAPI$^+$ and SOX10$^+$ cells was achieved by identifying round objects of a diameter between 5-10μm, thresholded against local background intensity. Each Z-step was then stitched together by connecting touching objects with a displacement of 4μm (Figure 6.2A-B). For axonal density, the integrated intensity of NF-H$^+$ staining was used as a proxy measure for the density of NF-H$^+$ axons as it was not possible to segment individual axons accurately (Figure 6.2C). To do so, a Simple Threshold was used to segment the total image area and the Connect by Touching tool was used to produce a volumetric measure for the entire acquisition site. The integrated intensity of NF-H$^+$ staining, as well as the total volume of segmented myelin (μm^3) and the number of SOX10+ and DAPI+ nuclei, were measured within this total image volume to produce a single score for each measurement.

Once again, practically, a single unit of analysis (i.e. a single acquisition site) would take approximately 6-7 minutes (1 myelinoid ~ 1.5h). However, using the MetaXpress PowerCore software, which enables the use of additional central processing units (CPUs), up to 9 units of analysis could be completed simultaneously, greatly increasing the analysis throughput. Downstream processing was performed using RStudio to process exported data tables, aggregate measurements for each myelinoid, and perform statistical analyses.

An important consideration is that since the initial threshold of either CNP$^+$ or MBP$^+$ immunostaining has the biggest downstream effect on total myelin area, it was necessary to optimise this for each experiment to account for changes in the staining intensity. The same settings were then used for each myelinoid and treatment conditions per experiment. All other analysis settings were also maintained. When comparisons between multiple experiments were made, the data were normalised to the mean value of the control condition for each experiment.

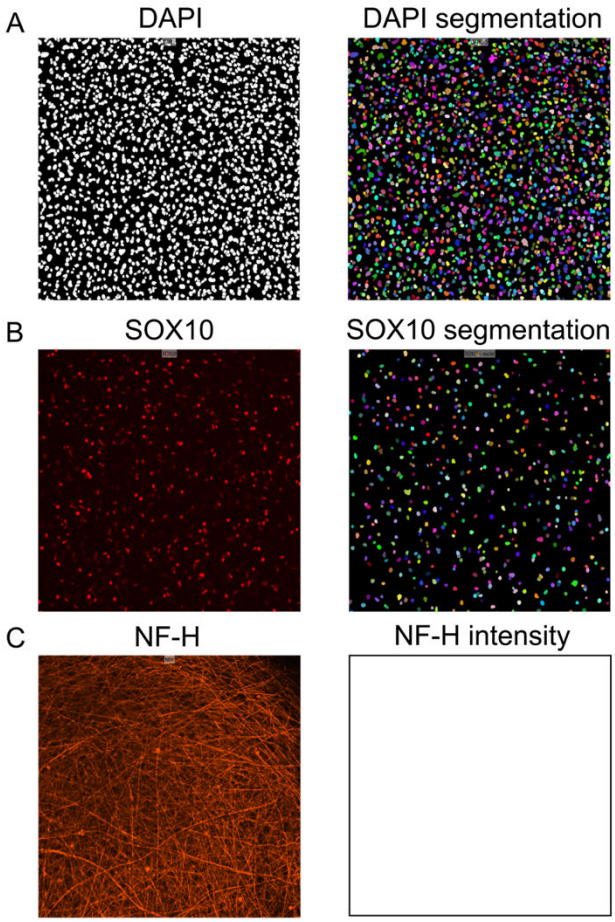

Figure 6.2 Automated segmentation of other cell-types

A) DAPI staining and segmentation.

B) SOX10 staining and segmentation.

C) NF-H staining and a box to represent extraction of the integrated intensity of NF-H+ pixels across the acquisition volume.

6.2.3 Automated analysis of myelinoids over time

In order to demonstrate the specificity of the automated analysis in recognising compact myelin, Figure 6.3 shows the myelin volume measured from individual myelinoids from MI-4, MI-8, and MI-12 alongside best projection images of those same myelinoids. Whilst the MI-4 myelinoid has an abundance of non-myelinating oligodendrocytes, only a small volume of compact myelin has been measured, thereby providing confidence that automated analysis of myelin volume is appropriately attributed.

Figure 6.4 shows a series of measurements obtained from a range of myelinoids across the time-course. Figure 6.4 A and B show the increase in myelin volume over time from both CNP and MBP-stained myelinoids. Figure 6.4C-E are ratiometric measurements of myelin volume normalised to NF-H intensity and the number of $SOX10^+$ nuclei respectively, and Figures 3.4D-H show the change in NF-H intensity, $DAPI^+$ cells, $SOX10^+$ cells, and the proportion of $SOX10^+$ cells compared to DAPI over the time-course. As demonstrated by the spread of myelin volume between MI-12 myelinoids, the degree of myelination observed between myelinoids can vary greatly. This is mostly accounted for by the heterogeneity between conversions of iPSCs, rather than between myelinoids of the same conversion. This is shown in Figure 6.4I, which compares the standard deviations of measurements obtained per timepoint and per batch. The smaller deviations per batch illustrates the need to account for data that is nested (i.e. per myelinoid, batch, or cell line) when performing inferential statistics (Aarts et al. 2014).

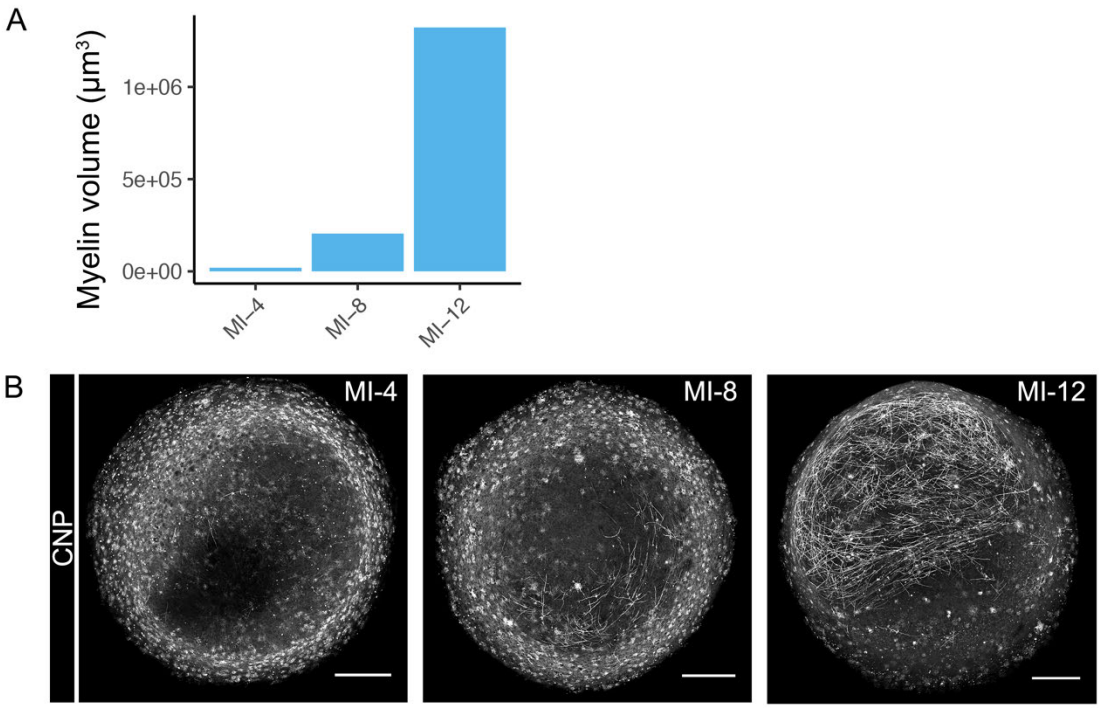

Figure 6.3 Automated analysis of individual myelinoids

A) Automated analysis of myelin volume over time measured from the same myelinoids shown in (B).

Scale = 250μm

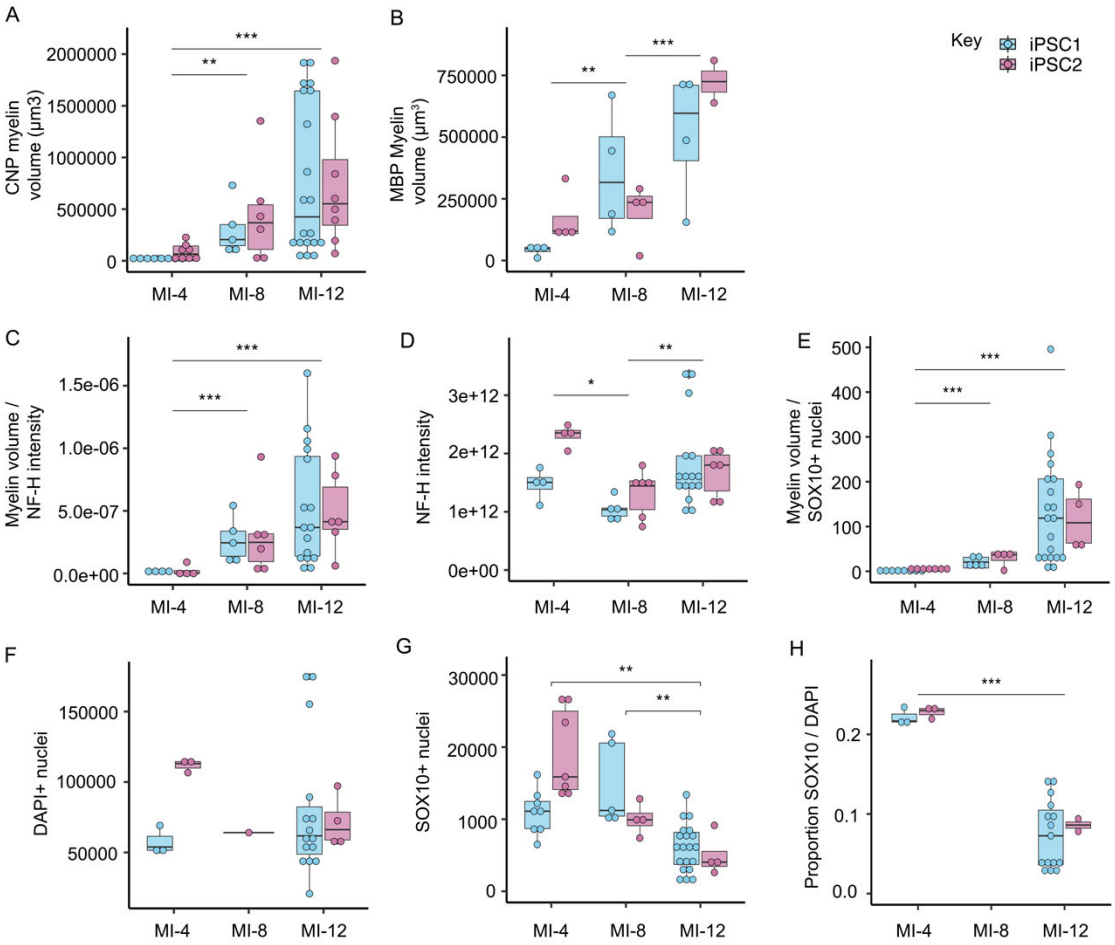

Figure 6.4 Automated analysis of myelin development

A) CNP+ myelin volume increased by over 40-fold between MI-4 and MI-8 ($p = 0.009$) and by over 80-fold by MI-12 ($p < 0.001$).

B) MBP+ myelin volume increased by 2.9-fold between MI-4 and MI-8 ($p = 0.02$) and by 6.4-fold by MI-12 ($p < 0.001$).

C) Myelin volume / NF-H+ intensity increased by 9-fold between MI-4 and MI-8 ($p < 0.001$) and by over 15-fold by MI-12 ($p < 0.001$).

D) NF-H+ intensity fluctuated minimally between timepoints with no change between MI-4 and MI-12. However, MI-8 myelinoids showed a 0.5-fold reduction compared to MI-4 ($p < 0.001$).

continued overleaf.

Figure 6.5 contd. Automated analysis of myelin development

E) Myelin volume / SOX10$^+$ nuclei increased by over 90-fold between MI-4 and MI-8 ($p <$ 0.001) and by over 400-fold by MI-12 ($p < 0.001$).

F) There was no change in DAPI$^+$ nuclei across the timepoints measured.

G) SOX10$^+$ nuclei steadily reduced in number over time with 0.4-fold as many SOX10+ nuclei at MI-12 than there was at MI-4 ($p < 0.001$).

H) Proportion of SOX10$^+$/DAPI$^+$ nuclei steadily reduced in number over time reaching 0.25X the starting population at MI-4 ($p < 0.001$).

Data collected from 23 myelinoids across 7 batches.

6.2.4 TeNT reduces global myelin volume

Having demonstrated that our automated analysis could faithfully measure myelin volume across myelinoids, we sought to use this method to compare myelin volume between experimental conditions.

I was interested in determining the effect of TeNT on global myelin volume as it has previously been shown that expression of the TeNT light chain resulted in a 40 % reduction in the number of myelinated axons in the spinal cord of zebrafish (Mensch et al. 2015). Additionally, given that we see a 22% reduction in the number of myelin sheaths per cell and no change in the density of myelinating oligodendrocytes, one might expect that global myelin volume would be equally disrupted.

Representative images show the distribution of CNP^+ myelin, $NF\text{-}H^+$ axons, and $SOX10^+$ nuclei in Ctrl and TeNT-treated myelinoids (Figure 6.6A). Across two cell lines, exposure to TeNT led to an overall reduction in myelin volume by 41% (p = 0.019, 95% CI: 8% to 62% reduction) (Figure 6.6B). On a subset of experiments, myelinoids that had been immunostained with MBP could also be used to measure myelin volume. Analysis of MBP^+ myelin volume mirrored the results using CNP showing a 39% reduction in myelin volume in TeNT-treated cultures (p = 0.054) (Figure 6.6C). This result also demonstrates the specificity of the automated analysis in removing CNP^+ oligodendrocyte cell bodies and processes from the final mask to leave only compact myelin, which is easily visualised with MBP due to its accumulation in the sheath proper.

There was no change in $NF\text{-}H^+$ intensity between Ctrl and TeNT-treated myelinoids across both cell lines (Figure 6.6D) and so the ratio between myelin volume and $NF\text{-}H^+$ intensity was expectedly reduced (32% reduction, p = 0.028, 95% CI: 4% to 52% reduction) (Figure 6.6E). Whilst there was no overall difference in the number of $SOX10^+$ nuclei between Ctrl and TeNT myelinoids. Breakdown per cell line showed that the number of $SOX10^+$ cells was reduced in iPSC2 (15% reduction, p = 0.031, 95% CI: 9.5% to 87% reduction) (Figure 6.6F). However, as we were only able to attain one iPSC-conversion for this cell line, it is difficult to draw a hard conclusion from this. The four other iPSC-conversions used in this experiment were from another cell line (iPSC1) and do not show a difference in the number of $SOX10^+$ nuclei. Finally,

the ratio between myelin volume and SOX10 number was unchanged between Ctrl and TeNT-treated myelinoids (Figure 6.6G).

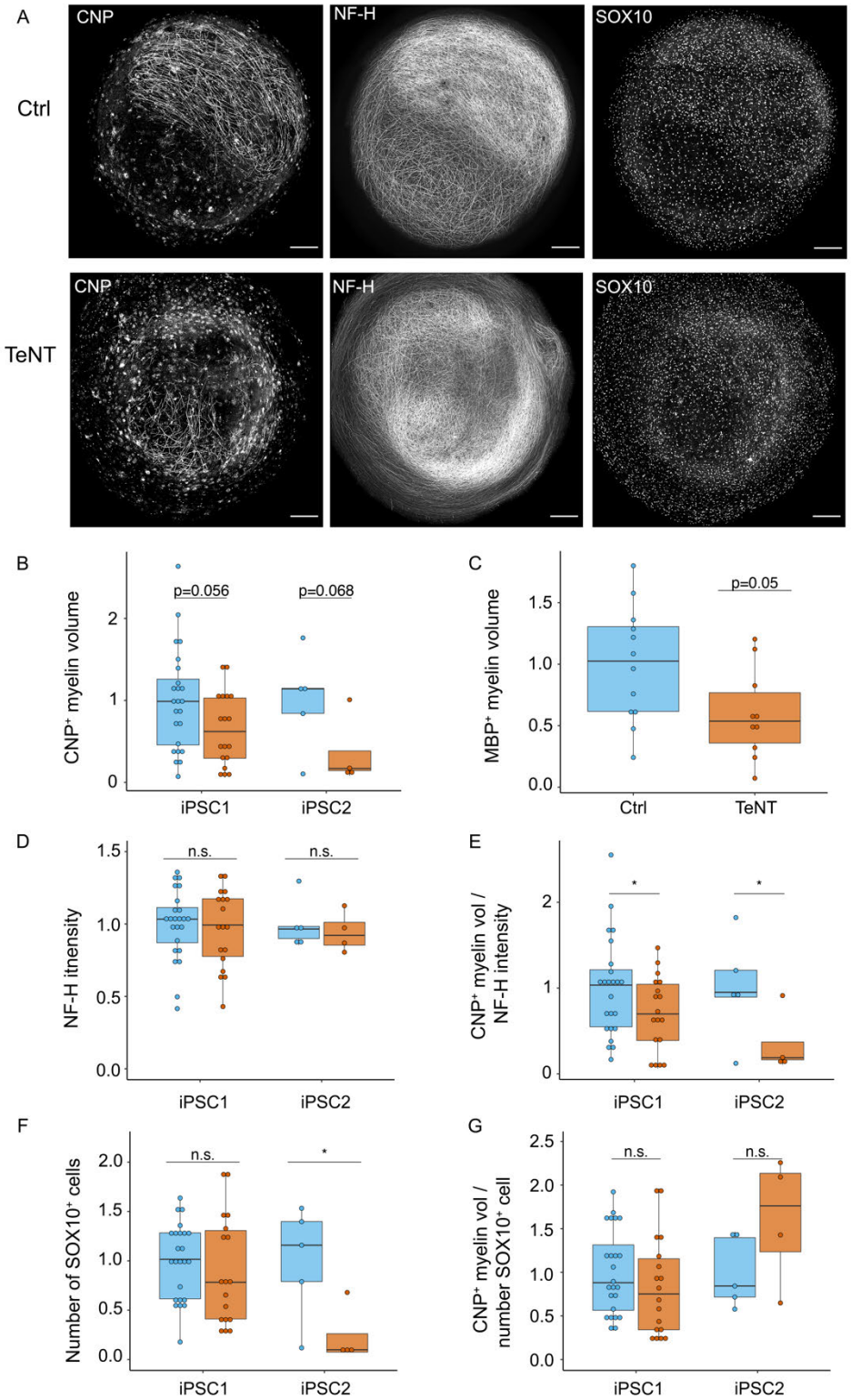

Figure 6.6 TeNT reduces global myelin volume

A) Representative images from CNP⁺ myelin, NF-H⁺ axons and SOX10⁺ oligodendroglia from same myelinoid. Scale = 250μm.

Contd. overleaf

Figure 6.5 TeNT reduces global myelination contd.

B) CNP^+ myelin volume was reduced in TeNT-treated myelinoids. iPSC1; 36% reduction, $p = 0.056$. iPSC2; 64% reduction, $p = 0.068$. The overall effect reported in the main text is greater due to increased strength of generalised mixed model.

C) MBP^+ myelin volume was reduced in TeNT-treated myelinoids (39% reduction, $p = 0.05$).

D) $NF\text{-}H^+$ intensity was not different between Ctrl and TeNT-treated myelinoids.

E) CNP^+ myelin volume / $NF\text{-}H^+$ intensity was reduced in TeNT-treated myelinoids. iPSC1: 35% reduction, ($p = 0.043$, 95% CI: 1.4% to 57% reduction). iPSC2: 65% reduction, ($p = 0.041$, 95% CI: 4% to 87% reduction).

F) Quantification of $SOX10^+$ number. iPSC1; no change. iPSC2; 15% reduction, ($p = 0.031$, 95% CI: 9.5% to 87% reduction).

G) No change in CNP^+ myelin volume / $SOX10^+$ nuclei in TeNT-treated myelinoids.

Data collected from 40 myelinoids from 5 batches across two 2 cell lines.

< 0.05 * generalised mixed model with each batch of myelinoids included as a random effect.

6.2.5 BDNF treatment increases global myelin volume

As discussed above, BDNF has been shown to potentiate myelin volume and can directly act upon oligodendrocytes via their expression of TrkB. In iPSC myelinoids BDNF treatment increased the density of myelinating oligodendrocytes but had no effect on myelin sheath number or mean sheath length per cell (Figure 5.6) In order to see whether the increased density of myelinating oligodendrocytes contributed towards a greater myelin content overall, automated analysis of myelin volume was performed.

Figure 6.7A shows representative images of DAPI, SOX10, CNP, and NF-H staining in Ctrl and BDNF-treated myelinoids. Analysis of $DAPI^+$ nuclei showed no difference between the two treatment groups (Figure 6.7B) and whilst a trend towards an increase in the number of $SOX10^+$ nuclei is seen in BDNF-treated cultures, neither $SOX10^+$ number nor the proportion of SOX10 / DAPI nuclei were significantly different between the two conditions (Figure 6.7C-D). However, BDNF treatment did increase myelin volume by 83 %. NF-H intensity was unchanged and thus the ratio of myelin volume / NFH intensity was also increased, by 75 %. There was no change in the ratio of myelin volume / $SOX10^+$ nuclei. This is likely due to the increasing trend of $SOX10^+$ cells in BDNF treated myelinoids.

Thus, BDNF acts to potentiate myelination in iPSC myelinoids by increasing the density of myelinating oligodendrocytes and total myelin, similarly to rodent derived cultures (Xiao et al. 2010).

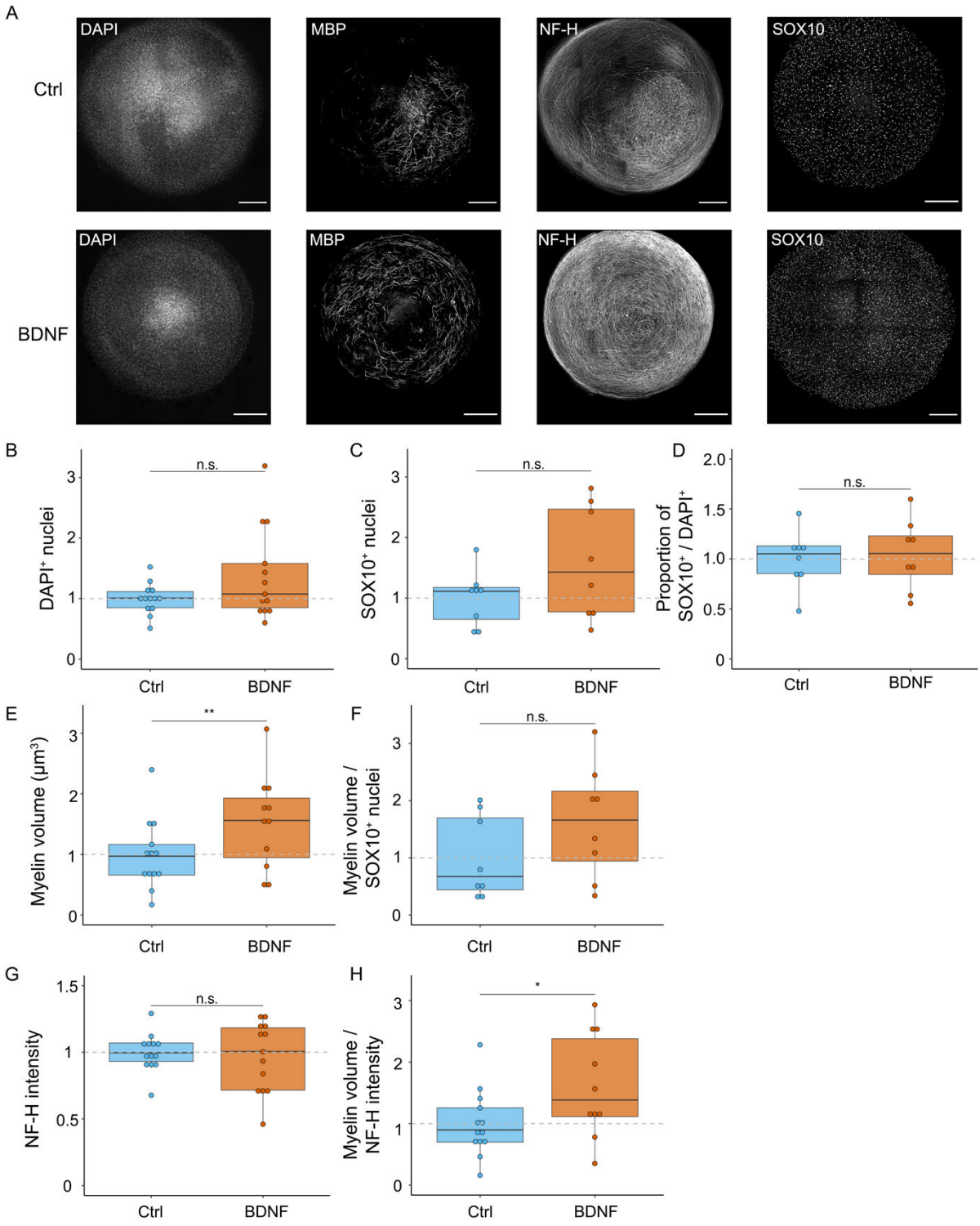

Figure 6.7 BDNF increases total myelin volume

A) Representative images of Ctrl and BDNF-treated myelinoids showing DAPI⁺ nuclei, MBP⁺ myelin, NF-H⁺ axons SOX10⁺ oligodendroglia (scale 340μm).

B-D) There was no change in the number of DAPI+ nuclei (B), SOX10+ nuclei (C) or the proportion of

Contd. overleaf

Figure 6.6 BDNF increases total myelin volume contd.

oligodendroglial cells (D) in BDNF treated myelinoids.

E) BDNF increased myelin volume by 83% ($p = 0.0067$) #.

F)There was no change in the ratio of myelin volume to SOX10$^+$ nuclei) in BDNF treated myelinoids.

G) There was no change in NF-H$^+$ intensity) in BDNF treated myelinoids.

H) BDNF increased the ratio of myelin volume to NF-H intensity by 75% ($p = 0.0131$, 95% CI: 12% to 274% increase) ##.

Data collected from 26 myelinoids across 3 conversions. # mixed linear model with treatment as fixed effect and each conversion as a random effect. ## glm with treatment as fixed effect and each conversion as a random effect. * < 0.05, ** < 0.01

6.3 Conclusions

In this chapter, I have demonstrated the development of an automated method of image acquisition and image analysis that permits unbiased quantification of myelin development in iPSC myelinoids. Using the ImageXpress micro confocal and a custom designed MetaXpress image analysis pipeline, it is possible to measure $DAPI^+$ number, $SOX10^+$ number, myelin volume, and $NF\text{-}H^+$ intensity in a three-dimensional environment.

With this platform, I have shown that myelin development increases between MI and MI-12, that global myelin volume is reduced in TeNT-treated myelinoids and is potentiated in BDNF-treated myelinoids, corroborating the pattern of myelination by individual oligodendrocytes in all conditions.

6.4 Discussion

To overcome the limitation of pixel-based analysis of myelin volume, I have developed a more robust and volumetric method that rapidly identifies compact areas of myelin and avoids retention of non-sheath-like objects by filtering segmentation masks on their elliptical shape, identifying and removing cell bodies and associated process, and filtering neighbouring objects based on their combined area across z-stacks. Recently, a deep-learning protocol for high-throughput analysis of myelination was reported that was capable of single cell resolution (Y. K. T. Xu et al. 2019). Such reports encourage wide-spread adoption of powerful and sophisticated methods of data analysis that will improve the reproducibility and generalise findings between studies. However, since this tool was not available at the time, the data presented in this chapter are based on the ImageXpress pipeline that I have outlined.

Automated segmentation of myelin in iPSC myelinoids reflects the myelin content observed by eye in individual myelinoids. By combining intensity thresholds with size and shape filtration of segmented objects, both pre-myelinating oligodendrocytes with dim and thin processes or those with expansive sheet-like membrane protrusions were excluded, leaving only bright, thick, and linear myelin sheaths. Furthermore, similar measurements of myelin volume between CNP-labelled and MBP-labelled myelin reflects the specificity of this analysis in identifying internodal myelin. Using this method, I've shown that myelin volume increases over the time-course. Furthermore, the number of $SOX10^{+}$ cells goes down expectedly over time, reflecting the *in vivo* scenario where the majority of oligodendrocytes that differentiate do not survive (Barres et al. 1992; Hughes et al. 2018). Therefore, automated analysis of myelin development provides an accurate representation of CNS myelin development.

Using this assay, I was also able to corroborate earlier findings of activity regulated myelin development in iPSC myelinoids. TeNT exposure was shown to reduce total myelin volume—a phenotype that would be expected following a reduction in the number of sheaths per cell whilst maintaining normal numbers of myelinating oligodendrocytes. That NF-H intensity was not changed by TeNT treatment supports the normal viability of neurons after long-term exposure to TeNT. A reduction in

SOX10^{+} nuclei was found for one of the cell lines used. However, as mentioned, since only one conversion of myelinoids was made using this cell line, it is difficult to conclusively say whether this is a true effect of TeNT exposure. Nevertheless, these results support the opinion that iPSC-derived cultures participate in activity-regulated myelination by the global reduction in myelin volume following blockade of vesicular release, which can be explained by a reduction in the number of myelin sheaths per cell.

In the previous chapter, I demonstrated that BDNF treatment resulted in an increase in the number of myelinating oligodendrocytes with normal sheath number and lengths per cell. Therefore, as one might predict, total myelin volume was also increased in BDNF treated myelinoids, similar to what has been shown using rodent derived cultures (Xiao et al. 2010). In their study, using Campenot chambers that physically separate the cell bodies of DRGs and oligodendrocytes, Xiao et al. showed that the BDNF-dependent increase in myelin observed was via direct action on oligodendrocytes. In this study however, BDNF is likely acting on multiple cell types and may also potentiate myelination by increasing neuronal activity.

Overall, this chapter reports a novel automated pipeline for unbiased quantification of myelin and that changes in total myelin volume reflect those at the level of individual oligodendrocytes.

Chapter 7 A platform for testing pro-myelinating compounds

7.1 Introduction

Oligodendrocyte or myelin disruption contributes to several neurological disorders including perinatal hypoxia (Buser et al. 2012); the childhood leukodystrophies (Powers 2004); neurodevelopmental disorders such autism spectrum disorder (Ameis & Catani 2015), schizophrenia (Fitzsimmons et al. 2013; Hakak et al. 2001), and major mental illness (Haroutunian et al. 2014); and neurodegenerative disorders such as multiple sclerosis (Noseworthy et al. 2000), motor neurone disease (Kang et al. 2013), Huntington's disease (B. Huang et al. 2015; J. Zhang et al. 2018), and Alzheimer's disease (Bartzokis 2011). However, in contrast to the prevailing view of CNS tissue regeneration, myelin can be repaired spontaneously following damage. Remyelination is neuroprotective against inflammatory damage, restores efficient conduction velocity to denuded axons, and is associated with functional recovery (Franklin & ffrench-Constant 2017).

Though mature oligodendrocytes are capable of myelin remodelling (Snaidero et al. 2014; Auer et al. 2018) and despite recent evidence suggests that they contribute to repair in humans and large animal models (Yeung et al. 2019; Duncan et al. 2018) (see chapter 2.6), the dominant view from mouse studies is that remyelination proceeds via the following distinct stages: resident OPC recruitment and colonisation of demyelinated lesions, differentiation into mature oligodendrocytes, myelin wrapping, and reorganisation of myelinated axon subdomains (Franklin & ffrench-Constant 2017). During ageing, the efficiency of remyelination progressively declines. This has significant consequences for chronically demyelinating diseases such as multiple sclerosis, where remyelination ultimately fails, leading to neurodegeneration and accumulating disability. Enhancing remyelination is therefore of substantial clinical interest. Significantly, the regenerative capacity of OPCs in adult mice was shown to be enhanced when stimulated with the milieu of a young mouse during heterochronic parabiosis (Ruckh et al. 2012) and, more recently, by the fasting mimetic, metformin (Neumann et al. 2019). These studies initially indicated, and subsequently demonstrated, that the reduced differentiation potential of aged OPCs could be reversed pharmacologically and that the oligodendrocyte lineage may be tractable for the treatment of disease (Franklin et al. 2012).

However, given the complex series of signalling pathways driving each of the steps involved in (re)myelination—as well as the abundance of inhibitory factors that arise in disease (Franklin & ffrench-Constant 2017)—the identification of compounds that modulate each of these processes in turn will enable treatments to be tailored to particular disease pathology. This is relevant for disorders such as multiple sclerosis where neuropathological studies have indicated heterogeneity between lesions and disruption at multiple stages in the repair process. For example, over 30% of multiple sclerosis lesions were found to contain low numbers of OPCs, which is suggestive of recruitment failure (Boyd et al. 2013), whilst others have substantial numbers of OPCs but few differentiated oligodendrocytes, and still others show an abundance of pre-myelinating oligodendrocytes (Lucchinetti et al. 2000; Chang et al. 2002). Furthermore, remyelinated axons are typified by short and thin myelin sheaths (Prineas & Connell 1979; Duncan et al. 2017).

The abundance of multiple sclerosis lesions demonstrating impaired differentiation has led to several high-content phenotypic screens that aimed to identify inducers of oligodendrocyte differentiation as a mode to promote remyelination (Deshmukh et al. 2013; Mei et al. 2014; Najm et al. 2015; Mei et al. 2016; Early et al. 2018; Lariosa-Willingham et al. 2016; Hubler et al. 2018). Several hit compounds have since been validated *in vivo* and one, clemastine fumarate, was recently shown to have beneficial effects on optic nerve conduction velocity in a double-blind clinical trial (Green et al. 2017). Significantly, clemastine fumarate has also demonstrated positive effects in treating other animal models of disease, including Williams syndrome and perinatal hypoxia, as well as in a human adult with hypoxic brain injury (Barak et al. 2019; F. Wang et al. 2018; Cree et al. 2017).

Mostly, these studies have relied on purified cultures of primary rodent- or mouse ES-derived OPCs. This is an important consideration given the differences in the timing and scale of human oligodendrogenesis and the possible exclusion of compounds that promote myelin wrapping. Indeed, both a miniaturised myelination assay derived from embryonic rat cortical cells and an *in vivo* screen of myelinating oligodendrocytes in developing zebrafish identified classes of compounds that promoted myelination, which were not found in OPC differentiation screens (Lariosa-Willingham et al. 2016; Early et al. 2018). Furthermore, a human iPSC-derived high-content screen of oligodendrocyte differentiation has also identified pro-differentiating compounds in

drug classes not previously reported, which indicates that species-specific differences might exist in the regulation of oligodendrogenesis (Magnani, Telford-Cooke et al., manuscript in preparation). Whilst these studies are not directly comparable, due to the use of different cellular and animal models, these findings support the view that differentiation and myelination are distinct cellular processes and that a combinatorial treatment that targets each of them is a favourable strategy for treating white matter disorders. Moreover, due to the high attrition of neuroscience-related drug discovery, it has been suggested that more physiologically complex—and potentially species-specific—models of drug discovery/validation are required to support the development of novel treatments (Silva & Haggarty 2019; Garner 2014; McGraw et al. 2017).

iPSC myelinoids, when paired with an automated and unbiased method of quantifying myelin volume, provide a unique opportunity to test the oligodendrogenic and myelinogenic propensity of candidate compounds in a human model of myelination. In this chapter, I sought to determine whether automated analysis could be used to measure drug-induced changes in oligodendrogenesis and myelination in iPSC myelinoids. First, I determined how the regional densities of different cell-types correlated with each other, in order to identify a potential bottleneck or rate-limiting step in myelinoid myelin formation. Next, I treated myelinoids with miconazole nitrate, a previously identified potent inducer of oligodendrocyte differentiation (Najm et al. 2015), and SGCCBP30, a pro-differentiating compound that was identified in an in-house automated screen of iPSC-derived oligodendrocyte differentiation.

7.2 Results

7.2.1 Myelination is driven by high axonal density

As discussed, myelination takes place in the periphery of myelinoid cultures, which provides a large area of myelin that can be easily visualised in 3D in whole-mounted myelinoids. However, even within this compartment, myelin appears randomly distributed across the surface of myelinoids. I was interested, therefore, in determining whether the density of DAPI$^+$ cells, SOX10$^+$ cells, or NF-H$^+$ intensity was associated with changes in myelin volume and drew correlations between these markers from automated measurements of robustly myelinated myelinoids (see Methods).

Figure 7.1A shows an example myelinoid with uniform expression of SOX10 and extensive myelination that appears constrained to areas of high NF-H density. Figures 7.1B-E show scatter plots correlating the densities of different cell-types. Summary statistics show that DAPI$^+$ and SOX10$^+$ nuclei are closely distributed, with an adjusted $R^2 = 0.76$, and that myelin volume is not dependent on high numbers of SOX10$^+$ cells ($R^2 = 0.07$) but rather high NF-H$^+$ intensities ($R^2 = 0.6$). Finally, a more sophisticated analysis with adjustment for the number of oligodendroglial cells present shows that myelin volume is predicted by axonal density ($R^2 = 0.67$, $p < 2.2e\text{-}16$).

These data suggest that myelin formation is highly dependent on axonal density and that the density of axons may act as a rate-limiting step in myelinoid myelin development, should dense axonal area become saturated with myelin. This is a useful consideration for the analysis of compounds whose mechanism of action is unknown, as off-target effects on neurons and axonal density may indirectly modulate myelin formation. Furthermore, potentiating oligodendrocyte differentiation in the absence of high axonal density may underrepresent the promyelinative capacity of drug compounds.

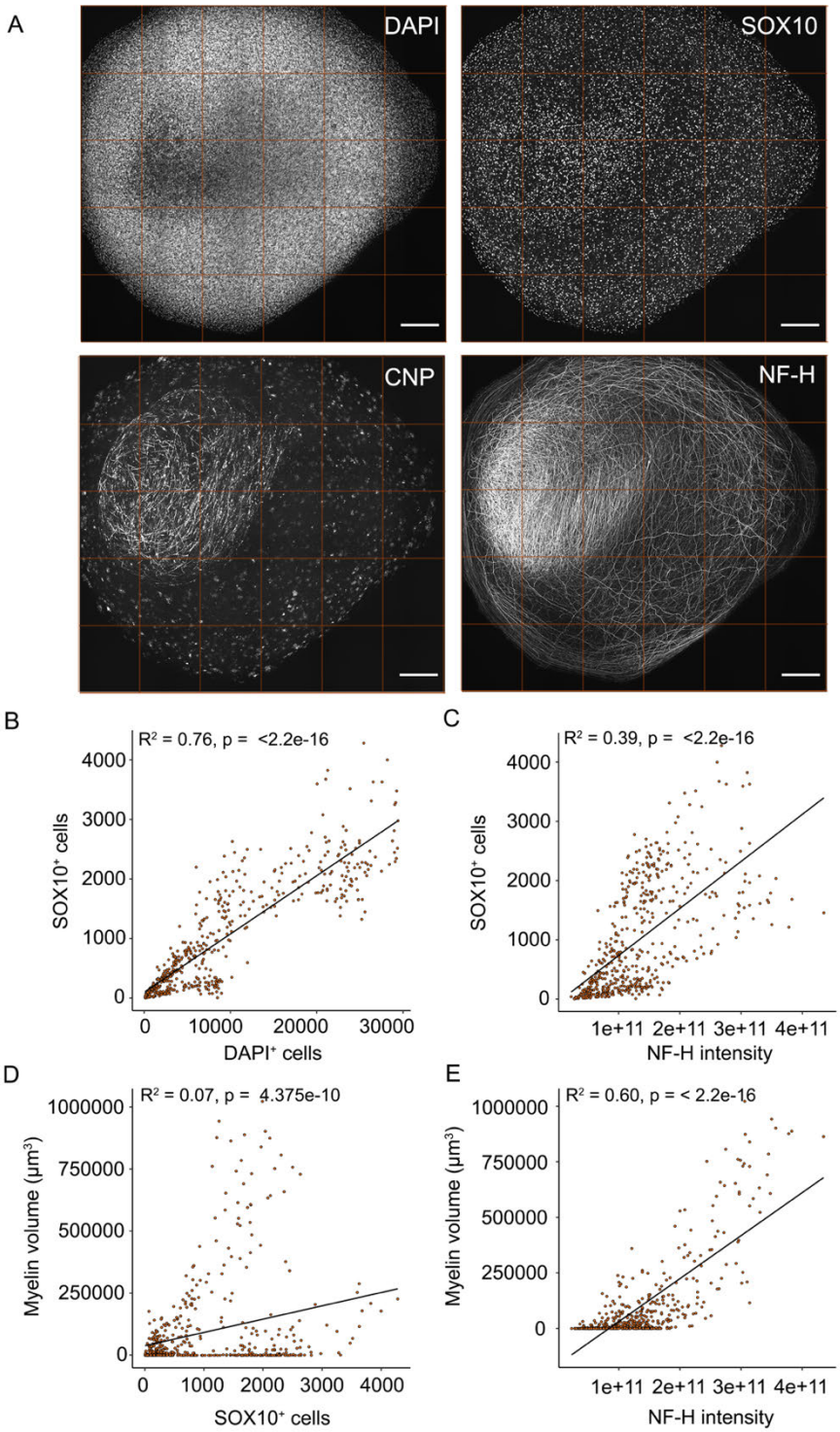

Figure 7.1 Distribution correlations of myelinoid cell-types

A) Representative images of different cell-types within myelinoids overlaid by example grid representing individual acquisition sites for automated analysis (scale 250μm).

B) Correlation between SOX10$^+$ oligodendroglial cells and total DAPI$^+$ nuclei.

Figure 7.1 Distribution correlations of myelinoid cell-types contd.
C) Correlation between SOX10^{+} oligodendroglial cells and NF-H^{+} intensity. D) Correlation between myelin volume and SOX10^{+} oligodendroglial cells. E) Correlation between Myelin volume and NF-H^{+} intensity.
Each dot represents a single square grid (acquisition site). Over 500 data points were analysed from 28 myelinoids at MI-12 across 6 conversions. Linear model with robust standard errors.

7.2.2 Miconazole nitrate

Miconazole nitrate is an antifungal agent that was found to potentiate OPC differentiation from mouse pluripotent epiblast stem cells *in vitro* and which alleviated disease severity in the experimental autoimmune encephalomyelitis (EAE) mouse model of progressive multiple sclerosis (Najm et al. 2015). Miconazole nitrate, similar to several recently identified pro-differentiating compounds, exerts its effects on OPC differentiation by targeting CYP51A, an essential enzyme involved in cholesterol biosynthesis (Hubler et al. 2018).

Given the extensive timeframe required for myelinoid myelination, choosing an appropriate treatment strategy proved challenging. Figure 7.2 shows the results from a single experiment in which myelinoids were cultured continuously with increasing concentrations of miconazole (MIC) for 12 weeks between MI and MI-12 (Figure 7.2A). This treatment strategy had a dose-dependent toxic effect on myelinoids Illustrated by the representative images of MBP^+ myelin and the quantification of $SOX10^+$ cell numbers, myelin volume, and NF-H intensity (Figure 7.2B-C).

An alternative strategy which involved 8 weeks of treatment between MI and MI-8 showed that, whilst there was widespread myelination in drug-treated myelinoids, there was no difference in the number of $SOX10^+$ cells, nor in the ratio of myelin volume to either SOX10 number or $NF\text{-}H^+$ intensity between the two groups (Figure 7.3).

These data show that treatment with miconazole nitrate did not enhance oligodendrocyte differentiation in iPSC myelinoids and that long-term exposure of miconazole had a toxic influence on cell viability.

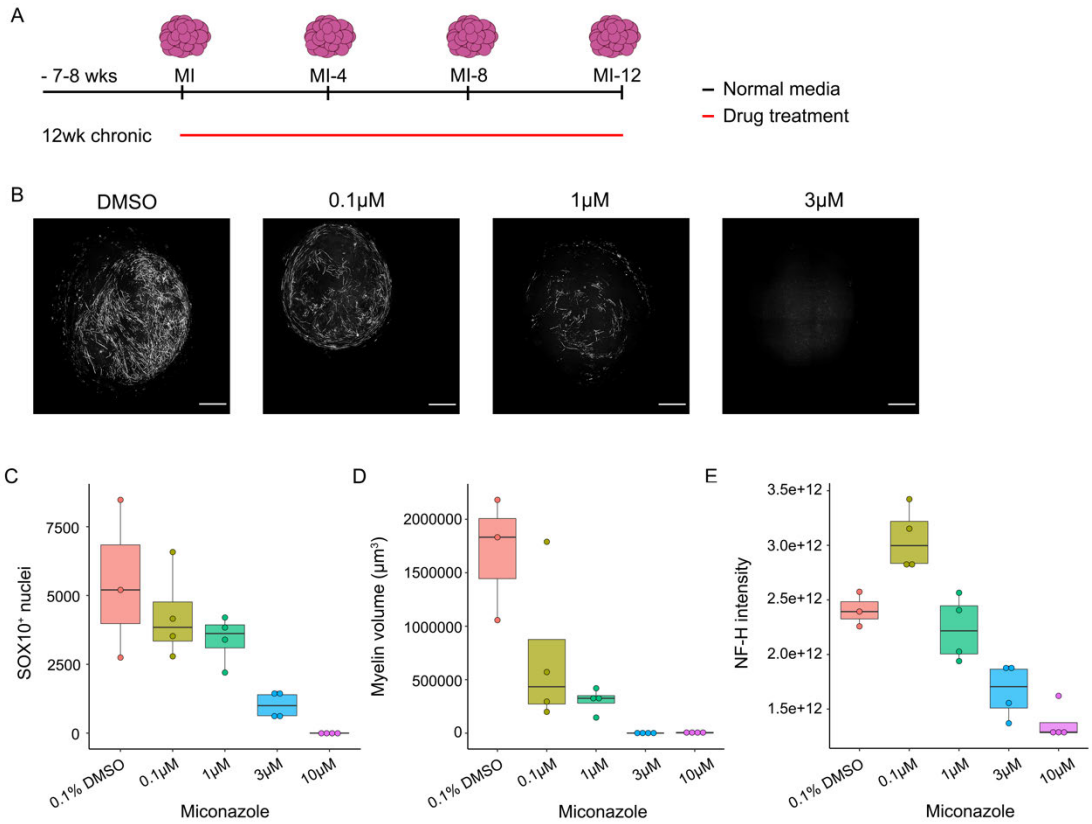

Figure 7.2 Optimising drug treatment paradigm

A) Schematic outlining 12-week miconazole treatment paradigm.

B) Representative images of MBP+ myelin from MI-12 myelinoids following dose-response (scale = 340μm).

C-E) SOX10+ nuclei, myelin volume and NF-H+ intensity each showed a dose-dependent reduction indicative of drug-induced toxicity.

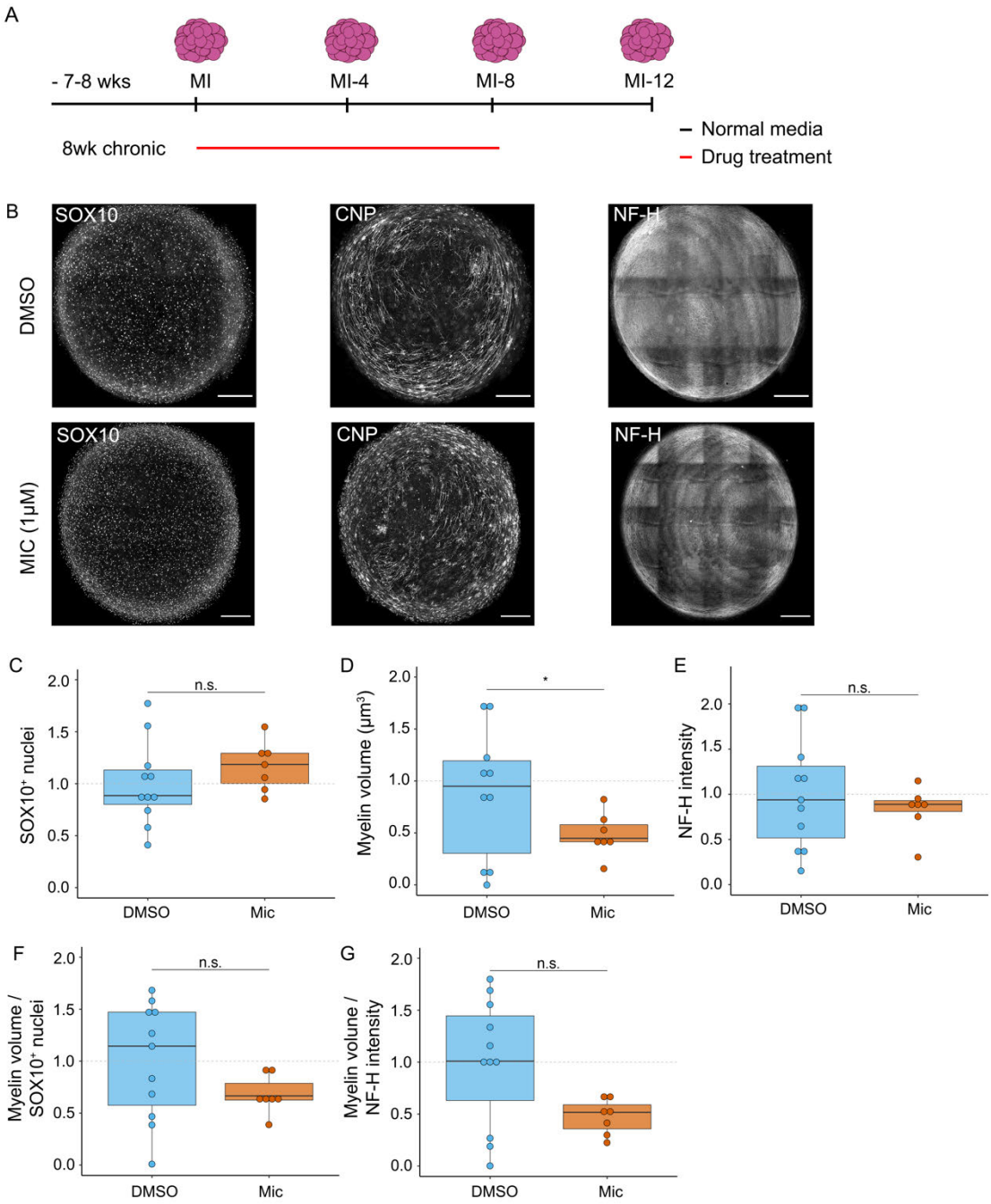

Figure 7.3 Miconazole nitrate did not increase myelin volume in iPSC myelinoids

A) Schematic outlining 8-week 1μM miconazole treatment paradigm.

B) Representative images of MBP$^+$ myelin from DMSO and MIC-treated MI-8 myelinoids (scale 250μm).

C) No difference in the number of SOX10$^+$ nuclei between DMSO and MIC-treated myelinoids.

D) Myelin volume was reduced in MIC-treated myelinoids (52 % reduction $p = 0.046$).

Figure 7.3 Miconazole nitrate did not increase myelin volume in iPSC myelinoids contd.

E) No difference was found in NF-H$^+$ intensity between DMSO and MIC-treated myelinoids.

F) No difference was found in myelin volume normalised to either SOX10$^+$ cell number or NF-H$^+$ intensity between DMSO and MIC-treated myelinoids.

Data collected from 18 myelinoids across 2 conversions.

< 0.05 * linear mixed model with each batch of myelinoids included as a random effect.

7.2.3 SGCCBP30

For another study in the Chandran lab (separate to this thesis), Dr Dario Magnani established a high-content phenotypic screen to identify compounds that promoted the differentiation of iPSC-derived oligodendrocytes. A novel epigenetic modulator of oligodendrocyte differentiation was identified, SGCCBP30, that greatly increased the number of mature oligodendrocytes (Magnani, Telford-Cooke et al., manuscript in preparation). A CBP/P300 histone acetyltransferase, SGCCBP30 is a structural analogue of another compound, C646, that was independently identified to increase oligodendrocyte numbers in the dorsal spinal cord of developing zebrafish (Early et al. 2018).

To determine whether SGCCBP30 (hereafter referred to as SGC) increased the number of oligodendrocytes and total myelin volume in iPSC myelinoids, cultures were exposed to a short dose-response of SGC between MI and MI-8. After 4 weeks of culture, SGC-treated myelinoids demonstrated a widespread increase in the number of $SOX10^+$ nuclei and the proportion of oligodendroglial cells identified by $SOX10^+$ / $DAPI^+$ nuclei (Figure 7.4). A substantial increase in the number of oligodendrocytes was observed by eye at MI-4 though no myelination is observed (Figure 7.4B). Analysis at MI-8 revealed that both the increased proportion of $SOX10^+$ nuclei and the increased number of oligodendrocytes are maintained (Figure 7.5D-E). However, there was no increase in compact myelin compared to DMSO-treated cultures (Figure 7.5F-G). Whilst these data suggest that SGC treatment robustly increased oligodendrocyte number and detrimentally effected myelin formation, a major caveat of this experiment is that the degree of myelination observed in control cultures was minimal. Unfortunately, this was reflective of a wider cell culture problem that led to a reduction in myelinoid quality and a failure to generate myelinating cultures for the remainder of this PhD. Therefore, conclusive demonstration of small molecule-mediated potentiation of myelin formation in iPSC myelinoids was not possible.

Nevertheless, these results show that it is possible to measure changes in the number of oligodendroglial cells and of compact myelin in a human stem cell-derived culture

model, using automation thereby providing a platform for investigating the effect of candidate compounds in promoting human myelination.

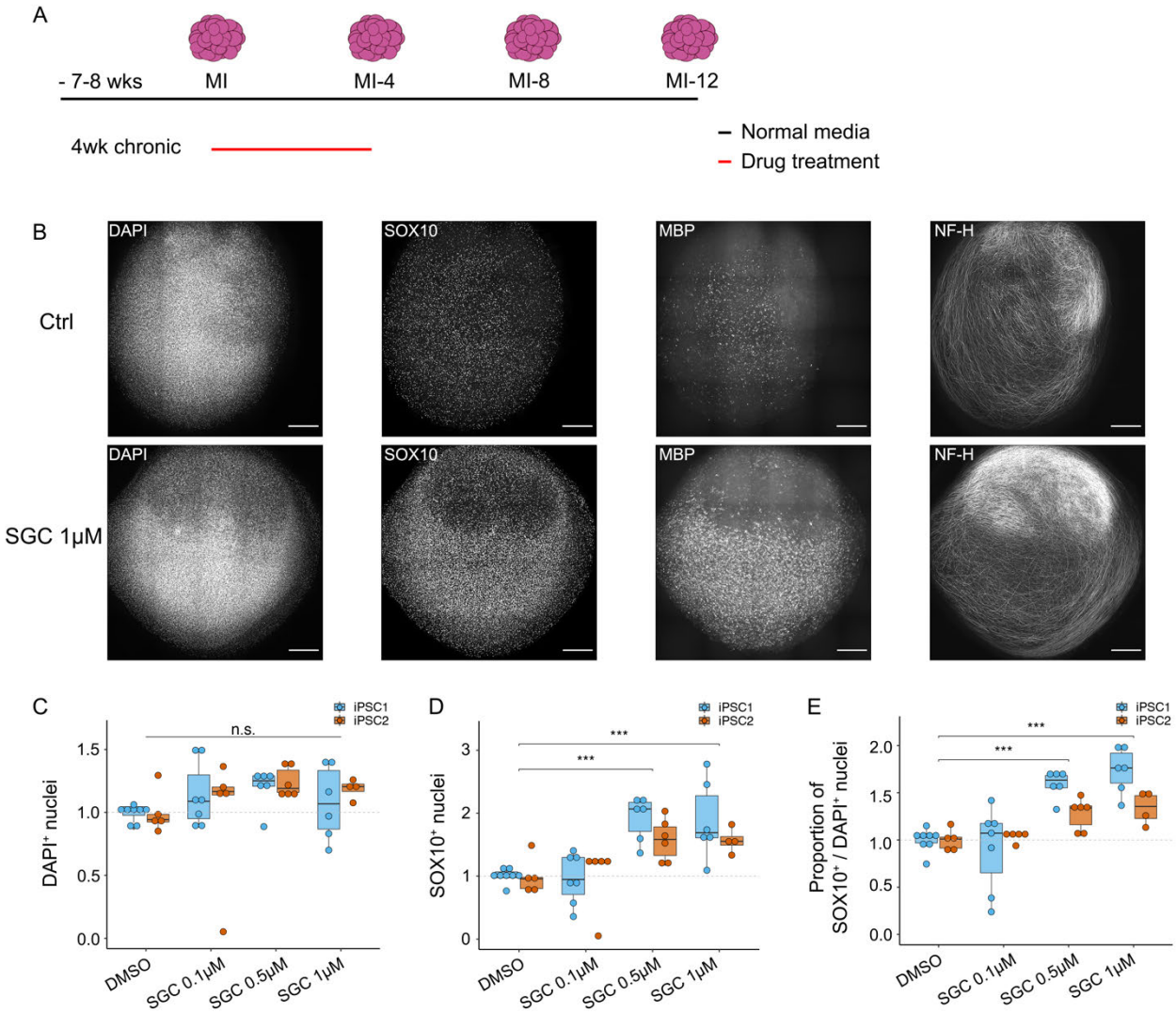

Figure 7.4 SGCCBP30 increases oligodendrogenesis at MI-4

A) Schematic illustration of 8-week drug treatment paradigm for SGC.

B) Representative images from the same myelinoid of DAPI, SOX10, MBP, and NF-H staining in Ctrl and 1μM SGC-treated myelinoids (scale = 250μm).

C) There was no significant difference in DAPI number between control and SGC-treated myelinoids.

D) SOX10 number significantly increases in a dose-dependent fashion in SGC-treated myelinoids: 77% increase at 0.5μM ($p < 0.001$, 95% CI: 30% to 240% increase), 73% increase at 1μM ($p < 0.001$, 95% CI: 26% to 239% increase).

E) The proportion of SOX10 / DAPI+ nuclei also increased in a dose-dependent fashion in SGC-treated myelinoids: 59% increase at 0.5μM ($p < 0.001$, 95% CI: 31% to 92% increase), 76% increase at 1μM ($p <$ 0.001, 95% CI: 26% to 215% increase).

Data collected from 47 myelinoids across 3 conversions and averaged across 2 cell lines.

< 0.001 *** generalised mixed model with each conversion of myelinoids included as a random effect.

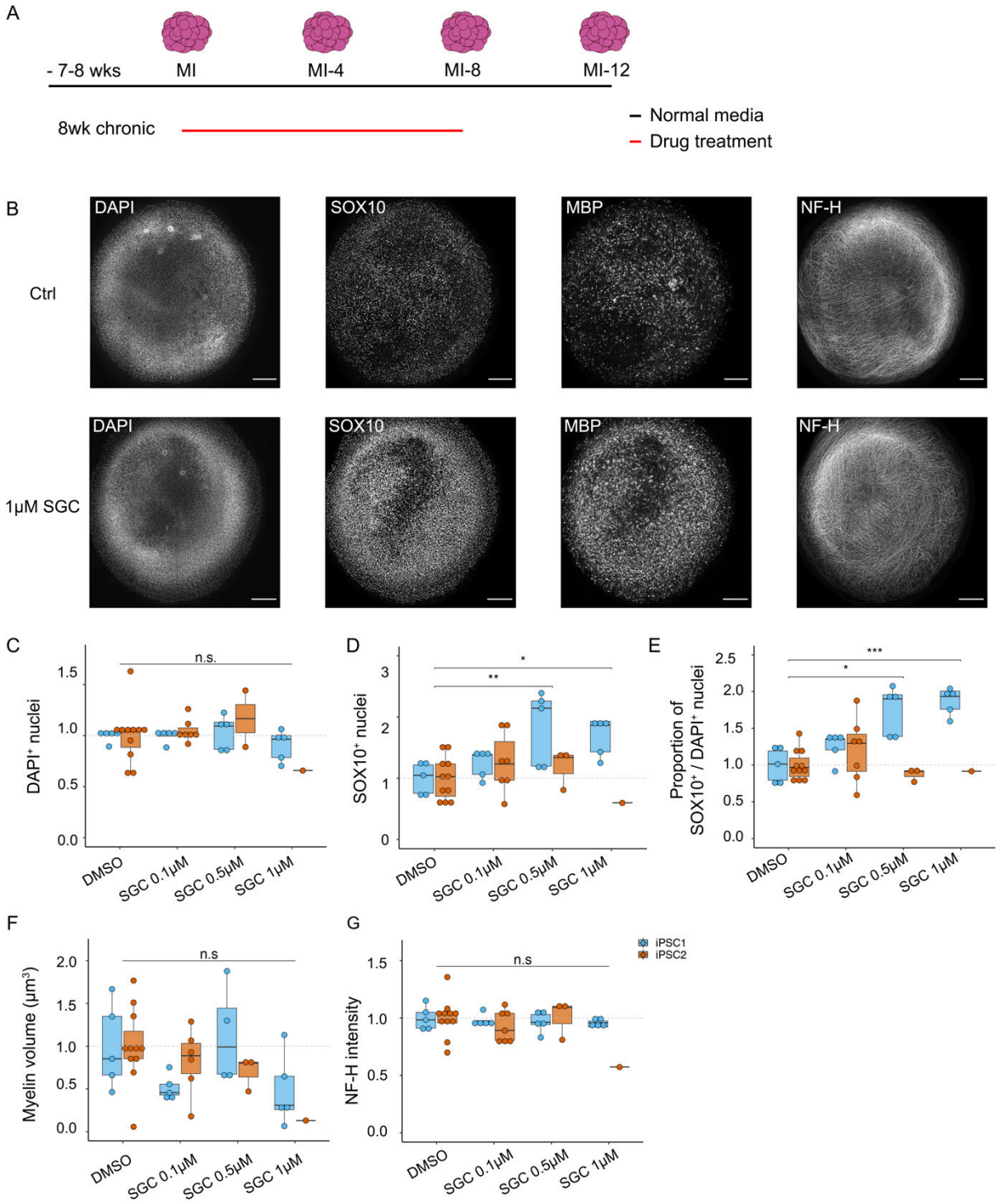

Figure 7.5 SGCCBP30 increases oligodendrogenesis at MI-8

A) Schematic illustration of 8-week drug treatment paradigm for SGC.

B) Representative images from the same myelinoid of DAPI, SOX10, MBP, and NF-H staining in Ctrl and 1μM SGC-treated myelinoids (scale = 250μm).

C) There was no significant difference in DAPI number between control and SGC-treated myelinoids.

Figure 7.5 SGCCBP30 increases oligodendrogenesis at MI-8 contd.

D) SOX10 number significantly increases in a dose-dependent fashion in SGC-treated myelinoids: 55% increase at 0.5μM (p = 0.002, 95% CI: 17% to 205% increase), 38% increase at 1μM (p = 0.0049, 95% CI: 0% to 90% increase).

E) The proportion of SOX10 / DAPI+ nuclei also increased in a dose-dependent fashion in SGC-treated myelinoids: 32% increase at 0.5μM (p = 0.018, 95% CI: 4.7% to 65% increase), 57% increase at 1μM (p < 0.001, 95% CI: 26% to 200% increase).

F) No change in myelin volume between DMSO and SGC-treated myelinoids.

G) No change in NF-H+ intensity between DMSO and SGC-treated myelinoids.

Data collected from 42 myelinoids across three 3 conversions and averaged across two cell lines.

p < 0.05 * p < 0.01 ** p < 0.001 *** generalised mixed model with each conversion of myelinoids included as a random effect.

7.3 Conclusions

In this chapter, I assessed the application of iPSC myelinoids as a platform for the validation of prodifferentiating/promyelinating compounds. I demonstrated that small molecule induced oligodendrogenesis can be measured using the automated pipeline outlined in the previous chapter. Specifically, 4- or 8-week exposure of myelinoids to SGCCBP30, a CBP/P300 histone acetyltransferase, increased the proportion of $SOX10^{+}$ nuclei. Further work is required to confirm whether this compound has a promyelinating effect in iPSC myelinoids. I also demonstrate the close association of myelination with high axonal densities. Whilst only preliminary, these results support the use and experimental optimisation of iPSC myelinoids in candidate studies of potentiators of human oligodendrogenesis and myelin development.

7.4 Discussion

The potential application of myelinoids—paired with an automated quantitative analysis of myelination—as a platform for testing promyelinating compounds was examined. However, similarly to the promotion of neuronal activity, pharmacological potentiation of myelination elicits practical considerations. Most drug screens are performed at either 1 or 10 μM for short periods of time over the course of days—not weeks—and there is limited data available on the half-life or EC50 of drug compounds for cell culture assays. One approach that has been employed to model oligodendrogenesis in three dimensional cultures was to transiently expose spheroids to drug compounds during glial patterning to inflate the number of OPCs, which eventually yielded high numbers of MYRF^{+} oligodendrocytes with continued culture (Madhavan et al. 2018). However, rather than simply potentiating oligodendrogenesis, myelinoids permit the identification of compounds that modulate the myelinating potential of single oligodendrocytes as well as the total volume of myelin, as I have shown with blebbistatin, TeNT, and BDNF treatment. This is important as, given the complex signalling pathways involved late in (re)myelination and that many lesions are occupied by pre-myelinating oligodendrocytes not engaged in remyelination, the assumption that myelin wrapping and myelinated axon sub-domain (re)organisation will naturally follow oligodendrocyte differentiation may not be justified (Chang et al. 2002; Nawaz, Sánchez, Schmitt, Snaidero, Mitkovski, Velte, Brückner, Alexopoulos, Czopka, Jung, Rhee, Janshoff, Witke, Schaap, Lyons & Simons 2015b; Franklin & ffrench-Constant 2017). The identification of compounds that, either alone or in combination, lead to enhanced myelin volume is therefore key.

Here, I exposed myelinoids to different compounds chronically for 4, 8, or 12 weeks. I found that 12 weeks of chronic exposure to miconazole had a detrimental effect on myelin development. However, given that these data came from only two conversions of myelinoids, further work repeating this experiment with measurements at MI-4 and MI-8 will hopefully provide further clarity.

In contrast to miconazole nitrate, exposure of myelinoids to SGCCBP30 did promote oligodendrogenesis. Analysis at both MI-4 and MI-8 showed a significantly increased proportion of SOX10^{+} cells. Representative images also demonstrated a robust

increase in the number of MBP$^+$ oligodendrocytes. However, the effect of SGC in promoting myelin formation was not able to be addressed due to concurrent tissue culture problems outside of our control, leading to a failure of iPSC myelinoids to form myelin—even in control conditions. Unfortunately, this failure was maintained in a number of subsequent conversions, rendering any further analysis of drug-treated myelinoids impossible. Though frustrating, such complications in stem cell-derived cultures are not uncommon. Nevertheless, the data demonstrated here shows that automated analysis of drug-induced oligodendrogenesis in iPSC myelinoids is a suitable and complementary assay to existing capacities.

Finally, analysis of individual acquisition sites across the surface of myelinoids shows that myelin volume is significantly correlated with axonal density (NF-H intensity). Axonal density has previously been identified to regulate the fraction of myelinating oligodendrocytes in co-culture (Lundgaard et al. 2013). Additionally, increasing the number of normal target axons in the developing spinal cord of zebrafish led to an increase in total myelin content without affecting the number of oligodendrocytes (Almeida et al. 2011). However, in iPSC myelinoids, it appears that it is the initiation of myelination that is dependent on high axonal density. One explanation for this could be that those non-myelinated, sparse axons possess a calibre below the threshold for myelination (approximately 0.2μm) (Lee et al. 2012; Goebbels et al. 2016). Whilst rare, the observation of myelinoids with seemingly saturated levels of myelin within constrained regions of axonal density identifies a potential ceiling effect in the enhancement of myelination in some cultures. This could be resolved by considering earlier time-points for analysis. Compounds that accelerate the rate of myelin formation will equally be of significant interest.

Future considerations

Future studies relating to the use of myelinoids in investigations of pro-myelinating compounds should consider alternative treatment paradigms that I performed during the course of my PhD study, but are not presented in this thesis. For example, if the mechanism of action is known to target early stage progenitor cells, transient exposure early-on, followed by continued culture for 6-7 weeks may be suitable, as was employed by (Madhavan et al. 2018). However, for compounds expected to target late oligodendrocyte progenitors and pre-myelinating oligodendrocytes, a

repetitive treatment strategy that continually targets differentiating oligodendrocytes might be better suited with drug exposure once per week, thereby limiting drug-induced toxicity whilst continually targeting newly differentiated oligodendrocytes throughout the time-course. Future studies should also consider the use of a fluorescent reporter line under the control of MBP or MYRF to quickly screen for drug effects and to identify appropriate treatment paradigms.

Chapter 8 Disease modelling

8.1 Introduction

A major application of this model system, which takes advantage of the source material, is the generation of myelinoids from patient-derived iPSCs for *in vitro* modelling of neurological disorders.

Disparities exist between humans and mice in terms of evolutionary divergence, anatomical disproportions, developmental time-courses, divergent gene expression profiles, and physiology, which are thought to contribute to the incomplete recapitulation of human disorders in rodent models of disease (S L Eaton 2017; Xu et al. 2018). Whilst animal models remain an instrumental tool with which to investigate cellular mechanism, disease pathogenesis, and preclinical studies of therapeutic interventions and drug safety, the rate of translation between drug trials and development of therapies is very low—particularly for neurological disorders (Garner 2014; McGraw et al. 2017). Both methodological flaws in animal studies and disease-specific differences between animals and humans have been shown to contribute to translational failure (van der Worp et al. 2010). Large animal models have been suggested to better recapitulate the human condition due to the relatively advanced genetic homology observed, especially in primates, and the presence of naturally occurring neurological disorders in pigs and sheep (S L Eaton 2017). However, the availability and advanced lifecycle of these animals precludes the wide-spread adoption of them for research purposes.

Though reductionist in nature, human iPSC derived cultures offer a powerful resource that complements animal studies. With an accessible *in vitro* environment for physiological interrogation and drug delivery, a theoretically unlimited supply of material, the ability to compare familial and sporadic forms of disease, and integration with clinical and pathology information, iPSC-derived cultures are well-suited for both mechanistic studies and drug-discovery purposes. A number of studies have revealed disease-associated phenotypes, novel drug targets, and drug combinations using patient-derived iPSCs (Silva & Haggarty 2019). Patient-derived iPSCs have been used to draw mechanistic insight into disease (Selvaraj et al. 2018), and iPSC-based discovery and screening has led to the initiation of a clinical trial for ALS (Wainger et al. 2014; McNeish et al. 2015). Organoid cultures provide an additional method for

studying the interaction of different cell-types and the function of cells in a more physiologically relevant environment. Indeed, organoid cultures have so far been employed to model disorders including microcephaly (Lancaster et al. 2013), Costello syndrome (Krencik et al. 2017), major psychiatric disease (Johnstone et al. 2019), Timothy syndrome (Birey et al. 2017), and Miller-Dieker syndrome (Iefremova et al. 2017). Therefore, stem cell-derived cultures have great potential in terms of stand-alone discovery, as well as to complement animal models by demonstrating the efficacy of compounds in a human cellular environment and, thus, supporting the progression of candidate hits to clinical trial.

However, whilst *in vitro* modelling with patient-derived material provides an opportunity to study the effect of disease-causing mutations on cell- and non-cell autonomous processes, it has not been possible to model functional oligodendroglial-axon interactions and the consequences of disease-causing mutations on this structure *in vitro* until now.

Mutations in several genes specific to myelinating glia have been associated with neurodevelopmental disorders, leukodystrophies and congenital hypomyelinating neuropathies (CHN) (Nave et al. 2007; Vallat et al. 2016; Inoue et al. 2002; Powers 2004a). These mutations result in myelin pathology but also negatively impact on the wider CNS and can present clinically with hypotonia, weakness, areflexia, slow nerve conduction and often culminate in early mortality. For example, there have been several reports of severe neurodevelopmental disorders arising through distinct mechanisms that result in disrupted NoR or PNJ formation. Mutations in GLDN and LGI4, which encode secreted cell adhesion molecules involved in NoR formation, lead to lethal arthrogryposis (Maluenda et al. 2016; S et al. 2017) and mutations in CNTNAP1 result in a rare CHN with paranodal lesions due to the loss of CASPR expression (Vallat et al. 2016). Recently, a novel mutation was described that also resulted in PNJ disruption due to a recessive homozygous nonsense mutation (NM_015090.3 c.2491C>T, p.Arg831Ter) in the *NFASC* gene (Smigiel et al. 2018). Importantly, this mutation was shown to selectively disrupt the transcription of glial Nfasc155 without affecting axonal isoforms (Nfasc186 and Nfasc140), which are implicated in the assembly and maintenance of the NoR (Smigiel et al. 2018; Zhang et al. 2015). A severe clinical phenotype that included hypotonia, amimia and areflexia was reported, and immunocytochemical staining of a skin biopsy demonstrated

disrupted paranode formation by the absence of both Nfasc155 and CASPR at the paranode.

Mice that lack both major isoforms of *NFASC* are embryonically lethal. However, specific loss of glial Nfasc155 disrupts paranode formation and results in a severe motor coordination phenotype and premature death by 17 days. Nfasc155$^{-/-}$ mice demonstrate widespread myelination and intact nodal clustering of voltage-gated Na^+ channels (Sherman et al. 2005). However, conduction velocity is estimated to be reduced by 50% (Roche et al. 2014). The clinical severity of Nfasc155$^{-/-}$ mice is somewhat surprising, as simply disrupting paranode formation only leads to mild motor symptoms, as has been shown in Caspr$^{-/-}$ mice. What additional functions Nfasc155 might be carrying out is currently unknown.

Oligodendroglial or myelin pathology are also observed across classical neurodegenerative diseases where the contribution of glial pathology to disease onset and progression remains unclear (Kang et al. 2013; Huang et al. 2015; Nasrabady et al. 2018). ALS has previously been described in this thesis as a progressive and fatal neurodegenerative disease characterised by the loss of upper and lower motor neurons. Oligodendrocyte pathology is prevalent in ALS (Kang et al. 2013; Lee et al. 2012; Ebstein et al. 2019). However, the mechanism by which oligodendroglia contribute to disease pathogenesis is not understood. Though the majority (90%) of ALS cases are sporadic, a striking similarity in key pathological features and phenotype largely indistinguishable from that of familial ALS (fALS) emphasises the value of studying fALS for drawing mechanistic insight into this fatal disease.

TDP-43—as has already been described above—is an integral DNA/RNA binding protein involved in RNA splicing, translation, and transport (Ratti & Buratti 2016). Whilst *TARDBP* mutations account for ~3% of fALS and ~1.5% of sporadic ALS cases (Lagier-Tourenne & Cleveland 2009), a defining pathological hallmark for the majority of ALS cases is the accumulation of large TDP-43$^+$ cytoplasmic aggregates in both neurons and glial cells (Neumann et al. 2006; Arai et al. 2006; Mackenzie et al. 2010), highlighting the importance of this protein in disease pathogenesis. The impact of *TARDBP* mutations on oligodendrocyte function remains unknown. Furthermore, whether *TARDBP* mutations lead to TDP-43 loss of function or toxic gain of function remains unclear and has been challenging to study with animal models of TDP-43

knockdown and overexpression as TDP-43 auto-regulates its mRNA levels through a negative feedback loop (Ayala et al. 2011). Patient-derived iPSCs therefore provide a unique opportunity to study the impact of ALS-causing mutations in *TARDBP*—expressed at endogenous levels—within a disease-susceptible genetic landscape.

In order to demonstrate the utility of iPSC myelinoids in modelling neurological disorders *in vitro*, I sought to recapitulate a monogenic disorder of myelinated axon organisation (Nfasc155 deficiency) and investigated myelin formation in the context of an ALS-causing mutation using patient-derived and gene-corrected iPSCs.

8.2 Results

8.2.1 Nfasc-155$^{-/-}$ patient-derived myelinoids recapitulate paranodal dysfunction

In order to demonstrate that iPSC-myelinoids are able to phenocopy known features of a myelin disease and to emphasise the unique ability of myelinoids to appropriately organise myelinated axon domains, we sought to model a recently reported case of a severe neurodevelopment disorder that resulted from a homozygous *NFASC* mutation which is predicted to specifically affect expression of the glial isoform Nfasc155 (Smigiel et al. 2018). Fibroblasts from the proband were reprogrammed and two clonal iPSC lines were obtained in collaboration with Professor Peter J. Brophy at the University of Edinburgh, Dr Robert Smigiel at Wroclaw Medical University, Poland and Cedars-Sinai. iPSCs were confirmed to be karyotypically normal and presence of the *NFASC* mutation was confirmed by PCR amplification and Sanger sequencing of ctrl and Nfasc155$^{-/-}$ DNA (Figure 8.1A).

Myelinoids generated from patient-derived iPSCs demonstrated intact widespread myelination, as has been previously been shown in Nfasc155$^{-/-}$ mice (Sherman et al. 2005) (Figure 8.1B). To assess paranode formation, 10 μm cryosections were obtained from Cs00ink-n1 (Nfasc155$^{-/-}$ clone 1), Cs00ink-n2 (Nfasc155$^{-/-}$ clone 2), and control MI-12 myelinoids. Figure 8.1C-D show that, whilst nodal expression of Nfasc186 and ANKYRIN-G were comparable between control and Nfasc155$^{-/-}$ myelinoids, patient-derived cultures lacked expression of glial Nfasc155 and its binding partner, CASPR, at the paranode. The expression of CLAUDIN-11 (which is not dependent on PNJ assembly) at the distal ends of Nfasc155$^{-/-}$ myelin sheaths demonstrates normal tight-junction formation between myelin lamellae, indicating that myelin wrapping is intact in patient-derived cultures (Figure 8.1E).

These data mirror those from the patient biopsy, as well as those from Nfasc155$^{-/-}$ mice and show that iPSC-myelinoids can recapitulate the key cellular pathology of a compact myelin disorder, *in vitro*.

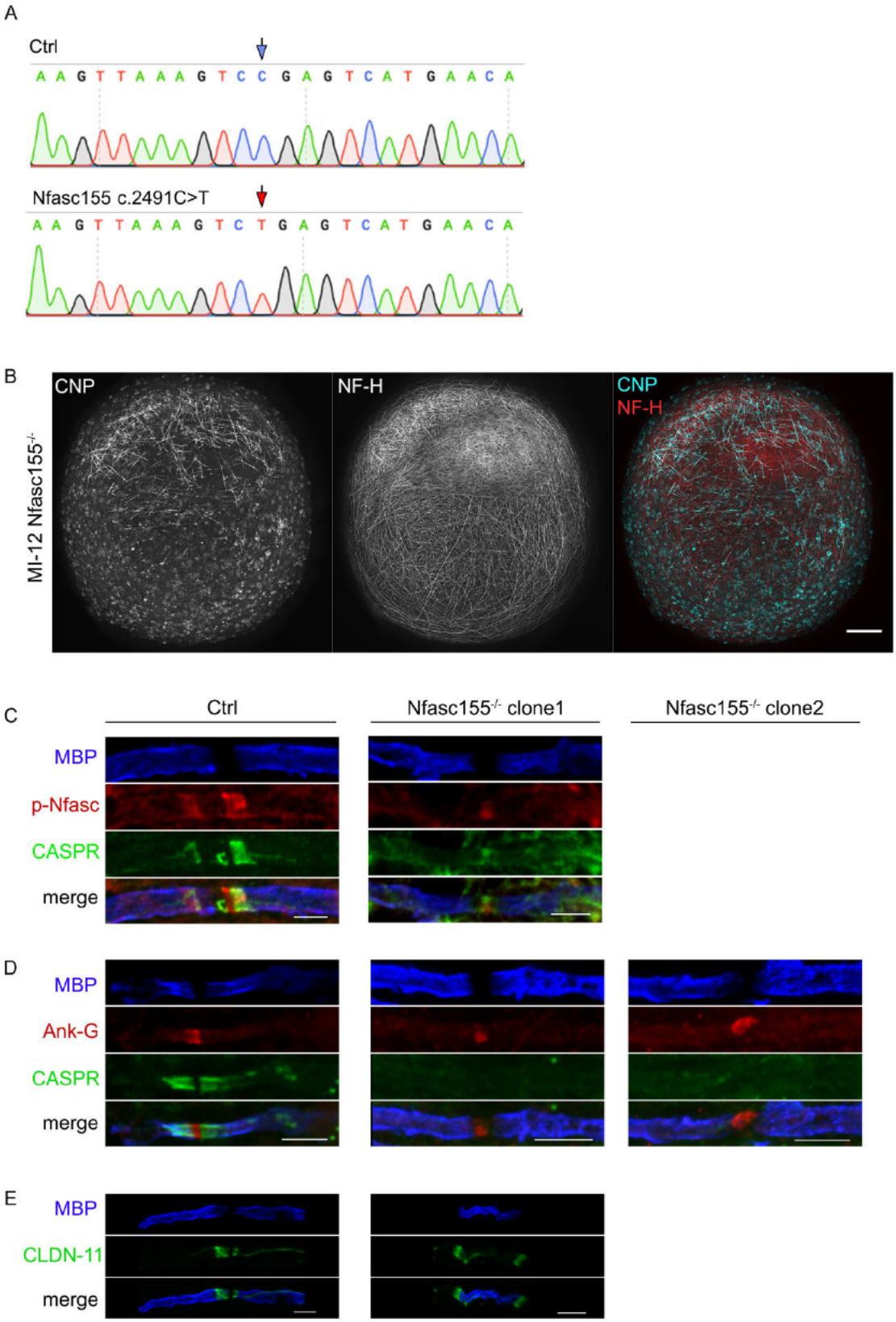

Figure 8.1 Nfasc155$^{-/-}$ myelinoids show disrupted paranode formation

A) Sanger sequencing identifies the c.2491C>T (p.Arg831Ter) mutation in patient-derived iPSCs.

Figure 8.1 Nfasc155$^{-/-}$ myelinoids show disrupted paranode formation contd.
B) Representative images of Nfasc155$^{-/-}$ myelinoids at MI-12 (scale = 250μm).
C) 10 μm cryosections stained with a pan-Neurofascin antibody shows normal nodal expression of Nfasc186 but loss of Nfasc155 and CASPR expression at PNJ in patient-derived myelinoids (scale = 5μm).
D) 10μm cryosections stained with ANKYRIN-G and CASPR shows normal clustering of nodal domain and loss of PNJs in patient-derived myelinoids (scale = 5μm)
E) 10μm cryosections stained with CLAUDIN-11 shows normal expression at tight junctions at the distal ends of MBP^{+} internodes, demonstrating myelin wrapping. Data collected from > 10 nodes each from 4 separate myelinoids (scale = 5μm).

8.2.2 Gene targeting and correction of mutant *TARDBP* in patient-derived iPSCs

In order to investigate the impact of TARDBP^{G298S} on oligodendrocyte biology and myelination, I first generated an isogenic gene-corrected cell line via CRISPR/Cas9 gene targeting.

The *TARDBP*^{G298S} mutation results from a c.892G>A substitution that gives rise to a rare but particularly aggressive form of fALS (Corcia et al. 2012). Both *TARDBP*^{G298S} and *TARDBP*^{M337V} iPSCs were generated in-house from patient-derived fibroblasts obtained from Professor Chris Shaw, King's College London. To correct the G298S mutation, a CRISPR/Cas9-mediated targeting strategy was employed to integrate a 180bp ssODN carrying the correct gene sequence at exon 6 of the *TARDBP* gene (Figure 8.2A).

TARDBP^{G298S} is an autosomal dominant mutation. Therefore, guide RNAs were designed to selectively bind the mutant allele and induce a double-stranded break (DSB) close to the mutation site (Figure 8.2A). Guide RNA design was performed by by Dr Bhuvaneish Selvaraj in the Chandran lab. Further experiments involving plasmid construction, gene-correction and screening was performed by myself. To test the gRNA-Cas9 targeting efficiency, gRNAs were cloned into a pSp-Cas9-2A-GFP plasmid and, together with a vector conferring puromycin resistance, were transfected into *TARDBP*^{G298S} iPSCs. Following puromycin treatment, DNA was extracted from the transfected cells and a T7 endonuclease assay was performed on the PCR-amplified target locus. T7 endonuclease selectively cleaves heterologous base pairs, which are regularly introduced following non-homologous end joining (NHEJ), the dominant—yet error-prone—repair response to DSBs. Figure 8.2B demonstrates successful gene targeting and formation of heterologous base pairs by the formation of two products corresponding to 191bp and 262bp. Note, as an autosomal dominant mutation, G298S itself introduces heterologous base pairs following denaturation and reannealing of PCR products, which results in T7 endonuclease-mediated cleavage in the patient-derived untransfected DNA (Figure 8.2B).

A 180bp ssODN containing the WT genomic sequence with 90bp arms flanking either side of the cut site was designed and ordered as single-stranded DNA from Integrated Device Technologies. To limit repeat DSB formation following ssODN integration, redundant nucleotides at the 3' end of the gRNA binding site (c.903C>T and c.906T>C) were substituted to create 'silent mutations' that reduced the binding efficiency of gRNAs without modifying the coding sequence. To create the isogenic control line, 800,000 *TARDBP*^{G298S} iPSCs were transfected with the pSp-Cas9-2A-GFP plasmid, the pMTL23-gRNA7 vector, the EGFP-Puro vector, and the ssODN, using the Lonza 4D nucleofector (programme #CA137). The concentration of each transfected reagent is provided in the methods. Transfected hiPSCs were split between two wells of a 6wp and, the next day, treated with puromycin for 24 hours. To isolate clonal populations of targeted cells, between 1000 and 5000 cells were plated onto matrigel- or laminin 511-coated 10 cm dishes as single cells and cultured for 1 week. Using an EVOS imaging system, 480 individual colonies were picked and passaged into matrigel-coated 96-well plates and, after 10 days, were passaged 1:2 using EDTA to give 3 sets of replica plates. From 1 set of plates, DNA was isolated from each well (see methods) and the target locus amplified by PCR. Confirmation of ssODN integration was achieved by restriction digestion and gel electrophoresis. The silent mutation c.906T>C within the gRNA-binding site of the ssODN introduced a novel BsaJ1 restriction site that produced a 191bp product identified by gel electrophoresis (Figure 8.2C).

Thirty one (6.5%) clones demonstrated integration of the ssODN via BsaJ1 restriction digestion. Of those, 3 (0.6%) were devoid of indel mutations, identified by Sanger sequencing. Two of the three correctly targeted clones displayed monoallelic integration of the ssODN on the mutant allele and one displayed biallelic integration of the ssODN. Figure 8.2 shows the Sanger sequencing results from the parental G298S cell line, a gene-corrected G298G cell line with monoallelic integration of the ssODN, and a second gene-corrected G298G cell line with biallelic integration of the ssODN. The remaining clones exhibited indel mutations on either the mutant or WT allele that resulted in disruptive missense mutations downstream of the DSB site. Karyotype analysis demonstrated no chromosomal abnormalities in either the parental *TARDBP*^{G298S} or the gene-corrected *TARDBP*^{G298G} cell lines. These data demonstrate successful gene-correction of *TARDBP*^{G298S} ALS patient-derived iPSCs.

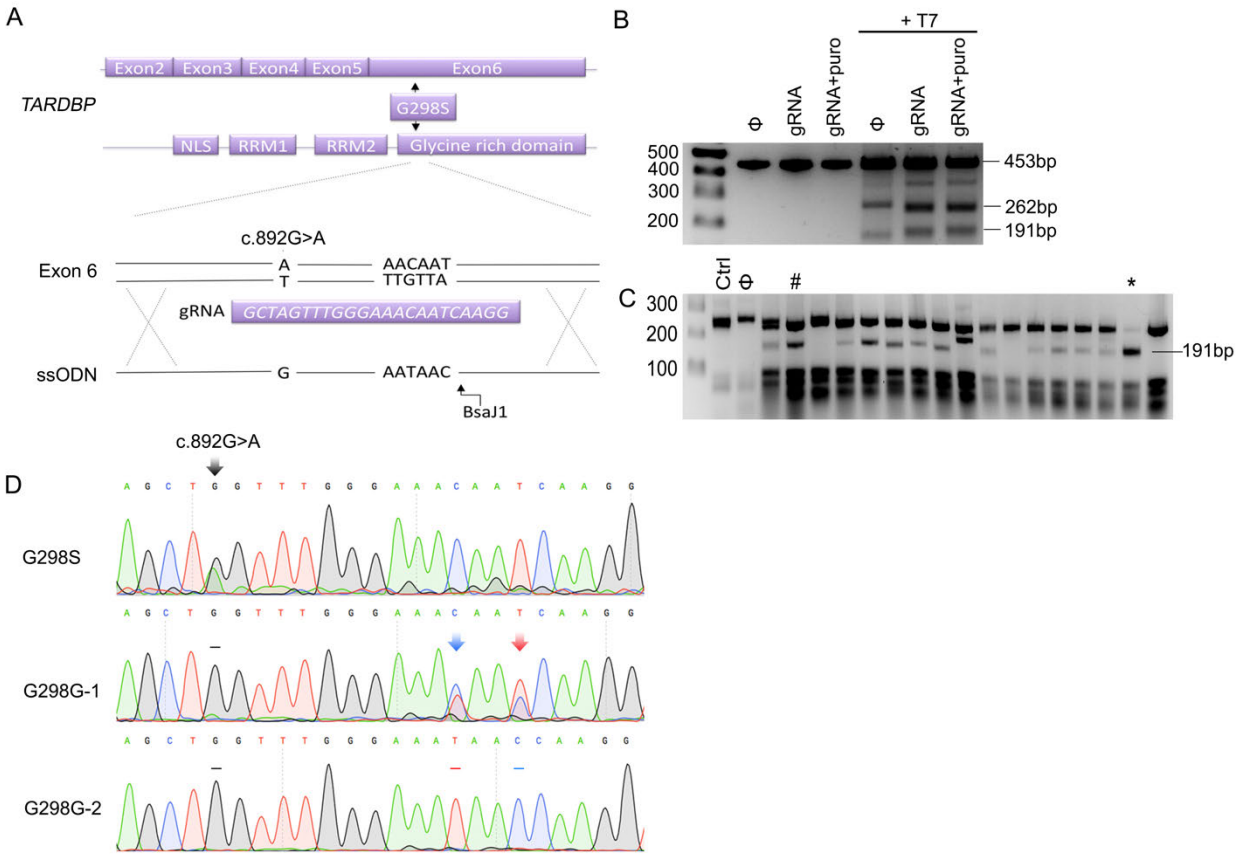

Figure 8.2 Targeted gene correction of TARDBP G298S ALS patient-derived iPSCs

A) Schematic overview of G298S mutation and targeting strategy for integration of ssODN.

B) T7 endonuclease assay shows the expected sizes of cleaved products, demonstrating appropriate targeting of Cas9.

C) Gel electrophoresis of BsaJ1 restriction digest dependent on ssODN integration. Neither control DNA from another cell line, nor untransfected DNA show cleavage by BsaJ1 (Ctrl and Φ). # shows monoallelic integration of ssODN and * shows biallelic integration of ssODN.

D) Sanger sequencing traces of *TARDBP* exon 6 showing presence of the G298S mutation in the parental line and correction in two different clones. G298G-1 shows monoallelic integration of ssODN on the mutant allele with integration of silent mutations (blue and red arrows). G2982G-2 shows biallelic integration of ssODN.

8.2.3 *TARDBP*^{G298S} mutation does not affect myelin formation

Drs Samantha Barton and Dario Magnani investigated the impact of *TARDBP*^{G298S} on oligodendrocyte function. They found that *TARDBP*^{G298S} derived oligodendrocytes develop TDP-43^{+} inclusions, which are resolved following targeted gene-correction. However, despite the presence of a TDP-43 proteinopathy, no differences were seen in oligodendrocyte maturation, morphology, or function between mutant and control oligodendrocytes (Barton, Magnani et al., manuscript in preparation).

In order to probe the impact of mutant TDP-43 in myelin formation, myelinoids were generated from the mutant and gene-corrected G298G iPSCs (with biallelic ssODN integration), as well as from a second patient-derived cell line harbouring the *TARDBP*^{M337V} mutation. Figure 8.3A demonstrates efficient myelin induction across the three cell lines.

Analysis of sheath number per cell at MI-12 showed no difference between the two mutant TDP-43 cell lines and the isogenic gene-corrected cell line (Figure 8.3B). Mean sheath length per cell and the frequency distribution of sheath lengths were equally unaffected across the three cell lines (Figure 8.3C-D). Nearest neighbour analysis showed that whilst there was a trend for an increase in the number of myelinating and total oligodendrocytes per 100μm radius between the mutant vs gene-corrected and M337V cell line, this did not reach significance (36% increase in number of myelinating oligodendrocytes in G298S vs G298G, $p = 0.0898$ and 26% increase in the total number of oligodendrocytes in G298S vs G298G, $p = 0.1911$).

These data demonstrate that myelinoids can be derived from ALS patient-derived iPSCs, which shows normal myelination. This mirrors data derived in-house from dissociated cultures of iPSC-derived oligodendrocytes showing that the *TARDBP*^{G298S} has no detrimental effect on the maturation or function of oligodendrocytes.

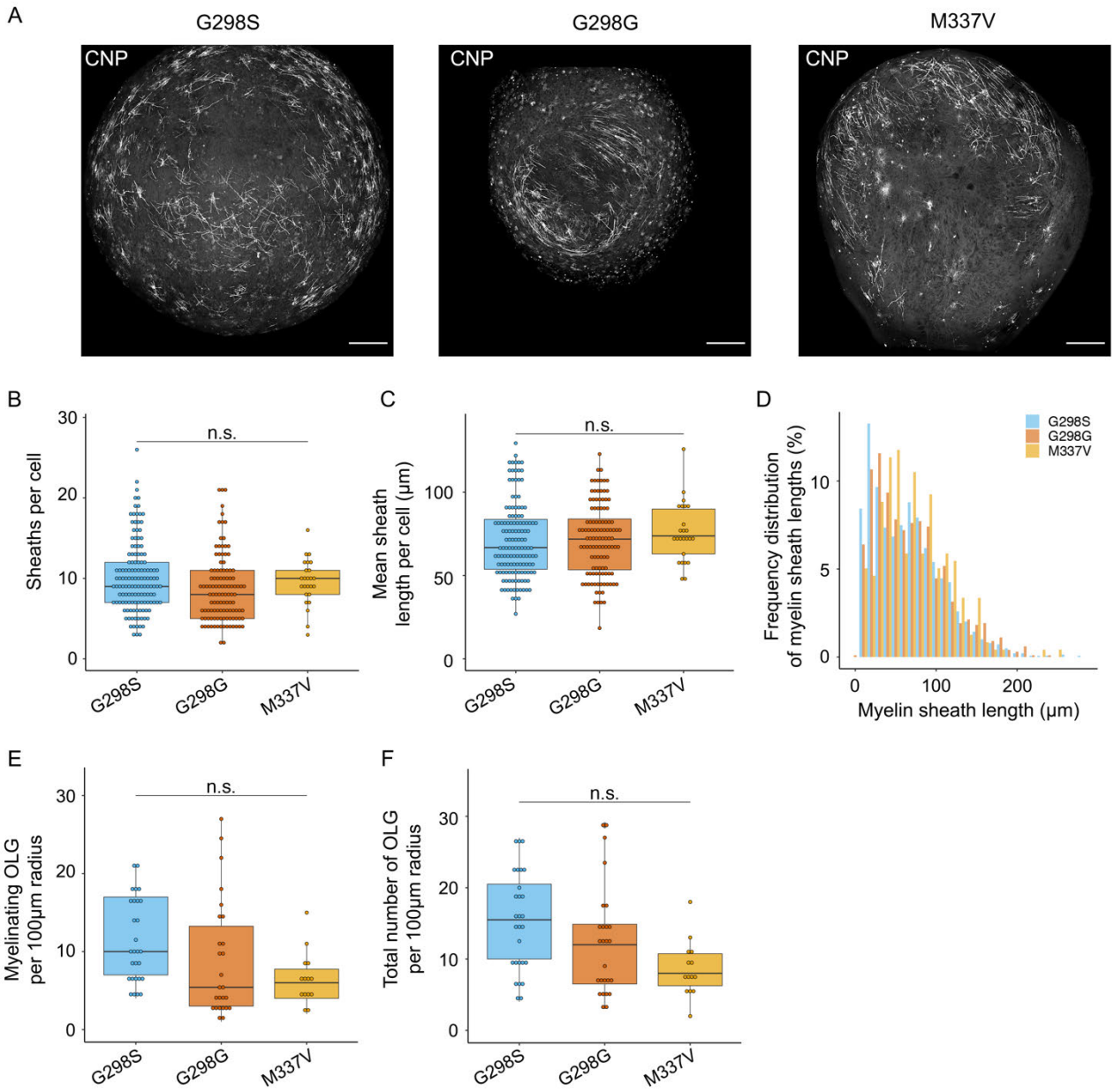

Figure 8.3 TARDBP^{G298S} mutation does not impact myelin development

A) Representative images of CNP+ myelin from G298S, G298G and M337V myelinoids (scale 250μm).

B) No difference was found in sheath number per cell between the three lines *.

C) No difference was found in mean sheath length per cell between the three lines *.

D) Frequency distribution of all sheath lengths shows no differences between the three lines *.

E) The number of myelinating (E) and total (F) oligodendrocytes per 100μm radius was the same for all three lines *.

Data were collected from 20 myelinoids from three separate conversions (1 conversion only for M337V). * $p < 0.05$, glm with each cell line as fixed effects and each conversion as a random effect.

8.3 Conclusion

This chapter concerned the use of iPSC myelinoids in modelling disease. I demonstrated that myelinoids generated from patient-derived cell lines carrying a monogenic disease-causing mutation that causes Nfasc155 deficiency are able to accurately phenocopy the key pathology of human patients and mouse models. Specifically, whilst nodal organisation of Nfasc186 was intact in mutant myelinoids, PNJ formation was disrupted and paranodal expression of Nfasc155 and CASPR was absent.

In order to investigate whether ALS-causing mutations in the gene for TDP-43 would specifically disrupt myelin development in iPSC myelinoids, I performed CRISPR/Cas9 gene targeting on a patient-derived cell line in order to generate an isogenic gene-corrected control cell line. Using these tools, I found that presence of the disease-causing mutation does not affect sheath number per cell, sheath length, or oligodendrocyte density. These results were comparable to another ALS patient-derived cell line carrying a different *TARDBP* mutation.

8.4 Discussion

iPSC-based modelling of different CNS disorders is gaining traction due to continual development of protocols that yield both more restricted and more diverse cell-types and regionality (Kelava & Lancaster 2016). Whilst organoids have been used to model healthy and pathological cell-cell interactions *in vitro* (Krencik et al. 2017), arguably, no other interaction is as complex as the axo-myelin unit. Modelling human compact myelin formation *in vitro* is, therefore, a substantial step forward that enables studies of pathogenic myelination in the context of environmental, pharmacological, or genetic perturbations.

In this chapter, I have demonstrated that patient-derived myelinoids carrying a missense mutation in the *NFASC* gene reveal specific disruption to the organisation of myelinated axon domains, which accurately mirrors the human condition. These data show, for the first time, that disorders of compact myelin can be phenocopied in a human stem cell-derived culture model, thus paving the way for further studies of pathogenic myelin development for disorders that urgently require therapeutic interventions (Powers 2004b). Additionally, given that Nfasc155$^{-/-}$ mice prematurely die between P17-P20, investigations into the long-term impact of Nfasc155 deficiency or other lethal glial mutations on nodal domain stability and axonal health may be well served using iPSC myelinoids (Pillai et al. 2009; Roche et al. 2014).

Interest has been placed on the role of oligodendrocytes in contributing to the pathogenesis of ALS (Kang et al. 2013; Nonneman et al. 2014; Philips et al. 2013; Barton et al. 2019). TDP-43 is of significant interest to the ALS field due to the presence of TDP-43^{+} inclusions in nearly all ALS cases and the discovery of several ALS-causing mutations in the *TARDBP* gene. The mechanism by which TDP-43-dependent neurodegeneration occurs remains unclear: whilst aggregation of TDP-43 in nuclear and cytoplasmic aggregates are thought to sequester the protein and lead to a toxic loss of function (Vanden Broeck et al. 2014), certain gain of function properties have been described—in which age-dependent neurodegeneration occurs without loss of normal TDP-43 levels (Arnold et al. 2013; Ebstein et al. 2019). Ubiquitous TDP-43 knockdown, as well as either MN or oligodendrocyte-specific depletion of TDP-43, leads to age-dependent neurodegeneration (Yang et al. 2014;

Wu et al. 2012; Iguchi et al. n.d.; Wang et al. 2018). However, given that TDP-43 is essential for cell survival and knock-out animals are not viable (Wu et al. 2010; Kraemer et al. 2010), more appropriate modelling of mutant TDP-43 at physiological levels of expression are likely to be of greater relevance to the human condition. Recently, it was shown that endogenous expression of two common *TARDBP* disease-associated alleles (M337V and G298S) results in age-dependent MN degeneration, demonstrating that physiological levels of mutant TDP-43 are sufficient to initiate disease (Ebstein et al. 2019). The authors, however, did not comment on whether oligodendroglial pathology was present in these mice.

TDP-43 mutant myelinoids did not shown any clear functional differences in myelin development compared to the gene-corrected control. This is surprising, given the evidence supporting a role for oligodendrocyte pathology in ALS. It is possible that mutant TDP-43 does not produce as overt a phenotype as do TDP-43 conditional knock-outs and that, given this is a late-onset disease, defects in iPSC myelinoids may become apparent with extended culture time. Given the emphasis of excitotoxicity in the pathophysiology of ALS (Van Den Bosch et al. 2006), it would be interesting to test whether exposing myelinoids to elevated levels of neuronal activity would exacerbate a myelin-related phenotype compared to isogenic gene-corrected controls. However, as discussed previously, boosting neuronal activity in iPSC myelinoids is not straightforward.

Nevertheless, these data show that iPSC myelinoids offer a tractable platform for *in vitro* modelling of human disease.

Chapter 9 Discussion

In this thesis, I set out to establish a robust, human iPSC-derived, *in vitro* model of myelination that would enable investigations into the biology and pathology of myelin development using patient-derived iPSCs and that would serve as a platform to identify pharmacological modulators of human oligodendrogenesis and myelination.

I set out to address the paucity of *in vitro* models of human myelination and established an organoid-like culture model that demonstrates substantial myelin formation with physiologically appropriate thickness and organisation of myelinated axon architecture. I showed that iPSC myelinoids can be generated from a number of healthy and patient-derived cell lines, that myelin development is temporally and (to an extent) spatially predictable, and that myelin formation can be pharmacologically modulated both at the level of individual cells and across entire myelinoids. An automated method of measuring myelin volume enabled comparisons between whole-myelinoid changes in myelin volume and the myelinogenic output of individual cells.

I characterised the maturation and temporal profile of myelin formation and examined the myelinating profile of individual cells and the subtypes of neurons that are myelinated in this system. Furthermore, using this platform, I demonstrated—for the first time—that human myelinating oligodendrocytes respond to regulation of axonal vesicular release, indicating that human myelin development is also regulated by changes in neuronal activity and showed that myelinoids recapitulated a monogenic disease of myelinated axon organisation, demonstrating the feasibility of modelling human neurodevelopmental disorders *in vitro.* Finally, I generated a gene-corrected isogenic control from an ALS patient-derived cell line carrying a TDP-43 mutation ($TARDBP^{G298S}$) and showed that presence of this mutation had no effect on oligodendrogenesis or myelin development in iPSC myelinoids.

An integral component of this thesis that directly relates to the wider context of the field is that robust, compact myelin formation is a critical component of oligodendroglial function and is something that should not be overlooked in organoid, pharmacological or genetic studies of oligodendrocyte biology. Cerebral organoids have advanced dramatically in recent years to include oligodendrocytes, microglia or functional networks between CNS and peripheral tissue (Abud et al. 2017; Giandomenico et al. 2019; Faustino Martins et al. 2020). However, functional

maturation of the nervous system requires myelination, which has largely been overlooked in the above studies. Axonal transport, axon calibre, neuronal gene expression, cytoskeletal composition and posttranslational modification of cytoskeletal proteins are all impacted by compact myelination, as demonstrated in studies of the dysmyelinating shiverer mouse (Brady et al. 1999). To date, organoid/spheroid cultures comprising oligodendrocytes show only limited myelin ensheathment and compaction whilst structural organisation of paranodal and nodal domains is not recapitulated (Madhavan, Nevin, Shick, Garrison, Clarkson-Paredes, Karl, Clayton, Factor, Allan, Barbar, Jain, Douvaras, Fossati, R. H. Miller & Tesar 2018a). The model described in this thesis contains compact and appropriately organised myelinated axons and thus represents a significant step towards establishing functionally mature iPSC-derived neural networks. As discussed in Chapter 4.4, regional and developmental variation in the timing of human myelination may account for the maturation differences between these findings and those of previous studies. The caudalisation of our cultures with retinoic acid generates spinal cord-patterned tissue, which contrasts with previous studies that generated cortical-patterned spheroids by the omission of retinoic acid (Madhavan, Nevin, Shick, Garrison, Clarkson-Paredes, Karl, Clayton, Factor, Allan, Barbar, Jain, Douvaras, Fossati, R. H. Miller & Tesar 2018a; Marton et al. 2019). During human development, the emergence of ventral spinal-cord derived oligodendrocytes occurs as early as 10 gestational weeks (gw) *in utero* and is followed by the appearance of myelinated fibres up to 4 weeks later (Weidenheim et al. 1993). In contrast, MBP^+ forebrain-derived oligodendrocytes are identified around 17-20 gw but emerge several months before the onset of cortical myelination (Back et al. 2002; Jakovcevski et al. 2009). It would follow that considerably longer culture times would be required for forebrain-patterned cultures to show—beyond myelin ensheathment—the assembly of nodal structures. One way to potentially accelerate compact myelin formation in forebrain-patterned cultures would be to promote neuronal maturation through extended exposure to growth factors such as BDNF. This would be particularly exciting as cerebral organoids generate a diverse range of neuronal subtypes that have greater relevance to the study of neurodevelopmental diseases compared to spinal cord patterned myelinoids. Ultimately, a goal in the neuroscience community will be to generate iPSC-derived cultures comprising distinct brain regions as well as central and peripheral tissues connected by functional networks. Whether or not such tracts would

segregate into rudimentary white and grey matter regions would be very interesting. Such a model would enable manifold questions to be asked surrounding axon targeting, network maturation, activity regulated myelination and oligodendrocyte heterogeneity, to name but a few examples.

The formation of compact myelin is also important in the context of drug discovery. Screening for compounds that might promote remyelination is technically challenging and has so far been addressed by identifying modulators of oligodendrocyte differentiation in enriched cultures of oligodendrocyte progenitor cells. However, the presence of neurons induces significant changes in glial gene expression and function (Hasel et al. 2017) and both a miniaturised myelination assay and zebrafish screen of myelinating oligodendrocytes identified distinct classes of pro-myelinating compounds not found in OPC differentiation screens (Early et al. 2018; Lariosa-Willingham et al. 2016). One may consider, therefore, the capability of testing drug-induced changes in human myelination with iPSC myelinoids to demonstrate putative action of candidate promyelinating compounds. The automated platform for measuring total myelin volume developed during this thesis will be essential for such studies through unbiased and higher throughput analysis.

Additionally, appropriate axo-glial interaction, as demonstrated in this model, enables the study of several biological processes and disease mechanisms may now be examined. These include the long-term impact of disrupted paranode formation on nodal stability and the trophic support of axons and its potential perturbation in ALS.

There are also areas in which this model system could be improved and parts of this work that could be extended. Firstly, a source of variability in myelinoid cultures comes from sphere diameter, which varies both within and between batches of myelinoids. Changes in sphere diameter will impact the concentration of patterning factors that is exposed to neural precursor cells within the developing spheroid. One method that has been employed in other organoid models to circumvent this is to seed single iPSCs into 96-well-plates or specialised plastic-wear to generate uniformly sized spheroids (Marton et al. 2019). Secondly, the culture of myelinoids on cell culture inserts in 6-well-plates limits their use in high throughput applications such as phenotypic drug screening. Miniaturisation with 24-well-plate cell culture inserts would be most analogous to the current method. However, adaptations that would enable

long-term culture of spheroids in 96- or 384-well-plates without the use of inserts would be most advantageous.

Unfortunately, during this PhD, I was not able to characterise the extent of network formation in myelinoid cultures or directly demonstrate reduced neuronal activity in TeNT-treated cultures. To do so, one may use multi-electrode arrays, which have been used to study network formation and firing synchrony in organoid cultures (Giandomenico et al. 2019). This would significantly add to the characterisation of this model and to the study of myelinated axon physiology. Whether changes in network formation can be identified with ongoing myelination would be of interest and a valuable assay in modelling various diseases.

Finally, the data presented in this thesis raise a number of questions that would be interesting to address in the future:

1) Why do human stem cell-derived oligodendrocytes take so long to myelinate?

Human myelin development is prolonged in comparison to other species (D. J. Miller et al. 2012; Yeung et al. 2014). However, even the initiation of myelin formation following oligodendrocyte differentiation has been shown to be delayed in humans (Jakovcevski et al. 2009). These differences appear to be cell-intrinsic, as human OPCs transplanted into the shiverer mouse maintain a protracted period of proliferation and delayed myelination compared to transplanted rodent-derived cells (Dietz et al. 2016). In iPSC myelinoids, it is surprising to see so many premyelinating oligodendrocytes at MI-4 and so little myelin at MI-8. It is likely that, similar to the *in vivo* scenario, oligodendrocytes are overproduced during myelinoid development and that changes in axonal properties dictate the initiation of myelination. Live-cell imaging studies have demonstrated the rapid development of myelin sheaths by zebrafish oligodendrocytes (Czopka et al. 2013). Oustanding questions include: do human oligodendrocytes similarly establish internodes quickly, after the initiation of myelination? Or, is the process of sheath stabilisation, retraction, and eventual myelination equally prolonged in humans? If so, are human oligodendrocytes more vulnerable to environmental stressors during the myelination programme? Finally, what are the transcriptional changes that accompany the initiation of myelin formation,

and are there species-specific differences compared to rodent-derived myelinating cultures? iPSC myelinoids are well-suited to answering these questions through the generation of an MBP promoter-driven reporter line. Surprisingly, the transcriptomic changes underlying the initiation of CNS myelination are not currently known and—given the protracted and temporally regulated programme of myelination in myelinoids—picking apart the different stages of myelin development for such studies should be relatively straight forward.

2) Does myelin targeted to different subtypes of neurons differ in length or thickness and does interneuron myelin deposition change in the context of neuropsychiatric disease?

I have shown that oligodendrocytes in myelinoids myelinate PV^+ interneurons with equal frequency to that of PV axons, suggesting no neuronal subtype bias in axon selection. Furthermore, individual oligodendrocytes were shown to myelinate both excitatory and inhibitory axons simultaneously. However, whether or not differences in sheath length or thickness exist between neuronal subtypes is a question which is currently outstanding. Both interneuron and myelin-related pathologies have been implicated in neuropsychiatric disorders, including schizophrenia (J Stedehouder 2017). Therefore, to investigate abnormal myelin development, it would be of great interest to interrogate interneuron myelination in control myelinoids (in the absence and presence of TeNT, to rule out selection bias of active axons) and in schizophrenia patient-derived myelinoids. Interestingly, I also identified evidence of myelinated neuronal cell bodies in iPSC myelinoids (Figure 9.1). Studies in zebrafish revealed the surprising frequency with which this phenomenon occurs under normal conditions and that it can be exacerbated when oligodendrocyte number excessively outweighs axonal area (Almeida et al. 2018). Another molecule, Jam2, was identified as a somatodendritic inhibitor of myelination. When Jam2 was knocked out, extensive myelination of $Pax2^+$ dorsal spinal cord interneuron cell bodies in both zebrafish and mouse was observed (Redmond et al. 2016). Myelinated neuronal cell bodies in iPSC myelinoids were shown to be positive for PV, suggesting that the mistargeting of myelin to inhibitory neuron cell bodies is an evolutionarily shared phenomenon, which

provides an assay that may be useful for studies investigating myelin mistargeting in different diseases.

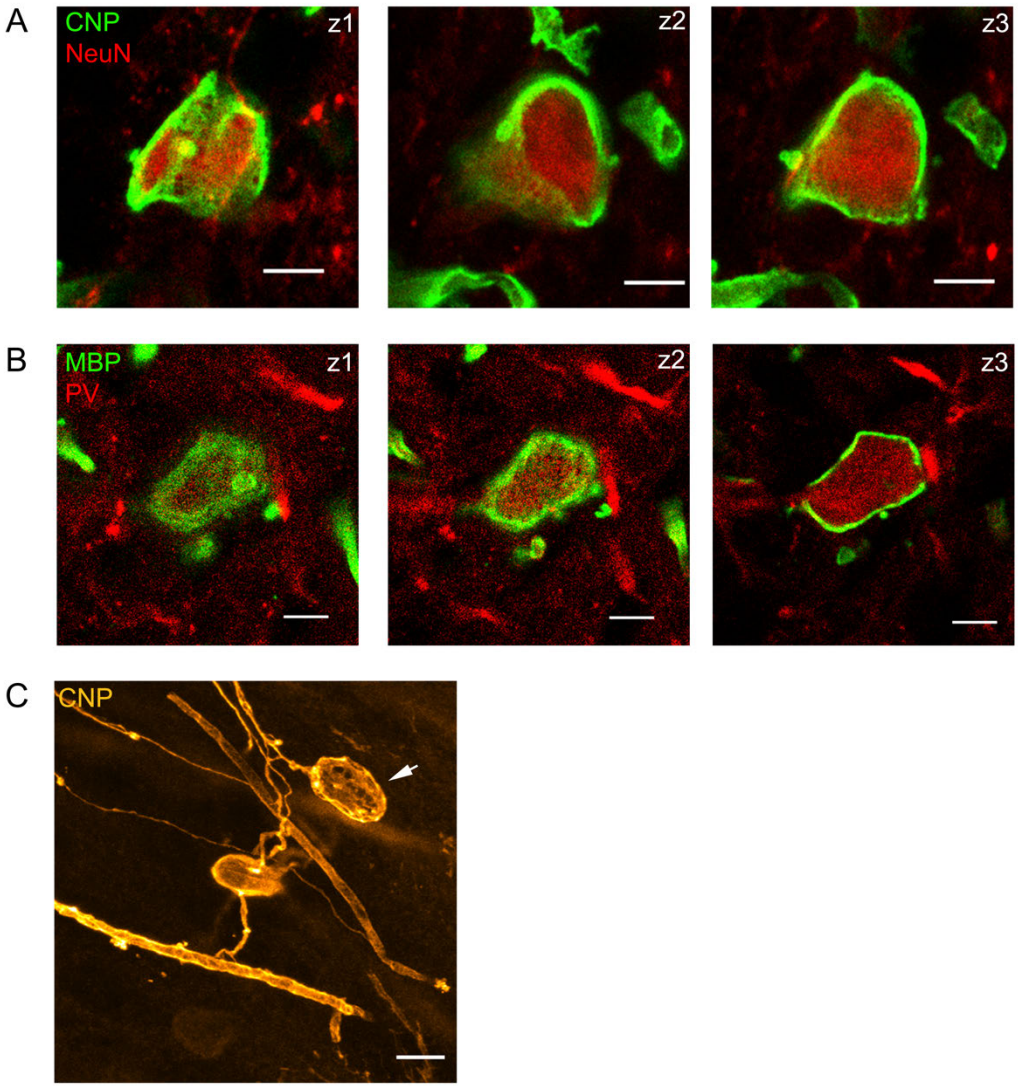

Figure 9.1 Myelinated neuronal cell bodies

A) Myelinated cell bodies were identified by acquiring serial z-steps by confocal microscopy to show CNP^+ myelin surrounding $NeuN^+$ neuronal cell bodies (scale 5μm). B) Myelinated cell bodies were found to be positive for PV (scale 5μm).

C) CNP^+ oligodendrocytes can be found to extend processes that form normal myelin sheaths as well as spherical objects indicative of cell bodies (arrow), scale = 10μm.

3) Does increasing neuronal activity in iPSC myelinoids lead to an increase in sheath number per cell?

I have shown that TeNT reduces the number of myelin sheaths per cell, as well as causing a global reduction in myelin volume in iPSC myelinoids. Several groups have demonstrated the reverse phenotype, whereby potentiating neuronal activity increased the number of myelin sheaths per cell, the number of oligodendrocytes, and total myelin (Mensch et al. 2015; Gibson et al. 2014). However, such studies are typically performed over a short period of time and my efforts at increasing neuronal activity in myelinoids proved challenging. Intermittent KCl treatment did not increase myelin sheath number or total myelin volume. Myelinoids were exposed to KCl in 2-hour intervals, once or three times per week, for 12 weeks. It is possible that this paradigm led to chronic depolarization of neurons and a reduction in their intrinsic excitability (O'Leary et al. 2010). Future work may consider much shorter exposure times to KCl (e.g. 1-minute exposure, three times per week). Alternatively, optogenetic tools may provide greater temporal control of over neuronal activation, as has been shown previously (Gibson et al. 2014). However, in such a closed system, identifying the appropriate strength and frequency of optogenetic stimulation will inevitably be challenging.

4) What treatment strategy is best suited for potentiating oligodendrogenesis and myelin formation in iPSC myelinoids?

A more complete discussion of this question can be found in Chapter 7. Just as the promotion of neuronal activity, the pharmacological potentiation of myelination throws up practical considerations. Most drug screens are performed at either 1 or 10 μM for short periods of time, over the course of days—not weeks—and there is limited data available on the half-life or EC50 of drug compounds for cell culture assays. One approach used to model oligodendrogenesis in three dimensional cultures involved transiently exposing spheroids to drug compounds during glial patterning to inflate the number of OPCs. This led to increased numbers of oligodendrocytes with continued culture (Madhavan, Nevin, Shick, Garrison, Clarkson-Paredes, Karl, Clayton, Factor, Allan, Barbar, Jain, Douvaras, Fossati, R. H. Miller & Tesar 2018b). However, rather

than simply potentiating oligodendrogenesis, myelinoids permit the identification of modulators of the myelination process. Therefore, drug exposure should overlap with peak myelin formation, which is between MI-8 to MI-12. In this thesis, I exposed myelinoids to different compounds chronically for 4, 8, or 12 weeks. I found that 12 weeks of chronic exposure to miconazole had a detrimental effect on myelin development. However, both 4- and 8-week exposure to SGCCBP30 increased the number of $SOX10^+$ cells and MBP^+ oligodendrocytes. Unfortunately, it was not possible to explore this further due to technical problems with the cell cultures that affected myelin formation in iPSC myelinoids. Future studies should consider the use of a fluorescent reporter line under the control of MBP or MYRF to quickly screen for drug effects and to identify appropriate treatment paradigms.

5) How might microglia contribute to myelin development and disease in iPSC myelinoids?

Microglia are essential regulators of CNS development and have important functions in stimulating neurogenesis, network wiring, and phagocytosing apoptotic cells (Ueno et al. 2013; Squarzoni et al. 2014; Sierra et al. 2010). Microglia also play an integral role in myelin development by regulating oligodendrocyte cell numbers (Hagemeyer et al. 2017) and in remyelination by clearing myelin debris and orchestrating pro- and anti-inflammatory cues that drive the repair process (Miron et al. 2013). I was interested in adapting myelinoid cultures so as to ask questions such as: can microglia be integrated into myelinoids? What effect might microglia have on myelin development? Would it be possible to model demyelination and remyelination in microglia-containing myelinoids? To begin this process, iPSC-derived microglia were generated by Dr. Poulomi Banerjee (manuscript in preparation) and were added onto myelinoids at MI by seeding 50,000 cells in a total of 5 μl of media. Microglia could be seen surrounding myelinoids, with some having landed on top and others surrounding the base. It was hoped that microglia would migrate into the myelinoid via chemotaxic signalling. Three days after co-culture, myelinoids were fixed, sectioned, and stained for microglia markers. Figure 9.2 shows the presence of multiple $IBA\text{-}1^+$ microglia within myelinoids that are exhibiting ramified and amoeboid morphologies and expressing TMEM-119 or P2YRY12, reflecting homeostatic and activated states,

respectively (Bennett et al. 2016). This preliminary data demonstrates successful integration of microglia into myelinoids, which will allow us to interrogate their role in the development and degradation of myelin. Future questions investigating whether microglia generated from different patient-derived cell lines show differences in their regulation of myelin development would be of great interest.

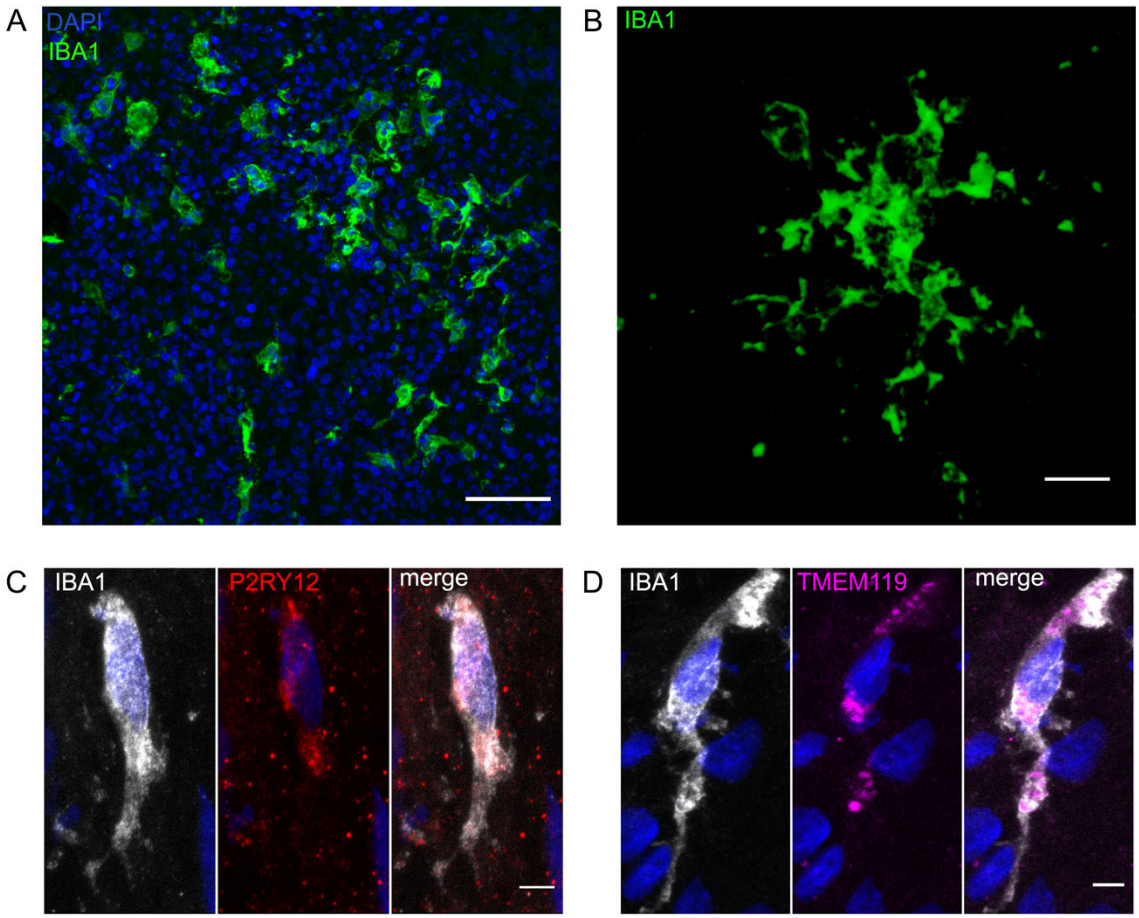

Figure 9.2 Myelinoid-microglia co-culture

A) Widespread integration of iPSC derived microglia in myelinoids at MI (scale 50μm) B) 3D projection of single microglia demonstrating highly ramified projections (scale 10μm). C-D) iPSC microglia display activated (P2RY12) and quiescent (TMEM119) markers (scale 5μm).

In summary, this thesis describes the successful development of an *in vitro* model of myelination using human iPSCs that displays appropriate hallmarks of maturity. Using this platform, I have shown that human myelination can be modulated by pharmacological and physiological manipulation, including changes in neuronal activity. I have developed an automated, unbiased, and whole-spheroid analysis of myelin volume and have used this pipeline to corroborate findings made at the level of individual oligodendrocytes. Finally, using patient-derived cell lines, I showed the feasibility of modelling human myelin disorders *in vitro.* It is hoped that this model will be of interest to myelin researchers for application in studies of the physiology and pathology of myelin development.

Chapter 10 Appendix

10.1 ImageJ macro for blinding and randomising filenames

```
// This macro renames files with an identifying experimental name + a random number.
// A .csv table is created in the output directory with both blinded and original filename

print("\\Clear");
dir=getDirectory("Select a folder of files");
newDir=getDirectory("select an output folder to save files");
list=getFileList(dir);
name = "[Blind table]";

Dialog.create("Experiment name?");
identifyingname="";
Dialog.addString("Provide an identifying name for the experiment",identifyingname);
Dialog.show();
identifyingname = Dialog.getString();

f = name;
makeTable();

for (i=0; i<list.length; i++){
        k=i+1;
        filename=dir+list[i];
        newName= newDir+ identifyingname + random + ".lsm";
        print(f, k+"\t"+filename+"\t" +newName+"\t");
        File.copy(filename, newName);
}

function makeTable() {
name = "[Blind table]";
 run("New... ", "name="+name+" type=Table");
 f = name;
 print(f, "\\Headings:#\tfilename\tnewName\tdir\tnewDir");
}
selectWindow("Blind table");
saveAs("results", newDir +"Blinded_fileNames.csv");
```

10.2 ImageJ macro for stitching and exporting best projection images from ImageXpress

```
// This macro organises best projection images exported from the ImageXpress microscope.
// It transfers images across all sites from each well into individual Well+Channel subfolders (maximum 4 wavelengths).
// The macro user then selects which subfolder of images to stitch together and the fused image is displayed
// and saved in new Directory.
// This macro uses the grid coordinates to stitch tiles together. Ensure you know the grid coordinates before running macro.
// Author: Owen Gwydion James s1470204@sms.ed.ac.uk
// Dementia Research Institute, Chancellor's Building, University of Edinburgh
// 26-2-2018

dir=getDirectory("Choose ImageXpress plate folder eg.747");
newDir=getDirectory("Where do you want to save the output images?");

list=getFileList(dir);
listOfWell =newArray();

for(i=0; i<list.length; i++){
		if(endsWith(list[i],".tif") || endsWith(list[i], ".TIF")){

		//Retrieves well name from file name
		indexWell=indexOf(list[i], "_");
			//Example filename = "....._A01_s1_w1.....tif"
		wellName=substring(list[i],indexWell+1,indexWell+4 );
		listOfWell = Array.concat(listOfWell, wellName);
		Array.print(listOfWell);
}}


	// Extracting unique well name from well array (uses the sorted well array)
	sortedListOfWell=Array.sort(listOfWell);
	uniqueWell=newArray(sortedListOfWell[0]);
		for (k=1; k<sortedListOfWell.length; k++){
			if (sortedListOfWell[k] != sortedListOfWell[k-1]){
			uniqueWell=Array.concat(uniqueWell, sortedListOfWell[k]);
			Array.print(uniqueWell);
}}

	// PadZero for siteName (replaces s_1 with s_01)
	for(i=0; i<list.length; i++){
		if(endsWith(list[i],".tif") || endsWith(list[i], ".TIF")){
			indexSite=indexOf(list[i], "_s");
			indexEndSite=indexOf(list[i], "_w");
			siteName=substring(list[i],indexSite+2,indexEndSite );
```

```
                        fullSiteName=substring(list[i], indexSite, indexEndSite);
                        lengthOfSiteName=lengthOf(siteName);
                        print(siteName);
                        print(fullSiteName);
                        print(lengthOfSiteName);
                                if (lengthOfSiteName==1){ padZero= "0"; }
                                if (lengthOfSiteName==2){ padZero= ""; }
                                if (lengthOfSiteName>2){exit("Error padding zero");}
                                                firstPart=substring(list[i], 0,
indexSite+2);
                                                secondPart=substring(list[i],
indexSite+2, lengthOf(list[i]));

        newName=firstPart+padZero+secondPart;
                                                print(newName);
                                                File.rename(dir+list[i], dir+newName);
}}

// Identify files with different wavelengths and copy into new subfolders

m=0; i=0; j=0;
for (m=0; m<uniqueWell.length; m++){

//For each unique well name (eg.A01) process the following:

        for(i=0; i<list.length; i++) {
                if(endsWith(list[i],".tif") ll endsWith(list[i], ".TIF")){
                indexChannel=indexOf(list[i], "_w");
                firstChannelPart=substring(list[i], 0, indexChannel+2);
                channelName=substring(list[i],indexChannel+1,indexChannel+3 );
                print(channelName);
                matchWell=".*_"+uniqueWell[m]+".*";

if((matches(list[i], ".*_w1.*")) && (matches(list[i], matchWell) && (matches(list[i],
".*thumb.*") != 1))){

//finds files of wavelength 1

        print(list[i]);

        newDirName=newDir+"Well_"+uniqueWell[m]+"_Channel_1";
        File.makeDirectory(newDirName);
        print(newDirName);
        File.copy(dir+list[i], newDirName+File.separator+list[i]);

//Copies files into new directory
                        }

if((matches(list[i], ".*_w2.*")) && (matches(list[i], matchWell) && (matches(list[i],
".*thumb.*") != 1))){
```

```
//Same again for wavelength 2

        print(list[i]);

        newDirName=newDir+"Well_"+uniqueWell[m]+"_Channel_2";
                                File.makeDirectory(newDirName);
                                print(newDirName);
                                File.copy(dir+list[i], newDirName+File.separator+list[i]);
                        }
        if((matches(list[i], ".*_w3.*")) && (matches(list[i], matchWell) &&
(matches(list[i], ".*thumb.*") != 1))){

//Same again for wavelength 3

        print(list[i]);

        newDirName=newDir+"Well_"+uniqueWell[m]+"_Channel_3";
                                File.makeDirectory(newDirName);
                                print(newDirName);
                                File.copy(dir+list[i], newDirName+File.separator+list[i]);
                        }
        if((matches(list[i], ".*_w4.*")) && (matches(list[i], matchWell) &&
(matches(list[i], ".*thumb.*") != 1))){

//Same again for wavelength 4

        print(list[i]);

        newDirName=newDir+"Well_"+uniqueWell[m]+"_Channel_4";
                                File.makeDirectory(newDirName);
                                print(newDirName);
                                File.copy(dir+list[i], newDirName+File.separator+list[i]);
                        }
                }
        }
}



// Creating a list of the Well+Channel subfolders
        newDirlist=getFileList(newDir);
        wellChannelList=newArray();
                for(j=0; j<newDirlist.length; j++){
                        if(matches(newDirlist[j], ".*.tif.*") != 1){
                        wellChannelList=Array.concat(wellChannelList, newDirlist[j]);
                        Array.print(wellChannelList);
}}

//Automated determining of tile configuration. In nearly all cases, Xtile is greater than
//Ytile. Beware of this assumption.
```

```
print("determining the number of tiles using the number of files in the folder");
copiedList=getFileList(newDirName);
for(v=0;v<copiedList.length;v++){
if(endsWith(copiedList[v],".tif")){
        print(copiedList.length);

if(copiedList.length==9){
        Xtile = 3;
        Ytile = 3;
}
if(copiedList.length==12){
        Xtile = 4;
        Ytile = 3;
}
if(copiedList.length==16){
        Xtile = 4;
        Ytile = 4;
}
if(copiedList.length==20){
        Xtile = 5;
        Ytile = 4;
}
if(copiedList.length==25){
        Xtile = 5;
        Ytile = 5;
}
if(copiedList.length==30){
        Xtile = 6;
        Ytile = 5;
}
if(copiedList.length==36){
        Xtile = 6;
        Ytile = 6;
}
}}


for(f=0; f<wellChannelList.length; f++){
        tempDir=newDir+wellChannelList[f];
                print("the TempDir is: "+ tempDir);
                ChoiceIndex=indexOf(tempDir, "Well");
                ChoiceNameEnd=lengthOf(tempDir);
                ChoiceName=substring(tempDir, ChoiceIndex, ChoiceNameEnd-1);

//Extracts the name of the chosen file to be used for saving stitched image

print("the choiceName is: "+ ChoiceName);
                File.makeDirectory(tempDir);
                File.isDirectory(tempDir);
```

```
		tempList=getFileList(tempDir);
		Array.print(tempList);

		for(i=0; i<tempList.length; i++){

// identifies the full site name and replaces with variable {ii}

		if(endsWith(tempList[i],".tif") || endsWith(tempList[i], ".TIF") &&
(matches(tempList[i], ".*Stitched.*") != 1)){
				currentName=tempDir+tempList[i];
				indexSiteX=indexOf(tempList[i], "_s");
				indexEndSiteX=indexOf(tempList[i], "_w");
				firstPart=substring(tempList[i], 0, indexEndSiteX+3);
				shortenedName=firstPart + ".tif";
				print("the ShortenedName is: " + shortenedName);
				newTempName=tempDir+shortenedName;
		tempSiteName=substring(tempList[i], indexSite, indexEndSite);

	genericFileName=replace(shortenedName, tempSiteName, "_s{ii}");
				File.rename(currentName, newTempName);
				print("the generic File Name is: " + genericFileName);

				}}

// run grid/collection stitching

	run("Grid/Collection stitching", "type=[Grid: row-by-row] order=[Right & Down
] grid_size_x=Xtile grid_size_y=Ytile tile_overlap=10 first_file_index_i=1
directory=[&tempDir] file_names=[&genericFileName]
output_textfile_name=TileConfiguration.txt fusion_method=[Linear Blending]
regression_threshold=0.30 max/avg_displacement_threshold=2.50
absolute_displacement_threshold=3.50 computation_parameters=[Save memory
(but be slower)] image_output=[Fuse and display]");

saveAs("tiff", newDir + shortenedName + "_Stitched_image" + ".tif");

}

for(x=0; x<wellChannelList.length; x++){
	print(wellChannelList[x]);
	File.isDirectory(newDir+wellChannelList[x]+File.separator);
	File.delete(newDir+wellChannelList[x]+File.separator);
	File.isDirectory(newDir+wellChannelList[x]+File.separator);

	}
```

Chapter 11 Bibliography

Aarts, E. et al., 2014. A solution to dependency: using multilevel analysis to accommodate nested data. *Nat Neurosci*, 17(4), pp.491–496.

Abud, E.M. et al., 2017. iPSC-Derived Human Microglia-like Cells to Study Neurological Diseases. *Neuron*, 94(2), pp.278–293.

Aguado, F. et al., 2003. BDNF regulates spontaneous correlated activity at early developmental stages by increasing synaptogenesis and expression of the K+/Cl- co-transporter KCC2. *Development*, 130(7), pp.1267–1280.

Ahmed, S., Reynolds, B.A. & Weiss, S., 1995. BDNF enhances the differentiation but not the survival of CNS stem cell- derived neuronal precursors. *J Neurosci*, 15(8), pp.5765–5778.

Aggarwal, S. et al., 2011. A Size Barrier Limits Protein Diffusion at the Cell Surface to Generate Lipid-Rich Myelin-Membrane Sheets. *Developmental cell*, 21(3), pp.445–456.

Alexander, A.L. et al., 2007. Diffusion Tensor Imaging of the Brain. *Neurotherapeutics : the journal of the American Society for Experimental NeuroTherapeutics*, 4(3), pp.316–329.

Alexandra I, M., Constanze, D. & Klaus-Armin, N., 2018. An emerging role of dysfunctional axon-oligodendrocyte coupling in neurodegenerative diseases. *Dialogues in Clinical Neuroscience*, 20(4), pp.283–292.

Allamargot, C., Pouplard-Barthelaix, A. & Fressinaud, C., 2001. A single intracerebral microinjection of platelet-derived growth factor (PDGF) accelerates the rate of remyelination in vivo. *Brain Research*, 918(1-2), pp.28–39.

Almazan, G., Honegger, P. & Matthieu, J.-M., 1985. Triiodothyronine Stimulation of Oligodendroglial Differentiation and Myelination. *Developmental Neuroscience*, 7(1), pp.45–54.

Almeida, R.G. & Lyons, D.A., 2014. On the resemblance of synapse formation and CNS myelination. *Neuroscience*, 276, pp.98–108.

Almeida, R.G. & Lyons, D.A., 2017. On Myelinated Axon Plasticity and Neuronal Circuit Formation and Function. *J Neurosci*, 37(42), pp.10023–10034.

Almeida, R.G. et al., 2011. Individual axons regulate the myelinating potential of single oligodendrocytes in vivo. *Development*, 138(20), pp.4443–4450.

Almeida, R.G. et al., 2018. Myelination of Neuronal Cell Bodies when Myelin Supply Exceeds Axonal Demand. *Current Biology*, 28(8), pp.1296–1305.

Althaus, H.H. et al., 1984. Isolation and cultivation of mature oligodendroglial cells. *Naturwissenschaften*, 71(6), pp.309–315.

Ambrose, C.T., 2017. An amended history of tissue culture: Concerning Harrison, Burrows, Mall, and Carrel. *Journal of Medical Biography*, 27(2), pp.95–102.

Ameis, S.H. & Catani, M., 2015. Altered white matter connectivity as a neural substrate for social impairment in Autism Spectrum Disorder. *Cortex*, 62, pp.158–181.

Anderson, J.A.E. et al., 2018. Effects of bilingualism on white matter integrity in older adults. *NeuroImage*, 167, pp.143–150.

Andrew M Ravanelli, B.A., 2015. Motor neurons and oligodendrocytes arise from distinct cell lineages by progenitor recruitment. *Genes & Development*, 29(23), pp.2504–2515.

Arai, T. et al., 2006. TDP-43 is a component of ubiquitin-positive tau-negative inclusions in frontotemporal lobar degeneration and amyotrophic lateral sclerosis. *Biochemical and biophysical research communications*, 351(3), pp.602–611.

Arancibia Carcamo, I.L. et al., 2017. Node of Ranvier length as a potential regulator of myelinated axon conduction speed. *eLife*, 6, p.521.

Arnold, E.S. et al., 2013. ALS-linked TDP-43 mutations produce aberrant RNA splicing and adult-onset motor neuron disease without aggregation or loss of nuclear TDP-43. *Proc Natl Acad Sci USA*, 110(8), pp.E736–E745.

Auer, F., Vagionitis, S. & Czopka, T., 2018. Evidence for Myelin Sheath Remodeling in the CNS Revealed by In Vivo Imaging. *Current Biology*, 28(4), pp.549–559.e3.

Ayala, Y.M. et al., 2011. TDP-43 regulates its mRNA levels through a negative feedback loop. *The EMBO Journal*, 30(2), pp.277–288.

Back, S.A. et al., 2002. Selective vulnerability of late oligodendrocyte progenitors to hypoxia-ischemia. *J Neurosci*, 22(2), pp.455–463.

Back, S.A. et al., 2002. Arrested Oligodendrocyte Lineage Progression During Human Cerebral White Matter Development: Dissociation Between the Timing of Progenitor Differentiation and Myelinogenesis. *Journal of Neuropathology & Experimental Neurology*, 61(2), pp.197–211.

Bading, H., Ginty, D.D. & Greenberg, M.E., 1993. Regulation of gene expression in hippocampal neurons by distinct calcium signaling pathways. *Science*, 260(5105), pp.181–186.

Bakken, T.E. et al., 2016. A comprehensive transcriptional map of primate brain development. *Nature*, 535(7612), pp.367–375.

Balkowiec, A. & Katz, D.M., 2000. Activity-Dependent Release of Endogenous Brain-Derived Neurotrophic Factor from Primary Sensory Neurons Detected by ELISAIn Situ. *J Neurosci*, 20(19), pp.7417–7423.

Barak, B. et al., 2019. Neuronal deletion of Gtf2i , associated with Williams syndrome, causes behavioral and myelin alterations rescuable by a remyelinating drug. *Nature Neuroscience*, 22(5), pp.700–708.

Barres, B.A. & Raff, M.C., 1993. Proliferation of oligodendrocyte precursor cells depends on electrical activity in axons. *Nature*, 361(6409), pp.258–260.

Barres, B.A. et al., 1992. Cell death and control of cell survival in the oligodendrocyte lineage. *Cell*, 70(1), pp.31–46.

Barres, B.A. et al., 1993. Multiple extracellular signals are required for long-term oligodendrocyte survival. *Development*, 118(1), pp.283–295.

Barton, S.K. et al., 2019. Could an Impairment in Local Translation of mRNAs in Glia be Contributing to Pathogenesis in ALS? *Frontiers in Molecular Neuroscience*, 12, p.7482.

Bartzokis, G. et al., 2001. Age-Related Changes in Frontal and Temporal Lobe Volumes in Men: A Magnetic Resonance Imaging Study. *Archives of General Psychiatry*, 58(5), pp.461–465.

Bechler, M.E., Byrne, L. & ffrench-Constant, C., 2015. CNS Myelin Sheath Lengths Are an Intrinsic Property of Oligodendrocytes. *Current biology : CB*, 25(18), pp.2411–2416.

Bechler, M.E., Swire, M. & ffrench-Constant, C., 2017. Intrinsic and adaptive myelination-A sequential mechanism for smart wiring in the brain P. Cassacia & G. Corfas, eds. *Developmental neurobiology*, 78(2), pp.68–79.

Ben Emery et al., 2009. Identification of Myelin-gene Regulatory Factor as a Critical Transcriptional Regulator Required for CNS Myelination. *Cell*, 138(1), pp.172–185.

Ben Emery, Q.R.L., 2015. Transcriptional and Epigenetic Regulation of Oligodendrocyte Development and Myelination in the Central Nervous System. *Cold Spring Harb Perspect Biol*, 7(9), p.a020461.

Benes, F.M., 1989. Myelination of cortical-hippocampal relays during late adolescence. *Schizophrenia Bulletin*, 15(4), pp.585–593.

Bennett, M.L. et al., 2016. From the Cover: PNAS Plus: New tools for studying microglia in the mouse and human CNS. *Proceedings of the National Academy of Sciences of the United States of America*, 113(12), pp.E1738–E1746.

Bengtsson, S.L. et al., 2005. Extensive piano practicing has regionally specific effects on white matter development. *Nat Neurosci*, 8(9), pp.1148–1150.

Bergles, D.E. et al., 2000. Glutamatergic synapses on oligodendrocyte precursor cells in the hippocampus. *Nature*, 405(6783), pp.187–191.

Beske, P.H. et al., 2016. Botulinum and Tetanus Neurotoxin-Induced Blockade of Synaptic Transmission in Networked Cultures of Human and Rodent Neurons. *Toxicological Sciences*, 149(2), pp.503–515.

Billings-Gagliardi, S. et al., 1984. Cultures of shiverer mutant cerebellum injected with normal oligodendrocytes make both normal and shiverer myelin. *Proc Natl Acad Sci USA*, 81(8), pp.2558–2561.

Billon, N. et al., 2002. Normal timing of oligodendrocyte development from genetically engineered, lineage-selectable mouse ES cells. *J Cell Sci*, 115(18), pp.3657–3665.

Bin, J.M. et al., 2012. Oligodendrocyte precursor cell transplantation into organotypic cerebellar shiverer slices: a model to study myelination and myelin maintenance. M. Stangel, ed. *PLoS ONE*, 7(7), pp.e41237–8.

Birey, F. et al., 2017. Assembly of functionally integrated human forebrain spheroids. *Nature*, 545(7652), pp.54–59.

Bjartmar, C., Hildebrand, C. & Loinder, K., 1994. Morphological heterogeneity of rat oligodendrocytes: Oligodendrocytes: Electron microscopic studies on serial sections. *Glia*, 11(3), pp.235–244.

Blakemore, W.F., 1974. Pattern of remyelination in the CNS. *Nature*, 249(5457), pp.577–578.

Blakemore, W.F., 1969. Schmidt-Lantermann incisures in the central nervous system. *Journal of Ultrastructure Research*, 29(5-6), pp.496–498.

Blumenfeld-Katzir, T. et al., 2011. Diffusion MRI of Structural Brain Plasticity Induced by a Learning and Memory Task Y.-P. Tang, ed. *PLoS ONE*, 6(6), p.e20678.

Boullerne, A.I., 2016. The history of myelin. *Exp Neurol*, 283(Pt B), pp.431–445.

Boyd, A., Zhang, H. & Williams, A., 2013. Insufficient OPC migration into demyelinated lesions is a cause of poor remyelination in MS and mouse models. *Acta Neuropathologica*, 125(6), pp.841–859.

Brady, S.T. et al., 1999. Formation of Compact Myelin Is Required for Maturation of the Axonal Cytoskeleton. *J Neurosci*, 19(17), pp.7278–7288.

Brill, M.H. et al., 1977. Conduction velocity and spike configuration in myelinated fibres: computed dependence on internode distance. *J Neurol Neurosurg Psychiatry*, 40(8), pp.769–774.

Brinkmann, B.G. et al., 2008. Neuregulin-1/ErbB signaling serves distinct functions in myelination of the peripheral and central nervous system. *Neuron*, 59(4), pp.581–595.

Brooks, M.E. et al., 2017. glmmTMB Balances Speed and Flexibility Among Packages for Zero-inflated Generalized Linear Mixed Modeling. *The R Journal*, 9(2), pp.378–400.

Brown, A.M., Tekkök, S.B. & Ransom, B.R., 2004. Glycogen Regulation and Functional Role in Mouse White Matter. *The Journal of Physiology*, 549(2), pp.501–512.

Buchet, D. et al., 2011. Human neural progenitors from different foetal forebrain regions remyelinate the adult mouse spinal cord. *Brain*, 134(4), pp.1168–1183.

Buser, J.R. et al., 2012. Arrested pre-oligodendrocyte maturation contributes to myelination failure in premature infants. *Annals of neurology*, 71(1), pp.93–109.

Buttery, P.C. & ffrench-Constant, C., 1999. Laminin-2/Integrin Interactions Enhance Myelin Membrane Formation by Oligodendrocytes. *Molecular and Cellular Neuroscience*, 14(3), pp.199–212.

Campagnoni, A.T., Carey, G.D. & Yu, Y.T., 1980. In Vitro Synthesis of the Myelin Basic Proteins: Subcellular Site of Synthesis. *Journal of neurochemistry*, 34(3), pp.677–686.

Carletti, F. et al., 2012. Alterations in White Matter Evident Before the Onset of Psychosis. *Schizophrenia Bulletin*, 38(6), pp.1170–1179.

Carrel, A., 1912. On the permanent life of tissues outside of the organism. *Journal of Experimental Medicine*, 15(5), pp.516–528.

Cassandra Sampaio-Baptista, H.J.-B., 2017. White Matter Plasticity in the Adult Brain. *Neuron*, 96(6), pp.1239–1251.

Câmara, J. et al., 2009. Integrin-mediated axoglial interactions initiate myelination in the central nervous system. *The Journal of Cell Biology*, 185(4), pp.699–712.

Chan, J.R. et al., 2001. Inaugural article by a Recently Elected Academy Member:Neurotrophins are key mediators of the myelination program in the peripheral nervous system. *Proceedings of the National Academy of Sciences of the United States of America*, 98(25), pp.14661–14668.

Chan, J.R. et al., 2004. NGF Controls Axonal Receptivity to Myelination by Schwann Cells or Oligodendrocytes. *Neuron*, 43(2), pp.183–191.

Chandran, S. et al., 2003. FGF-dependent generation of oligodendrocytes by a hedgehog-independent pathway. *Development*, 130(26), pp.6599–6609.

Chandran, S. et al., 2004. Differential generation of oligodendrocytes from human and rodent embryonic spinal cord neural precursors. *Glia*, 47(4), pp.314–324.

Chang, A. et al., 2002. Premyelinating Oligodendrocytes in Chronic Lesions of Multiple Sclerosis. *The New England journal of medicine*, 346(3), pp.165–173.

Chanoumidou, K. et al., 2019. Stem cell derived oligodendrocytes to study myelin diseases. *Glia*, 19(6), p.1129.

Chen, S. et al., 2005. Robust axonal sprouting and synaptogenesis in organotypic slice cultures of rat cerebellum exposed to increased potassium chloride. *Brain Research*, 1057(1-2), pp.88–97.

Chen, S. et al., 2016. A Comparative Study of Three Interneuron Types in the Rat Spinal Cord S. Lei, ed. *PLoS ONE*, 11(9), p.e0162969.

Chernoff, G.F., 1981. Shiverer: an autosomal recessive mutant mouse with myelin deficiency. *Journal of Heredity*, 72(2), pp.128–128.

Chomiak, T. & Bin Hu, 2009. What Is the Optimal Value of the g-Ratio for Myelinated Fibers in the Rat CNS? A Theoretical Approach D. Finkelstein, ed. *PLoS ONE*, 4(11), p.e7754.

Christopherson, K.S. et al., 2005. Thrombospondins Are Astrocyte-Secreted Proteins that Promote CNS Synaptogenesis. *Cell*, 120(3), pp.421–433.

Chong, S.Y.C., Rosenberg, S.S., Fancy, S.P.J., Zhao, C., Shen, Y.-A.A., Hahn, A.T., McGee, A.W., Xu, X., Zheng, B., Zhang, L.I., Rowitch, D.H., Franklin, R.J.M., Lu, Q.R. & Chan, J.R., 2012. Neurite outgrowth inhibitor Nogo-A establishes spatial segregation and extent of oligodendrocyte myelination. *Proc Natl Acad Sci USA*, 109(4), pp.1299–1304.

Chun, S.-J. et al., 2003. Integrin-linked kinase is required for laminin-2–induced oligodendrocyte cell spreading and CNS myelination. *The Journal of Cell Biology*, 163(2), pp.397–408.

Clevers, H., 2016. Modeling Development and Disease with Organoids. *Cell*, 165(7), pp.1586–1597.

Clowry, G.J. et al., 2000. Changing pattern of expression of parvalbumin immunoreactivity during human fetal spinal cord development. *Journal of Comparative Neurology*, 423(4), pp.727–735.

Colcombe, S.J. et al., 2006. Aerobic Exercise Training Increases Brain Volume in Aging Humans. *Journal of Gerontology MEDICAL SCIENCES*, 61A(11), pp.1166–1170.

Colman, D.R. et al., 1982. Synthesis and incorporation of myelin polypeptides into CNS myelin. *The Journal of Cell Biology*, 95(2 Pt 1), pp.598–608.

Colognato, H. et al., 2002. CNS integrins switch growth factor signalling to promote target-dependent survival. *Nature Cell Biology*, 4(11), pp.833–841.

Corcia, P. et al., 2012. Phenotype and genotype analysis in amyotrophic lateral sclerosis with TARDBP gene mutations. *Neurology*, 78(19), pp.1519–1526.

Crain, S.M., 1966. Development of “Organotypic” Bioelectric Activities in Central Nervous Tissues During Maturation in Culture. *International Review of Neurobiology*, 9, pp.1–43.

Crawford, A.H. et al., 2016. Pre-Existing Mature Oligodendrocytes Do Not Contribute to Remyelination following Toxin-Induced Spinal Cord Demyelination. *The American journal of pathology*, 186(3), pp.511–516.

Cree, B.A.C. et al., 2017. Clemastine rescues myelination defects and promotes functional recovery in hypoxic brain injury. *Brain*, 141(1): 85–98.

Croft, C.L. et al., 2017. Membrane association and release of wild-type and pathological tau from organotypic brain slice cultures. *Cell Death Dis*, 8(3), pp.e2671–e2671.

Czopka, T., ffrench-Constant, C. & Lyons, D.A., 2013. Individual Oligodendrocytes Have Only a Few Hours in which to Generate New Myelin Sheaths In Vivo. *Developmental cell*, 25(6), pp.599–609.

de Rosbo, N.K. et al., 1990. Demyelination Induced in Aggregating Brain Cell Cultures by a Monoclonal Antibody Against Myelin/Oligodendrocyte Glycoprotein. *Journal of neurochemistry*, 55(2), pp.583–587.

de Vrij, F.M. et al., 2019. Candidate CSPG4 mutations and induced pluripotent stem cell modeling implicate oligodendrocyte progenitor cell dysfunction in familial schizophrenia. *Molecular Psychiatry*, 24(5), pp.757–771.

Deary, I.J. et al., 2006. White matter integrity and cognition in childhood and old age. *Neurology*, 66(4), pp.505–512.

Demerens, C. et al., 1996. Induction of myelination in the central nervous system by electrical activity. *Proceedings of the National Academy of Sciences of the United States of America*, 93(18), pp.9887–9892.

Deoni, S.C.L. et al., 2015. Cortical maturation and myelination in healthy toddlers and young children. *NeuroImage*, 115, pp.147–161.

Derfuss, T. et al., 2010. Axo-glial antigens as targets in multiple sclerosis: implications for axonal and grey matter injury. *Journal of Molecular Medicine*, 88(8), pp.753–761.

Deshaies, J.-E. et al., 2018. TDP-43 regulates the alternative splicing of hnRNP A1 to yield an aggregation-prone variant in amyotrophic lateral sclerosis. *Brain*, 141(5), pp.1320–1333.

Deshmukh, V.A. et al., 2013. A regenerative approach to the treatment of multiple sclerosis. *Nature*, 502(7471), pp.327–332.

Diemel, L.T. et al., 2004. Remyelination of cytokine- or antibody-demyelinated CNS aggregate cultures is inhibited by macrophage supplementation. *Glia*, 45(3), pp.278–286.

Dietz, K.C. et al., 2016. Targeting human oligodendrocyte progenitors for myelin repair. *Exp Neurol*, 283(Pt B), pp.489–500.

Domingues, H.S. et al., 2017. Mechanical plasticity during oligodendrocyte differentiation and myelination. *Glia*, 66(1), pp.5–14.

Douvaras, P. et al., 2014. Efficient Generation of Myelinating Oligodendrocytes from Primary Progressive Multiple Sclerosis Patients by Induced Pluripotent Stem Cells. *Stem Cell Reports*, 3(2), pp.250–259.

Douvaras, P. et al., 2015. Generation and isolation of oligodendrocyte progenitor cells from human pluripotent stem cells. *Nat Protoc*, 10(8), pp.1143–1154.

Du, Y. et al., 2017. Differential subnetwork of chemokines/cytokines in human, mouse, and rat brain cells after oxygen–glucose deprivation. *Journal of Cerebral Blood Flow & Metabolism*, 37(4), pp.1425–1434.

Duncan, I.D. et al., 2018. The adult oligodendrocyte can participate in remyelination. *Proc Natl Acad Sci USA*, 115(50), pp.E11807–E11816.

Duncan, I.D. et al., 2017. Thin myelin sheaths as the hallmark of remyelination persist over time and preserve axon function. *Proc Natl Acad Sci USA*, 114(45), pp.E9685–E9691.

Duvanel, C.B., Honegger, P. & Matthieu, J.-M., 2001. Antibodies directed against rubella virus induce demyelination in aggregating rat brain cell cultures. *J Neurosci Res*, 65(5), pp.446–454.

Dylan A Galloway, C.S.M., 2016. miRNAs As Emerging Regulators of Oligodendrocyte Development and Differentiation. *Frontiers in Cell and Developmental Biology*, 4(13), p.274.

Dzhashiashvili, Y. et al., 2007. Nodes of Ranvier and axon initial segments are ankyrin G–dependent domains that assemble by distinct mechanisms. *The Journal of Cell Biology*, 177(5), pp.857–870.

Early, J.J. et al., 2018. An automated high-resolution in vivo screen in zebrafish to identify chemical regulators of myelination. *eLife*, 7, p.4443.

Ebstein, S.Y., Yagudayeva, I. & Shneider, N.A., 2019. Mutant TDP-43 Causes Early-Stage Dose-Dependent Motor Neuron Degeneration in a TARDBP Knockin Mouse Model of ALS. *CellReports*, 26(2), pp.364–373.

Ehrlich, M. et al., 2017. Rapid and efficient generation of oligodendrocytes from human induced pluripotent stem cells using transcription factors. *Proceedings of the National Academy of Sciences of the United States of America*, 114(11), pp.201614412–E2252.

Erickson, K.I. et al., 2011. Exercise training increases size of hippocampus and improves memory. *Proc Natl Acad Sci USA*, 108(7), pp.3017–3022.

Eroglu, Ç. et al., 2009. The Gabapentin Receptor α2δ-1 is the Neuronal Thrombospondin Receptor Responsible for Excitatory CNS Synaptogenesis. *Cell*, 139(2), pp.380–392.

Evans, M.J. & Kaufman, M.H., 1981. Establishment in culture of pluripotential cells from mouse embryos. *Nature*, 292(5819), pp.154–156.

Faustino Martins, J.-M. et al., 2020. Self-Organizing 3D Human Trunk Neuromuscular Organoids. *Cell Stem Cell*, 26(2), pp.172–186.

Fernandez, P.-A. et al., 2000. Evidence that Axon-Derived Neuregulin Promotes Oligodendrocyte Survival in the Developing Rat Optic Nerve. *Neuron*, 28(1), pp.81–90.

Ferraiuolo, L. et al., 2016. Oligodendrocytes contribute to motor neuron death in ALS via SOD1-dependent mechanism. *Proc Natl Acad Sci USA*, 113(42), pp.E6496–E6505.

Field, E.J., Hughes, D. & Raine, C.S., 1969. Electron microscopic observations on the development of myelin in cultures of neonatal rat cerebellum. *Journal of the Neurological Sciences*, 8(1), pp.49–60.

Fields, R.D., 2011. Nonsynaptic and nonvesicular ATP release from neurons and relevance to neuron–glia signaling. *Seminars in Cell & Developmental Biology*, 22(2), pp.214–219.

Fields, R.D., 2008. White matter in learning, cognition and psychiatric disorders. *Trends in Neurosciences*, 31(7), pp.361–370.

Fitzsimmons, J., Kubicki, M. & Shenton, M., 2013. Review of functional and anatomical brain connectivity findings in schizophrenia. *Current Opinion in Psychiatry*, 26(2), pp.172–187.

Fletcher, J.L., Murray, S.S. & Xiao, J., 2018. Brain-Derived Neurotrophic Factor in Central Nervous System Myelination: A New Mechanism to Promote Myelin Plasticity and Repair. *International Journal of Molecular Sciences*, 19(12), p.4131.

Follett, P.L. et al., 2000. NBQX Attenuates Excitotoxic Injury in Developing White Matter. *The Journal of Neuroscience*, 20(24), pp.9235–9241.

Ford, M.C. et al., 2015. Tuning of Ranvier node and internode properties in myelinated axons to adjust action potential timing. *Nature Communications*, 6(1), p.101.

Fraichard, A. et al., 1995. In vitro differentiation of embryonic stem cells into glial cells and functional neurons. *J Cell Sci*, 108(10), pp.3181–3188.

Franklin, R.J.M. & ffrench-Constant, C., 2008. Remyelination in the CNS: from biology to therapy. *Nat Rev Neurosci*, 9(11), pp.839–855.

Franklin, R.J.M. & ffrench-Constant, C., 2017. Regenerating CNS myelin — from mechanisms to experimental medicines. *Nat Rev Neurosci*, 18(12), pp.753–769.

Franklin, R.J.M. et al., 2012. Neuroprotection and repair in multiple sclerosis. *Nature Publishing Group*, 8(11), pp.624–634.

Freyberg, Z. et al., 2016. Mechanisms of amphetamine action illuminated through optical monitoring of dopamine synaptic vesicles in Drosophila brain. *Nature Communications*, 7(1), pp.1–15.

Friston, K. et al., 2016. The dysconnection hypothesis (2016). *Schizophrenia research*, 176(2-3), pp.83–94.

Fu, H. et al., 2002. Dual origin of spinal oligodendrocyte progenitors and evidence for the cooperative role of Olig2 and Nkx2.2 in the control of oligodendrocyte diffe... *Development*, 129(3), pp.681–693.

Fünfschilling, U., Supplie, L.M., Mahad, D., Boretius, S., Saab, A.S., Edgar, J., Brinkmann, B.G., Kassmann, C.M., Tzvetanova, I.D., Möbius, W., Diaz, F., Meijer, D., Suter, U., Hamprecht, B., Sereda, M.W., Moraes, C.T., Frahm, J., Goebbels, S. & Nave, K.-A., 2012a. Glycolytic oligodendrocytes maintain myelin and long-term axonal integrity. *Nature*, 485(7399), pp.517–521.

Garner, J.P., 2014. The Significance of Meaning: Why Do Over 90% of Behavioral Neuroscience Results Fail to Translate to Humans, and What Can We Do to Fix It? *ILAR Journal*, 55(3), pp.438–456.

Gasser, A. et al., 2012. An AnkyrinG-Binding Motif Is Necessary and Sufficient for Targeting Nav1.6 Sodium Channels to Axon Initial Segments and Nodes of Ranvier. *J Neurosci*, 32(21), pp.7232–7243.

Gasset-Rosa, F. et al., 2019. Cytoplasmic TDP-43 De-mixing Independent of Stress Granules Drives Inhibition of Nuclear Import, Loss of Nuclear TDP-43, and Cell Death. *Neuron*.

Gautier, H.O.B. et al., 2015. Neuronal activity regulates remyelination via glutamate signalling to oligodendrocyte progenitors. *Nature Communications*, 6, p.8518.

Ge, Y. et al., 2002. Age-Related Total Gray Matter and White Matter Changes in Normal Adult Brain. Part I: Volumetric MR Imaging Analysis. *American Journal of Neuroradiology*, 23(8), pp.1327–1333.

Geng, X. et al., 2012. Quantitative Tract-Based White Matter Development from Birth to Age Two Years. *NeuroImage*, 61(3), pp.542–557.

Geraghty, A.C. et al., 2019. Loss of Adaptive Myelination Contributes to Methotrexate Chemotherapy-Related Cognitive Impairment. *Neuron*, 103(2), pp.250–265.

Giandomenico, S.L. et al., 2019. Cerebral organoids at the air–liquid interface generate diverse nerve tracts with functional output. *Nature Neuroscience*, 22(4), pp.669-679.

Gibson, E.M. et al., 2014. Neuronal Activity Promotes Oligodendrogenesis and Adaptive Myelination in the Mammalian Brain. *Science*, 344(6183), pp.1252304–1252304.

Goebbels, S. et al., 2017. A neuronal PI(3,4,5)P 3 -dependent program of oligodendrocyte precursor recruitment and myelination. *Nature Neuroscience*, 20(1), pp.10–15.

Goldenberg, M.M., 2012. Multiple sclerosis review. *P & T : a peer-reviewed journal for formulary management*, 37(3), pp.175–184.

Goldman, S.A. & Kuypers, N.J., 2015. How to make an oligodendrocyte. *Development*, 142(23), pp.3983–3995.

Goldman, S.A., Nedergaard, M. & Windrem, M.S., 2012. Glial Progenitor Cell–Based Treatment and Modeling of Neurological Disease. *Science*, 338(6106), pp.491–495.

Goldsberry, G. et al., 2011. Accelerated myelination with motor system involvement in a neonate with immediate postnatal onset of seizures and hemimegalencephaly. *Epilepsy & Behavior*, 22(2), pp.391–394.

Gonchar, Y. & burkhalter, A., 1997. Three distinct families of GABAergic neurons in rat visual cortex. | Cerebral Cortex | Oxford Academic. *Cerebral Cortex*.

Gow, A. et al., 1999. CNS Myelin and Sertoli Cell Tight Junction Strands Are Absent in Osp/Claudin-11 Null Mice. *Cell*, 99(6), pp.649–659.

Gow, A., Southwood, C.M. & Lazzarini, R.A., 1998. Disrupted proteolipid protein trafficking results in oligodendrocyte apoptosis in an animal model of Pelizaeus-Merzbacher disease. *The Journal of Cell Biology*, 140(4), pp.925–934.

Green, A.J. et al., 2017. Clemastine fumarate as a remyelinating therapy for multiple sclerosis (ReBUILD): - Google Search. *The Lancet*, 390(10111), pp.2481–2489.

Griffiths, I. et al., 1998. Axonal swellings and degeneration in mice lacking the major proteolipid of myelin. *Science*, 280(5369), pp.1610–1613.

Grydeland, H. et al., 2013. Intracortical Myelin Links with Performance Variability across the Human Lifespan: Results from T1- and T2-Weighted MRI Myelin Mapping and Diffusion Tensor Imaging. *J Neurosci*, 33(47), pp.18618–18630.

Gurney, M.E. et al., 1994. Motor neuron degeneration in mice that express a human Cu,Zn superoxide dismutase mutation. *Science*, 264(5166), pp.1772–1775.

Gyllensten, L. & Malmfors, T., 1963. Myelinization of the optic nerve and its dependence on visual function--a quantitative investigation in mice. *Journal of embryology and experimental morphology*, 11(1), pp.255–266.

Hagemeyer, N. et al., 2017. Microglia contribute to normal myelinogenesis and to oligodendrocyte progenitor maintenance during adulthood. *Acta Neuropathologica*, 134(3), pp.441–458.

Hajihosseini, M., Tham, T.N. & Dubois-Dalcq, M., 1996. Origin of Oligodendrocytes within the Human Spinal Cord. *J Neurosci*, 16(24), pp.7981–7994.

Hakak, Y. et al., 2001. Genome-wide expression analysis reveals dysregulation of myelination-related genes in chronic schizophrenia. *Proceedings of the National Academy of Sciences*, 98(8), pp.4746–4751.

Halter, J.A. & Clark, J.W., Jr, 1991. A distributed-parameter model of the myelinated nerve fiber. *Journal of Theoretical Biology*, 148(3), pp.345–382.

Haroutunian, V. et al., 2014. Myelination, oligodendrocytes, and serious mental illness C. Matute & P. K. Stys, eds. *Glia*, 62(11), pp.1856–1877.

Harrison, R.G. et al., 1907. Observations of the living developing nerve fiber. *The Anatomical Record*, 1(5), pp.116–128.

Hartline, D.K. & Colman, D.R., 2007. Rapid Conduction and the Evolution of Giant Axons and Myelinated Fibers. *Current Biology*, 17(1), pp.R29–R35.

Hasel, P. et al., 2017. Neurons and neuronal activity control gene expression in astrocytes to regulate their development and metabolism. *Nature Communications*, 8(1), pp.1–18.

Haynes, R.L. et al., 2003. Nitrosative and Oxidative Injury to Premyelinating Oligodendrocytes in Periventricular Leukomalacia. *Journal of Neuropathology & Experimental Neurology*, 62(5), pp.441–450.

Highley, J.R. et al., 2014. Loss of nuclear TDP-43 in amyotrophic lateral sclerosis (ALS) causes altered expression of splicing machinery and widespread dysregulation of RNA splicing in motor neurones. *Neuropathology and Applied Neurobiology*, 40(6), pp.670–685.

Hildebrand, C. & Hahn, R., 1978. Relation between myelin sheath thickness and axon size in spinal cord white matter of some vertebrate species. *Journal of the Neurological Sciences*, 38(3), pp.421–434.

Hildebrand, C. et al., 1993. Myelinated nerve fibres in the CNS. *Progress in Neurobiology*, 40(3), pp.319–384.

Hill, R.A., Li, A.M. & Grutzendler, J., 2018. Lifelong cortical myelin plasticity and age-related degeneration in the live mammalian brain. *Nat Neurosci*, 21(5), pp.683–695.

Hines, J.H. et al., 2015. Neuronal activity biases axon selection for myelination in vivo. *Nat Neurosci*, 18(5), pp.683–689.

Hoch-Kraft, P., Trotter, J. & Gonsior, C., 2019. Missing in Action: Dysfunctional RNA Metabolism in Oligodendroglial Cells as a Contributor to Neurodegenerative Diseases? *Neurochemical Research*, 23(12), pp.1–14.

Hodge, R.D. et al., 2019. Conserved cell types with divergent features in human versus mouse cortex. *Nature*, 536, pp.171–8.

Hofman, M.A., 1985. Size and shape of the cerebral cortex in mammals. I. The cortical surface. *Brain, Behavior and Evolution*, 27(1), pp.28–40.

Huang, B. et al., 2015. Mutant huntingtin downregulates myelin regulatory factor-mediated myelin gene expression and affects mature oligodendrocytes. *Neuron*, 85(6), pp.1212–1226.

Huang, J.K. et al., 2011. Retinoid X receptor gamma signaling accelerates CNS remyelination. *Nature Neuroscience*, 14(1), pp.45–53.

Hubler, Z. et al., 2018. Accumulation of 8,9-unsaturated sterols drives oligodendrocyte formation and remyelination. *Nature*, 560(7718), pp.372–376.

Hughes, E.G. et al., 2018. Myelin remodeling through experience-dependent oligodendrogenesis in the adult somatosensory cortex. *Nature Neuroscience*, 21(5), pp.696–706.

Hughes, E.G. et al., 2013. Oligodendrocyte progenitors balance growth with self-repulsion to achieve homeostasis in the adult brain. *Nature Neuroscience*, 16(6), pp.668–676.

Ibrahim, M., Butt, A.M. & Berry, M., 1995. Relationship between myelin sheath diameter and internodal length in axons of the anterior medullary velum of the adult rat. *Journal of the Neurological Sciences*, 133(1-2), pp.119–127.

Iefremova, V. et al., 2017. An Organoid-Based Model of Cortical Development Identifies Non-Cell-Autonomous Defects in Wnt Signaling Contributing to Miller-Dieker Syndrome. *CellReports*, 19(1), pp.50–59.

Iguchi, Y. et al., Loss of TDP-43 causes age-dependent progressive motor neuron degeneration | Brain | Oxford Academic. *Brain*, (136), pp.1371–1382.

Inoue, K. et al., 2002. Congenital hypomyelinating neuropathy, central dysmyelination, and Waardenburg–Hirschsprung disease: Phenotypes linked by SOX10 mutation. *Annals of neurology*, 52(6), pp.836–842.

Insel, T.R., 2010. Rethinking schizophrenia. *Nature*, 468(7321), pp.187–193.

Ishibashi, T. et al., 2006. Astrocytes Promote Myelination in Response to Electrical Impulses. *Neuron*, 49(6), pp.823–832.

Ishii, A. et al., 2009. Human myelin proteome and comparative analysis with mouse myelin. *Proc Natl Acad Sci USA*, 106(34), pp.14605–14610.

Izrael, M. et al., 2007. Human oligodendrocytes derived from embryonic stem cells: Effect of noggin on phenotypic differentiation in vitro and on myelination in vivo. *Molecular and Cellular Neuroscience*, 34(3), pp.310–323.

Jarjour, A.A. et al., 2012. In vitro modeling of central nervous system myelination and remyelination. *Glia*, 60(1), pp.1–12.

Jäkel, S. et al., 2019. Altered human oligodendrocyte heterogeneity in multiple sclerosis. *Nature*, 566(7745), pp.543–547.

Jakovcevski, I. et al., 2009. Oligodendrocyte Development and the Onset of Myelination in the Human Fetal Brain. *Frontiers in Neuroanatomy*, 3, p.5.

Jankowska, E., 2013. Spinal Interneurons. In *Neuroscience in the 21st Century*. New York, NY: Springer, New York, NY, pp. 1063–1099.

Jenna M Gaesser, S.L.F.-M., 2016. Intracellular Signaling Pathway Regulation of Myelination and Remyelination in the CNS. *Exp Neurol*, 283(Pt B), pp.501–511.

Jensen, S.K. & Yong, V.W., 2016. Activity-Dependent and Experience-Driven Myelination Provide New Directions for the Management of Multiple Sclerosis. *Trends in Neurosciences*, 39(6), pp.356–365.

Johnstone, M. et al., 2019. Reversal of proliferation deficits caused by chromosome 16p13.11 microduplication through targeting NFκB signaling: an integrated study of patient-derived neuronal precursor cells, cerebral organoids and in vivo brain imaging. *Molecular Psychiatry*, 24(2), pp.294–311.

Jones, K.J. et al., 2001. The expanding phenotype of laminin α2 chain (merosin) abnormalities: case series and review. *Journal of Medical Genetics*, 38(10), pp.649–657.

Kabashi, E. et al., 2008. TARDBP mutations in individuals with sporadic and familial amyotrophic lateral sclerosis. *Nature Genetics*, 40(5), pp.572–574.

Kang, S.H. et al., 2013. Degeneration and impaired regeneration of gray matter oligodendrocytes in amyotrophic lateral sclerosis. *Nature Neuroscience*, 16(5), pp.571–579.

Kang, S.M. et al., 2007. Efficient Induction of Oligodendrocytes from Human Embryonic Stem Cells. *Stem Cells*, 25(2), pp.419–424.

Kelava, I. & Lancaster, M.A., 2016. Stem Cell Models of Human Brain Development. *Cell Stem Cell*, 18(6), pp.736–748.

Kerman, B.E. et al., 2015. In vitro myelin formation using embryonic stem cells. *Development*, 142(12), pp.2213–2225.

Kim, H. et al., 2019. Pluripotent Stem Cell-Derived Cerebral Organoids Reveal Human Oligodendrogenesis with Dorsal and Ventral Origins. *Stem Cell Reports*, 12(5), pp.890–905.

Kim, S.U., 1972. Formation of synapses and myelin sheaths in cultures of dissociated chick embryonic spinal cord. *Experimental Cell Research*, 73(2), pp.528–530.

Kim, Y.I. et al., 1984. Miniature end-plate potentials in rat skeletal muscle poisoned with botulinum toxin. *The Journal of Physiology*, 356(1), pp.587–599.

Koudelka, S. et al., 2016. Individual Neuronal Subtypes Exhibit Diversity in CNS Myelination Mediated by Synaptic Vesicle Release. *Current Biology*, 26(11), pp.1–10.

Krämer, E.M., Schardt, A. & Nave, K.-A., 2001. Membrane traffic in myelinating oligodendrocytes H. H. Althaus & G. Jeserich, eds. *Microscopy Research and Technique*, 52(6), pp.656–671.

Kraemer, B.C. et al., 2010. Loss of murine TDP-43 disrupts motor function and plays an essential role in embryogenesis. *Acta Neuropathologica*, 119(4), pp.409–419.

Krencik, R. et al., 2017. Systematic Three-Dimensional Coculture Rapidly Recapitulates Interactions between Human Neurons and Astrocytes. *Stem Cell Reports*, 9(6), pp.1745–1753.

Kukley, M., Capetillo-Zarate, E. & Dietrich, D., 2007. Vesicular glutamate release from axons in white matter. *Nature Neuroscience*, 10(3), pp.311–320.

Lagier-Tourenne, C., Polymenidou, M. & Cleveland, D.W., 2010. TDP-43 and FUS/TLS: emerging roles in RNA processing and neurodegeneration. *Human Molecular Genetics*, 19(R1), pp.R46–R64.

Lai, H.C., Seal, R.P. & Johnson, J.E., 2016. Making sense out of spinal cord somatosensory development. *Development*, 143(19), pp.3434–3448.

Lancaster, M.A. & Knoblich, J.A., 2014a. Generation of cerebral organoids from human pluripotent stem cells. *Nat. Protocols*, 9(10), pp.2329–2340.

Lancaster, M.A. & Knoblich, J.A., 2014b. Organogenesis in a dish: modeling development and disease using organoid technologies. *Science*, 345(6194), pp.1247125–1247125.

Lancaster, M.A. et al., 2013. Cerebral organoids model human brain development and microcephaly. *Nature*, 501(7467), pp.373–379.

Lappe-Siefke, C. et al., 2003. Disruption of Cnp1 uncouples oligodendroglial functions in axonal support and myelination. *Nature Genetics*, 33(3), pp.366–374.

Lariosa-Willingham, K.D. et al., 2016. A high throughput drug screening assay to identify compounds that promote oligodendrocyte differentiation using acutely dissociated and purified oligodendrocyte precursor cells. *BMC Research Notes*, 9(1), p.419.

Lee, S.-K. et al., 2005. Olig2 and Ngn2 function in opposition to modulate gene expression in motor neuron progenitor cells. *Genes & Development*, 19(2), pp.282–294.

Lee, Y., Morrison, B.M., Li, Y., Lengacher, S., Farah, M.H., Hoffman, P.N., Liu, Y., Tsingalia, A., Jin, L., Zhang, P.-W., Pellerin, L., Magistretti, P.J. & Rothstein, J.D., 2012a. Oligodendroglia metabolically support axons and contribute to neurodegeneration. *Nature*, 487(7408), pp.443–448.

Lee, S. et al., 2012. A culture system to study oligodendrocyte myelination processes using engineered nanofibers. *Nature Methods*, 9(9), pp.917–922.

Leegwater, P.A.J. et al., 2001. Subunits of the translation initiation factor eIF2B are mutant in leukoencephalopathy with vanishing white matter. *Nature Genetics*, 29(4), pp.383–388.

Leong, S.Y. et al., 2014. Heterogeneity of oligodendrocyte progenitor cells in adult human brain. *Ann Clin Transl Neurol*, 1(4), pp.272–283.

Li, Q. et al., 2010. Electrical stimulation of the medullary pyramid promotes proliferation and differentiation of oligodendrocyte progenitor cells in the corticospinal tract of the adult rat. *Neuroscience Letters*, 479(2), pp.128–133.

Liu, J. et al., 2016. Epigenetic control of oligodendrocyte development: adding new players to old keepers. *Current Opinion in Neurobiology*, 39, pp.133–138.

Liu, J. et al., 2012. Impaired adult myelination in the prefrontal cortex of socially isolated mice. *Nature Neuroscience*, 15(12), pp.1621–1623.

Livesey, M.R., Magnani, D., Cleary, E.M., Vasistha, N.A., James, O.T., Selvaraj, B.T., Burr, K., Story, D., Shaw, C.E., Kind, P.C., Hardingham, G.E., Wyllie, D.J.A. & Chandran, S., 2016b. Maturation and electrophysiological properties of human pluripotent stem cell-derived oligodendrocytes. *Stem Cells*, 34(4), pp.1040–1053.

Lock, C. et al., 2002. Gene-microarray analysis of multiple sclerosis lesions yields new targets validated in autoimmune encephalomyelitis. *Nat Med*, 8(5), pp.500–508.

Longair, M.H., Baker, D.A. & Armstrong, J.D., 2011. Simple Neurite Tracer: open source software for reconstruction, visualization and analysis of neuronal processes | Bioinformatics | Oxford Academic. *Bioinformatics*, 27(17), pp.2453–2454.

Lu, P.H. et al., 2013. Myelin breakdown mediates age-related slowing in cognitive processing speed in healthy elderly men. *Brain and Cognition*, 81(1), pp.131–138.

Lubetzki, C. et al., 1993. Even in culture, oligodendrocytes myelinate solely axons. *Proc Natl Acad Sci USA*, 90(14), pp.6820–6824.

Lucchinetti, C. et al., 2000. Heterogeneity of multiple sclerosis lesions: implications for the pathogenesis of demyelination. *Annals of neurology*, 47(6), pp.707–717.

Lundgaard, I. et al., 2013. Neuregulin and BDNF Induce a Switch to NMDA Receptor-Dependent Myelination by Oligodendrocytes B. A. Barres, ed. *PLOS Biology*, 11(12), p.e1001743.

Mack, C.M. et al., 1995. Sex differences in the distribution of axon types within the genu of the rat corpus callosum. *Brain Research*, 697(1-2), pp.152–156.

Mackenzie, I.R., Rademakers, R. & Neumann, M., 2010. TDP-43 and FUS in amyotrophic lateral sclerosis and frontotemporal dementia. *Lancet Neurology*, 9(10), pp.995–1007.

Madhavan, M., Nevin, Z.S., Shick, H.E., Garrison, E., Clarkson-Paredes, C., Karl, M., Clayton, B.L.L., Factor, D.C., Allan, K.C., Barbar, L., Jain, T., Douvaras, P., Fossati, V., Miller, R.H. & Tesar, P.J., 2018b. Induction of myelinating oligodendrocytes in human cortical spheroids. *Nature Methods*, 15(9), pp.700–706.

Maheras, K.J. et al., 2018. Absence of Claudin 11 in CNS Myelin Perturbs Behavior and Neurotransmitter Levels in Mice. *Sci Rep*, 8(1), pp.1–16.

Makinodan, M. et al., 2012. A critical period for social experience-dependent oligodendrocyte maturation and myelination. *Science*, 337(6100), pp.1357–1360.

Maluenda, J. et al., 2016. Mutations in GLDN , Encoding Gliomedin, a Critical Component of the Nodes of Ranvier, Are Responsible for Lethal Arthrogryposis. *The American Journal of Human Genetics*, 99(4), pp.928–933.

Marques, S. et al., 2016. Oligodendrocyte heterogeneity in the mouse juvenile and adult central nervous system. *Science*, 352(6291), pp.1326–1329.

Martin, G.R., 1981. Isolation of a pluripotent cell line from early mouse embryos cultured in medium conditioned by teratocarcinoma stem cells. *Proc Natl Acad Sci USA*, 78(12), pp.7634–7638.

Martin, M. et al., 2006. Myelin deficiencies visualized in vivo: Visually evoked potentials and T2-weighted magnetic resonance images of shiverer mutant and wild-type mice. *J Neurosci Res*, 84(8), pp.1716–1726.

Marton, R.M. et al., 2019. Differentiation and maturation of oligodendrocytes in human three-dimensional neural cultures. *Nature Neuroscience*, 22(3), pp.484–491.

Matthieu, J.M. et al., 1978. Myelination in rat brain aggregating cell cultures. *Neuroscience*, 3(6), pp.565–572.

Mayoral, S.R. et al., 2018. Initiation of CNS Myelination in the Optic Nerve Is Dependent on Axon Calibre. *CellReports*, 25(3), pp.544–550.

McCarthy, K.D. & de Vellis, J., 1980. Preparation of separate astroglial and oligodendroglial cell cultures from rat cerebral tissue. *The Journal of Cell Biology*, 85(3), pp.890–902.

McGraw, C.M., Ward, C.S. & Samaco, R.C., 2017. Genetic rodent models of brain disorders: Perspectives on experimental approaches and therapeutic strategies G. S. Fisch, ed. *American Journal of Medical Genetics Part C: Seminars in Medical Genetics*, 175(3), pp.368–379.

McKenzie, I.A. et al., 2014. Motor skill learning requires active central myelination. *Science*, 346(6207), pp.318–322.

McNeish, J. et al., 2015. From Dish to Bedside: Lessons Learned While Translating Findings from a Stem Cell Model of Disease to a Clinical Trial. *Cell Stem Cell*, 17(1), pp.8–10.

Mei, F. et al., 2016. Identification of the Kappa-Opioid Receptor as a Therapeutic Target for Oligodendrocyte Remyelination. *J Neurosci*, 36(30), pp.7925–7935.

Mei, F. et al., 2014. Micropillar arrays as a high-throughput screening platform for therapeutics in multiple sclerosis. *Nat Med*, 20(8), pp.954–960.

Meireles, A.M. et al., 2018. The Lysosomal Transcription Factor TFEB Represses Myelination Downstream of the Rag-Ragulator Complex. *Developmental cell*, 47(3), pp.319–330.

Menichella, D.M. et al., 2003. Connexins Are Critical for Normal Myelination in the CNS. *J Neurosci*, 23(13), pp.5963–5973.

Mensch, S. et al., 2015. Synaptic vesicle release regulates myelin sheath number of individual oligodendrocytes in vivo. *Nat Neurosci*, 18(5), pp.628–630.

Meyer, N. et al., 2018. Oligodendrocytes in the Mouse Corpus Callosum Maintain Axonal Function by Delivery of Glucose. *CellReports*, 22(9), pp.2383–2394.

Mi, S. et al., 2005. LINGO-1 negatively regulates myelination by oligodendrocytes. *Nat Neurosci*, 8(6), pp.745–751.

Michailov, G.V. et al., 2004. Axonal Neuregulin-1 Regulates Myelin Sheath Thickness. *Science*, 304(5671), pp.700–703.

Mikael Simons, K.-A.N., 2016. Oligodendrocytes: Myelination and Axonal Support. *Cold Spring Harb Perspect Biol*, 8(1), p.a020479.

Miller, D.J. et al., 2012. Prolonged myelination in human neocortical evolution. *Proc Natl Acad Sci USA*, 109(41), pp.16480–16485.

Miron, V.E. et al., 2013. M2 microglia and macrophages drive oligodendrocyte differentiation during CNS remyelination. *Nat Neurosci*, 16(9), pp.1211–1218.

Mitew, S. et al., 2018. Pharmacogenetic stimulation of neuronal activity increases myelination in an axon-specific manner. *Nature Communications*, 9(1), p.306.

Molina-Gonzalez, I. & Miron, V.E., 2019. Astrocytes in myelination and remyelination. *Neuroscience Letters*, 713, p.134532.

Morell, P. & Quarles, R.H., 1999. Characteristic Composition of Myelin. In *Basic Neurochemistry: Molecular, Cellular and Medical Aspects. 6th edition*. Lippincott-Raven.

Moscona, A., 1957. The development in vitro of chimeric aggregates of dissociated embryonic chick and mouse cells. *Proc Natl Acad Sci USA*, 43(1), pp.184–194.

Moscona, A. & MOSCONA, H., 1952. The dissociation and aggregation of cells from organ rudiments of the early chick embryo. *Journal of Anatomy*, 86(3), pp.287–301.

Mota, B. & Herculano-Houzel, S., 2014. All brains are made of this: a fundamental building block of brain matter with matching neuronal and glial masses. *Frontiers in Neuroanatomy*, 8(4), p.532.

Mota, B. et al., 2019. White matter volume and white/gray matter ratio in mammalian species as a consequence of the universal scaling of cortical folding. *Proc Natl Acad Sci USA*, 116(30), pp.15253–15261.

Mozafari, S. et al., 2015. Skin-derived neural precursors competitively generate functional myelin in adult demyelinated mice. *The Journal of Clinical Investigation*, 125(9), pp.3642–3656.

Murtie, J.C., Macklin, W.B. & Corfas, G., 2007. Morphometric analysis of oligodendrocytes in the adult mouse frontal cortex. *J Neurosci Res*, 85(10), pp.Nasrabady, S.E. et al., 2018. White matter changes in Alzheimer's disease: a focus on myelin and oligodendrocytes. *Acta Neuropathologica Communications*, 6(1), pp.1–10.

Najm, F.J. et al., 2015. Drug-based modulation of endogenous stem cells promotes functional remyelination in vivo. *Nature*, 522(7555), pp.216–220.

Nasrabady, S.E. et al., 2018. White matter changes in Alzheimer's disease: a focus on myelin and oligodendrocytes. *Acta Neuropathologica Communications*, 6(1), pp.1–10.

Nave, K.-A. & Ehrenreich, H., 2014. Myelination and Oligodendrocyte Functions in Psychiatric Diseases. *JAMA Psychiatry*, 71(5), pp.582–584.

Nave, K.-A., Sereda, M.W. & Ehrenreich, H., 2007. Mechanisms of Disease: inherited demyelinating neuropathies—from basic to clinical research. *Nature Clinical Practice Neurology*, 3(8), pp.453–464.

Nawaz, S., Sánchez, P., Schmitt, S., Snaidero, N., Mitkovski, M., Velte, C., Brückner, B.R., Alexopoulos, I., Czopka, T., Jung, S.Y., Rhee, J.S., Janshoff, A., Witke, W., Schaap, I.A.T., Lyons, D.A. & Simons, M., 2015a. Actin Filament Turnover Drives Leading Edge Growth during Myelin Sheath Formation in the Central Nervous System. *Developmental cell*, 34(2), pp.139–151.

Nawaz, S., Sánchez, P., Schmitt, S., Snaidero, N., Mitkovski, M., Velte, C., Brückner, B.R., Alexopoulos, I., Czopka, T., Jung, S.Y., Rhee, J.S., Janshoff, A., Witke, W., Schaap, I.A.T., Lyons, D.A. & Simons, M., 2015b. Actin Filament Turnover Drives Leading Edge Growth during Myelin Sheath Formation in the Central Nervous System. *Developmental cell*, 34(2), pp.139–151.

Neumann, M. et al., 2006. Ubiquitinated TDP-43 in Frontotemporal Lobar Degeneration and Amyotrophic Lateral Sclerosis. *Science*, 314(5796), pp.130–133.

Nevin, Z.S. et al., 2017. Modeling the Mutational and Phenotypic Landscapes of Pelizaeus-Merzbacher Disease with Human iPSC-Derived Oligodendrocytes. *American Journal of Human Genetics*, 100(4), pp.617–634.

Nicholson, M. et al., 2018. BDNF haploinsufficiency exerts a transient and regionally different influence upon oligodendroglial lineage cells during postnatal development. *Molecular and Cellular Neuroscience*, 90, pp.12–21.

Niu, J. et al., 2012. Phosphorylated olig1 localizes to the cytosol of oligodendrocytes and promotes membrane expansion and maturation. *Glia*, 60(9), pp.1427–1436.

Nonneman, A., Robberecht, W. & Bosch, Den, L.V., 2014. The role of oligodendroglial dysfunction in amyotrophic lateral sclerosis. *Neurodegenerative Disease Management*, 4(3), pp.223–239.

Noseworthy, J.H. et al., 2000. Multiple sclerosis. *The New England journal of medicine*, 343(13), pp.938–952.

Oberheim, N.A. et al., 2009. Uniquely Hominid Features of Adult Human Astrocytes. *J Neurosci*, 29(10), pp.3276–3287.

Ogawa, S.-I. et al., 2011. Induction of oligodendrocyte differentiation from adult human fibroblast-derived induced pluripotent stem cells. *In Vitro Cellular & Developmental Biology - Animal*, 47(7), pp.464–469.

Ortiz, F.C. et al., 2019. Neuronal activity in vivo enhances functional myelin repair. *JCI Insight*, 4(9), p.149.

Osanai, Y. et al., 2016. Rabies virus-mediated oligodendrocyte labeling reveals a single oligodendrocyte myelinates axons from distinct brain regions. *Glia*, 65(1), pp.93–105.

Osipovitch, M. et al., 2018. Human ESC-Derived Chimeric Mouse Models of Huntington's Disease Reveal Cell-Intrinsic Defects in Glial Progenitor Cell Differentiation. *Cell Stem Cell*, 24(1), pp.107–122.

Ouyang, M. et al., 2017. Short-range connections in the developmental connectome during typical and atypical brain maturation. *Neuroscience and biobehavioral reviews*, 83, pp.109–122.

O'Leary, T., van Rossum, M.C.W. & Wyllie, D.J.A., 2010. Homeostasis of intrinsic excitability in hippocampal neurones: dynamics and mechanism of the response to chronic depolarization. *The Journal of Physiology*, 588(1), pp.157–170.

Pajevic, S., Basser, P.J. & Fields, R.D., 2014. Role of Myelin Plasticity in Oscillations and Synchrony of Neuronal Activity. *Neuroscience*, 276, pp.135–147.

Pan, B. et al., 2005. Myelin-associated glycoprotein and complementary axonal ligands, gangliosides, mediate axon stability in the CNS and PNS: Neuropathology and behavioral deficits in single- and double-null mice. *Exp Neurol*, 195(1), pp.208–217.

Paşca, A.M. et al., 2015. Functional cortical neurons and astrocytes from human pluripotent stem cells in 3D culture. *Nat Meth*, 12(7), pp.671–678.

Patrikios, P. et al., 2006. Remyelination is extensive in a subset of multiple sclerosis patients. *Brain*, 129(Pt 12), pp.3165–3172.

Pérez-Cerdá, F., Sanchez-Gomez, M.V. & Matute, C., 2015. Pío del Río Hortega and the discovery of the oligodendrocytes. *Frontiers in Neuroanatomy*, 9, p.92.

Pfaff, S.L. et al., 1996. Requirement for LIM Homeobox Gene Isl1 in Motor Neuron Generation Reveals a Motor Neuron– Dependent Step in Interneuron Differentiation. *Cell*, 84(2), pp.309–320.

Philips, T. et al., 2013. Oligodendrocyte dysfunction in the pathogenesis of amyotrophic lateral sclerosis. *Brain*, 136(Pt 2), pp.471–482.

Pillai, A.M. et al., 2009. Spatiotemporal Ablation of Myelinating Glia-Specific Neurofascin (NfascNF155) in Mice Reveals Gradual Loss of Paranodal Axoglial Junctions and Concomitant Disorganization of Axonal Domains. *J Neurosci Res*, 87(8), pp.1773–1793.

Powers, J.M., 2004. The Leukodystrophies. In *Myelin Biology and Disorders*. Elsevier, pp. 663–690.

Prineas, J.W. & Connell, F., 1979. Remyelination in multiple sclerosis. *Annals of neurology*, 5(1), pp.22–31.

Pulliam, L., Berens, M.E. & Rosenblum, M.L., 1988. A normal human brain cell aggregate model for neurobiological studies. *J Neurosci Res*, 21(2-4), pp.521–530.

Qian, X. et al., 2016. Brain-Region-Specific Organoids Using Mini-bioreactors for Modeling ZIKV Exposure. *Cell*, 165(5), pp.1238–1254.

Qiu, J. et al., 2016. Evidence for evolutionary divergence of activity-dependent gene expression in developing neurons. *eLife*, 5, p.e20337.

Quan Wen, D.B.C., 2005. Segregation of the Brain into Gray and White Matter: A Design Minimizing Conduction Delays. *PLoS computational biology*, 1(7), p.e78.

Rasband, M.N. et al., 1999. Dependence of Nodal Sodium Channel Clustering on Paranodal Axoglial Contact in the Developing CNS. *J Neurosci*, 19(17), pp.7516–7528.

Rasband, M.N. & Peles, E., 2015. The Nodes of Ranvier: Molecular Assembly and Maintenance. *Cold Spring Harb Perspect Biol*, 8(3), p.a020495.

Ratti, A. & Buratti, E., 2016. Physiological functions and pathobiology of TDP-43 and FUS/TLS proteins. *Journal of neurochemistry*, 138 Suppl 1(Pt B), pp.95–111.

Ravanelli, A.M. et al., 2018. Sequential specification of oligodendrocyte lineage cells by distinct levels of Hedgehog and Notch signaling. *Developmental Biology*, 444(2), pp.93–106.

Redmond, S.A. et al., 2016. Somatodendritic Expression of JAM2 Inhibits Oligodendrocyte Myelination. *Neuron*, 91(4), pp.824–836.

Remahl, S. & Hildebrand, C., 1990. Relations between axons and oligodendroglial cells during initial myelination. II. The individual axon. *Journal of neurocytology*, 19(6), pp.883–898.

Rivers, L.E. et al., 2008. PDGFRA/NG2 glia generate myelinating oligodendrocytes and piriform projection neurons in adult mice. *Nature Neuroscience*, 11(12), pp.1392–1401.

Roche, S.L. et al., 2014. Loss of Glial Neurofascin155 Delays Developmental Synapse Elimination at the Neuromuscular Junction. *The Journal of Neuroscience*, 34(38), pp.12904–12918.

Rohan, Z. et al., 2014. Oligodendroglial response in the spinal cord in TDP-43 proteinopathy with motor neuron involvement. *Neurodegenerative Diseases*, 14(3), pp.117–124.

Rosenberg, S.S. et al., 2008. The geometric and spatial constraints of the microenvironment induce oligodendrocyte differentiation. *Proc Natl Acad Sci USA*, 105(38), pp.14662–14667.

Rossant, J., 2011. The Impact of Developmental Biology on Pluripotent Stem Cell Research: Successes and Challenges. *Developmental cell*, 21(1), pp.20–23.

Roussos, P. & Haroutunian, V., 2014. Schizophrenia: susceptibility genes and oligodendroglial and myelin related abnormalities. *Frontiers in Cellular Neuroscience*, 8, p.5.

Rowitch, D.H., 2004. Glial specification in the vertebrate neural tube. *Nat Rev Neurosci*, 5(5), pp.409–419.

Ruckh, J.M. et al., 2012. Rejuvenation of regeneration in the aging central nervous system. *Cell Stem Cell*, 10(1), pp.96–103.

Rushton, W.A.H., 1951. A theory of the effects of fibre size in medullated nerve. *The Journal of Physiology*, 115(1), pp.101–122.

S L Eaton, T.M.W., 2017. Bridging the gap: large animal models in neurodegenerative research. *Mammalian Genome*, 28(7), pp.324–337.

S, X. et al., 2017. Loss-of-Function Mutations in LGI4, a Secreted Ligand Involved in Schwann Cell Myelination, Are Responsible for Arthrogryposis Multiplex Congenita. *American Journal of Human Genetics*, 100(4), pp.659–665.

Saab, A.S. et al., 2016. Oligodendroglial NMDA Receptors Regulate Glucose Import and Axonal Energy Metabolism. *Neuron*, 91(1), pp.119–132.

Saab, A.S., Tzvetanova, I.D. & Nave, K.-A., 2013. ScienceDirect The role of myelin and oligodendrocytes in axonal energy metabolism. *Current Opinion in Neurobiology*, 23(6), pp.1065–1072.

Salami, M. et al., 2003. Change of conduction velocity by regional myelination yields constant latency irrespective of distance between thalamus and cortex. *Proc Natl Acad Sci USA*, 100(10), pp.6174–6179.

Saliani, A. et al., 2017. Axon and Myelin Morphology in Animal and Human Spinal Cord. *Frontiers in Neuroanatomy*, 11, p.977.

Salzer, J.L. & Zalc, B., 2016. Myelination. *Current Biology*, 26(20), pp.R971–R975.

Salzer, J.L., 2003. Polarized Domains of Myelinated Axons. *Neuron*, 40(2), pp.297–318.

Sampaio-Baptista, C. et al., 2013. Motor Skill Learning Induces Changes in White Matter Microstructure and Myelination. *J Neurosci*, 33(50), pp.19499–19503.

Schiffmann, R. & van der Knaap, M.S., 2009. Invited Article: An MRI-based approach to the diagnosis of white matter disorders. *Neurology*, 72(8), pp.750–759.

Schlegel, A.A., Rudelson, J.J. & Tse, P.U., 2012. White Matter Structure Changes as Adults Learn a Second Language. *Journal of Cognitive Neuroscience*, 24(8), pp.1664–1670.

Schmahmann, J.D. et al., 2008. Cerebral White Matter. *Annals of the New York Academy of Sciences*, 1142(1), pp.266–309.

Schoenemann, P.T., Sheehan, M.J. & Glotzer, L.D., 2005. Prefrontal white matter volume is disproportionately larger in humans than in other primates. *Nat Neurosci*, 8(2), pp.242–252.

Scholz, J. et al., 2009. Training induces changes in white-matter architecture. *Nature Neuroscience*, 12(11), pp.1370–1371.

Seeds, N.W. & Vatter, A.E., 1971. Synaptogenesis in Reaggregating Brain Cell Culture. *Proc Natl Acad Sci USA*, 68(12), pp.3219–3222.

Sehmbi, M. et al., 2019. Age-related deficits in intracortical myelination in young adults with bipolar disorder type I. *Journal of Psychiatry & Neuroscience : JPN*, 44(2), pp.79–88.

Seidl, A.H. & Rubel, E.W., 2015. Systematic and differential myelination of axon collaterals in the mammalian auditory brainstem. *Glia*, 64(4), pp.487–494.

Seil, F. & Blank, N.K., 1981. Myelination of central nervous system axons in tissue culture by transplanted oligodendrocytes. *Science*, 212(4501), pp.1407–1408.

Selvaraj, B.T. et al., 2018. C9ORF72 repeat expansion causes vulnerability of motor neurons to Ca 2+ -permeable AMPA receptor-mediated excitotoxicity. *Nature Communications*, 9(1), p.347.

Sherman, D.L. & Brophy, P.J., 2005. Mechanisms of axon ensheathment and myelin growth. *Nat Rev Neurosci*, 6(9), pp.683–690.

Sherman, D.L. et al., 2005. Neurofascins Are Required to Establish Axonal Domains for Saltatory Conduction. *Neuron*, 48(5), pp.737–742.

Sierra, A. et al., 2010. Microglia shape adult hippocampal neurogenesis through apoptosis-coupled phagocytosis. *Cell Stem Cell*, 7(4), pp.483–495.

Silva, M.C. & Haggarty, S.J., 2019. Human pluripotent stem cell–derived models and drug screening in CNS precision medicine. *Annals of the New York Academy of Sciences*, 151, p.291.

Sim, F.J., Windrem, M.S. & Goldman, S.A., 2009. Fate determination of adult human glial progenitor cells. *Neuron Glia Biol*, 5(3-4), pp.45–55.

Simons, M. & Nave, K.-A., 2015. Oligodendrocytes: Myelination and Axonal Support. *Cold Spring Harb Perspect Biol*, 8(1), p.a020479.

Simons, M. et al., 2000. Assembly of Myelin by Association of Proteolipid Protein with Cholesterol- and Galactosylceramide-Rich Membrane Domains. *The Journal of Cell Biology*, 151(1), pp.143–154.

Smaers, J.B. et al., 2010. Frontal White Matter Volume Is Associated with Brain Enlargement and Higher Structural Connectivity in Anthropoid Primates A. Iwaniuk, ed. *PLoS ONE*, 5(2), p.e9123.

Smigiel, R. et al., 2018. Homozygous mutation in the Neurofascin gene affecting the glial isoform of Neurofascin causes severe neurodevelopment disorder with hypotonia, amimia and areflexia. *Human Molecular Genetics*, 27(21), pp.3669–3674.

Smith, K.J., Blakemore, W.F. & McDonald, W.I., 1979. Central remyelination restores secure conduction. *Nature*, 280(5721), pp.395–396.

Snaidero, N. & Simons, M., 2017. The logistics of myelin biogenesis in the central nervous system. *Glia*, 6, p.6122.

Snaidero, N. et al., 2014. Myelin Membrane Wrapping of CNS Axons by PI(3,4,5)P3-Dependent Polarized Growth at the Inner Tongue. *Cell*, 156(1-2), pp.277–290.

Söllner, T. et al., 1993. SNAP receptors implicated in vesicle targeting and fusion. *Nature*, 362(6418), pp.318–324.

Spalding, K.L. et al., 2005. Retrospective Birth Dating of Cells in Humans. *Cell*, 122(1), pp.133–143.

Squarzoni, P. et al., 2014. Microglia modulate wiring of the embryonic forebrain. *Cell Reports*, 8(5), pp.1271–1279.

Sreedharan, J. et al., 2008. TDP-43 Mutations in Familial and Sporadic Amyotrophic Lateral Sclerosis. *Science*, 319(5870), pp.1668–1672.

Stacpoole, S.R.L. et al., 2013. High Yields of Oligodendrocyte Lineage Cells from Human Embryonic Stem Cells at Physiological Oxygen Tensions for Evaluation of Translational Biology. *Stem Cell Reports*, 1(5), pp.437–450.

Stedehouder, J. & Kushner, S.A., 2016. Myelination of parvalbumin interneurons: a parsimonious locus of pathophysiological convergence in schizophrenia. *Molecular Psychiatry*, 22(1), pp.4–12.

Stedehouder, J. et al., 2018. Activity-dependent myelination of parvalbumin interneurons mediated by axonal morphological plasticity. *J Neurosci*, 38(15), pp.0074–18–3642.

Stefansson, H. et al., 2002. Neuregulin 1 and Susceptibility to Schizophrenia. *The American Journal of Human Genetics*, 71(4), pp.877–892.

Stevens, B. et al., 2002. Adenosine: a neuron-glial transmitter promoting myelination in the CNS in response to action potentials. *Neuron*, 36(5), pp.855–868.

Suminaite, D., Lyons, D.A. & Livesey, M.R., 2019. Myelinated axon physiology and regulation of neural circuit function. *Glia*, 67(11), pp.2050–2062.

Sun, L.O. et al., 2018. Spatiotemporal Control of CNS Myelination by Oligodendrocyte Programmed Cell Death through the TFEB-PUMA Axis. *Cell*, 175(7), pp.1811–1826.e21.

Susuki, K. et al., 2013. Three Mechanisms Assemble Central Nervous System Nodes of Ranvier. *Neuron*, 78(3), pp.469–482.

Svennerholm, L., Vanier, M.T. & Månsson, J.E., 1980. Krabbe disease: a galactosylsphingosine (psychosine) lipidosis. *Journal of Lipid Research*, 21(1), pp.53–64.

Svenningsen, Å.F. et al., 2003. Rapid method for culturing embryonic neuron–glial cell cocultures. *J Neurosci Res*, 72(5), pp.565–573.

Swire, M. et al., 2019. Endothelin signalling mediates experience-dependent myelination in the CNS. *eLife*, 8, p.4443.

Szuchet, S., Polak, P.E. & Yim, S.H., 1987. Mature Oligodendrocytes Cultured in the Absence of Neurons Recapitulate the Ontogenic Development of Myelin Membranes. *Developmental Neuroscience*, 8(4), pp.208–221.

Takahashi, K. & Yamanaka, S., 2006. Induction of Pluripotent Stem Cells from Mouse Embryonic and Adult Fibroblast Cultures by Defined Factors. *Cell*, 126(4), pp.663–676.

Takahashi, K. et al., 2007. Induction of Pluripotent Stem Cells from Adult Human Fibroblasts by Defined Factors. *Cell*, 131(5), pp.861–872.

Taveggia, C. et al., 2005. Neuregulin-1 Type III Determines the Ensheathment Fate of Axons. *Neuron*, 47(5), pp.681–694.

Thaler, J.P. et al., 2002. LIM factor Lhx3 contributes to the specification of motor neuron and interneuron identity through cell-type-specific protein-protein interactions. *Cell*, 110(2), pp.237–249.

Thomas Philips, J.D.R., 2017. Oligodendroglia: metabolic supporters of neurons. *The Journal of Clinical Investigation*, 127(9), pp.3271–3280.

Tomassy, G.S. et al., 2014. Distinct profiles of myelin distribution along single axons of pyramidal neurons in the neocortex. *Science*, 344(6181), pp.319–324.

Trapp, B.D. et al., 1979. Morphological differentiation of mechanically dissociated fetal rat brain in aggregating cell cultures. *Brain Research*, 160(1), pp.117–130.

Tyler, W.J. & Pozzo-Miller, L.D., 2001. BDNF Enhances Quantal Neurotransmitter Release and Increases the Number of Docked Vesicles at the Active Zones of Hippocampal Excitatory Synapses. *J Neurosci*, 21(12), pp.4249–4258.

Ueno, M. et al., 2013. Layer V cortical neurons require microglial support for survival during postnatal development. *Nature Neuroscience*, 16(5), pp.543–551.

Vallat, J.-M. et al., 2016. Contactin-Associated Protein 1 (CNTNAP1) Mutations Induce Characteristic Lesions of the Paranodal Region. *Journal of Neuropathology & Experimental Neurology*, 75(12), pp.1155–1159.

Van Den Bosch, L. et al., 2006. The role of excitotoxicity in the pathogenesis of amyotrophic lateral sclerosis. *Biochimica et Biophysica Acta (BBA) - Molecular Basis of Disease*, 1762(11-12), pp.1068–1082.

van der Worp, H.B. et al., 2010. Can Animal Models of Disease Reliably Inform Human Studies? *PLOS Medicine*, 7(3), p.e1000245.

Vanden Broeck, L., Callaerts, P. & Dermaut, B., 2014. TDP-43-mediated neurodegeneration: towards a loss-of-function hypothesis? *Trends in Molecular Medicine*, 20(2), pp.66–71.

Vasile, F., Dossi, E. & Rouach, N., 2017. Human astrocytes: structure and functions in the healthy brain. *Brain Structure and Function*, 222(5), pp.2017–2029.

Vasistha, N.A. et al., 2019. Familial t(1;11) translocation is associated with disruption of white matter structural integrity and oligodendrocyte-myelin dysfunction. *Molecular Psychiatry*, 511(4), p.421.

Velasco, S. et al., 2019. Individual brain organoids reproducibly form cell diversity of the human cerebral cortex. *Nature*, 570(7762), pp.523–527.

Venkatesh, H.S. et al., 2019. Electrical and synaptic integration of glioma into neural circuits. *Nature*, 573(7775), pp.539–545.

Visser, E.M. et al., 2012. A new prevalence study of multiple sclerosis in Orkney, Shetland and Aberdeen city. *J Neurol Neurosurg Psychiatry*, 83(7), pp.719–724.

Vondran, M.W. et al., 2010. BDNF+/– mice exhibit deficits in oligodendrocyte lineage cells of the basal forebrain. *Glia*, 58(7), pp.848–856.

Voyvodic, J.T., 1989. Target size regulates calibre and myelination of sympathetic axons. *Nature*, 342(6248), pp.430–433.

Wainger, B.J. et al., 2014. Intrinsic Membrane Hyperexcitability of Amyotrophic Lateral Sclerosis Patient-Derived Motor Neurons. *CellReports*, 7(1), pp.1–11.

Wake, H. et al., 2015. Nonsynaptic junctions on myelinating glia promote preferential myelination of electrically active axons. *Nature Communications*, 6, p.7844.

Wake, H., Lee, P.R. & Fields, R.D., 2011. Control of Local Protein Synthesis and Initial Events in Myelination by Action Potentials. *Science*, 333(6049), pp.1647–1651.

Walhovd, K.B. et al., 2005. Effects of age on volumes of cortex, white matter and subcortical structures. *Neurobiology of Aging*, 26(9), pp.1261–1270.

Walhovd, K.B., Johansen-Berg, H. & Káradóttir, R.T., 2014. Unraveling the secrets of white matter – Bridging the gap between cellular, animal and human imaging studies. *Neuroscience*, 276, pp.2–13.

Wang, F. et al., 2018. Enhancing Oligodendrocyte Myelination Rescues Synaptic Loss and Improves Functional Recovery after Chronic Hypoxia. *Neuron*, 99(4), pp.689–701.

Wang, H. et al., 2008. Myosin II has distinct functions in PNS and CNS myelin sheath formation. *The Journal of Cell Biology*, 182(6), pp.1171–1184.

Wang, Jia et al., 2018. Cell-autonomous requirement of TDP-43, an ALS/FTD signature protein, for oligodendrocyte survival and myelination. *Proc Natl Acad Sci USA*, 115(46), pp.E10941–E10950.

Wang, Jing et al., 2014. Transcription factor induction of human oligodendrocyte progenitor fate and differentiation. *Proceedings of the National Academy of Sciences of the United States of America*, 111(28), pp.E2885–E2894.

Wang, Su et al., 2013. Human iPSC-Derived Oligodendrocyte Progenitor Cells Can Myelinate and Rescue a Mouse Model of Congenital Hypomyelination. *Cell Stem Cell*, 12(2), pp.252–264.

Waxman, S.G. & Sims, T.J., 1984. Specificity in central myelination: evidence for local regulation of myelin thickness. *Brain Research*, 292(1), pp.179–185.

Weber, B. et al., 2019. Learning Unicycling Evokes Manifold Changes in Gray and White Matter Networks Related to Motor and Cognitive Functions. *Sci Rep*, 9(1), pp.1–11.

Weidenheim, K.M. et al., 1993. Neuroanatomical localization of myelin basic protein in the late first and early second trimester human foetal spinal cord and brainstem. *Journal of neurocytology*, 22(7), pp.507–516.

Weidenheim, K.M. et al., 1996. Temporal and Spatial Expression of Major Myelin Proteins in the Human Fetal Spinal Cord during the Second Trimester. *Journal of Neuropathology & Experimental Neurology*, 55(6), pp.734–745.

Welliver, R.R. et al., 2018. Muscarinic Receptor M3R Signaling Prevents Efficient Remyelination by Human and Mouse Oligodendrocyte Progenitor Cells. *J Neurosci*, 38(31), pp.6921–6932.

Westlye, L.T. et al., 2010. Life-Span Changes of the Human Brain White Matter: Diffusion Tensor Imaging (DTI) and Volumetry. *Cerebral Cortex*, 20(9), pp.2055–2068.

White, R. et al., 2008. Activation of oligodendroglial Fyn kinase enhances translation of mRNAs transported in hnRNP A2–dependent RNA granules. *The Journal of Cell Biology*, 181(4), pp.579–586.

Wiggins, R.C. et al., 1988. Development of axonal-oligodendroglial relationships and junctions during myelination of the optic nerve. *International Journal of Developmental Neuroscience*, 6(3), pp.233–243.

Wilson, R. & Brophy, P.J., 1989. Role for the oligodendrocyte cytoskeleton in myelination. *J Neurosci Res*, 22(4), pp.439–448.

Windrem, M.S. et al., 2014. A Competitive Advantage by Neonatally Engrafted Human Glial Progenitors Yields Mice Whose Brains Are Chimeric for Human Glia. *The Journal of Neuroscience*, 34(48), pp.16153–16161.

Windrem, M.S. et al., 2017. Human iPSC Glial Mouse Chimeras Reveal Glial Contributions to Schizophrenia. *Cell Stem Cell*, 21(2), pp.195–208.

Windrem, M.S. et al., 2008. Neonatal chimerization with human glial progenitor cells can both remyelinate and rescue the otherwise lethally hypomyelinated shiverer mouse. *Cell Stem Cell*, 2(6), pp.553–565.

Witt, S.H. et al., 2017. Genome-wide association study of borderline personality disorder reveals genetic overlap with bipolar disorder, major depression and schizophrenia. *Translational Psychiatry*, 7(6), pp.e1155–e1155.

Wood, P., Okada, E. & Bunge, R., 1980. The use of networks of dissociated rat dorsal root ganglion neurons to induce myelination by oligodendrocytes in culture. *Brain Research*, 196(1), pp.247–252.

Wu, L.-S., Cheng, W.-C. & Shen, C.K.J., 2012. Targeted depletion of TDP-43 expression in the spinal cord motor neurons leads to the development of

amyotrophic lateral sclerosis-like phenotypes in mice. *Journal of Biological Chemistry*, 287(33), pp.27335–27344.

Wu, L.-S. et al., 2010. TDP-43, a neuro-pathosignature factor, is essential for early mouse embryogenesis. *genesis*, 48(1), pp.56–62.

Xiao, L. et al., 2016. Rapid production of new oligodendrocytes is required in the earliest stages of motor skill learning. *Nature Neuroscience*, 19(9), pp.1210–1217.

Xiao, J. et al., 2010. Brain-derived neurotrophic factor promotes central nervous system myelination via a direct effect upon oligodendrocytes. *Neurosignals*, 18(3), pp.186–202.

Xiao, J., Kilpatrick, T.J. & Murray, S.S., 2009. The role of neurotrophins in the regulation of myelin development. *Neurosignals*, 17(4), pp.265–276.

Xu, X. et al., 2018. Species and cell-type properties of classically defined human and rodent neurons and glia. *eLife*, 7, p.868.

Xu, Y.K.T. et al., 2019. Deep learning for high-throughput quantification of oligodendrocyte ensheathment at single-cell resolution. *Communications Biology*, 2(1), pp.1–12.

Yang, C. et al., 2014. Partial loss of TDP-43 function causes phenotypes of amyotrophic lateral sclerosis. *Proc Natl Acad Sci USA*, 111(12), pp.E1121–E1129.

Yeung, M.S.Y. et al., 2014. Dynamics of Oligodendrocyte Generation and Myelination in the Human Brain. *Cell*, 159(4), pp.766–774.

Yeung, M.S.Y. et al., 2019. Dynamics of oligodendrocyte generation in multiple sclerosis. *Nature*, 566(7745), pp.538–542.

Young, K.M. et al., 2013. Oligodendrocyte Dynamics in the Healthy Adult CNS: Evidence for Myelin Remodeling. *Neuron*, 77(5), pp.873–885.

Yuen, T.J. et al., 2013. Identification of endothelin 2 as an inflammatory factor that promotes central nervous system remyelination. *Brain*, 136(4), pp.1035–1047.

Yuen, T.J. et al., 2014. Oligodendrocyte-encoded HIF function couples postnatal myelination and white matter angiogenesis. *Cell*, 158(2), pp.383–396.

Zalc, B., Goujet, D. & Colman, D., 2008. The origin of the myelination program in vertebrates. *Current Biology*, 18(12), pp.R511–R512.

Zatorre, R.J., Fields, R.D. & Johansen-Berg, H., 2012. Plasticity in gray and white: neuroimaging changes in brain structure during learning. *Nature Neuroscience*, 15(4), pp.528–536.

Zhang, A. et al., 2015. Neurofascin 140 Is an Embryonic Neuronal Neurofascin Isoform That Promotes the Assembly of the Node of Ranvier. *J Neurosci*, 35(5), pp.2246–2254.

Zhang, J. et al., 2018. In vivo characterization of white matter pathology in premanifest huntington's disease. *Annals of neurology*, 84(4), pp.497–504.

Zhang, S.-C. et al., 2001. In vitro differentiation of transplantable neural precursors from human embryonic stem cells. *Nat Biotech*, 19(12), pp.1129–1133.

Zhang, Y. et al., 2016. Purification and Characterization of Progenitor and Mature Human Astrocytes Reveals Transcriptional and Functional Differences with Mouse. *Neuron*, 89(1), pp.37–53.

Zhu, Z. & Huangfu, D., 2013. Human pluripotent stem cells: an emerging model in developmental biology. *Development*, 140(4), pp.705–717.

Ziskin, J.L. et al., 2007. Vesicular release of glutamate from unmyelinated axons in white matter. *Nature Neuroscience*, 10(3), pp.321–330.

Zonouzi, M. et al., 2019. Individual Oligodendrocytes Show Bias for Inhibitory Axons in the Neocortex. *CellReports*, 27(10), pp.2799–2808.

Zuchero, J.B. et al., 2015. CNS Myelin Wrapping Is Driven by Actin Disassembly. *Developmental cell*, 34(2), pp.152–167.